CONTRACTOR REPORT

SAND82-7105
Unlimited Release
UC-63c

Efficiency Improvement Study for GaAs Solar Cells

Final Report
For Period 03/31/80 through 09/30/81

J. A. Cape, J. R. Oliver, S. W. Zehr
Rockwell International
Thousand Oaks, California 91360

Prepared by Sandia National Laboratories Albuquerque, New Mexico 87185 and Livermore, California 94550 for the United States Department of Energy under Contract DE-AC04-76DP00789

Printed April 1982

When printing a copy of any digitized SAND Report, you are required to update the markings to current standards.

Issued by Sandia National Laboratories, operated for the United States Department of Energy by Sandia Corporation.

NOTICE: This report was prepared as an account of work sponsored by an agency of the United States Government. Neither the United States Government nor any agency thereof, nor any of their employees, nor any of their contractors, subcontractors, or their employees, makes any warranty, express or implied, or assumes any legal liability or responsibility for the accuracy, completeness, or usefulness of any information, apparatus, product, or process disclosed, or represents that its use would not infringe privately owned rights. Reference herein to any specific commercial product, process, or service by trade name, trademark, manufacturer, or otherwise, does not necessarily constitute or imply its endorsement, recommendation, or favoring by the United States Government, any agency thereof or any of their contractors or subcontractors. The views and opinions expressed herein do not necessarily state or reflect those of the United States Government, any agency thereof or any of their contractors or subcontractors.

Printed in the United States of America
Available from
National Technical Information Service
U.S. Department of Commerce
5285 Port Royal Road
Springfield, VA 22161

NTIS price codes
Printed copy: A08
Microfiche copy: A01

Distribution
Category UC-63c

SAND82-7105
Unlimited Distribution
Printed April 1982

EFFICIENCY IMPROVEMENT STUDY FOR GaAs SOLAR CELLS

J. A. Cape, J. R. Oliver, S. W. Zehr
Rockwell International
Thousand Oaks, California 91360

ABSTRACT

High-yield fabrication of good quality AlGaAs/GaAs concentration solar cells has been a limiting factor in widespread utilization of these high conversion efficiency (22-24%) photovoltaic cells. The study described here reports on a series of investigations to correlate solar cell yield with substrate quality, growth techniques, layer composition, and metallization processes. In addition, several diagnostic techniques are described to aid in device characterization.

Prepared for Sandia National Laboratories under Contract 49-1792.

TABLE OF CONTENTS

Page

1.0 INTRODUCTION 1

1.1 Background 1
1.2 Summary of Problem 3

2.0 CELL FABRICATION AND TESTING 5

2.1 Cell Design 5
2.2 Bulk Materials Growth 10
2.3 Epitaxial Growth 10
2.4 Cell Processing 11
2.5 Solar Cell Testing 14

3.0 RESULTS 18

3.1 Ohmic Contact Studies 18
3.2 Auger Analysis of Alloy Contacts 25
3.3 The Effect of Substrates 29
3.4 Photoresponse Studies 35
3.5 Discussion 45
3.6 Critique 46

REFERENCES 48

APPENDIX 1 49

APPENDIX 2 57

APPENDIX 3 142

LIST OF ILLUSTRATIONS

Page

Fig. 1. Ohmic contact grid..... 6

Fig. 2. A section of the solar cell showing the new ohmic contact technique for the top grid. The AlGaAs layer is selectively etched under the contact fingers such that the contact material can make contact to the underneath p^+-GaAs layer directly..... 7

Fig. 3. The GaAs concentrator cell efficiency as a function of concentration for a number of series resistance values..... 9

Fig. 4. (a) The schematic diagram of MO-CVD growth system, (b) research MO-CVD reactor for growth of AlGaAs/GaAs heterostructure devices..... 12

Fig. 5. Rockwell International natural sunlight concentrator test facility..... 15

Fig. 6. Schematic diagram of flash illumination I-V test apparatus.. 16

Fig. 7. Block diagram of the computer-controlled photoresponse test apparatus..... 17

Fig. 8. Ohmic contact resistance test pad configuration..... 19

Fig. 9. Predicted resistance vs. pad-to-pad separation..... 20

Fig. 10. Measured contact resistance data for LPE cell..... 22

Fig. 11. Measured contact resistance data for MO-CVD cell, MIT-224... 23

Fig. 12. Measured contact resistance data for MO-CVD cell, CS-265.... 24

Fig. 13. Typical scanning Auger chemical profile analysis of "good" ohmic contact to an LPE grown AlGaAs/GaAs solar cell structure prior to alloying..... 26

Fig. 14. Typical scanning Auger chemical profile analysis of alloyed "good" ohmic contact to LPE-grown AlGaAs/GaAs solar cell structure..... 27

LIST OF ILLUSTRATIONS (Cont.)

Page

Fig. 15. Typical scanning Auger chemical profile analysis of alloyed "poor" ohmic contact to an MO-CVD grown AlGaAs/GaAs solar cell structure. Contacts of this type behaved as Schottky barrier diodes bucking the cell p-n junction..... 28

Fig. 16. Electron Beam Induced Current (EBIC) scan for 10 μm LPE p-layer on n^+ bulk substrate. Junction at peak, p-layer to right..... 31

Fig. 17. Log of reciprocal lifetime (from EBIC data) vs. square of distance from junction..... 32

Fig. 18. EBIC scan of 1 μm p-layer on 10 μm n-buffer layer both grown by MO-CVD at 655°C..... 33

Fig. 19. Photoresponse and reflectivity for typical Mitsubishi substrate, Cell PR-308..... 36

Fig. 20. Photoresponse and reflectivity for Crystal Specialties substrate, Cell 308-8..... 37

Fig. 21 Computer fit to internal quantum efficiency for cell 308-8.. 38

Fig. 22. 1 SUN I-V for cell 308-8..... 39

Fig. 23. 500 SUNs I-V for cell 308-8..... 40

Fig. 24. Photoresponse curve for a high I_{sc} cell (28 mA/cm^2)..... 43

Fig. A-1 Distributed sheet resistance model..... 51

Fig. A-2 Computed 750X, 500X and 250X light I-V curves for a radial concentrator cell based on the model in Fig. A-1. Data points are for cell N7/M-186-3..... 53

Fig. A-3 Computed dark I-V curve. Dashed curve is actual measured data. Dotted curve is equivalent junction current derived from 750X data of Fig. A-2..... 55

1.0 INTRODUCTION

1.1 Background

The goal of this program was the achievement of high yields of high efficiency GaAs concentrator solar cells. To this end, the project focused on identifying the efficiency-limiting factors in cell materials and cell processing and in improving materials growth and cell fabrication procedures so as to mitigate these factors.

In a previous study (Sandia Contract #07-7274), we demonstrated a laboratory scale production yield of 62% for GaAs concentrator cells with $\eta >$ 18.5%. This yield at the end of the one-year program represented a great improvement over the less than 1% yields experienced at the beginning of the program. While this result represents a highly successful yield improvement, it falls far short of the potential suggested by individual GaAs cell results. By this time, certainly tens of GaAs cells have been fabricated which achieved AM1 efficiencies >24%. These remarkable performances which approach the theoretical maximum promised by GaAs, imply that acceptable yields of high efficiency cells can be achieved once the inherent efficiency degrading mechanisms can be identified and circumvented. Accordingly, an attempt was made to define and initiate a program of study to achieve the desired high yields. This report summarizes the results of the past year of study on this program.

The highest efficiency GaAs solar cells that have been fabricated thus far were fabricated using either liquid phase or vapor phase epitaxy to obtain material of sufficient quality. A minimum of two epitaxial layers have been required, one of which serves in part as a buffer layer to isolate the active regions of the cell from the substrate.

Currently available Czochralski-grown bulk single crystal GaAs is not of sufficient quality to yield high performance solar cells directly, without the use of epitaxial buffer layers. The major problems exhibited by these bulk materials are short minority carrier lifetimes and diffusion lengths. These are limited by electron-hole recombination processes. Recombination processes

are in turn affected by the nature and amounts of unwanted impurities, and the concentrations of crystalline imperfections such as point defects and dislocations. Consequently, solar cells fabricated on bulk substrates without a buffer layer tend to have low efficiencies.

To date, this problem has been somewhat mitigated by the growth of an intervening buffer layer. However, while the growth of a buffer layer greatly improves the yield of high efficiency cells, the yields remain undesirably low for cost-effective production purposes. The low efficiency cells prepared by this method exhibit similar characteristics to those grown without buffer layers. This suggests the possibility that certain defects propagate through the buffer layers into the active layers. For example, chromium is known to be a fast diffuser and dislocations may also propagate into the grown layers.

The low solar cell efficiencies frequently obtained with these materials appear to result from two problem areas. First, impurities and defects in the bulk of the active layers apparently cause reduction of the short circuit currents. The identity and nature of these imperfections is not well understood. Secondly, in many cells, the open circuit voltage is greatly reduced at low illumination levels. The most likely explanation of this problem is the presence of traps and recombination centers in the p-n junction. This problem characteristically occurs at isolated regions distributed about the area of the device as can be demonstrated by fabricating many small area cells on a single layer area (e.g., 1 cm^2) wafer. Thus, this problem is particularly inimical to high yields for large area devices such as solar cells. Again, what imperfections give rise to these effects are not known. Thus, there is a great need to identify these imperfections and reduce their level in bulk and epi-material. Moreover, cell processing has the potential for being simpler, faster, and less costly, if substrates with suitably long lifetimes and diffusions lengths become available. Ideally, the development of highest quality n^+ substrate materials can mean not only greatly increased yields but may lead to single layer epi-growth and thus greatly reduced cell cost.

1.2 Summary of Problem

The situation described in the previous section suggests basically three areas which may be critical for cell yields. There are, first of all, those factors which limit the diffusion length in the active layers and, hence, the cell current. Here one is probably concerned with recombination processes which reduce the minority carrier lifetime. Impurities and other defects are thought to be the causative agent but the origin of these defects is not known. They may be incorporated during crystal growth as impurities in the primary reactants or as diffusants from the underlying substrates. Alternatively, they may arise during processing, for example, as a result of ohmic contact alloying procedures. The latter possibility seems unlikely because it is hard to see how a significant fraction, if not the entire area of the active layers could be affected, as it must to significantly reduce the cell voltage.

A second area of concern is the quality of the p-n junction. Recombination centers in the junction or gross imperfections which provide leakage paths can severely reduce the cell voltage. A dramatic illustration of this effect occurs when one processes a large area (say 3 cm x 3 cm) wafer into a checkerboard of very small (0.025 cm^2) cells. Typically it is observed that many of the cells will have greatly reduced open circuit voltages though they will be surrounded by cells with more typical values of V_{oc}. This illustrates the highly local nature of the agents which cause degradation in the cell voltage. Unfortunately, solar cells being large area devices are particularly sensitive to such problems because a single low voltage region in the cell tends to govern the voltage of the entire cell. Here again, it is not known whether such defects are incorporated during growth -- and, if so, whether they arise in the substrate or in the reactants -- or whether they are caused during processing. In this case, it is much easier to envision processing failures, e.g. a diffusion of ohmic contact metallization into the junction region during alloying.

Finally, the third primary area of concern has to do with those factors which contribute to ohmic losses in the cell, i.e., give rise to unacceptably large effective series resistance. Certainly in this category must be

considered the ohmic contacting processing and electroplating which are critical steps in the formation of the contact grid.

In Section 3, we describe some of the studies and conclusions, in each of these problem areas, that have been carried out during the contact period.

2.0 CELL FABRICATION AND TESTING

2.1 Cell Design

Figure 1 shows the ohmic contact grid pattern selected for the cells to be studied on this program. Since these cells are designed for application at concentrations up to 1000X, the contact grid incorporates a large number of very fine grid fingers. The pattern consists of 5 concentric ring areas with 256 tapered radial fingers in the outermost ring, 128 in the second, and 64, 32 and 16 fingers, respectively, in the subsequent ring areas. This design provides an average finger spacing of 92 μm and an average shadowing ratio of $\sim$10% (the design goal was 7% but excessive "blossoming" of the fingers during plating leads to the larger value). In the Rockwell concentrator cell design, the contact grid is alloyed directly to the cell p-layer (see Fig. 2). This is accomplished by first selectively etching away the AlGaAs "window" layer where the contact metallization is to be applied. Thus, the relatively thin ($\sim$500Å) AlGaAs layer, other than acting as a preventative of surface recombination losses, is sensibly inactive, and the major contribution to the ohmic losses, by far, comes from the sheet resistance of the p-layer, ρ_p, the resistivity of the grid fingers, ρ_f, and the specific ohmic contact resistance, R_c^{sp}, of the metallization-p layer interface. The total resistance of the cell is given, to a good approximation by

$$R_s A = \rho_p b^2/12t_p + \rho_f A/12t_f r + R_c^{sp}/r \qquad (1)$$

where r is the shadowing ratio, A the cell area, and the three terms are respectively, the sheet resistance contribution, the contribution of the fingers, and the contribution of the contact resistance of the grid. For high quality p-material as grown by LPE, for example, $\rho_p \sim 0.03\Omega$-cm, and for a p-layer thickness of 1 μm with an average grid finger spacing of 92 μm, the first term gives ≈ 2 mΩcm^2.

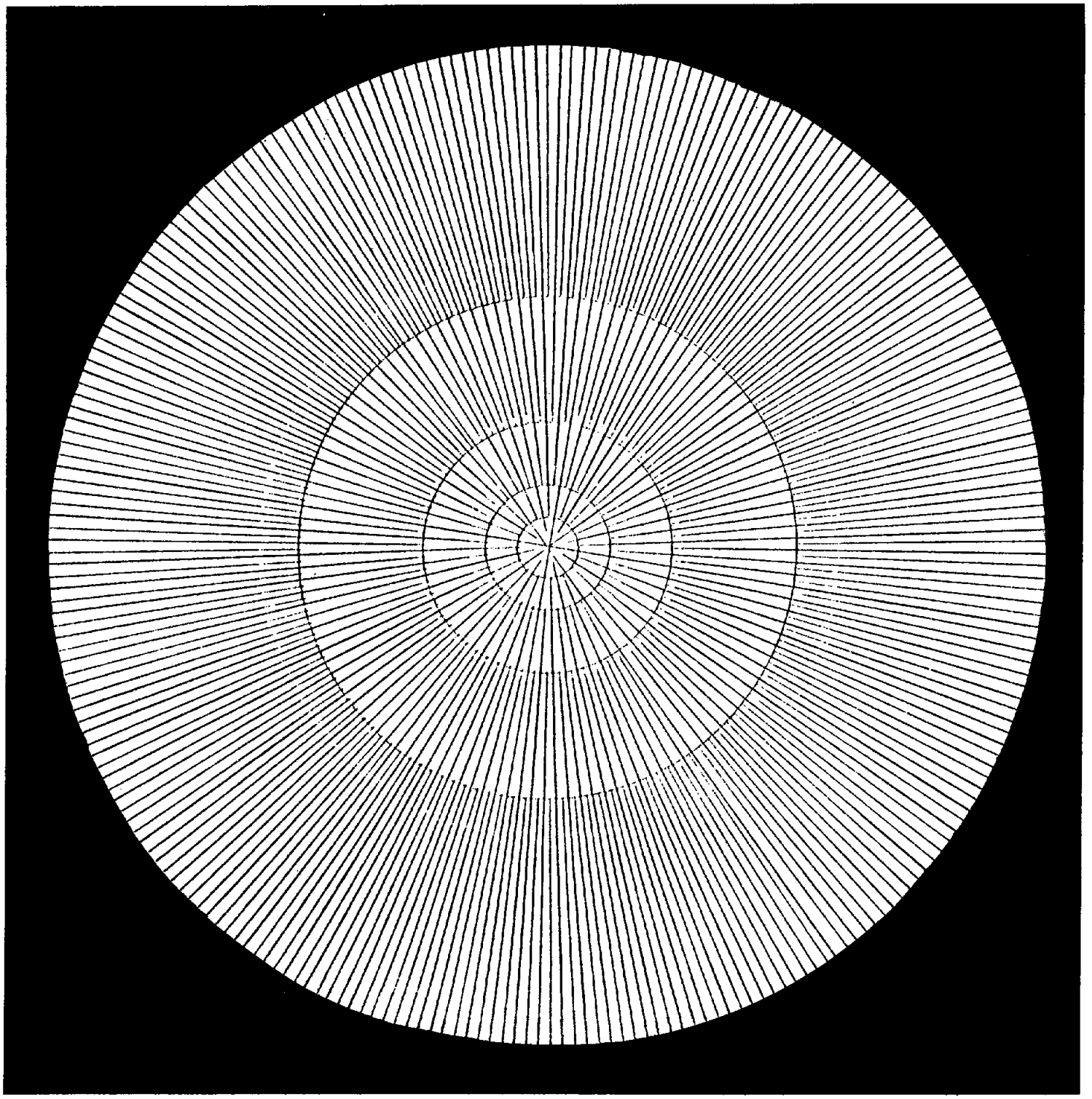

Fig. 1. Ohmic contact grid.

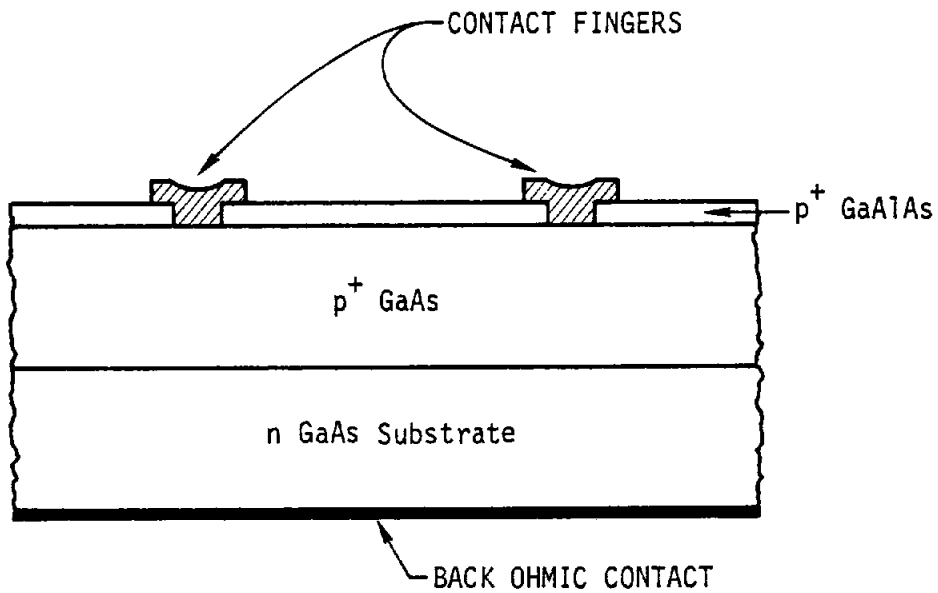

Fig. 2. A section of the solar cell showing the new ohmic contact technique for the top grid. The AlGaAs layer is selectively etched under the contact fingers such that the contact material can make contact to the underneath p^+-GaAs layer directly.

In the second term, if one takes the cell area A = 0.785 cm^2, a finger height of 5 μm and a 10% shadowing ratio, this term also yields $\sim$2 $m\Omega cm^2$. For this result, we have used the resistivity of pure silver (1.6 $\mu\Omega cm$) for the calibration. A value of R_c^{sp} of $10^{-4}\,\Omega\text{-}cm^2$ was assumed as an upper limit when this cell design was developed. This limiting value of the specific contact resistance appeared to be representative of our ohmic contacting technology for LPE materials and, when combined with the first two resistance terms, led to a predicted resistance-area product for the cell design of $\sim$5 $m\Omega\text{-}cm^2$ or about 6 $m\Omega$/cell. Such a value would be expected to permit high efficiency performance at concentrations up to $\sim$1000X as was the design goal (see Fig. 3). We shall see, however, the the measured values could be significantly less than 6 $m\Omega$/cell <u>and</u> could be much greater than that value. Some of these variations occur because of variations in the thickness and doping level of the p-layer and some are due to variations in the quality and amount of plating in the fingers, but the vast majority of this variability could be traced to unreliable ohmic contacting. Some of these experiments will be discussed in greater detail in the next section.

The contributions to the effective series resistance discussed above give insight into the trade-offs involved in the solar cell design. For example, if diffusion lengths greater than say, 3 μm can be dependably produced the p-layer thickness could be increased to perhaps 2 μm, thus reducing the sheet resistance contribution to $\sim$1 $m\Omega cm^2$. Conversely, if the diffusion lengths were more typically 2 μm or less, the external quantum efficiency (collection efficiency) of the cell would be severely reduced unless the p-layer thickness was $\leqslant$1 μm thus increasing the R_s value and compromising the high concentration performance. Similarly, increasing the finger thickness to say 10 μm can reduce the grid contribution to R_s, but it is characteristic of our plating procedure that increasing the finger height will concommitantly increase the shadowing ratio. Thus, while R_s may be lowered, the effective cell area and hence the cell current would be lowered. What remains unequivocal, however, is that quality ohmic contacts with R_c^{sp} values $\leqslant 10^{-4}\,\Omega\text{-}cm^2$ are critical for the achievement of high concentration cells.

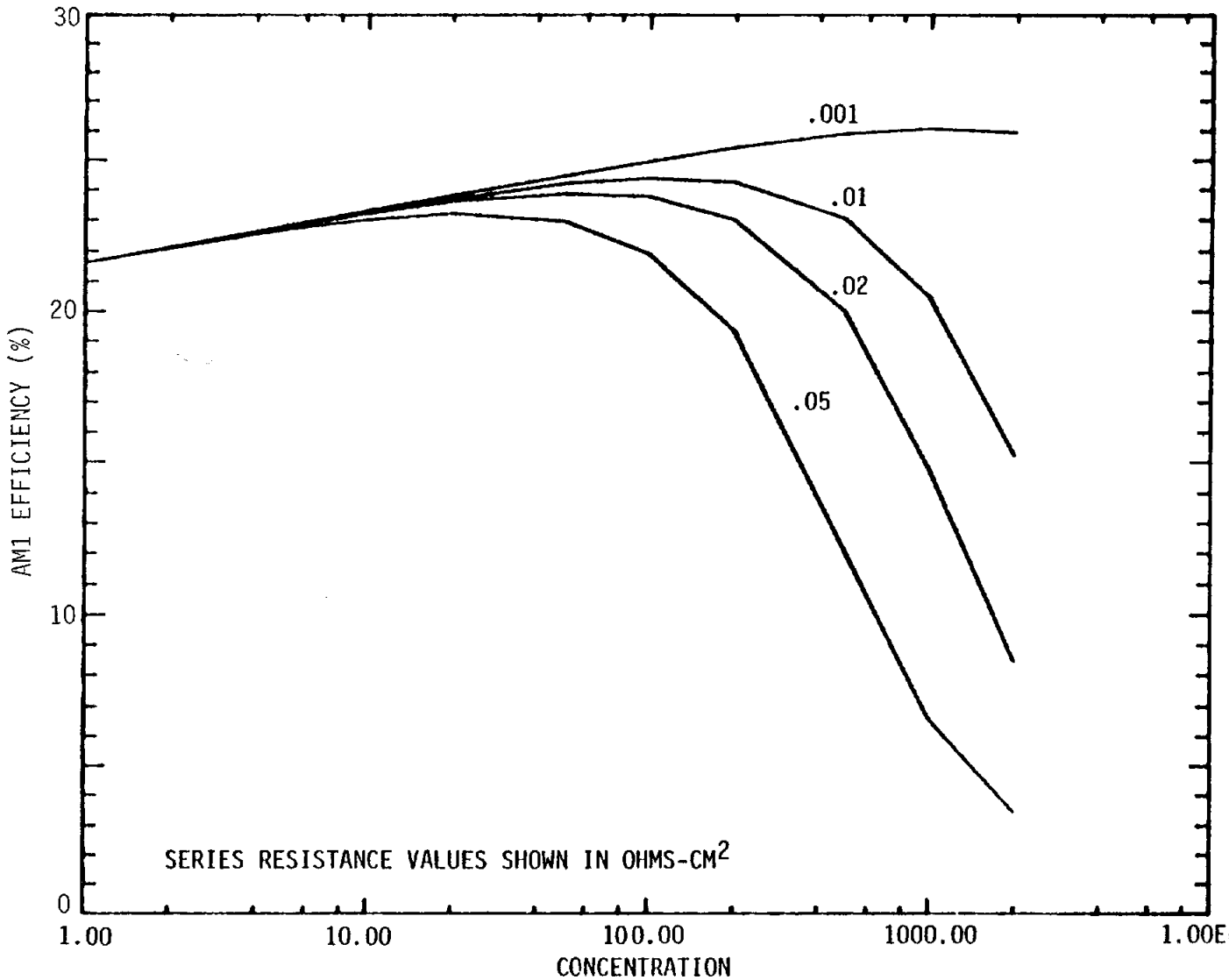

Fig. 3. The GaAs concentrator cell effficiency as a function of concentration for a number of series resistance values.

2.2 Bulk Materials Growth

The substrate materials used in this program were chosen from a variety of sources in the hope of establishing correlation between substrate quality and cell yield. Substrates were obtained from external suppliers (Crystal Specialties, Mitsubishi and Laser Diode Labs), and grown in-house using a Metals Research liquid encapsulant Czochralski (LEC) puller. The materials supplied by the external suppliers were, in each case, boat grown. The Mitsubishi (Mit.) material was specified as Si-doped, $1.4 \times 10^{18} < N < 3 \times 10^{18}$, $4.5 \times 10^{2} < EPD < 2.6 \times 10^{3}$. Wafers 1.4" x 1.4" were polished on one side and lapped on the other by the supplier. The Crystal Specialties (CS) material was specified as Te-doped, $n > 2 \times 10^{18}$. The material was supplied as unpolished 1.4" x 1.4" wafers. Polishing was performed in-house at Rockwell.

The Laser Diode (LD) materials were supplied in the form of small "D"-shaped wafers specified as Si-doped, $0.8 \times 10^{18} < N < 2.5 \times 10^{18}$, and $1700 < EPD < 2800$. Whereas generally, the CS and Mit wafers were processed simultaneously using a 3x3, nine-cell mask set, the LD wafers were processed from 1 to 6 cells simultaneously.

The in-house grown wafers were taken from three boules numbered N1/C, N6/C and N7/M. The "C" designation refers to boules grown (111)-oriented with a corracle so as to be precisely 2" in diameter. The "M" designated boules were (100) oriented with free-form boundary and were typically 3" in diameter. The LEC grown boules were Te-doped typically $1\text{-}2 \times 10^{18}$ with EPD's in the range 10^{4} to 10^{5}.

2.3 Epitaxial Growth

Prior to the initiation of this program, virtually all of the GaAs cells fabricated at Rockwell were made by liquid phase epitaxy (LPE). While LPE has generally produced the highest quality materials and the highest recorded efficiency solar cells[1], it suffers from several handicaps. For example, the method does not lend itself conveniently to mass production. A second, and perhaps more serious flaw is that it is difficult at best to obtain uniform growths on large area substrates. In contrast, vapor phase tech-

niques are fairly easily adapted to large area and multiple wafer production. For these reasons, principally, this program was initiated using metal-organic chemical vapor deposition (MO-CVD) as the method for epitaxial layer growth. Rockwell is certainly one of the most experienced laboratories in MO-CVD growth of III-V compounds, though comparatively little of this history has been specifically oriented towards solar cells. Nevertheless, our experience made it possible to get under way rapidly at the beginning of this contract period. A system dedicated to solar cell growth was set up. It features automatic microprocessor programmed control of the metal organic sources (see Fig. 4). All of the sources can be introduced sequentially during the same run, thus minimizing the possibility of contamination. In fact, it appears that the only significant source of impurities -- other than those present in the GaAs substrates -- may be the metal-alkyls and arsine which are used in the growth. Under a separate program (SERI Subcontract No. XS-0-9430-1), Rockwell is investigating this problem. The Rockwell MO-CVD reactor is shown in schematic in Fig. 4(a). The growth chamber features vertical flow of the gases and a horizontal susceptor and substrate.

The principal n-type dopant employed for solar cell applications is Se derived from H_2Se. Reproducible doping has been achieved over the range 10^{16}-10^{19} cm^{-3} using this source. The doping in the solid is linearly proportional to flow of H_2Se in the reactor. Similarly, control of p-type doping is achieved using Zn in the form of diethylzinc (DEZn). DEZn is a high vapor pressure liquid at room temperature and is transported to the reactor by passing H_2 over the liquid. The doping level has been varied over the range 10^{16}-10^{20} cm^{-3} by this method. Again, the doping varies linearly with the flow of H_2 through DEZn. These two dopants were used for all the cells studies during this program.

2.4 Cell Processing

A unique concentrator cell process developed by Sahai, Edwall and Harris[1,2] has been employed at Rockwell for several years. This process, which was adopted at the start of this program, is described briefly as follows:

SC78-2171

SCHEMATIC DIAGRAM OF MO-CVD REACTOR

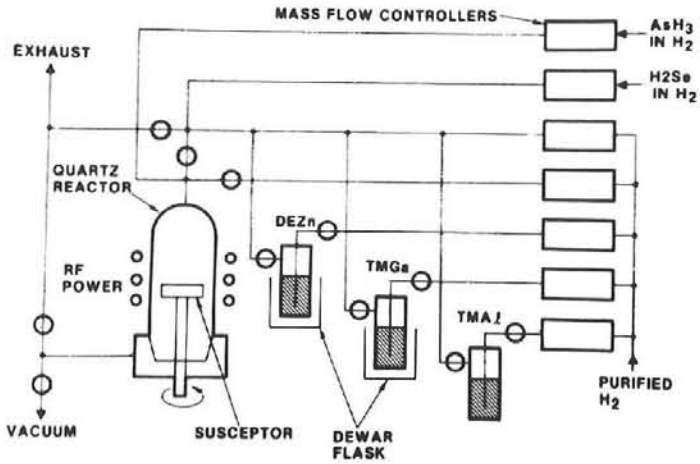

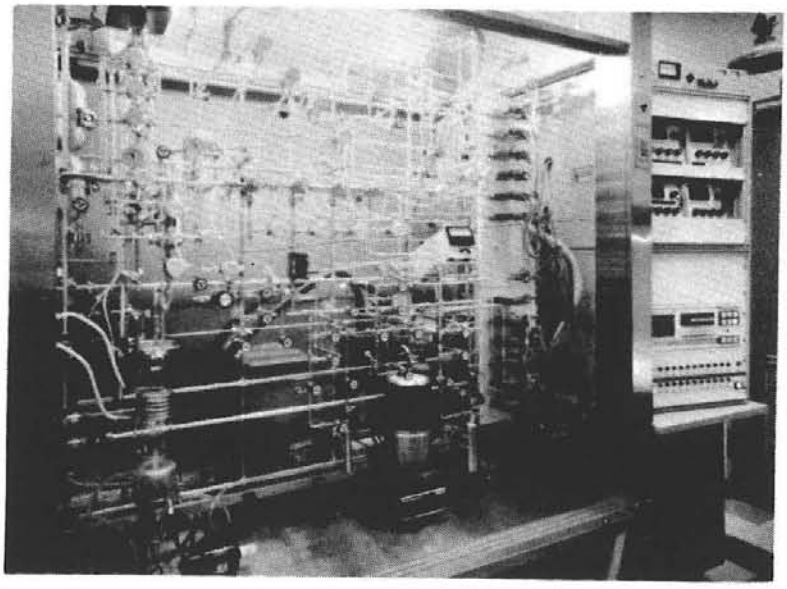

Fig. 4 (a) The schematic diagram of MO-CVD growth system, (b) research MO-CVD reactor for growth of AlGaAs/GaAs hetero-structure devices.

1. Etch channels in the AlGaAs layer for the contact grid pattern (see Fig. 2). This step exposes the GaAs p-layer in the channels. The etchant used is dilute HF.
2. A thin layer of Zn followed by a layer of Ag-Mn alloy is then evaporated into the channels. An Au-Ge-Pt complex is then deposited on the back face of the n-substrate.
3. These metal deposits are then alloyed to the p-GaAs and n-GaAs respectively.
4. The contact grid fingers and buss area (see Fig. 1) are then electroplated to $\sim 5\ \mu m$ thickness with Ag and capped with a thin (500Å) Au layer.
5. Mesas are etched around each of the 9-cells.
6. The wafer is sawed into 9 individual cells. Standard photolithography techniques are used throughout.

During the course of this study, as part of our effort to improve good ohmic contact yields, many variations in the above process were attempted. Some of these will be discussed in more detail in the following. For example, it was discovered that the addition of Zn in the front contact metallization was apparently superfluous.

Among the other variations that were studied, numerous etch procedures for removal of the AlGaAs layer were tried, since it was thought that the presence of oxide or other residue contaminants at the p-layer surface might be causing poor ohmic contact formation. The Al content of the AlGaAs window was varied. A marked increase in the p-layer dopant level at the interface was incorporated in many of the wafers. No concrete evidence was obtained that any of these process variations improved the quality of the ohmic contacts or cell performance.

2.5 Solar Cell Testing

The Rockwell test facilities include: (1) an automatic pnotoresponse system which yields spectral quantum efficiency and reflectivity data, (2) an automated I-V system for 1 SUN (simulated) I-V curves, (3) an automated pulse I-V system using a flash simulator which provides high concentration (10 SUNs to 10,000 SUNs) I-V curves as well as dark I-V up to 25 amperes, and (4) a high concentration (up to 1000 SUNs) facility for I-V data in natural sunlight. The natural sunlight facility is shown in Fig. 5.

The pulse I-V apparatus is shown in schematic form in Fig. 6. The solar cell is illuminated by a xenon arc lamp triggered by a Macsym II computer. When the cell voltage reaches the reference voltage, V_{REF}, the comparator turns on the transistor switch and draws a load current, I_L, sufficient to maintain the cell voltage at V_{REF}. This load current is monitored by a 0.25 ohm resistor in series with a 12,000 μF capacitor which is discharged to -16 volts between flash pulses. The low duty cycle of the system (1 flash/ 4 seconds) allows a low current power supply to be used for the capacitor discharge. A typical I-V curve requires 22-25 data points and shows excellent agreement with curves generated by continuous illumination.

Solar cell spectral response measurements are made using the apparatus shown in Fig. 7[3]. Calibrated quantum efficiency and reflectivity measurements are routinely performed over a wavelength range of 360-1000 nm in either dark or 1 SUN light level conditions. Stored AMO and AM1 solar spectra are convolved with the photoresponse measurements to obtain predicted values for AMO and AM1 current densities. Computed internal quantum efficiency data can be curve-fit by a mathematical model describing the predicted cell response[4] and extract minority carrier diffusion lengths, interfacial recombination velocity, and AlGaAs window layer Al content and thickness.

In addition to the above types of measurements which are performed routinely on all of the cells fabricated for this contract, a number of facilities are used more or less routinely for characterization of the cell materials. These include Hall measurements on epilayers, EBIC studies of junctions and active epilayers, and Auger profile analysis.

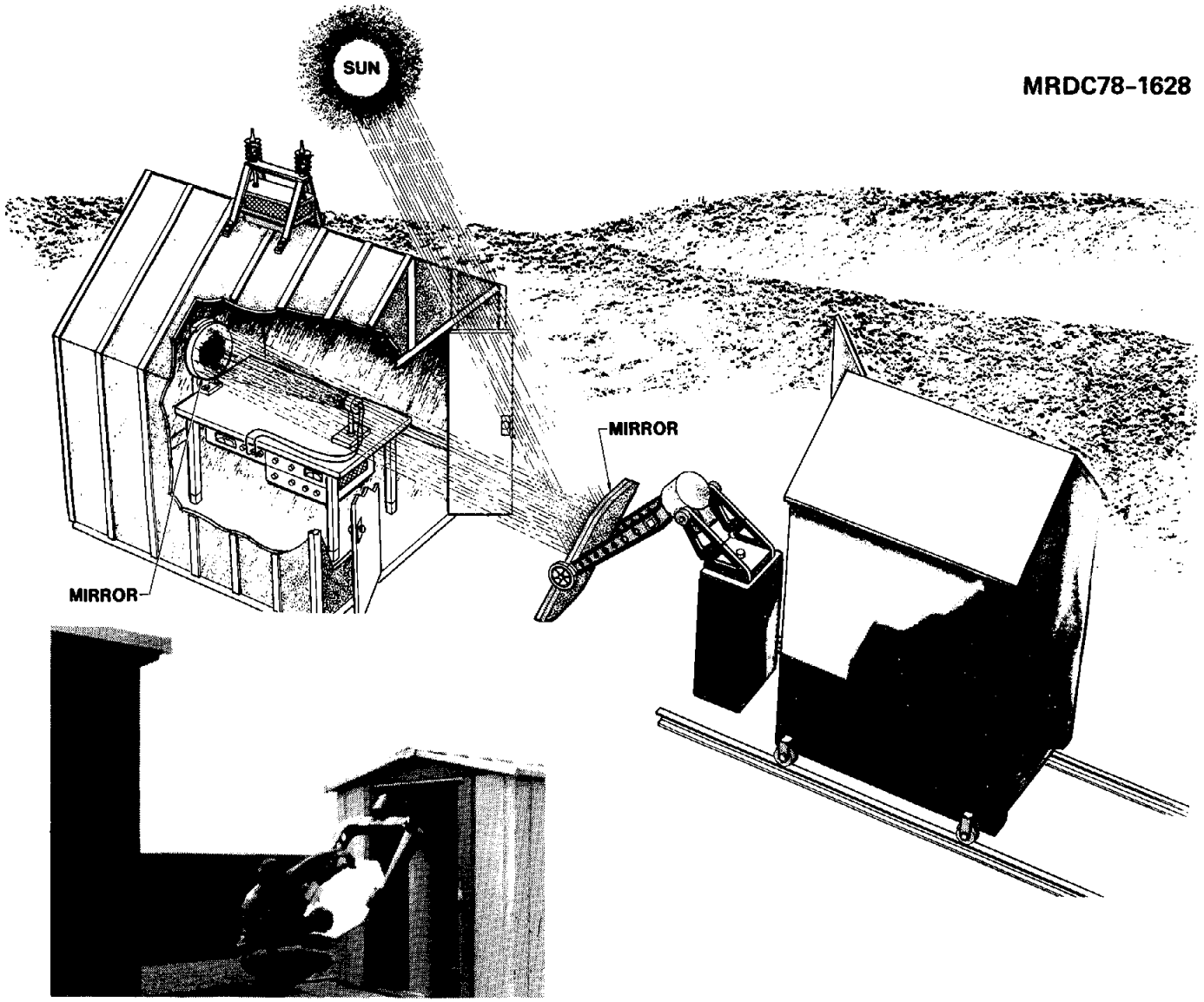

Fig. 5 Rockwell International natural sunlight concentrator test facility.

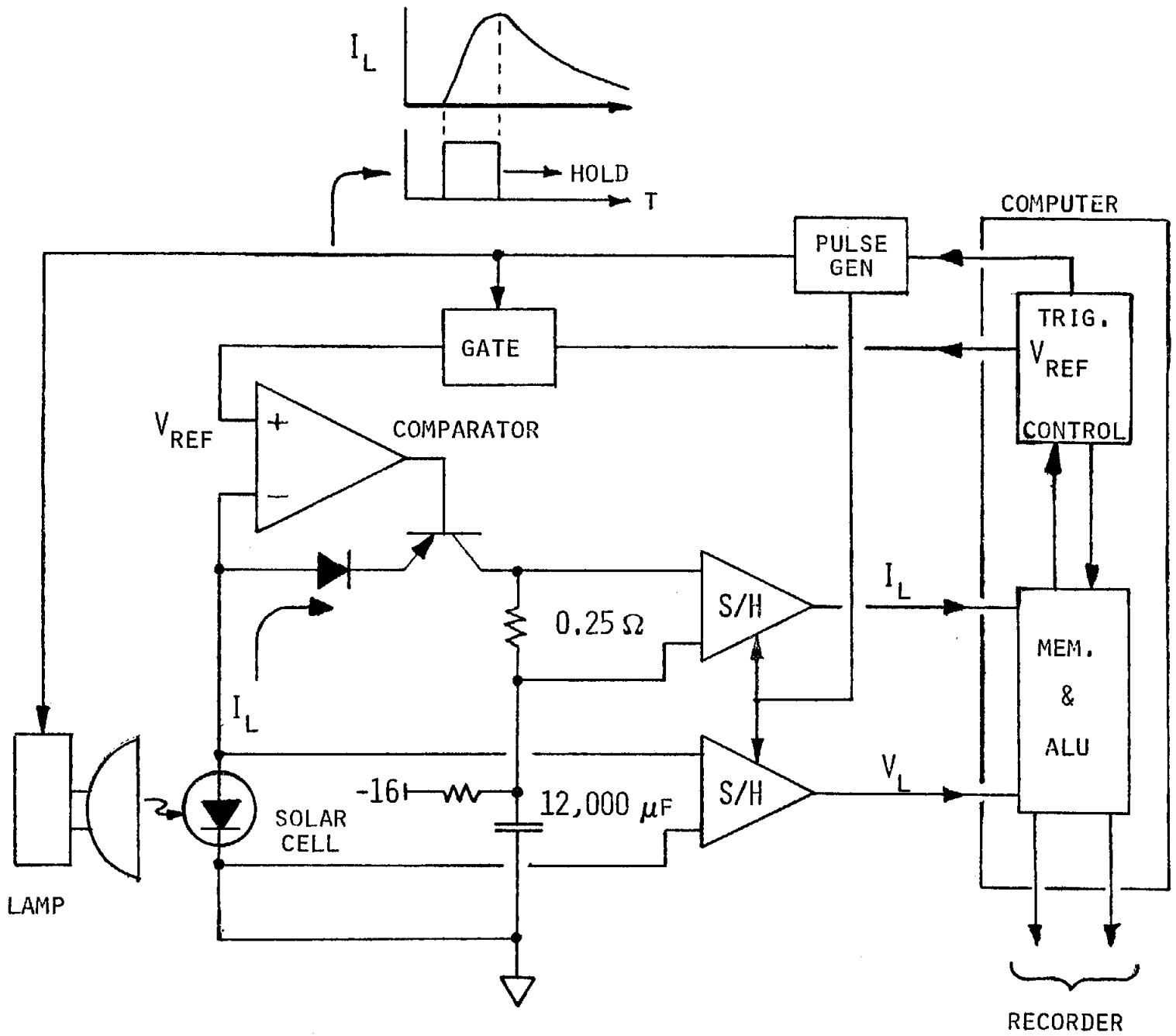

Fig. 6. Schematic diagram of flash illumination I-V apparatus.

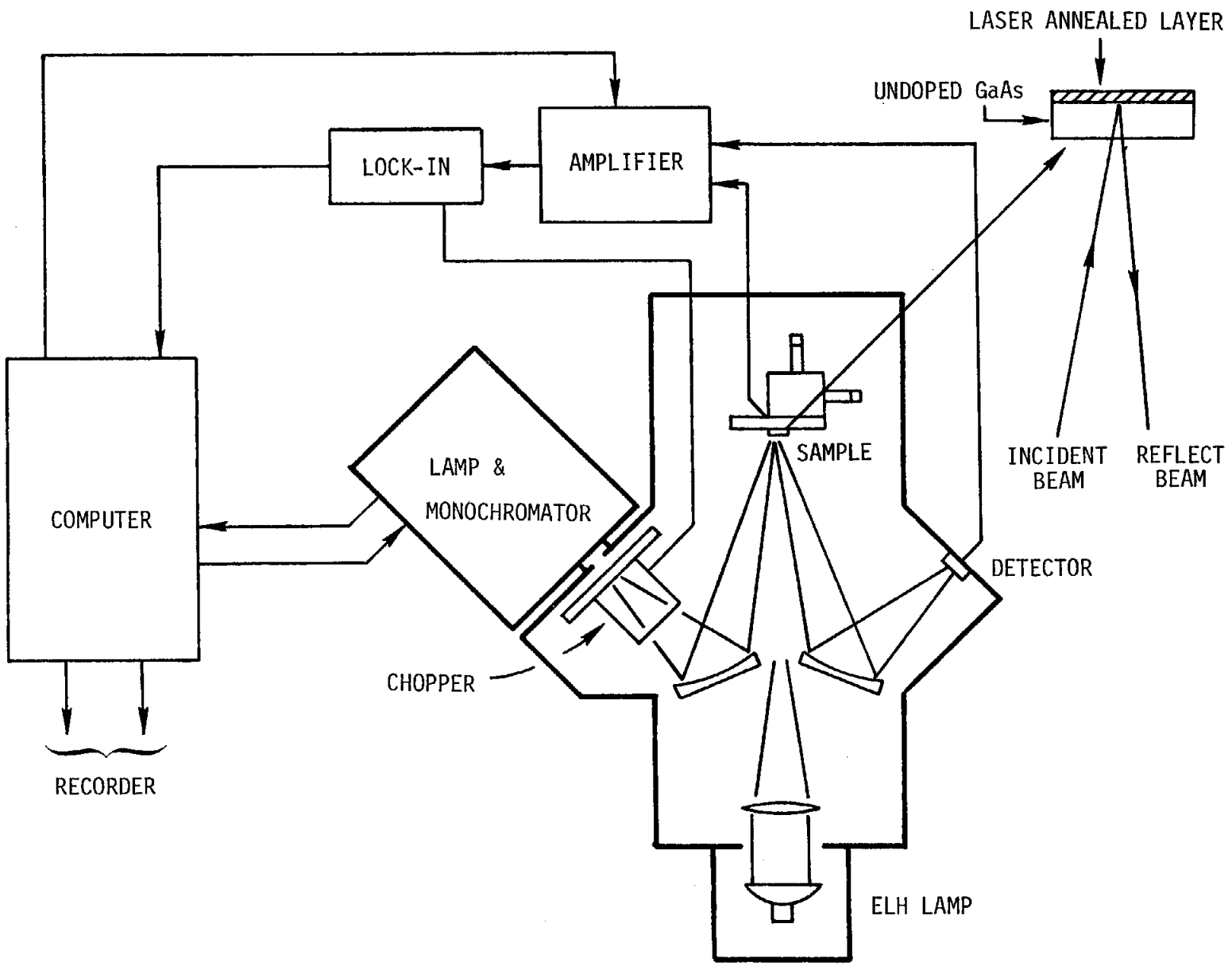

Fig. 7. Block diagram of the computer-controlled photoresponse test apparatus.

3.0 RESULTS

3.1 Ohmic Contact Studies

A perusal of the data in Appendix 2 will reveal that a wide variability of series resistance values were obtained during this program. In fact, in a number of instances, the contacts were very non-ohmic behaving rather like Schottky barriers and presenting much larger effective resistances to the I-V characteristics of the cells. This began to happen frequently, after a few months into the contract period after which a careful study of the problem was initiated.

Figure 8 shows the contact resistance test pad configuration which was used for determining specific contact resistance and sheet resistance values. For our purposes, a set of masks was fabricated producing contact pads approximately 100 μm square. These were processed simultaneously with and precisely in the same manner as our solar cells.

The individual contact pads are defined by the mesa etching, which is the last step, and leaves the contact pads separated by p-layer sections which increase in length from pad to pad -- in our case from 10 μm to 160 μm. The pad-to-pad resistance presented by this configuration has been calculated within the self-consistent approximation that the current density in the ohmic contact falls off exponentially from the leading edge of the contact, that is, from the edge in the direction of current flow in the p-layer. The resultant resistance between two consecutive pads, shown also in Fig. 8, is[5]

$$R_{ij} = 2(\rho_p R_c^{sp}/t_p)^{\frac{1}{2}} W + \rho_p d_{ij}/Wt_p \qquad (2)$$

where ρ_p is the p-layer resistivity, t_p its thickness, W the pad width, and d_{ij} the pad-to-pad separation.

If the resistance between successive pads is measured and plotted as a function of pad separation, Eq. 2 predicts a straight line as shown in Fig. 9. From the intercept, R_{int}, of the line, R_c^{sp} is given from Eq. 2 by

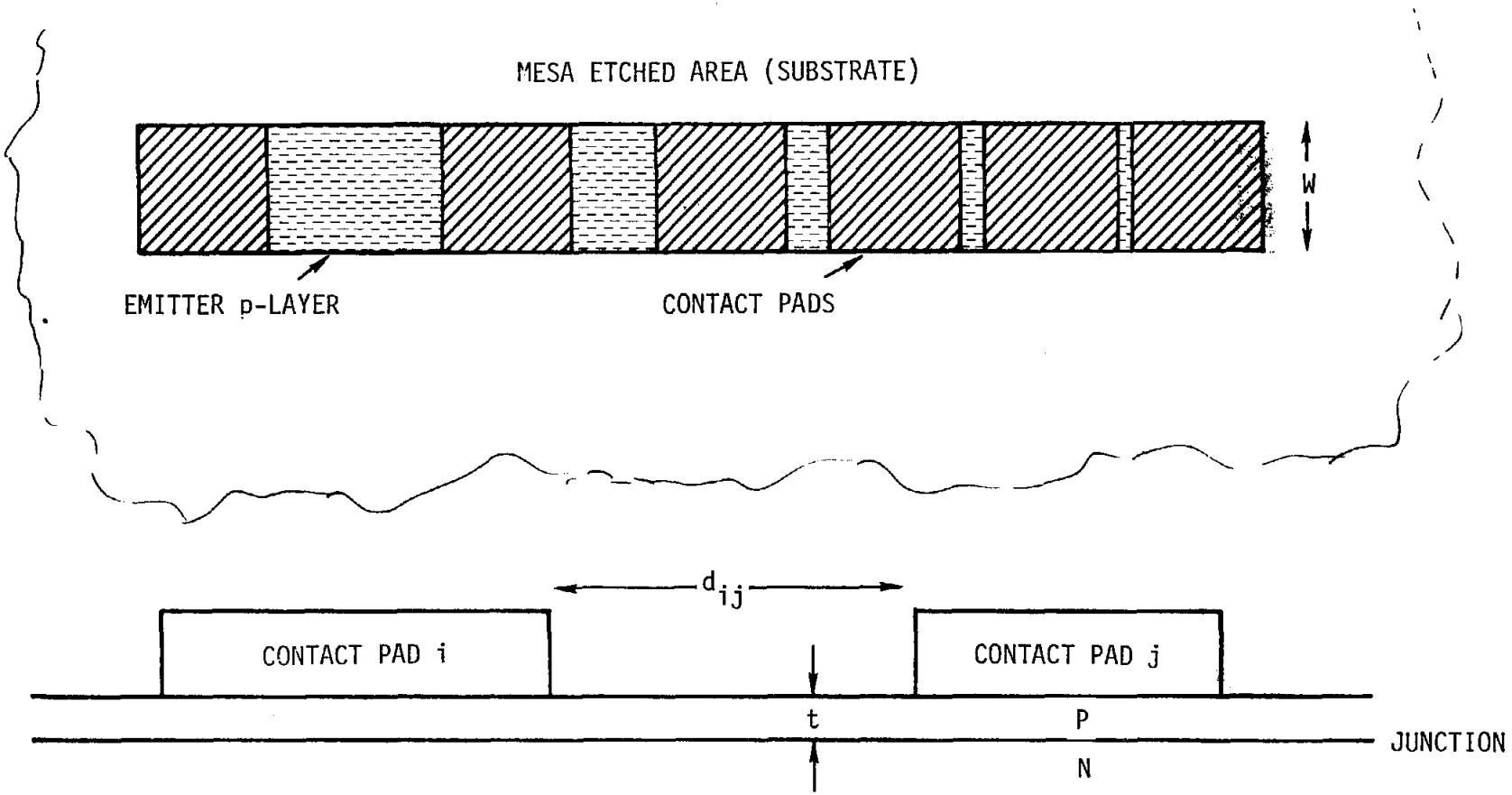

$$R_{ij} = 2(\rho_p R^c_{sp}/t)^{\frac{1}{2}}/W + \rho_p d_{ij}/Wt$$

Fig. 8. Ohmic contact resistance test pad configuration.

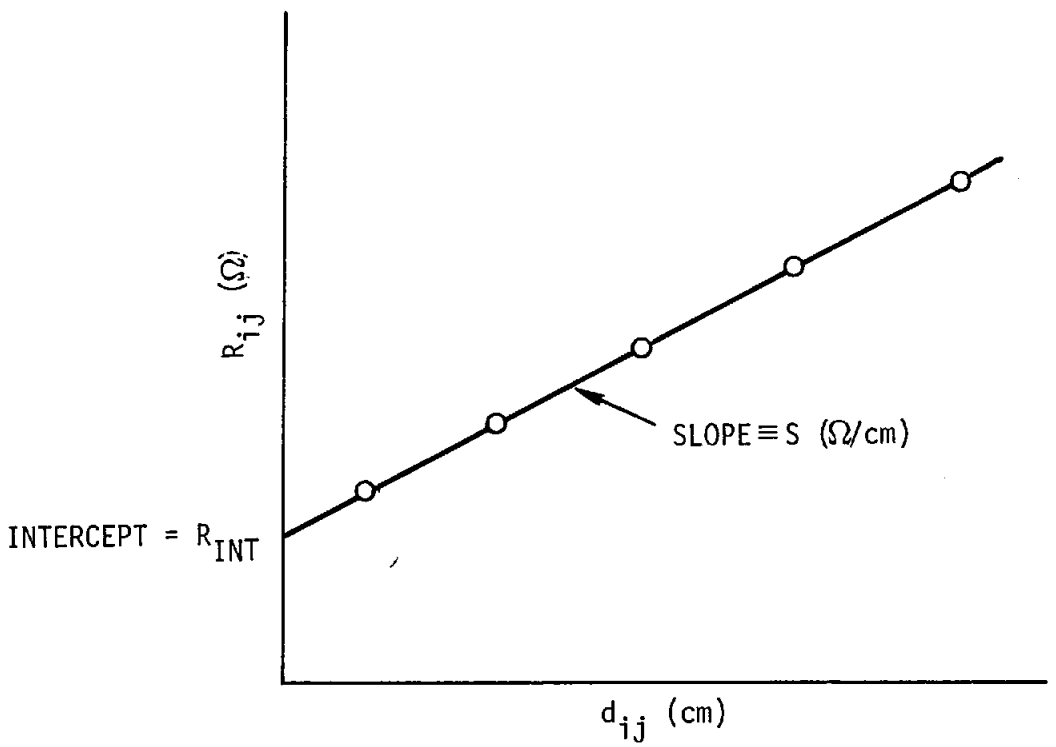

$$R^c_{sp} = R^2_{INT}W/4S; \quad \rho_p = SWt$$

Fig. 9. Ohmic contact test analysis.

$$R^{sp} = R_{int}^2 W/4S \tag{3}$$

where S is the slope of the line. The p-layer resistivity, from Eq. 2, is given by

$$\rho_p = SWt_p. \tag{4}$$

Using the mask set described above and the above analysis, we have examined the ohmic contacts of a large number of samples with a number of variations in the processing and growth. The first significant result was that our "standard" process which had been developed over a period of years, appeared to produce consistently good contacts on LPE growths. This is illustrated in Fig. 10 which indicates a very low specific contact resistance for the LPE layer. The results for two of the MO-CVD growths are shown in Table I and in Figs. 11 and 12. These are representative of successful ohmics on CVD materials. For sample #CS-265-1, the contact resistance contribution to the series resistance would be expected to be ~ 3 mΩ, which combined with the sheet and finger resistance would lead to a total predicted $R_sA \approx 8$ mΩcm^2. This compares reasonably well with the measured value of ~ 11 mΩcm^2. For Mit-274, the predicted value -- taking into account the higher sheet resistance -- is 12 mΩcm^2 compared to a measured value of ~ 9 mΩcm^2. The "measured" values are the values deduced from the slope of the high concentration ($\sim$500X) I-V curve at V_{oc} using the formula[6]

$$R_s = -(\partial V/\partial I)_{V_{oc}} - nkT/qI_{sc} \tag{5}$$

where a value of $n \approx 1$ is assumed unless otherwise measured. These results are typical in the respect that the measured effective series resistance values are very comparable to what would be expected when specific contact resistance and sheet resistance data are available.

The data of Figs. 11 and 12 are, however, by no means representative of the worst or the best ohmic contacts and series resistance obtained during

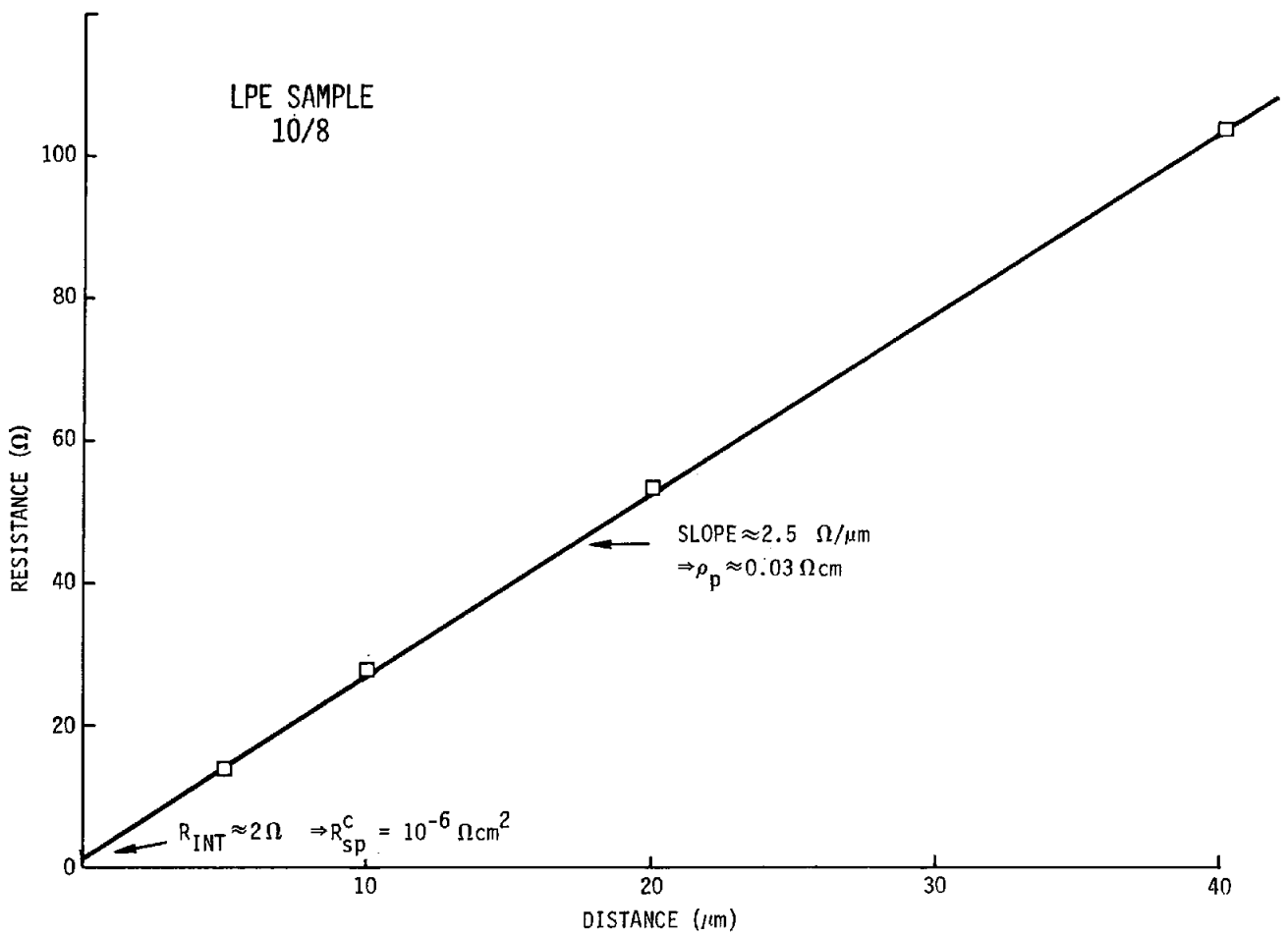

Fig. 10. Measured contact resistance data for LPE cell.

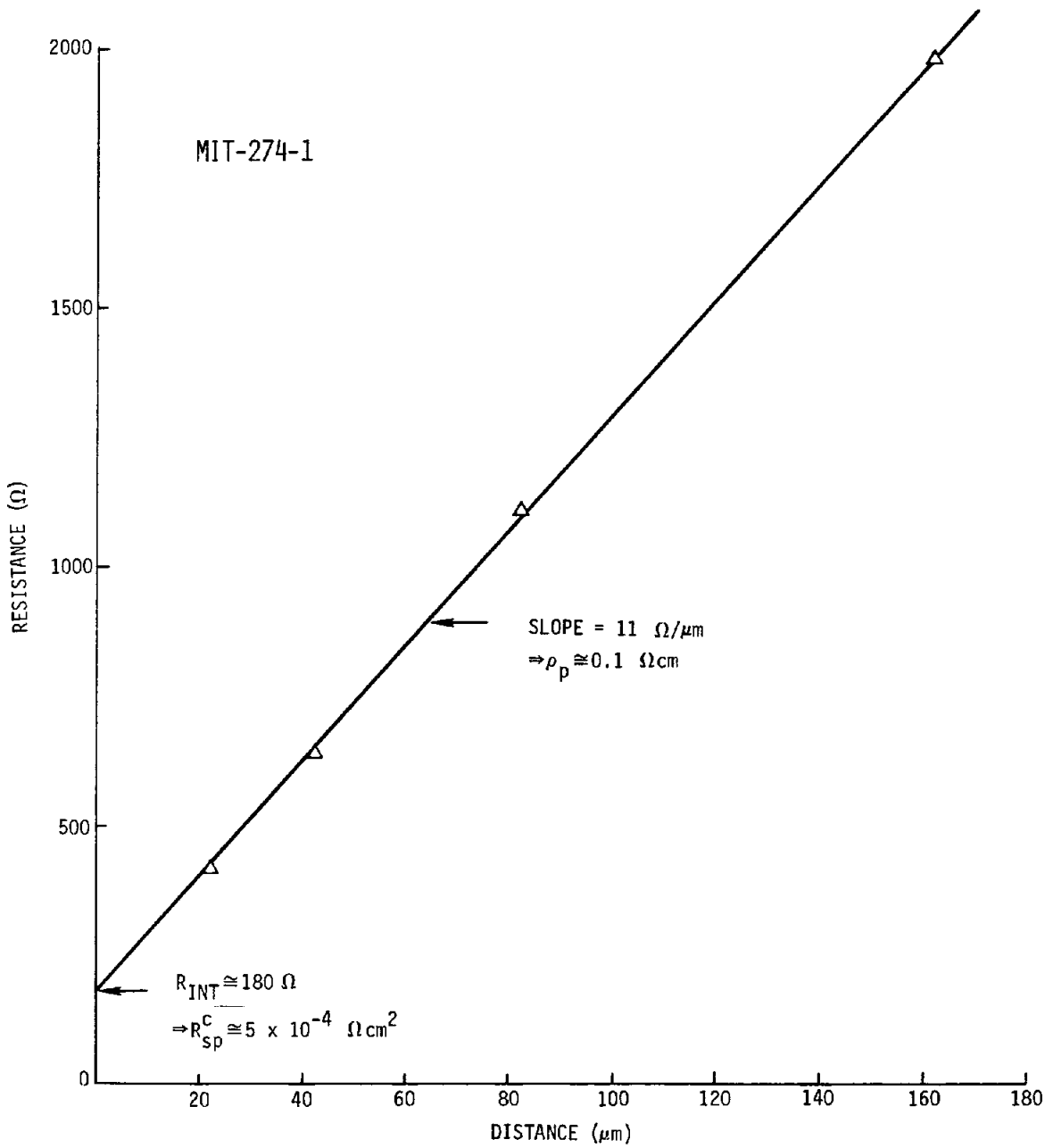

Fig. 11. Measured contact resistance data for MO-CVD cell, MIT-224.

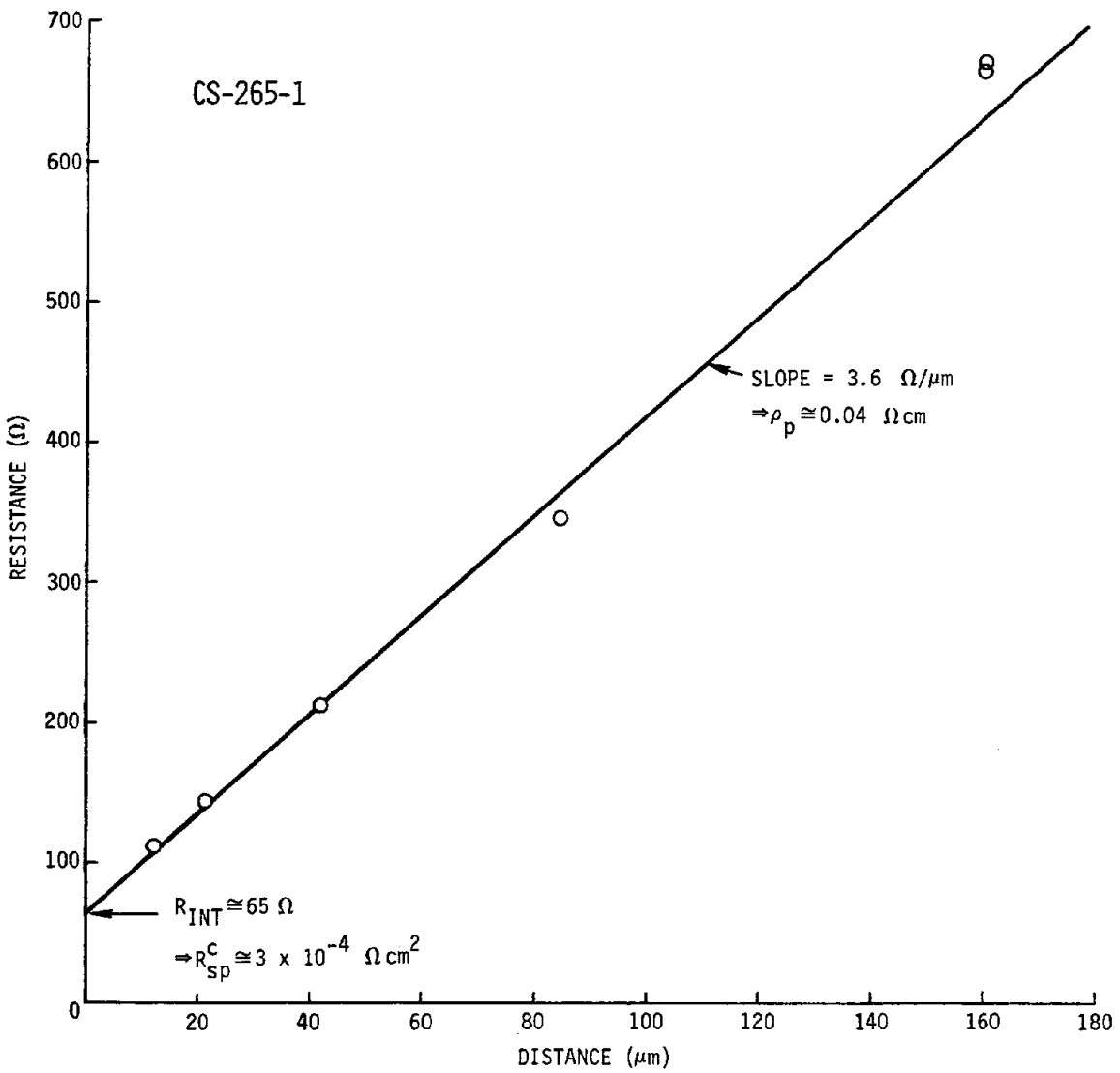

Fig. 12. Measured contact resistance data for MO-CVD cell, CS-265

this study. Of the cells reported in Appendix 2, a number have R_s values significantly less than 5 mΩ, some as small as 2 mΩ or less. Equally significant is the fact that many cells fabricated during this contract had extremely high R_s values, in some instances as high as 100 mΩ or more. Studies of contact resistance in these cases indicated that these contacts were generally non-ohmic and tended to exhibit Schottky barrier-like behavior. After some study, this problem was attributed primarily to contamination in one of the e-beam evaporators. When that evaporator was replaced with a new one, the ohmic contact yield improved dramatically. This is not to say, however, that vacuum and contamination conditions during processing were the sole causes of poor ohmics on our MO-CVD wafers. For example, as a result of the ohmic contact studies, we were led to improve our control of the DEZn and TMA sources in the MO-CVD reactor.

3.2 Auger Analysis of Alloy Contacts

Perhaps the most pertinent result to emerge from the ohmic contact studies was that the process which had provided reliable, very low resistance contacts for LPE layers was apparently much less satisfactory for MO-CVD materials. In drawing this conclusion, it must be remembered that the tests were conducted primarily during a period when problems were being encountered with the growth reactor and with an old e-beam evaporator which was finally replaced with a new one. For this reason, some of the apparent differences between processing MO-CVD wafers and LPE wafers may not be intrinsic. We have one set of experiments, however, which do appear to point to a definite difference. Our standard contact grid process was carried out on an MO-CVD growth and an LPE growth within a few days of each other. The process consists in the deposition by e-beam evaporation of ~25Å of Zn followed by 1500Å of Ag-Mn alloy and finally a 500Å cap layer. This structure is then alloyed in flowing H_2 gas at ~450°C for 1 minute. Contacts thus processed were analyzed by Auger-sputtering chemical profile both prior to and subsequent to the alloying step. The results are shown in Figs. 13 to 15. The salient features appear to be as follows:

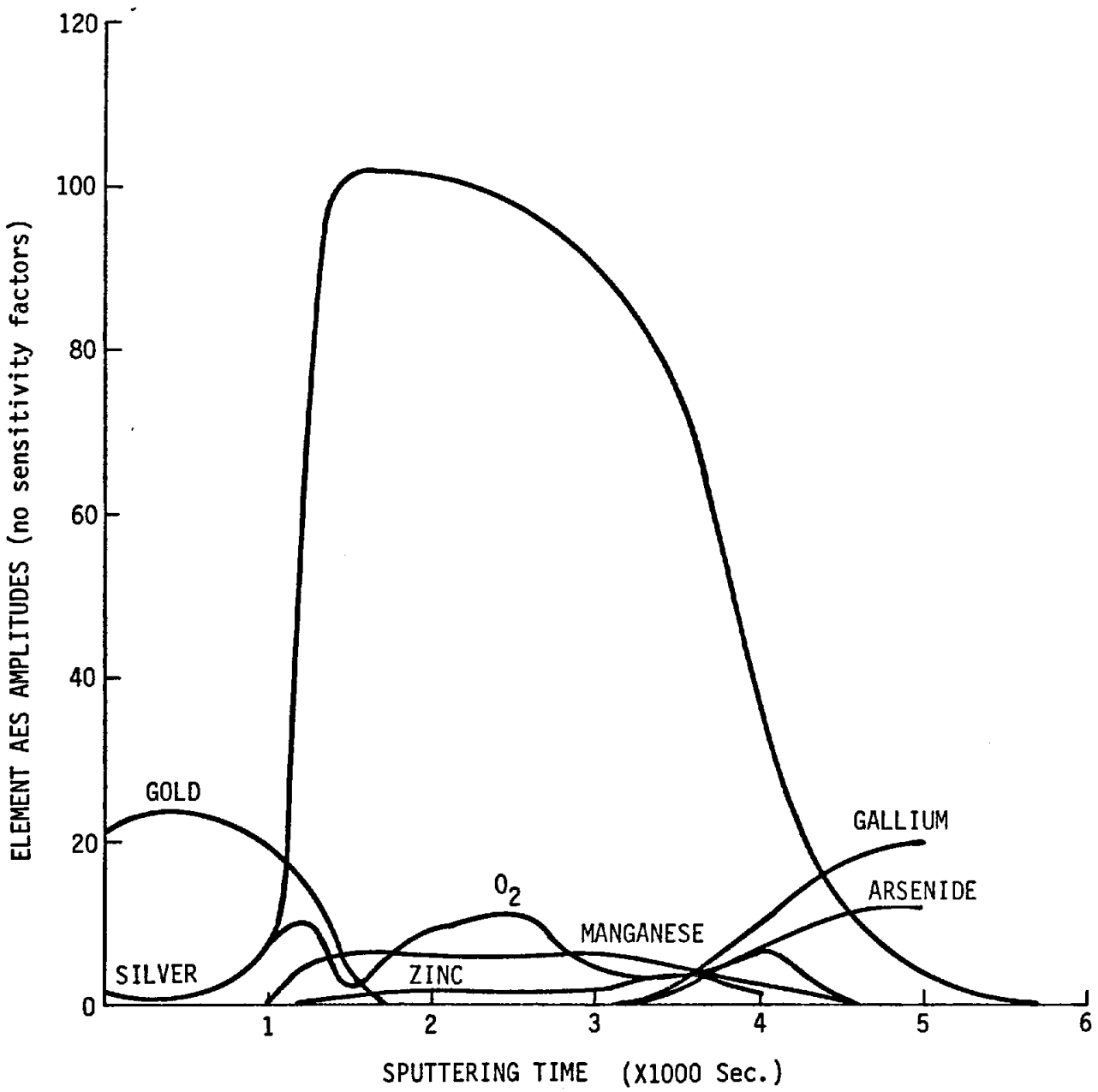

Fig. 13. Typical scanning Auger chemical profile analysis of "good" ohmic contact to an LPE growth AlGaAs/GaAs solar cell structure prior to alloying.

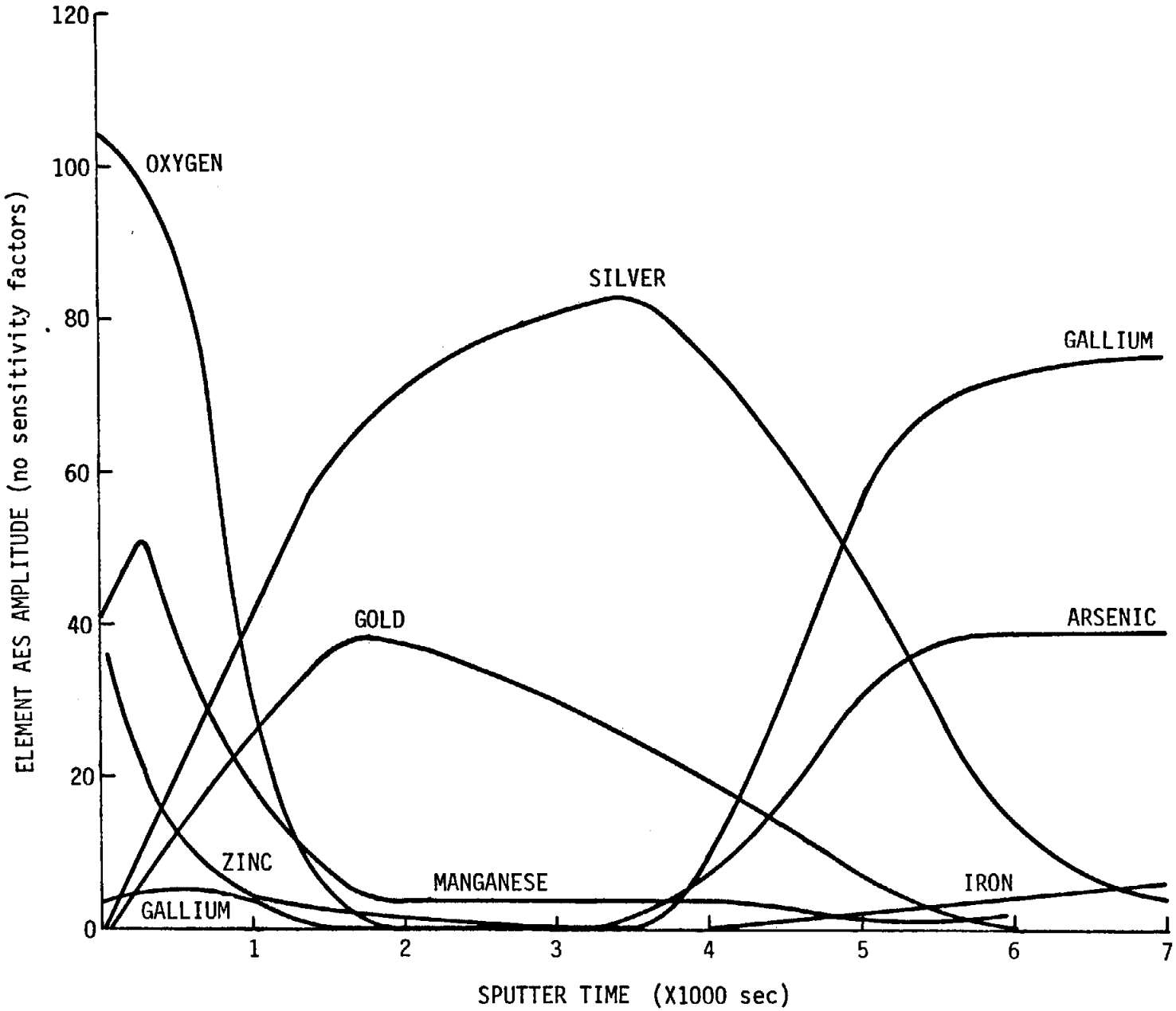

Fig. 14. Typical scanning Auger chemical profile analysis of alloyed "good" ohmic contact to LPE grown AlGaAs/GaAs solar cell structure.

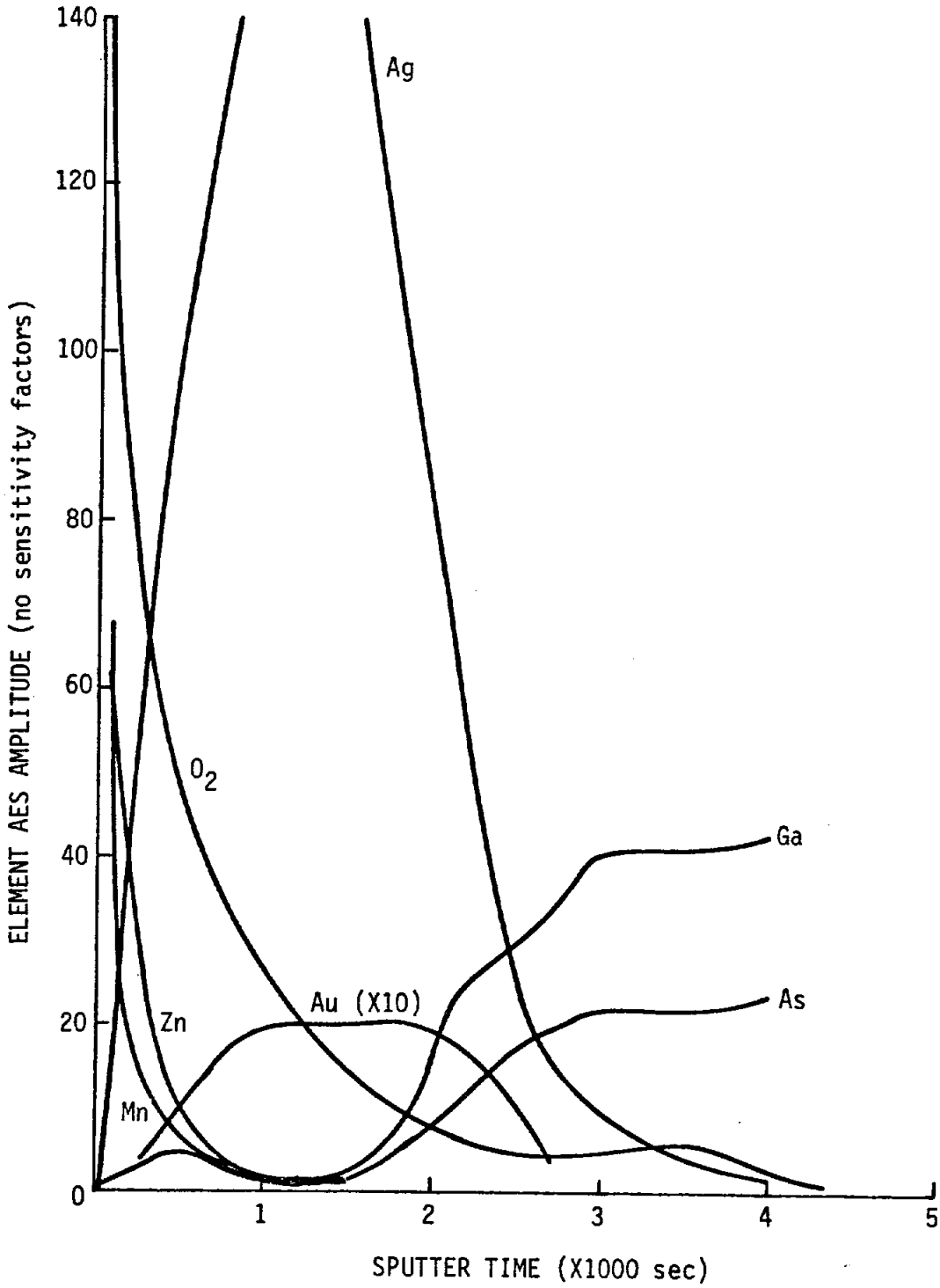

Fig. 15. Typical scanning Auger chemical profile analysis of alloyed "poor" ohmic contact to an MO-CVD grown AlGaAs/GaAs solar cell structure. Contacts of this type behaved as Schottky barrier diodes bucking the cell p-n junction.

In the case of the LPE material (Fig. 14), the p-dopant Mn has been incorporated well into the GaAs surface layer as has the Au and Ag. Some residual O_2 appears to be restricted to surface region in the Ag-Au overlayer. There is no evidence that any appreciable Zn is incorporated in the ohmic contact transition region but the presence of the Mn probably accounts for the high quality of these ohmics on LPE material.

For the MO-CVD materials (Fig. 15), the story is quite different. In this case, it is the oxygen which incorporates well into the GaAs material and the Mn appears to be restricted to the surface region well away from the transition region. This is quite opposite behavior to that on the LPE materials. From these results, it is perhaps not surprising that these contacts behaved like Schottky barriers with a very high differential resistivity at small voltages. Certainly, we now know that the contaminating environment of the old evaporator was contributing to the problem, but this does not explain why the interface chemistry should be so different for the MO-CVD material. We have considered the hypothesis that very slight differences in stoichiometry between the two growth techniques may be partially responsible and we attempted to vary the stoichiometry slightly by varying the AsH_3 source flow rate. This did not result in any improvement in results.

3.3 The Effect of Substrates

In the past, we have frequently fabricated solar cell structures by growing LPE p-layers directly on n^+ GaAs substrates. This procedure in some instances produced cells of very high efficiency. It was clearly established, however, during the "dense array" contract (Sandia #07-7274) that the yield of high efficiency LPE cells was greatly improved when an intervening n-buffer layer was grown prior to the p-layer. These results are not surprising since it is expected that the quality of the epitaxial material should be significantly better than that of the bulk grown substrate. However, the frequent occurrence of poor junction quality (leaky cells and/or low open circuit voltages) and of reduced diffusion lengths suggests that even with buffer layers, unwanted defects are incorporated in the growths.

To explore the hypothesis that the defects may diffuse from the substrate into the grown regions, we have carried out a series of EBIC (electron beam induced current) scans of as-grown layers in cross-section. Examples of these studies are shown in Figs. 16 and 18.

Figure 16 shows the EBIC scan for a cell consisting of a bulk grown n^+ substrate on which a ~10 μm thick p-layer has been grown by LPE. The distance along the cross-section of the device is the abscissa. The current peak occurs at approximately the junction with the substrate to the left and the p-layer to the right. If we make the usual assumption that $(d\,\ell nI/dx)^{-1} = L$, the minority carrier diffusion length, the data indicate that L increases from very small values (~1 μm) near the junction to perhaps 7-8 μm near the surface 10 μm away. This effect is consistent with the assumption that lifetime reducing recombination centers have diffused into the p-layer from the bulk material to the left. Using these diffusion length values and assuming a value of 3000 for the electron mobility in the p-layer, we have calculated the minority carrier lifetimes and obtained the plot shown in Fig. 17. From the slope of the straight line and the growth time, a diffusivity of 2.3×10^{-11} cm^2/sec at 750°C is obtained for the diffused recombination centers*. Similar experiments carried out on layers grown at 900°C yield a value of 5×10^{-9} cm^2/sec. A number of conclusions can be drawn from these results.

First, for a 1 μm p-layer grown at 750°C, we would predict a diffusion length of less than 2 μm -- a result consistent with the low and extremely variable short circuit currents that such cells exhibit. Secondly, if we use the above values to deduce a diffusivity at lower temperatures, we can predict, for example, for growth at 655°C, diffusion lengths of ~5-6 μm.

Accordingly, during the sixth to eighth months of this program, we recalibrated our reactor control systems for growth at 655°C. In a sequence of 8 such growths, the cells produced had, with few exceptions, the highest I_{sc} values seen during this program. Figure 18 shows an EBIC scan of a structure consisting of a 1 μm p-layer on a 10 μm n^+ buffer layer grown on n^+ bulk

* Very nearly the same value is obtained if an infinite source (error function) analysis is used.

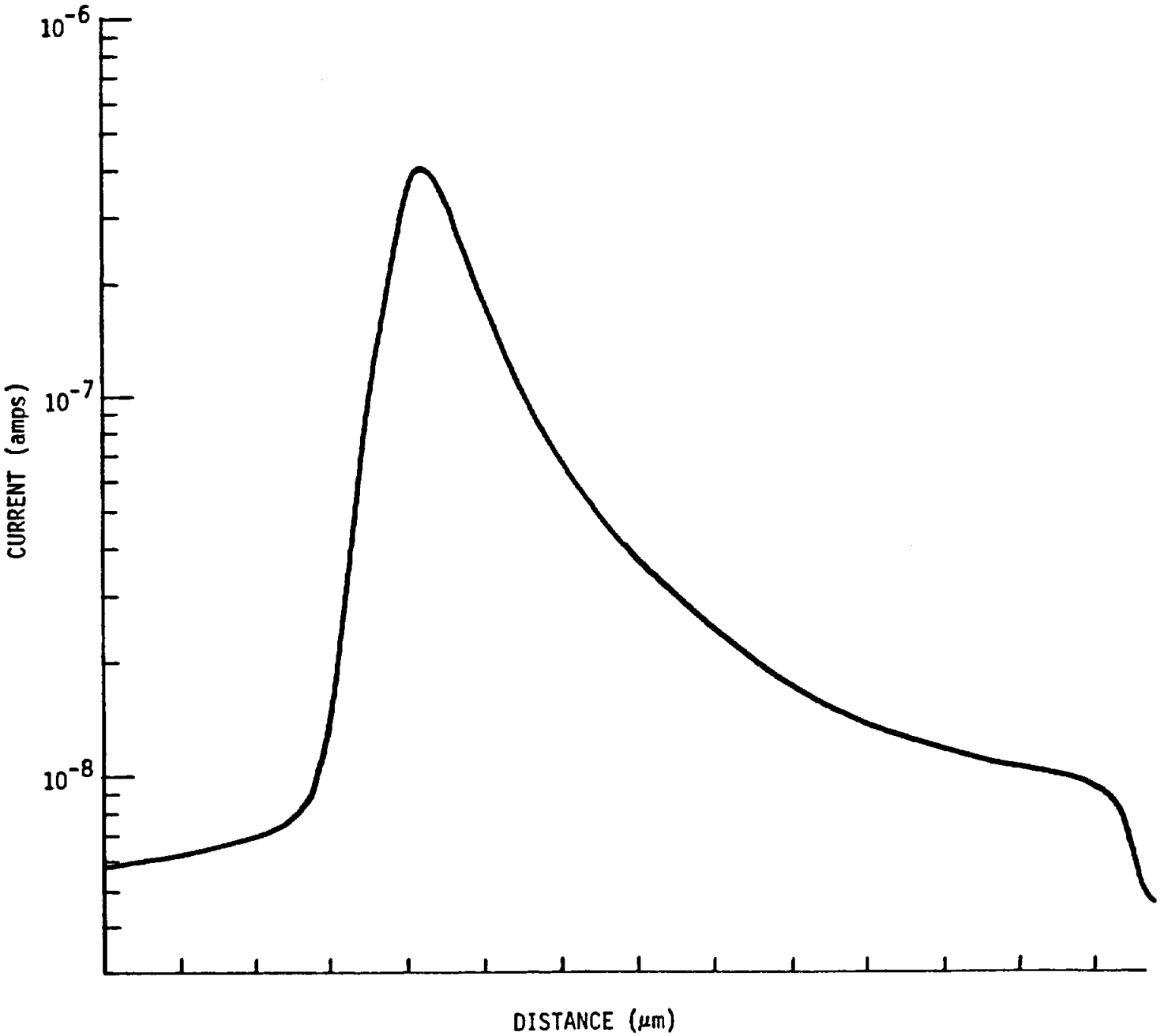

Fig. 16. Electron Beam Induced Current (EBIC) scan for 10 μm LPE p-layer on n^+ bulk substrate. Junction at peak, p-layer to right.

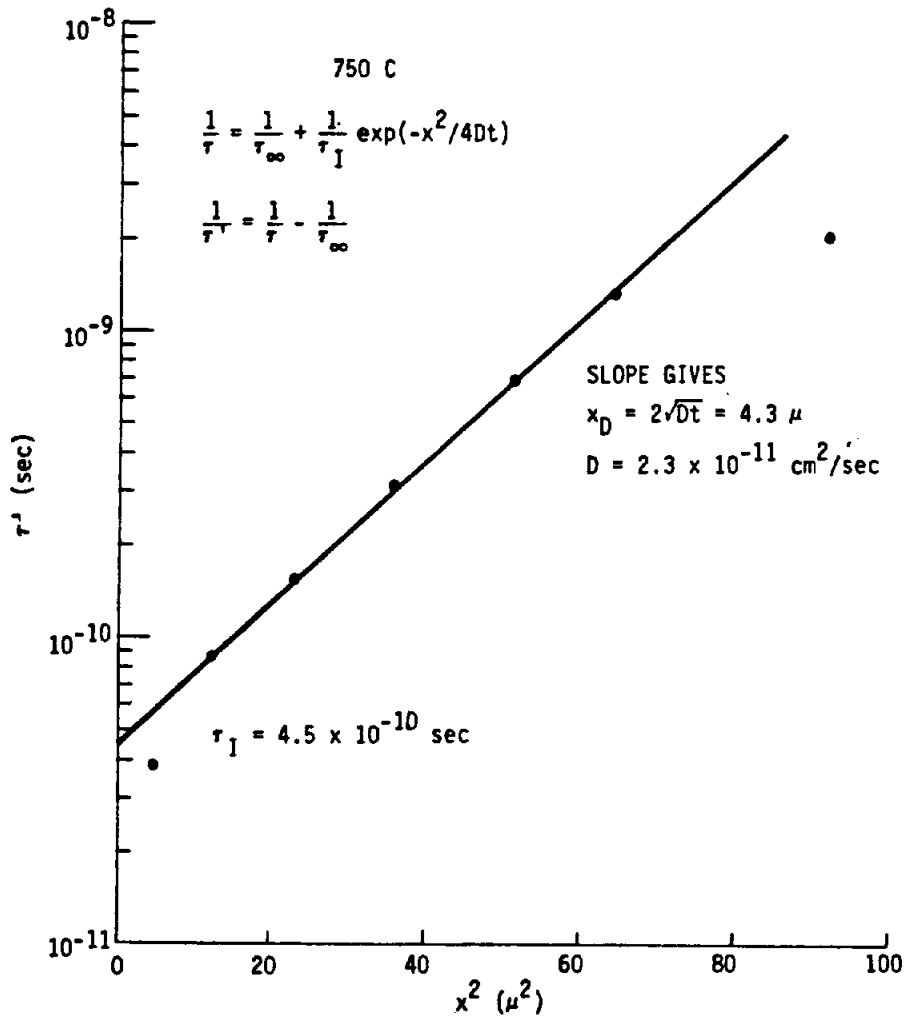

Fig. 17. Log of reciprocal lifetime (from EBIC data) vs. square of distance from junction.

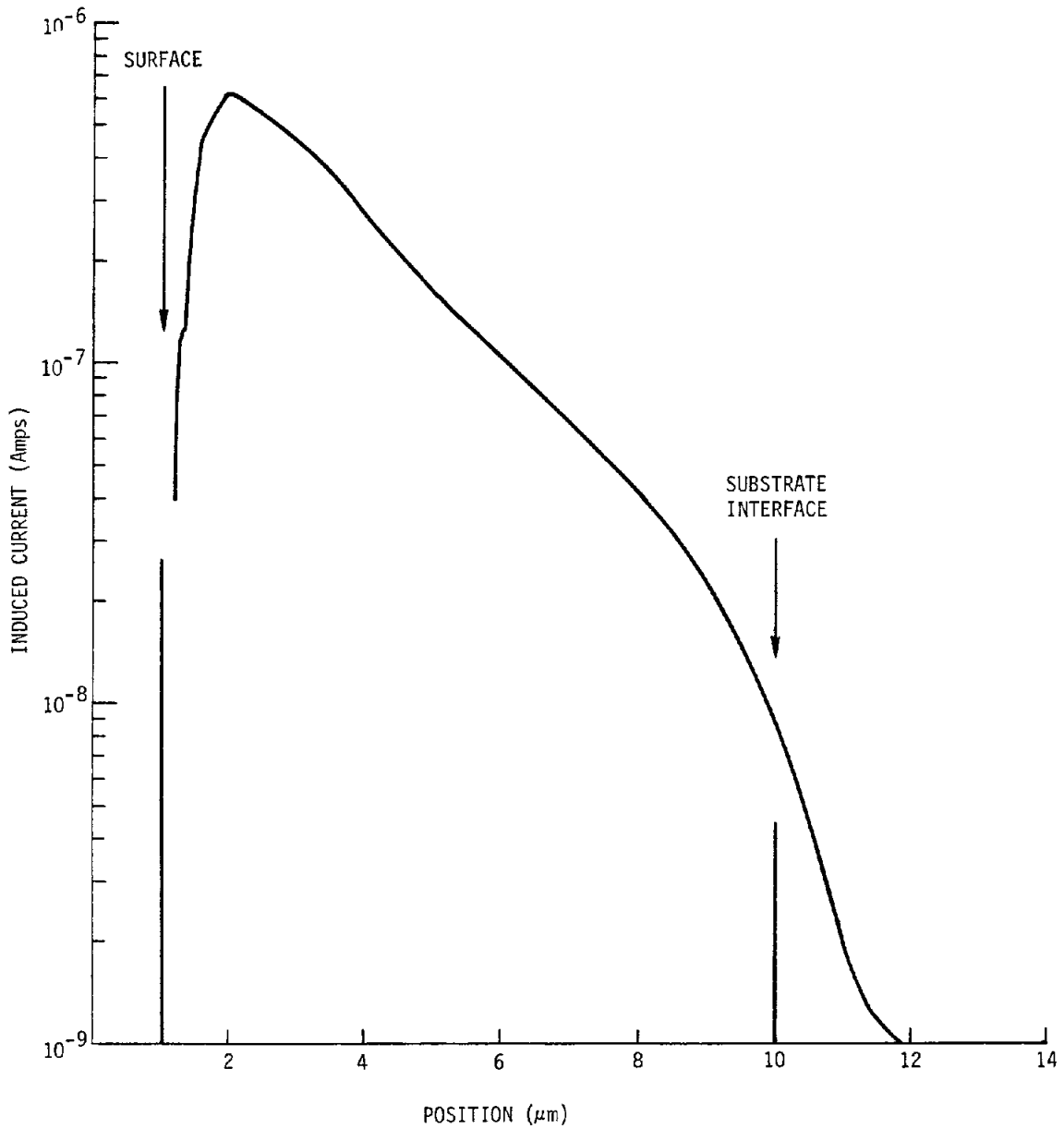

Fig. 18. EBIC scan of 1 μm p-layer on 10 μm n-buffer layer both grown by MO-CVD at 655°C.

material, at 655°C. In this case, the inferred minority carrier diffusion length in the n^+ buffer layer is very nearly constant at about 2 μm all the way across the layer until the beam is within about 1 μm of the substrate, after which L drops sharply. Since a value of 2 μm is very good for holes in n-material, one can conclude that the mean diffusion distance for the recombination centers at 655°C is less than 1 μm. This is in agreement with diffusion analysis such as Fig. 17.

These results suggested that good solar cells could be achieved with buffer layers as thin as 2-3 μm if the growths were done at ~650°C. However, when this was done, it was found that many of the cells grown at the low temperature exhibited undesirably high series resistance values and also a curious leakage behavior which increased with increasing irradiance. The latter effect caused poor fill factors at high concentrations. Whereas the cells would exhibit good 1-SUN fill factors, at high intensities the I-V curves (see Section 3.4) suggested a low shunt resistance type of behavior -- in effect, a "photoconductive shunt". Masking experiments showed that this unusual phenomenon was not an edge effect.

After much analysis, variation of the growth parameters, etc. we abandoned the low growth temperature and began again to grow at 750°C. The very first wafers yielded acceptable R_s values. This apparent immediate restoration of acceptable R_s values seemed to confirm the suspicion that some aspect of the low temperature growth was inimical to good ohmic contacting. Unfortunately, this conclusion has not been convincingly substantiated. One reason for this is that during the same time period, we were discovering the inadequacy of the evaporator and were exploring a number of other possible processing difficulties. Also, during the same time period, we stopped growing on LEC substrates which were known to have high (e.g., 10^5) dislocation densities and began to grow on Laser Diode and Crystal Specialties substrates which had much lower dislocation densities. The initial results showed much better R_s values but lower I_{sc}'s and V_{oc}'s. Also, during the same time period, a problem with doping control was again diagnosed, further complicating the interpretation of the results.

More recently, Mitsubishi substrates, which have the lowest EPD's of all (from 500/cm^2 to 2000/cm^2) were introduced. These substrates seemed to consistently yield poorer I_{sc}'s and electron diffusion lengths than the Crystal Specialties or Laser Diode wafers. This result could mean that defects not associated with dislocations -- e.g., impurity recombination centers -- were the primary diffusant agent and were responsible for the low diffusion lengths in material near the substrate. However, examination of mesa etches on the Mitsubishi cells showed possible evidence of polishing damage, whereas both the Crystal Specialties and Laser Diode substrates which were lapped and polished in our own laboratory, did not. Our own polishing process removes up to 0.01" of material whereas the Mitsubishi cells, which were polished by the supplier, had much less material removed. Thus, remnant polishing damage could possibly be a factor with the Mitsubishi substrates.

The Mitsubishi cells differed from the Laser Diode and Crystal Specialties cells in another way: that is, in their reflectivity. Figures 19 and 20 show typical reflectance spectra for a Mitsubishi cell and a Crystal Specialties cell. Characteristically, at ~900 nm, corresponding to the GaAs band edge, the reflectivity of the Crystal Specialty and Laser Diode cells rises sharply. Evidently, the cells become transparent at wavelengths greater than the bandgap and the increased reflectance is probably due to reflection from the metallized back face of the cell. The Mitsubishi cells, on the other hand, appear to continue to absorb in the long wavelength region -- perhaps due to free carriers. However, the specified dopant densities for these materials are not that different, varying from ~1.0×10^{18} cm^{-3} for the lowest (a Laser Diode wafer) to ~3×10^{18} cm^{-3} for the most highly doped Mitsubishi substrate.

3.4 Photoresponse Studies

Figures 20 and 21 show photoresponse curves for concentrator cell 308-8. The corresponding I-V curves are shown in Figs. 22 and 23. Figure 22 shows the external quantum efficiency and reflectivity as measured on the automatic photoresponse system. From these results, the internal quantum efficiency

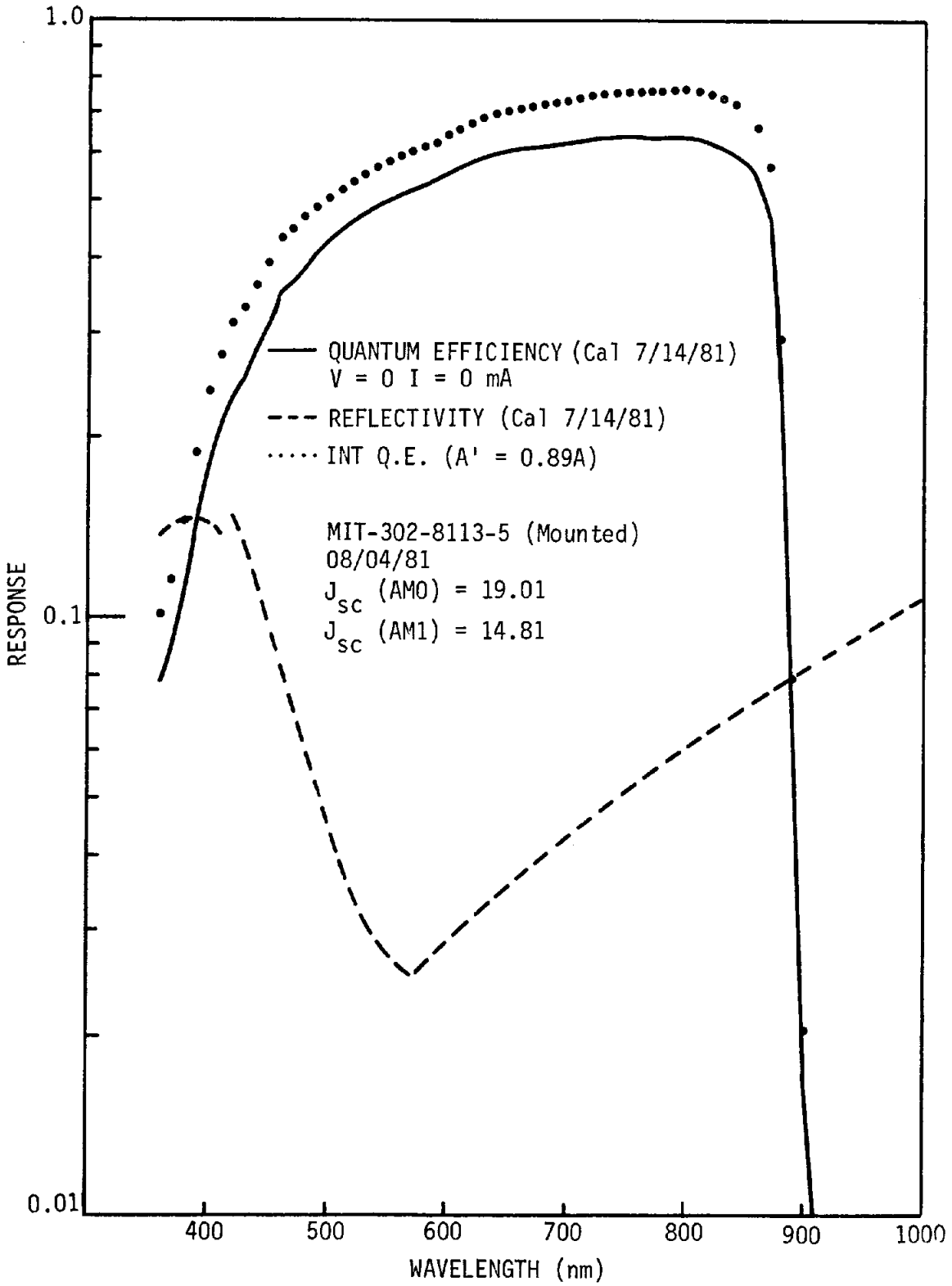

Fig. 19. Photoresponse and reflectivity for typical Mitsubishi substrate, cell PR-308.

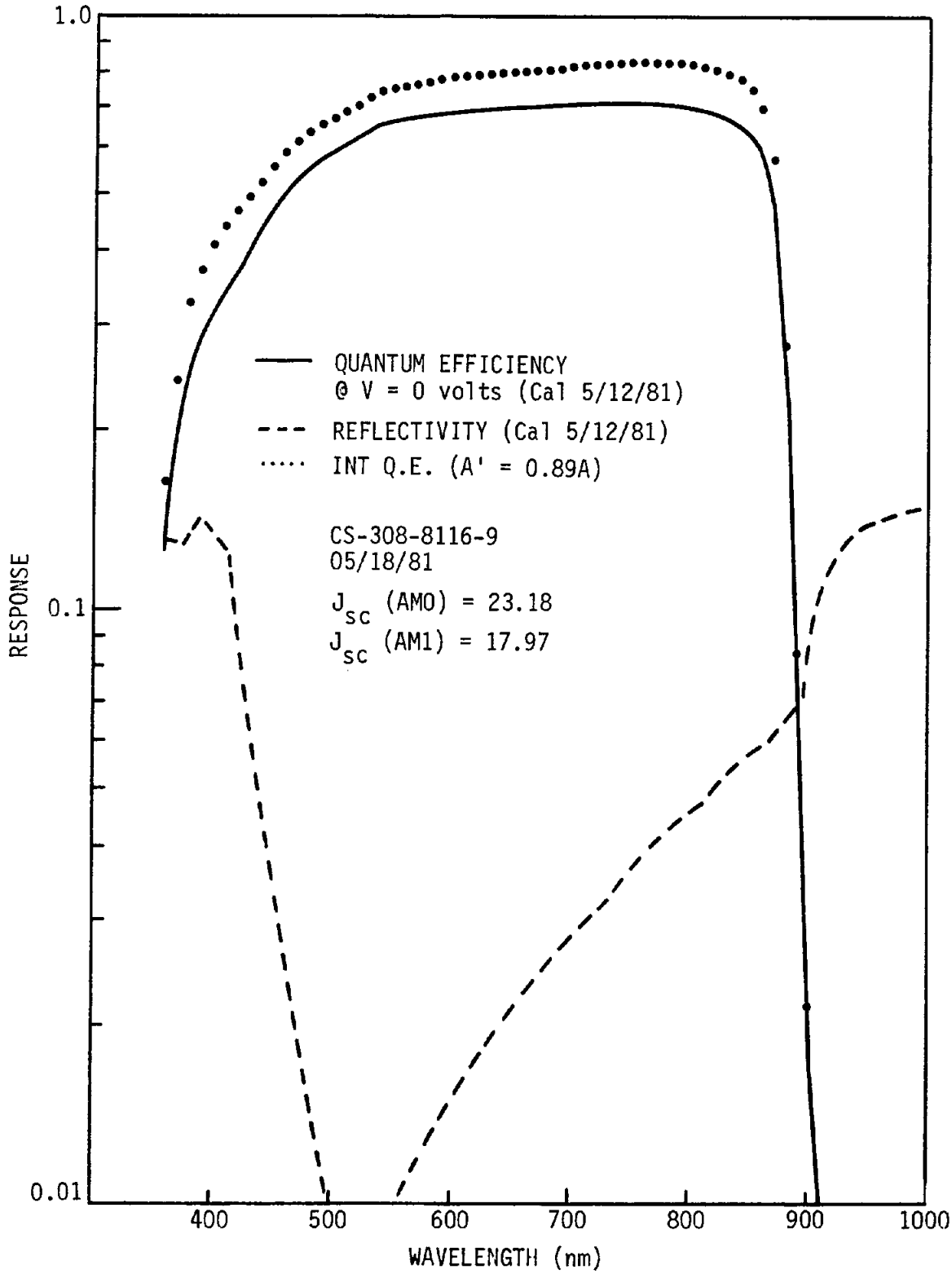

Fig. 20. Photoresponse and reflectivity for Crystal Specialties substrate, Cell 308-8.

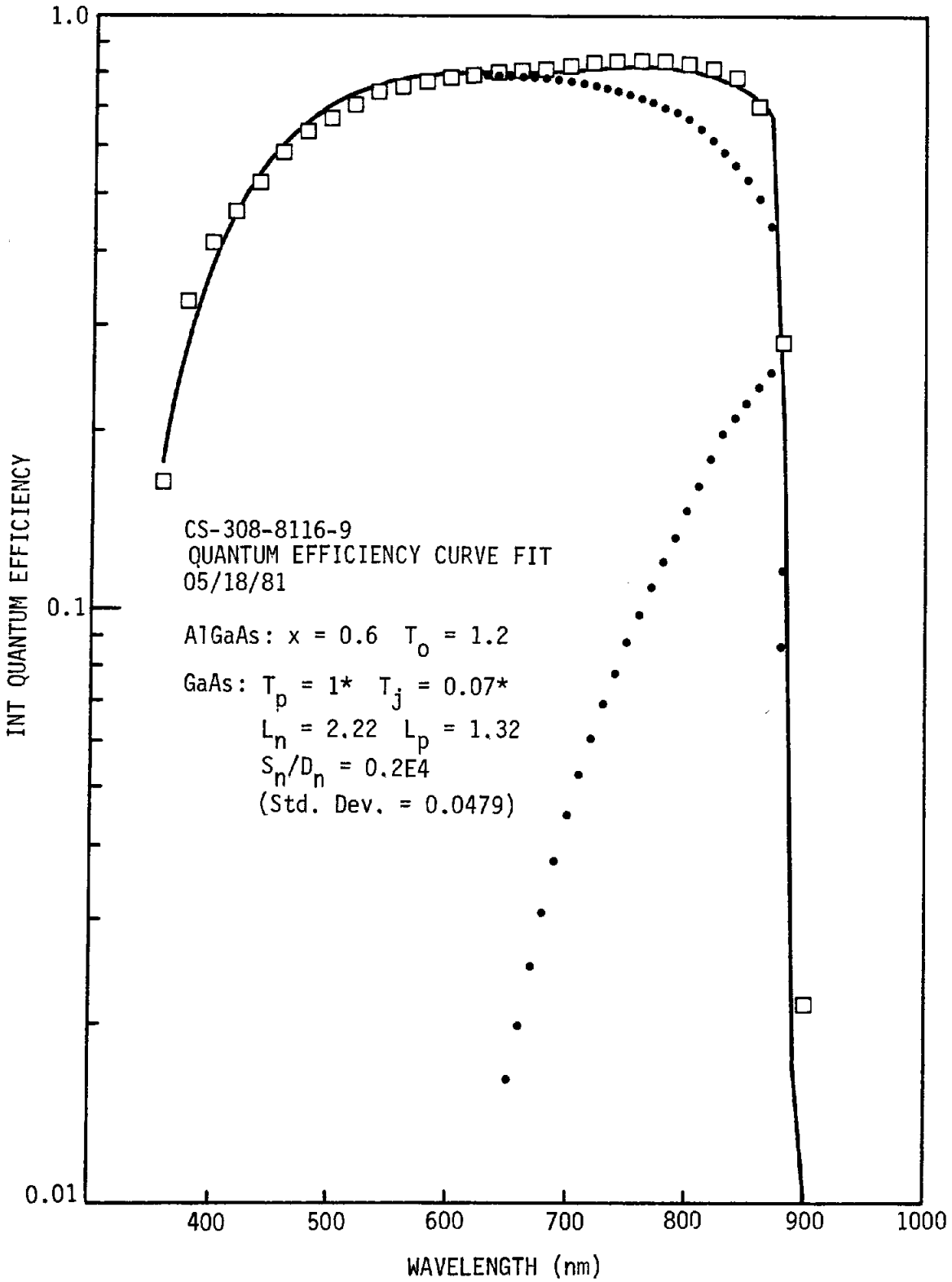

Fig. 21. Computer fit to internal quantum efficiency for cell 308-8.

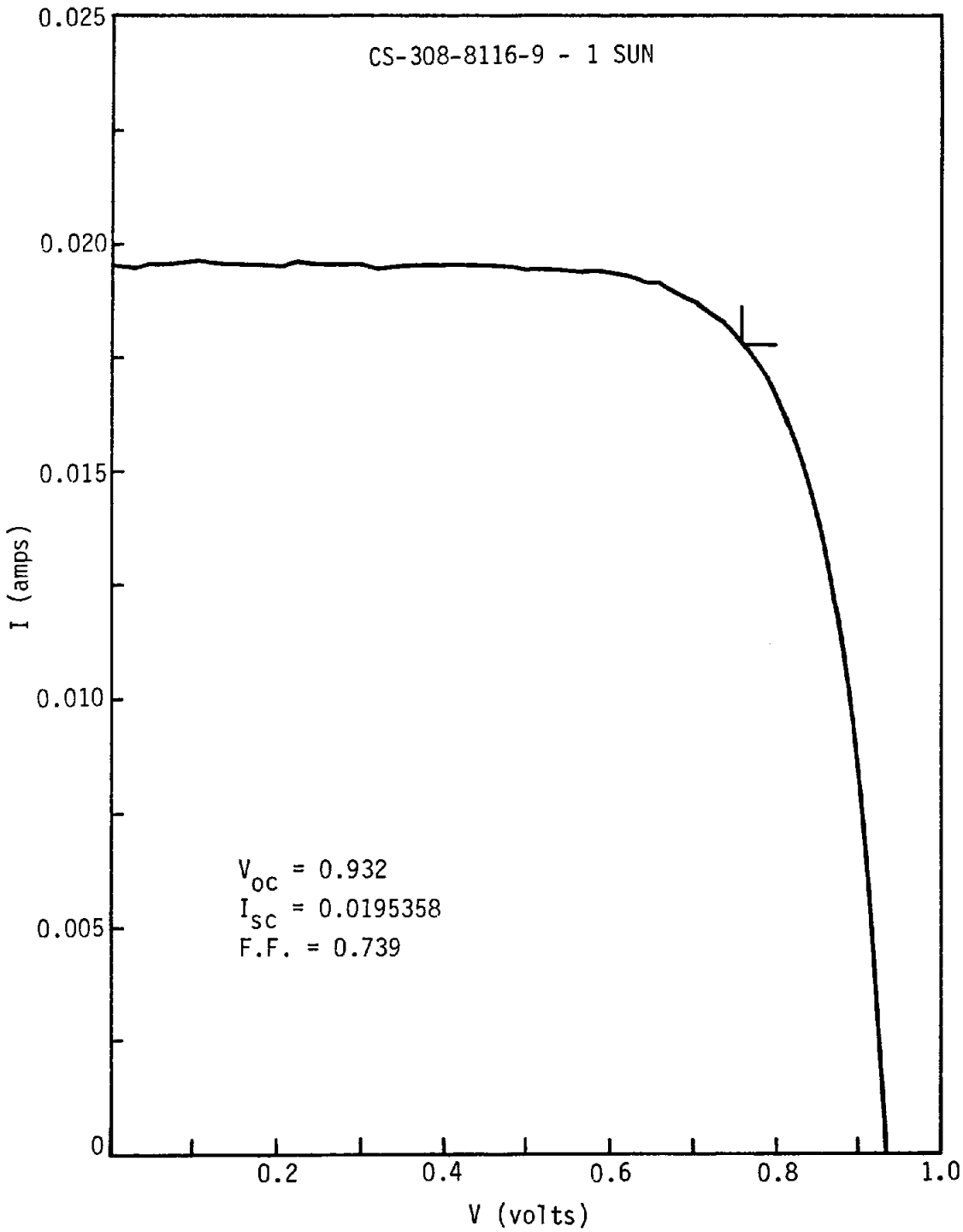

Fig. 22. 1 SUN I-V for cell 308-8.

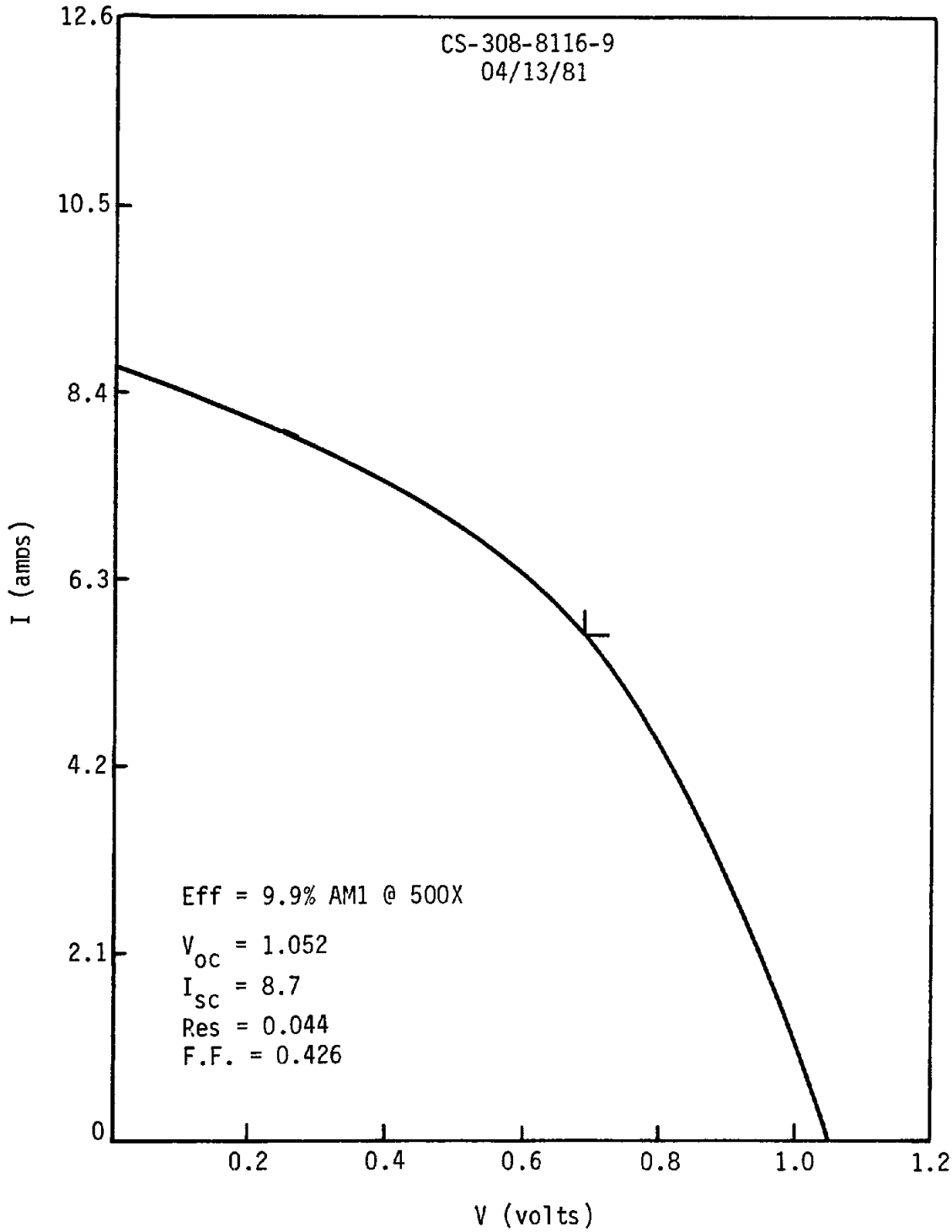

Fig. 23. 500 SUNs I-V for cell 308-8

is automatically calculated and plotted as the dotted curve. It is from the latter curve that diffusion lengths and information on the AlGaAs window length are obtained by curve-fitting. This also is done automatically by the computer. Figure 21 shows the results for cell 308-9. The dotted curves show the contribution of the n-layer(lower right) and p-layer (upper branch). Input values for the computer curve fitting routine are the junction depth, T_j, and the p-layer thickness, T_p. For the example shown, the best fit curve (standard deviation = 0.0479) is obtained for an AlGaAs window layer aluminum content of 0.6, a window layer thickness of 0.12 μm, a p-layer diffusion length of 2.2 μm and an n-layer diffusion length of 1.3 μm. The AlGaAs-GaAs interface recombination parameter S/D is found to be $\sim 2 \times 10^3$ cm^{-1}.

These results provide an explanation for the undesirably low short circuit current exhibited by this cell. We conclude that the primary current limiting factors are (1) the insufficient electron diffusion length (a value $L_n/T_p \sim 3$-4 would be adequate), and (2) the excessively thick AlGaAs layer which reduces the blue response (here a value of 0.05 μm would be much better). This cell exhibits another interesting but deleterious characteristic. This is illustrated by comparing Figs. 22 and 23, the 1 SUN and high concentration I-V curves. Note that at 1 SUN the I-V curve exhibits a reasonable fill factor (IF$\approx$0.74, $\eta \sim 17\%$). However, at 500X, the fill factor has fallen to 0.426 and it appears to be more a consequence of cell leakage than of series resistance though the latter is a factor (probably due to poor ohmic contacting as discussed in the previous section). This diminution in the fill factor, which increases with increasing concentration, does not seem to be explained by any elementary model. It implies a non-linear dependence on the luminance and, for this reason, we have referred to this effect as a "photoconductive shunt" (PCS) effect. Fortunately, it has occurred quite rarely but curiously most commonly during a period when we were experimenting with low temperature ($\sim$650°C) growths (see monthly reports #4-5).

The cells grown at 655°C exhibited very promising and generally superior 1 SUN behaviors, but because of the PCS effect, many of them were unacceptable for concentrator applications. For this reason, we abandoned the

low temperature growth after several weeks of effort.

Figure 24 shows a photoresponse curve fit for a good cell. Note that the critical electron diffusion length is very large and the AlGaAs layer thickness is nearly optimum. This cell exhibited an AM1 1 SUN short circuit current density of 29 mA/cm^2 as measured by a calibrated solar simulator.

Table I is a summary of photoresponse results for a number of cells grown on various substrates. The most noteworthy conclusions that might be drawn from these results are

(1) The lower temperature ($\sim 650°C$) growths consistently yield longer electron diffusion lengths, though the same, evidently, cannot be said for the n-layer hole diffusion length.

(2) A single instance of an exceptional p-layer diffusion length for a growth at 750°C is represented by growth 397 for which especially selected high purity TMGa was used. Growth 405, a matching growth with a commercial grade (Labolac) TMGa yielded a very poor L_n.

(3) The high base diffusion lengths, L_p, appear to occur only with low temperature and/or thick buffer layer growths.

(4) The aluminum content in the AlGaAs layer, as determined by the photoresponse curve fit, is consistently much lower than expected on the basis of calibration runs on thicker growths. This may be an erroneous consequence of the fitting procedure or it could mean that lower Al contents occur in the initial stages of AlGaAs layer growth and thus the average Al content for thin layers is lower than expected.

(5) The Al window layer thickness as indicated by the photoresponse fit is typically substantially greater than the calibrated growth rate value.

While the above conclusions are based on relatively poor statistics, we believe the evidence is convincing that lower temperature growth yields better diffusion lengths and correspondingly higher I_{sc} values. Unfortunately,

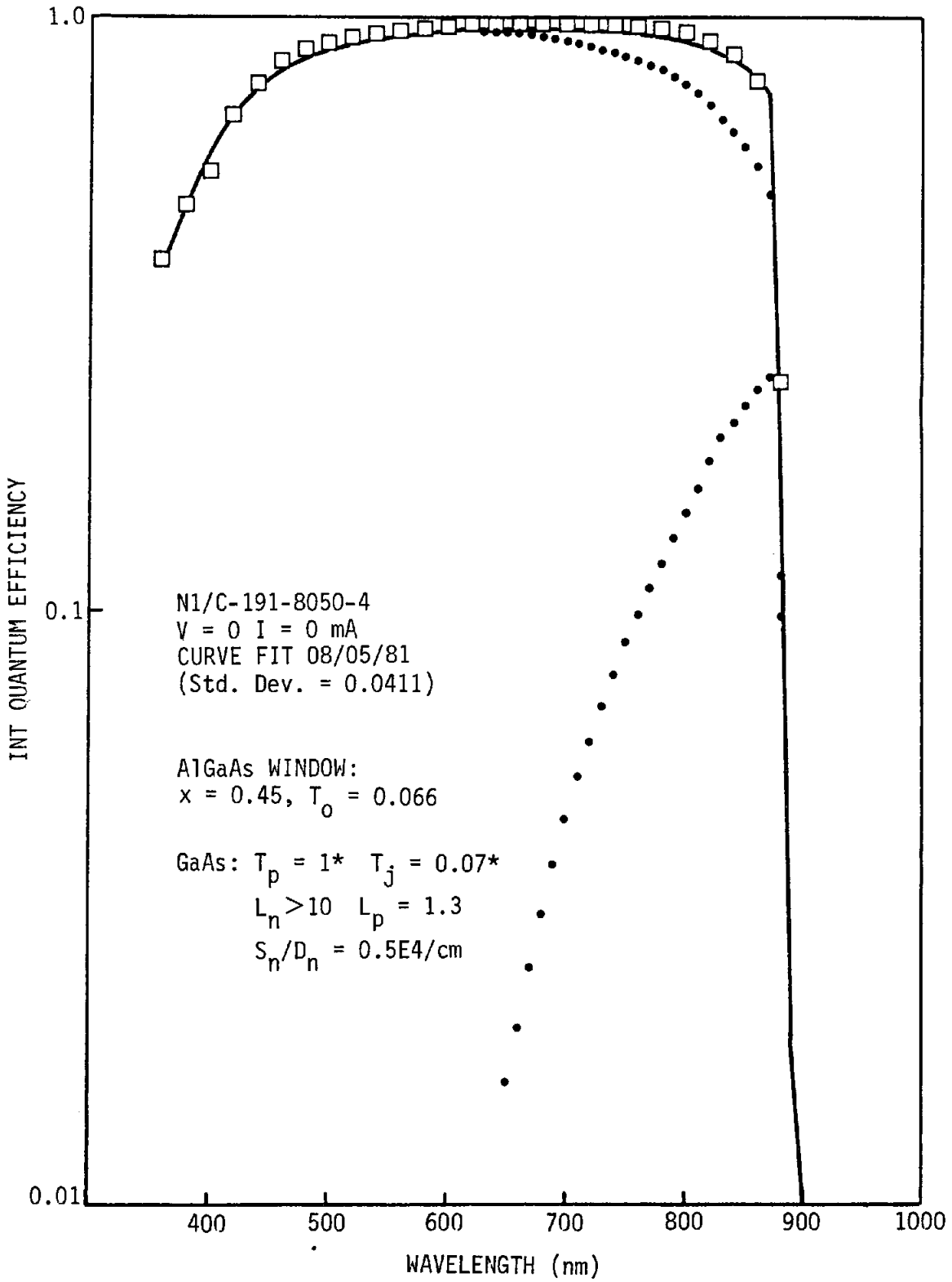

Fig. 24. Photoresponse curve for a high I_{sc} cell (28 mA/cm^2).

TABLE 1: Tabulation of Photoresponse Results for Various MO-CVD Growths

Substrate*	Growth	Growth Temp	Buffer Thickness	L_n (μm)	L_p (μm)	x	AlGaAs Thickness	Remarks
MIT	347	750	10 μm	1.2	2.6	0.4	0.09	
MIT	358	750	6 μm	0.4	1.3	0.4	0.12	
MIT	375	750	12 μm	1.3	0.6	0.4	0.08	
MIT	381	750	12 μm	0.8	2.4	0.4	0.10	
MIT	388	750	6 μm	2.1	1.2	0.4	0.07	
CS	194	675	10 μm	>5	1.1	0.6	0.09	Poor F.F.
CS	364	750	6 μm	2.2	0.5	0.4	0.09	
CS	365	750	6 μm	0.92	0.8	0.4	0.10	
LD	197	660	10 μm	3.1	0.4	0.55	0.06	Poor F.F.
LD	395	655	10 μm	3.3	4.7	0.4	0.07	
LD	396	750	10 μm	1.2	0.2	0.4	0.06	
LD	397	750	10 μm	>5	0.1	0.4	0.07	High purity materials
LD	405	750	10 μm	0.8	0.8	0.4	0.11	Poor materials
N7/M	169	655	10 μm	3.0	0.3	0.4	0.7	Poor F.F.
N1/C	191	655	10 μm	>5	1.3	0.45	0.7	Poor F.F.

* The substrate suppliers are respectively: MIT (Mitsubishi, CS (Crystal Specialties), LD (Laser Diode), N7/M (In-house LEC grown 100-oriented 3" boule), N/1C (In-house LEC grown 111-oriented, 2" boule grown with a corracle)

at present, the low temperature growths appear to yield poor fill factors particularly at high concentrations.

3.5 Discussion

We have presented above evidence from EBIC studies which suggest the possibility that substrate-originated recombination centers act to shorten diffusion lengths and hence cell short circuit currents. Indeed, cells grown at lower temperatures and/or with thick buffer layers appear to have much longer diffusion lengths. If diffusion of unwanted centers from the substrates is a significant problem, one must ask what are these defects and how might they be identified and controlled.

In the past decade, a great deal of evidence has been obtained at many laboratories, including this one, using a variety of techniques (DLTS, PITS[7], photoconductivity, etc.) which indicates that the primary recombination center (in LPE material, at least) is a donor located at 0.73 eV below the conduction band edge. This level originally attributed to oxygen is now believed to involve a vacancy complex. In this connection, we note that the diffusivities obtained from our EBIC studies are very comparable to vacancy diffusivity values. Recently, Wagner et al.[8] have conducted experiments indicating that this same level is responsible for recombination effects in GaAs solar cells. It appears more important than ever to identify this center and to seek ways to reduce its concentration in bulk grown substrate materials.

As a means of obviating the problem of substrate-originated impurities, the evidence presented here suggests that lower temperature growths when combined with thick buffer layers can greatly increase the diffusion lengths and short circuit currents. Unfortunately, this prescription seems to be accompanied frequently, if not regularly, by most undesirable side effects. Firstly, we have found a high percentage of poor p-layer ohmic contacts on these low temperature growths. It is, however, not yet clear whether this is an effect truly related to the lower temperature process or whether it has been caused by other processing failures. Only further work will tell.

The same can be said about the other problem which seems endemic to the low temperature growth -- that is the so-called "photoconductive shunt" -- though in this case the correlation with low temperature growth seems more convincing. Clearly, it would be highly desirable to overcome this problem so that substrates of marginal quality might be admissable.

One possible explanation that has been considered is that a shallow electron trap occurs slightly below the conduction band in these 655°C-grown p-layers. Under intense irradiance, the quasi-Fermi level is shifted above the trap, thus activating minority carrier recombination. Occurring in the interface region between the AlGaAs and GaAs, the effect could be thought of as producing an intensity-dependent interface recombination velocity. These speculations are preliminary to say the least. However, recent work shows that the PCS effect is due to two-dimensional distributed sheet resistance effects in the p-layer. Preliminary results from this work are given in Appendix 1.

Perhaps the most significant conclusion that can be drawn at this point is that the basic cell design is sound and superior. In every instance in which good layer quality and good ohmics have been achieved, these cells exhibit the lowest series resistance and the highest efficiencies in the 500-1000S range that have been reported. I-V and spectral response data for these cells are given in Appendix 2. It seems very probable that as the growth and process steps are further refined and controlled -- and reduced in number where possible -- this concentrator cell design will yield consistently very high efficiency, low resistance loss concentrator cells.

3.6 Critique

With the advantage of hindsight, it is possible to suggest how this program might have been more productive. Rather than focus on shortcomings in the program's concept and execution, it is perhaps most constructive to describe what a better scenario might have been.

The first point which should be made is that the emphasis would not have been on fabricating and delivering numerous high efficiency, large area

devices (for GaAs in the present state-of-the-art, 1 cm^2 is a large area). Rather, the emphasis would be on identifying and solving the materials and processing problems which prevent routine fabrication of high quality devices.

Secondly, it seems clear that a thoroughly evolved "process", i.e., one that would dependably produce good solar cells providing the materials and growths were excellent, could be developed methodically providing a tight control could be maintained on the process facilities. This was certainly not the case during the present program. The process laboratories and equipment were shared by a number of projects and as many as 10-15 researchers who reported to at least three different managers. It seems clear that the evaporator problem, which may well have been the key problem for ohmic contacts, was certainly a factor in this lack of process control.

Thirdly, rather than attempting to produce high efficiency large area devices, very simple small area cells would be fabricated while the process and growth parameters were being refined. There are several reasons for this, but the primary reason is that the use of small area devices greatly diminishes any problems arising from localized major defects, e.g., voids which are prevalent in current GaAs materials technology.

Simultaneously with the development of a dependable process technology using small area devices, the materials, substrates and epi-growths would be characterized and monitored much more thoroughly than was possible in a situation where the emphasis was on delivery of high efficiency devices.

Once either one of the two areas, growth and processing, could be regarded as "tight", the prospects for resolving any remaining problems in the other would be greatly improved. Only when this had been done would the final step, escalate the process technology to large area cells, be undertaken.

REFERENCES

1. R. Sahai, D. D. Edwall and J. S. Harris, Jr., 13th IEEE Photovoltaic Specialists Conference, New York, 1978.
2. R. Sahai, D. D. Edwall and J. S. Harris, Jr., Appl. Phys. Lett. 34, 147 (1979).
3. J. A. Cape, J. R. Oliver, D. L. Miller and M. D. Paul, 15th IEEE Photovoltaic Specialists Conference, 1981, p. 1195.
4. H. J. Hovel and J. M. Woodall, 10th IEEE Photovoltaic Specialists Conference, New York, 1973.
5. H. H. Berger, J. Electrochem. Soc.: Solid State Science and Technology 119, 507 (1972).
6. J. A. Cape and J. R. Oliver, Solar Cells 3, 215 (1981).
7. R. D. Fairman, J. R. Oliver and F. J. Morin, Gallium Arsenide and Related Compounds 1979, Inst. Phys. Conf. Ser. 45, p. 134.
8. E. E. Wagner, D. E. Mars, G. Hom and G. B. Stringfellow, J. Appl. Phys. 51, 5434 (1980).

APPENDIX 1 REFERENCES

9. C. R. Fang and J. R. Hauser, 13th IEEE Photovoltaic Specialists Conference, 1978.
10. R. T. Otterbein and D. L. Evans, 14th IEEE Photovoltaic Specialists Conference, 1980, p. 574.
11. M. O. Watanabe et al., Japanese Journal of Appl. Phys. 20, L429 (1981).

APPENDIX 1

ANALYSIS OF THE PHOTOCONDUCTIVE SHUNT EFFECT

APPENDIX 1

We have done an extensive investigation into the so-called "photoconductive shunt" (PCS) problem which has been evident at concentration with some cells. This problem causes a severe degradation in fill factor and is characterized by a significant non-zero slope of the I-V curve near I_{sc} and a sub-linear I_{sc} vs. concentration relationship above several hundred SUNs. It has appeared at random intervals during our MO-CVD growth development program, particularly with 655°C growths -- ironically, cells which have shown the best internal quantum efficiency to date.

One area we have investigated is the possibility of an intensity-dependent recombination velocity at the AlGaAs/GaAs interface. The presence of a large number of interface states will cause significant band-bending near the interface and effectively trap any short-wavelength-generated minority carriers (the so-called "dead zone" problem). One compelling argument against this effect is that identical I-V curves can be obtained with long wavelength (>700 nm) illumination for a given value of I_{sc} on cells which show the PCS effect. Furthermore, interfacial recombination, in general, tends to decrease rather than increase with higher illumination.

Another possibility is the effect of a distributed sheet resistance network. This problem has been considered by others[9-10], but, in general, has not been examined in detail for high illumination levels. We have recently developed computer programs which evaluate the dark and light I-V characteristics of the distributed network shown in Fig. A-1. The network is evaluated in terms of the variable I_{PH}*R(sheet), where I_{PH} is the total photogenerated current and R(sheet) is the total p-layer series resistance. The model takes into account the variation in the p-layer depletion width W(depl) with voltage, the shunting effect of the diode region underneath the contact metallization, and, in the case of radial cells, the variation of network parameters as a function of radius, i.e., a two-dimensional network.

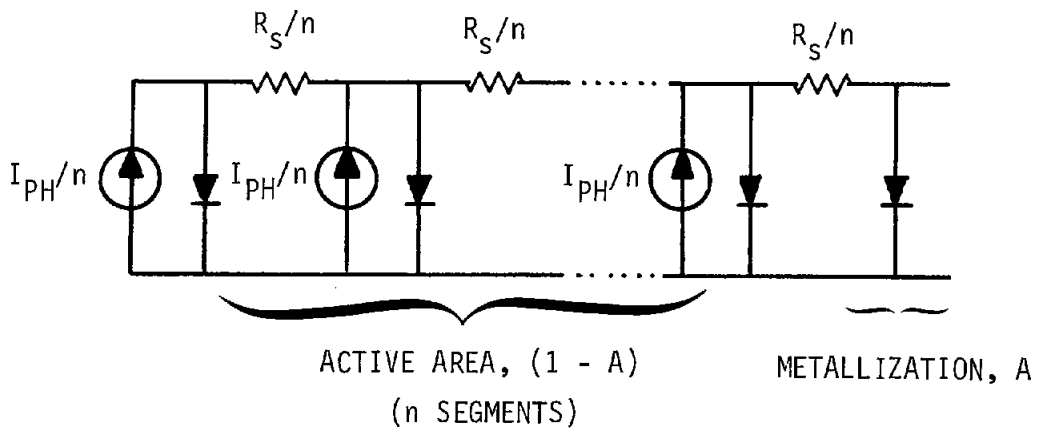

Fig. A-1 Distributed sheet resistance model.

Consider now the N7/M-186 growth. The cells from this 655°C growth all show the "PCS" effect at >200 SUNs while at the same time showing excellent photoresponse, high internal quantum efficiency, and excellent 1 SUN I-V curves with fill factors >0.8. Capacitance measurements around 0 volts indicate a large depletion width of 0.275 μm. Assuming an n-layer doping of $N_D = 4 \times 10^{17}$ cm^{-3}, this gives a p-layer doping of $N_A = 2.85 \times 10^{16}$ cm^{-3} and W(depl) = 0.256 μm, with a resistivity $\rho = 0.55\,\Omega$-cm. The I_{PH}*R(sheet) product is given by

$$I_{PH}*R(\text{sheet}) = (\rho\ell^2/4w_p)J_{PH}$$

where W_p = W(total) - W(depl), J_{PH} is the photogenerated current per unit active surface area, and ℓ is the average finger separation. In this example, for an average finger spacing of 92 μm less 10% metal obscuration, ℓ = 83 μm. I_{PH} is the maximum current at moderate reverse bias (-1 to -2 volts). For 750 SUNs illumination, I_{PH} = 15.65 amps for an active surface area of 0.71 cm^2. Hence, for W_p = 1.0 μm, we have

$$I_{PH}*R(\text{sheet}) = 2.10 \text{ v @ } 750X$$

$$W(\text{depl})/W = 0.204$$

Computed curves for 750X, 500X and 250X illumination are compared with measured normalized I-V curves for cell N7/M-186-3 in Fig. A-2. Best fit was achieved with W(depl)/W = 0.2 and I_{PH}*R(sheet) = 1.9 at 750X, in excellent agreement with the computed values given above. These curves were computed with a metallization coverage of 42% (finger + bus) and a min/max finger separation ratio of 0.5 appropriate to our radial cell contact geometry. The computed equivalent R(sheet), derived from the slope of the I-V curve at V = V_{oc}, is 6.0 mΩ in good agreement with the measured value of 4.8 mΩ. It should be noted that the equivalent sheet resistance is a factor of 20 smaller than the actual value for R(sheet).

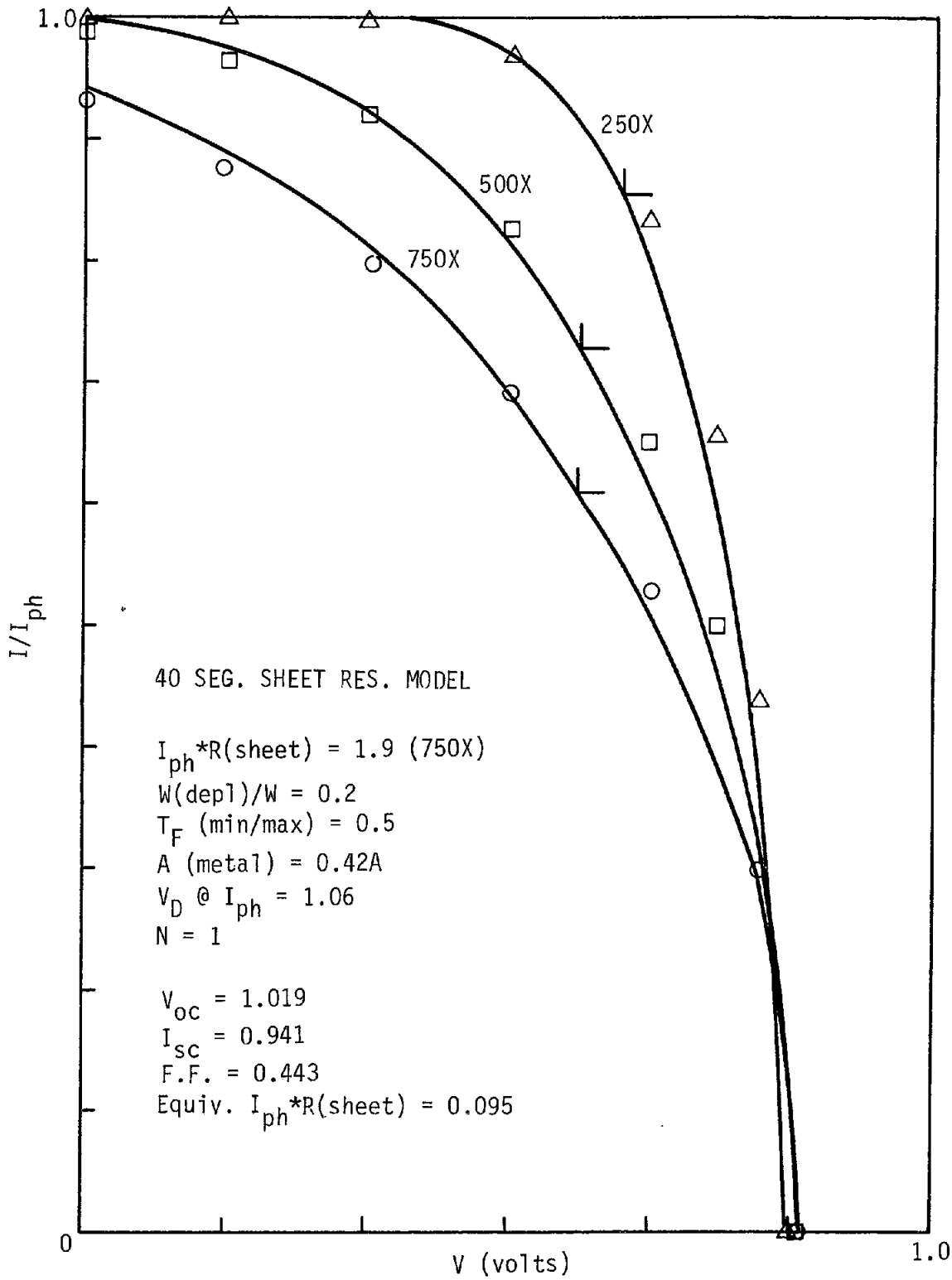

Fig. A-2 Computed 750X, 500X and 250X light I-V curves for a radial concentrator cell based on the model in Fig. A-1. Data points are for cell N7/M-186-3.

Figure A-3 shows the computed and measured normalized dark I-V characteristics for the same cell. It can be seen that the effect of the series sheet resistance is essentially undetectable. Also shown is the "apparent" junction current ($1 - I/I_{PH}$) taken from the 750X light I-V curve of Fig. A-2 (dotted curve). The latter deviates substantially from the actual dark I-V characteristic, and looks very much like cell shunt leakage -- hence the name "photoconductive shunt". We see, however, that the effect is actually due to the distributed two-dimensional nature of current generation and sheet resistance in the active region.

The excellent agreement between computed and measured curves for a number of different cells shows that the "PCS" effect is in fact due to high p-layer resistance. This effect cannot be modeled by a single lumped resistance element; in fact, the "soft" I-V characteristic is a trademark of distributed sheet resistance problems, except for possible variations in collection efficiency with depletion region width for cells with low diffusion lengths. A more detailed analysis and discussion of distributed sheet resistance effects will be published in a paper currently in progress.

It is evident that many of the problems associated with 655°C growths can be attributed to low p-layer doping, in spite of frequent calibration runs with the MO-CVD reactor. Low doping not only causes high p-layer resistance, it can create problems with adequate contacting as well. The low apparent series resistance obtained from the slope of the I-V curve near V_{OC} had led us to believe during the course of this program that sheet resistance problems were not the cause of low fill factors at 500 SUNs concentration. The above example shows, however, that a low apparent series resistance value is not inconsistent with large distributed sheet resistance. The fact that sheet resistance problems occurred more frequently with 655°C growths is reflected in the steeper TMZn flow rate vs. doping level calibration for our MO-CVD reactor. We are presently investigating modification to our TMZn source which will improve this situation.

We still feel that low temperature MO-CVD growths have the potential for highest solar cell efficiency as long as the p-layer doping can be adequately

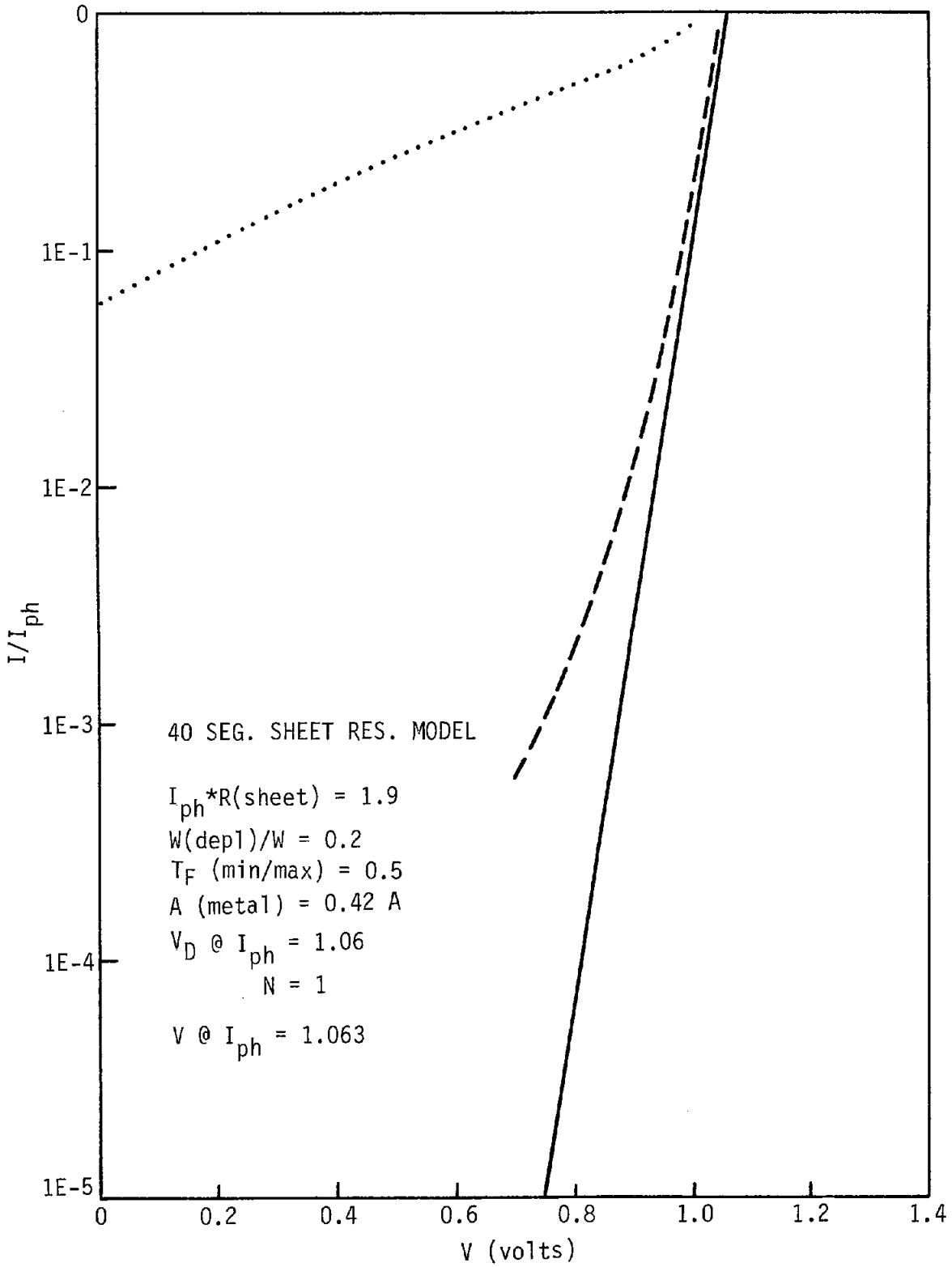

Fig. A-3 Computed dark I-V curves. Dashed curve is actual measured data. Dotted curve is equivalent junction current derived from 750X data of Fig. A-2.

controlled. In the example given here, a p-layer doping of $N_A \sim 3\text{-}5 \times 10^{17}$ cm^{-3} would have been sufficient to minimize sheet resistance problems at 500 SUNs, in addition to providing a corresponding improvement in V_{oc}. The excellent quantum efficiency for 655°C growths is reflected by recent work[11] which shows the the dominant recombination center EL2 located 0.73 eV below the conduction band ($\sim$0.8 eV apparent activation energy) decreases in concentration with lower MO-CVD growth temperatures. This level directly influences minority carrier lifetime, and therefore diffusion length. Its lower concentration with 655°C growths is consistent with our observation of excellent diffusion lengths from EBIC and photoresponse measurements, and diode quality factors which are near unity (Fig. A-3).

APPENDIX 2

CELL DATA FOR DELIVERED CELLS

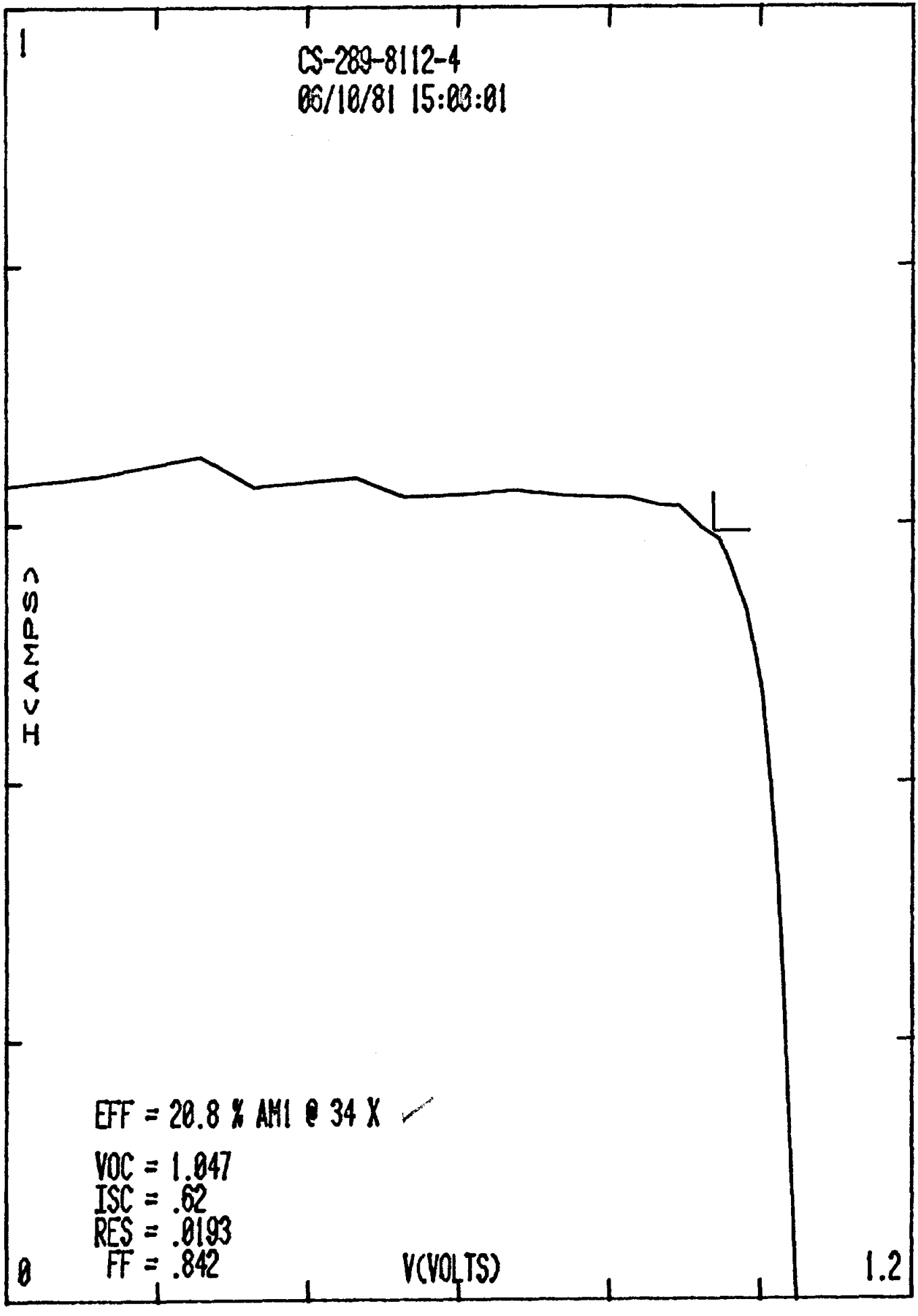
1
CS-289-8112-4
06/10/81 15:03:01
I(AMPS)
EFF = 20.8 % AM1 @ 34 X
VOC = 1.047
ISC = .62
RES = .0193
FF = .842
0
V(VOLTS)
1.2

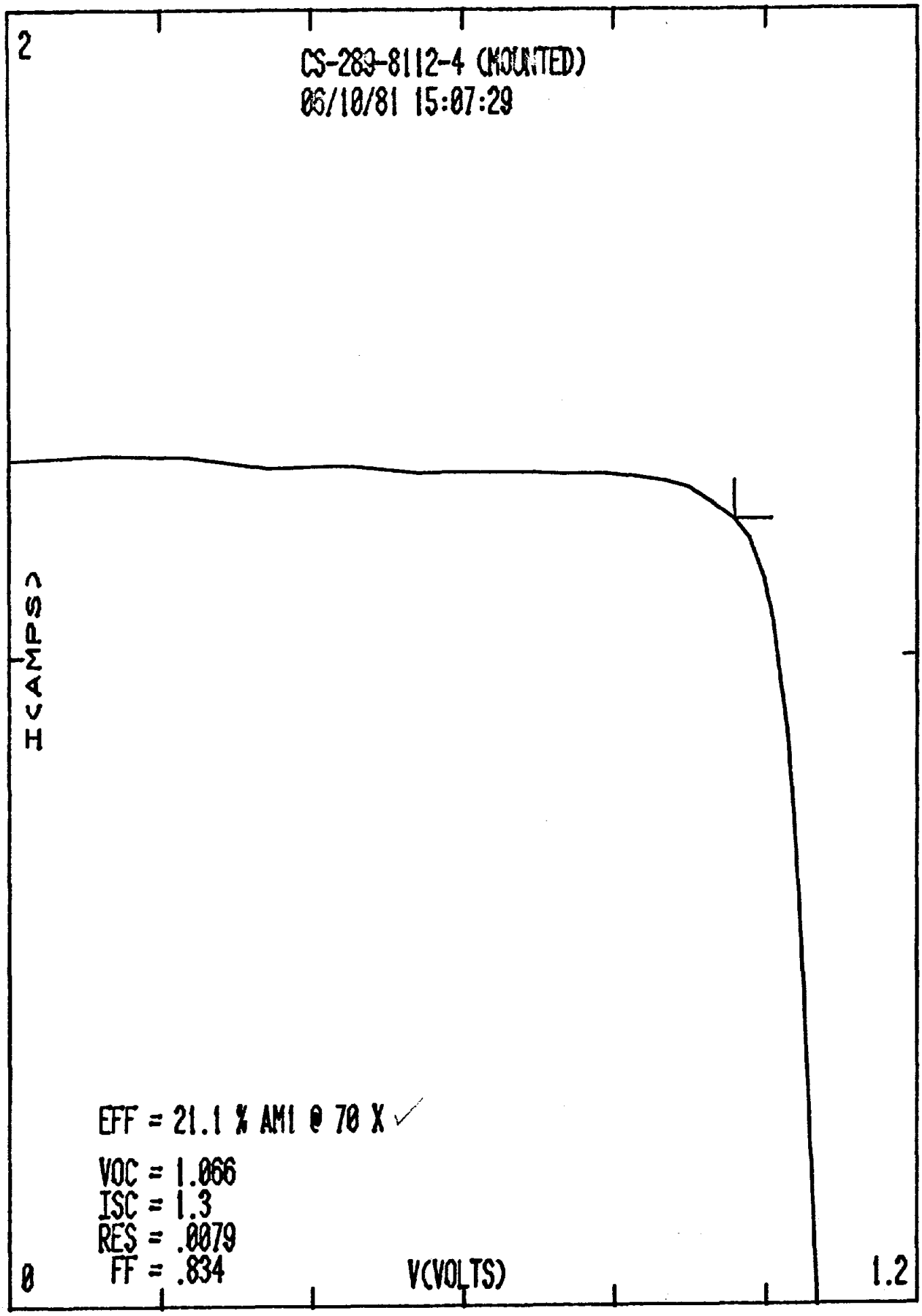
2
CS-289-8112-4 (MOUNTED)
06/10/81 15:07:29
I(AMPS)
EFF = 21.1 % AM1 @ 70 X
VOC = 1.066
ISC = 1.3
RES = .0079
FF = .834
0
V(VOLTS)
1.2

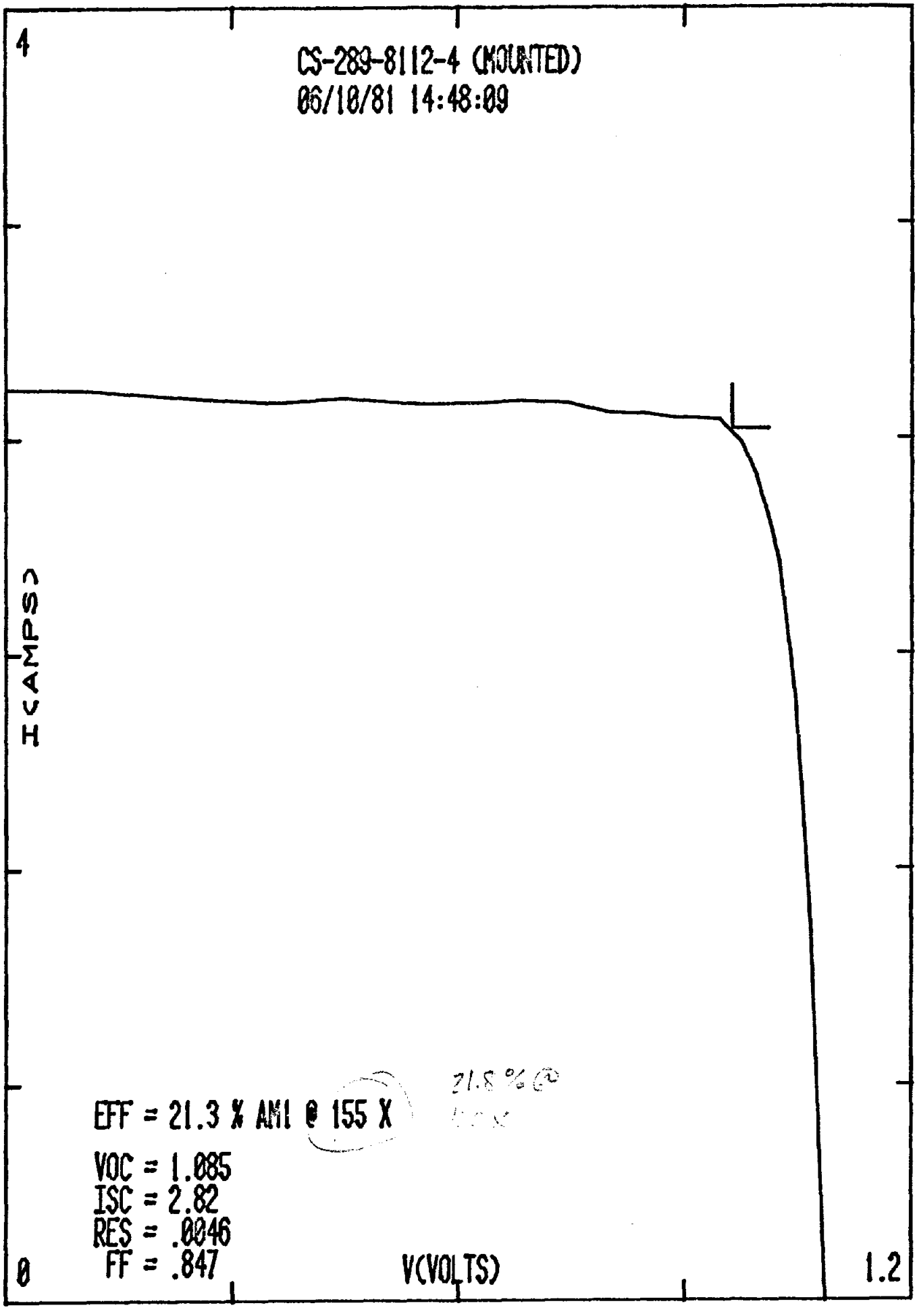
4
CS-289-8112-4 (MOUNTED)
06/10/81 14:48:09
I(AMPS)
EFF = 21.3 % AM1 @ 155 X
21.8 % @
VOC = 1.085
ISC = 2.82
RES = .0046
FF = .847
0
V(VOLTS)
1.2

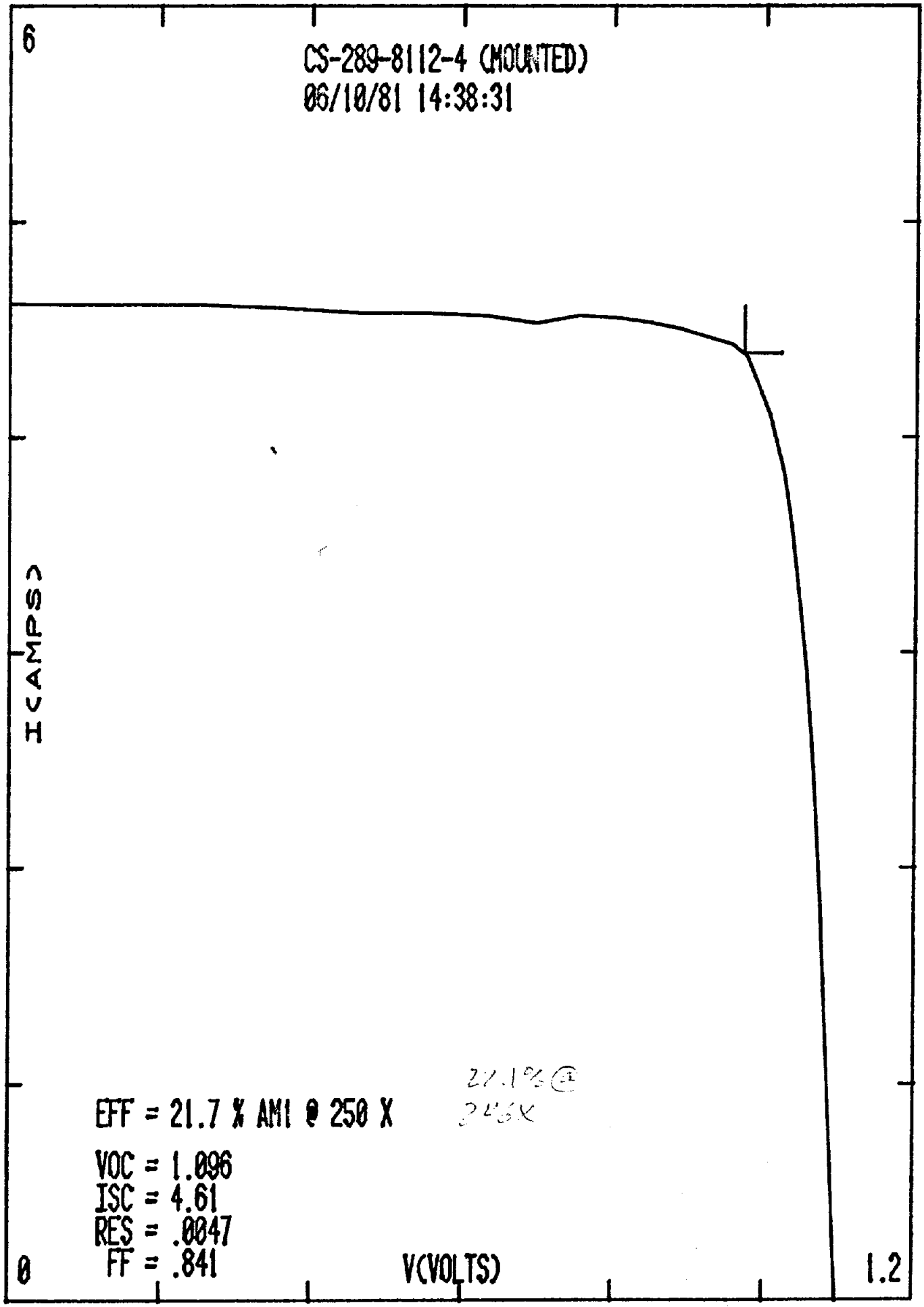
6
CS-289-8112-4 (MOUNTED)
06/10/81 14:38:31
I(AMPS)
EFF = 21.7 % AM1 @ 250 X
VOC = 1.096
ISC = 4.61
RES = .0047
FF = .841
0
V(VOLTS)
1.2

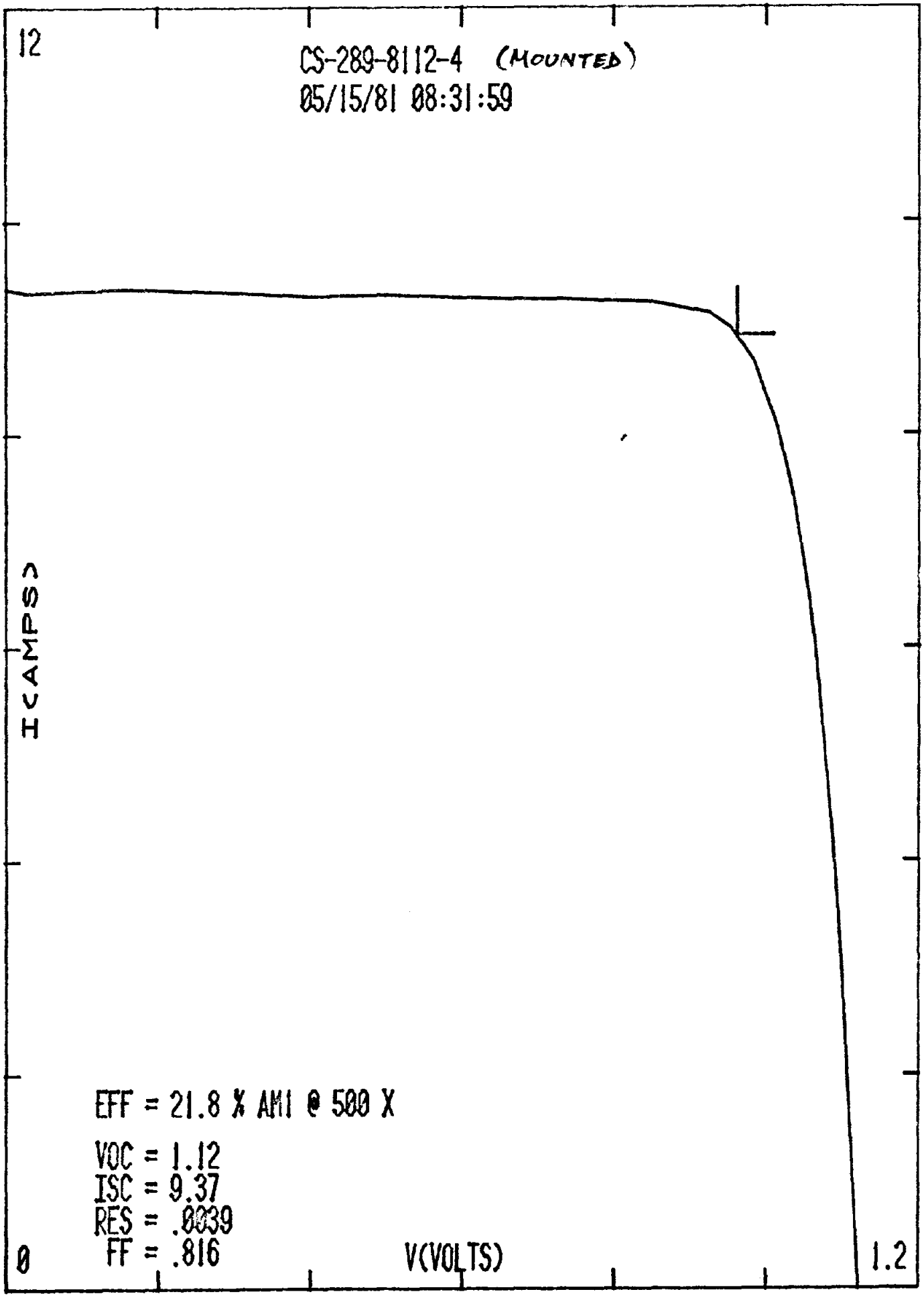
12
CS-289-8112-4 (MOUNTED)
05/15/81 08:31:59
I(AMPS)
EFF = 21.8 % AM1 @ 500 X
VOC = 1.12
ISC = 9.37
RES = .0039
FF = .816
0
V(VOLTS)
1.2

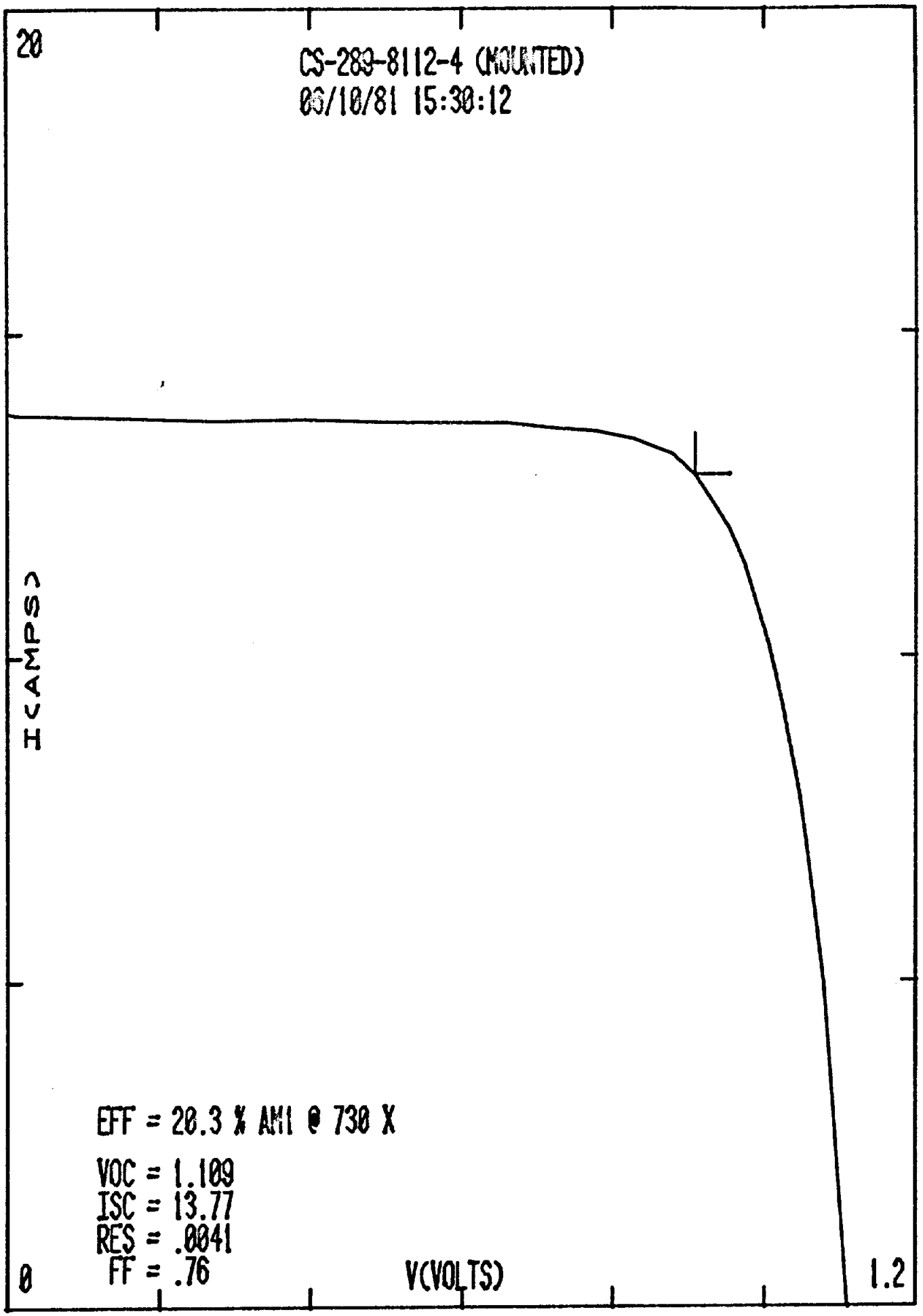
20
CS-289-8112-4 (MOUNTED)
06/10/81 15:30:12
I(AMPS)
EFF = 20.3 % AM1 @ 730 X
VOC = 1.109
ISC = 13.77
RES = .0041
FF = .76
0
V(VOLTS)
1.2

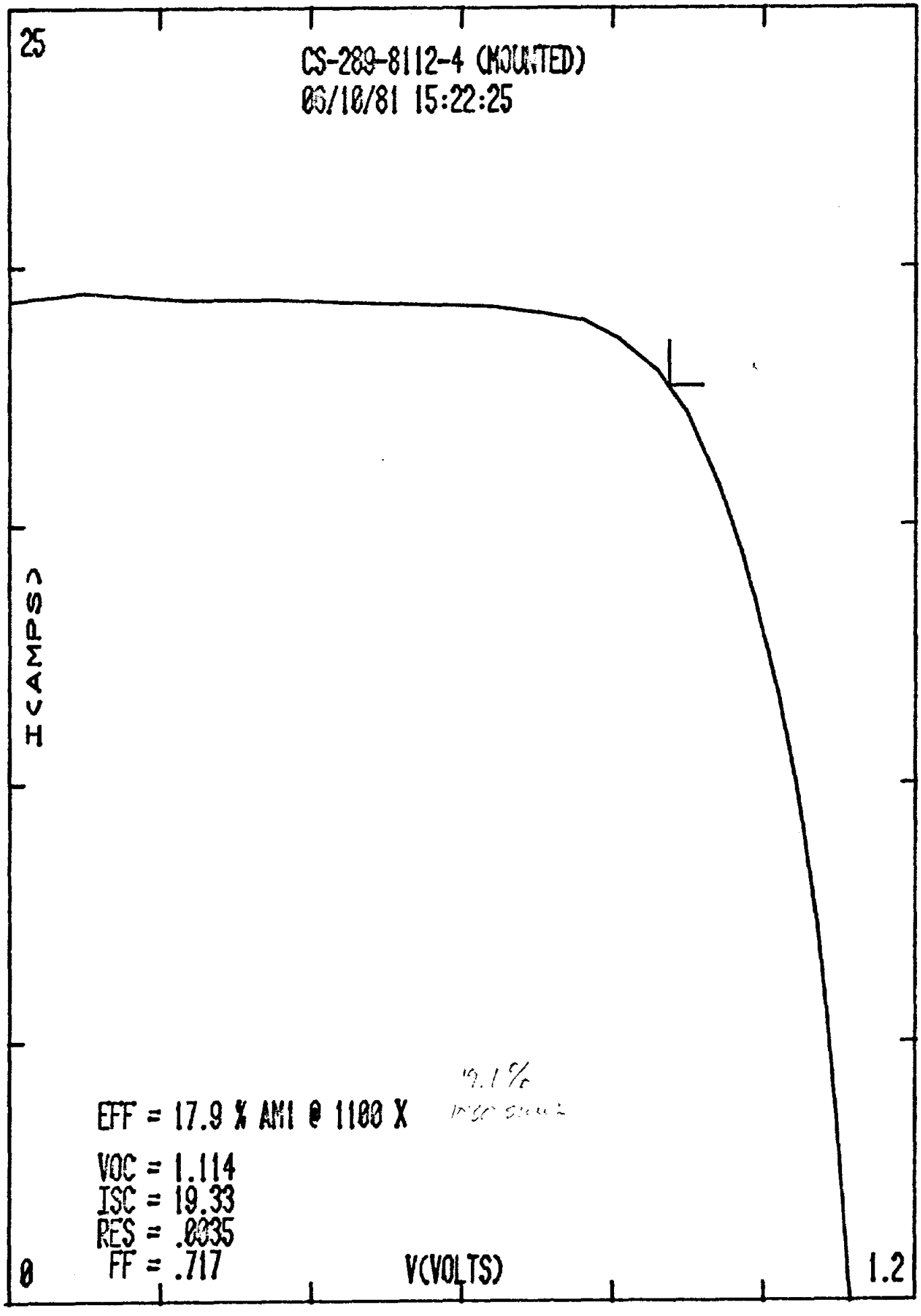
25
CS-289-8112-4 (MOUNTED)
06/10/81 15:22:25
I(AMPS)
EFF = 17.9 % AM1 @ 1100 X
VOC = 1.114
ISC = 19.33
RES = .0035
FF = .717
0
V(VOLTS)
1.2

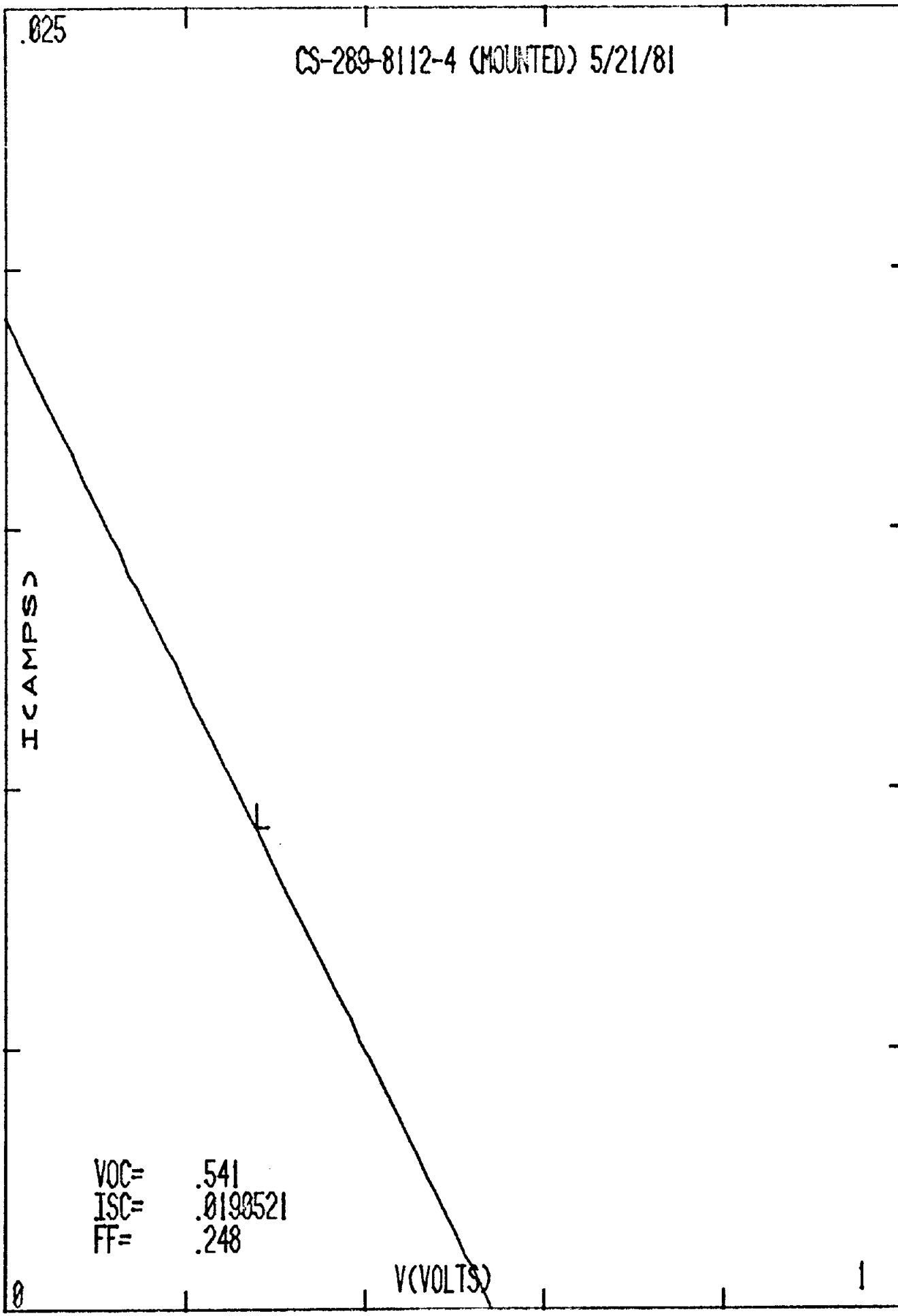
.025
CS-289-8112-4 (MOUNTED) 5/21/81
I(AMPS)
VOC= .541
ISC= .0190521
FF= .248
V(VOLTS)
0
1

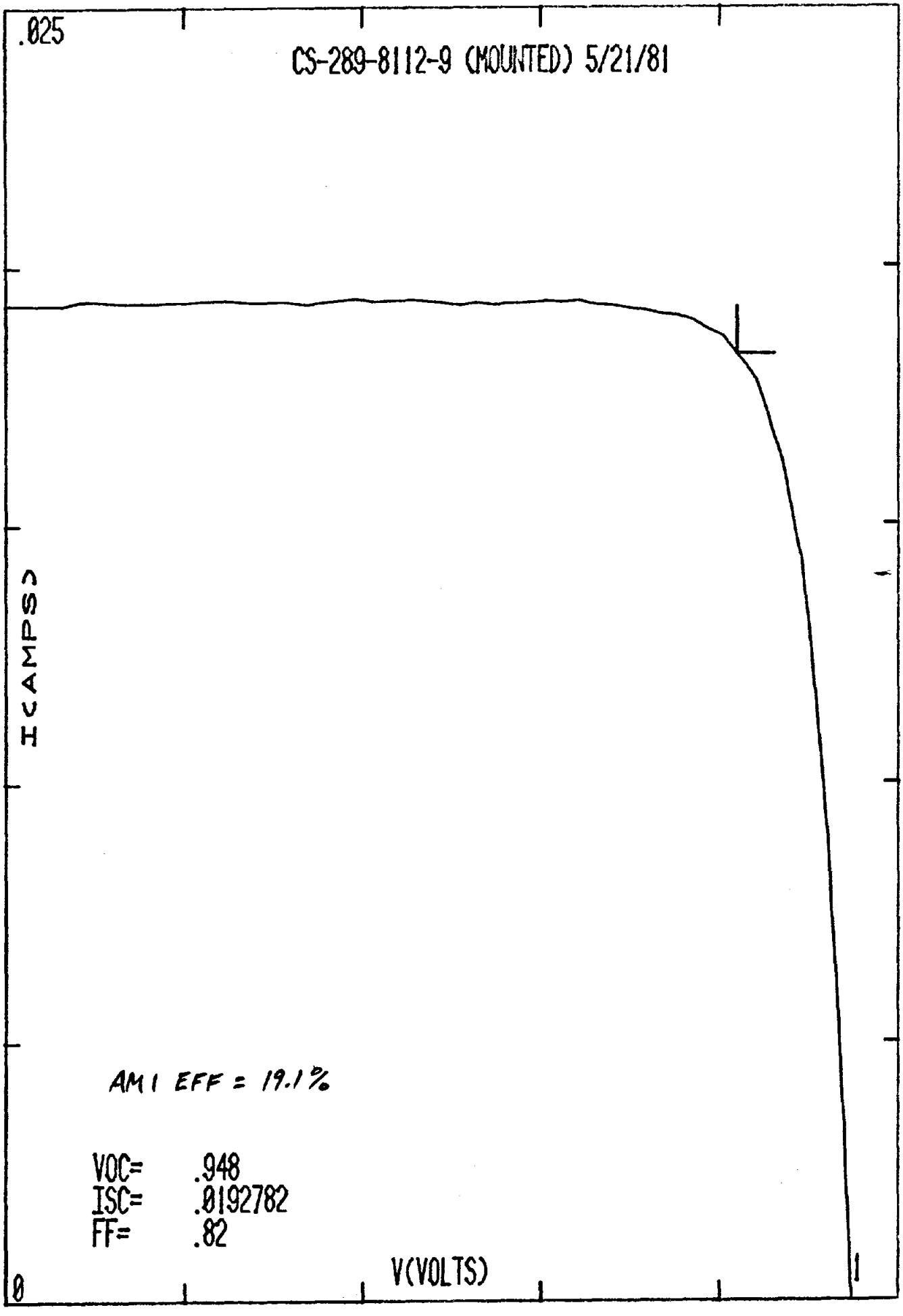
.025
CS-289-8112-9 (MOUNTED) 5/21/81
I(AMPS)
AM1 EFF = 19.1%
VOC= .948
ISC= .0192782
FF= .82
V(VOLTS)
0
1

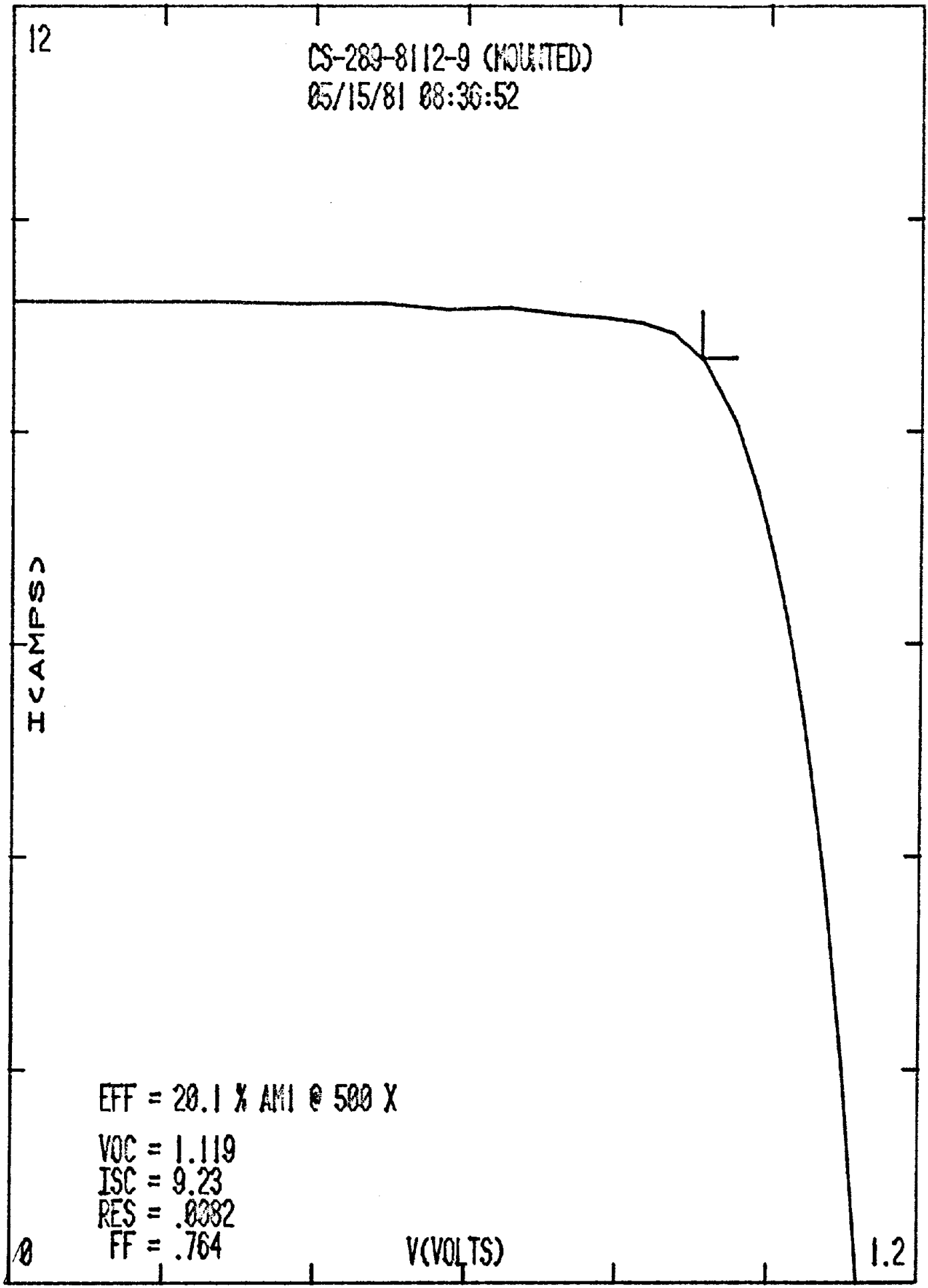
12
CS-283-8112-9 (MOUNTED)
05/15/81 08:36:52
I(AMPS)
EFF = 20.1 % AM1 @ 500 X
VOC = 1.119
ISC = 9.23
RES = .0082
FF = .764
0
V(VOLTS)
1.2

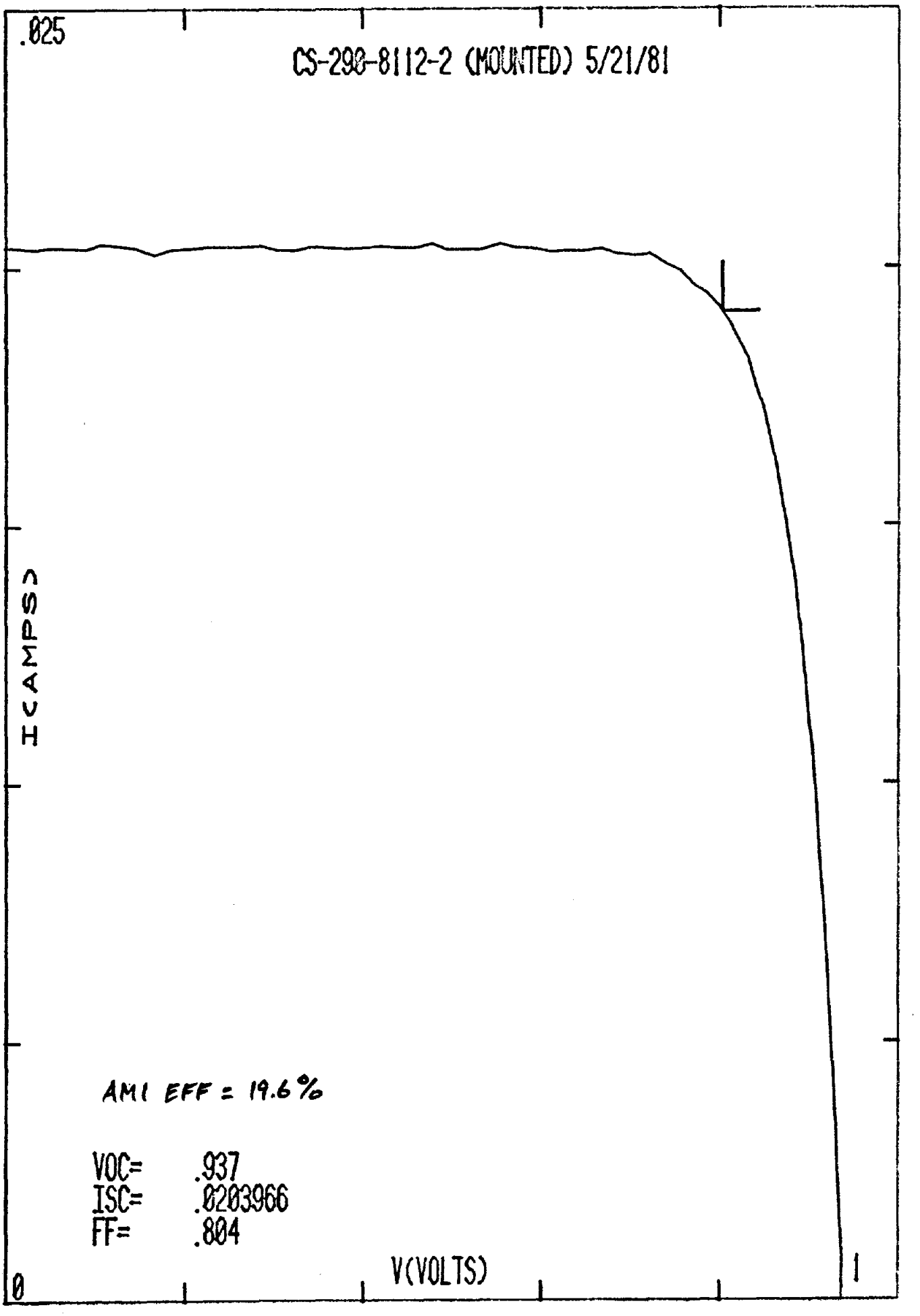
.025
CS-290-8112-2 (MOUNTED) 5/21/81
I(AMPS)
AM1 EFF = 19.6%
VOC= .937
ISC= .0203966
FF= .804
V(VOLTS)
0
1

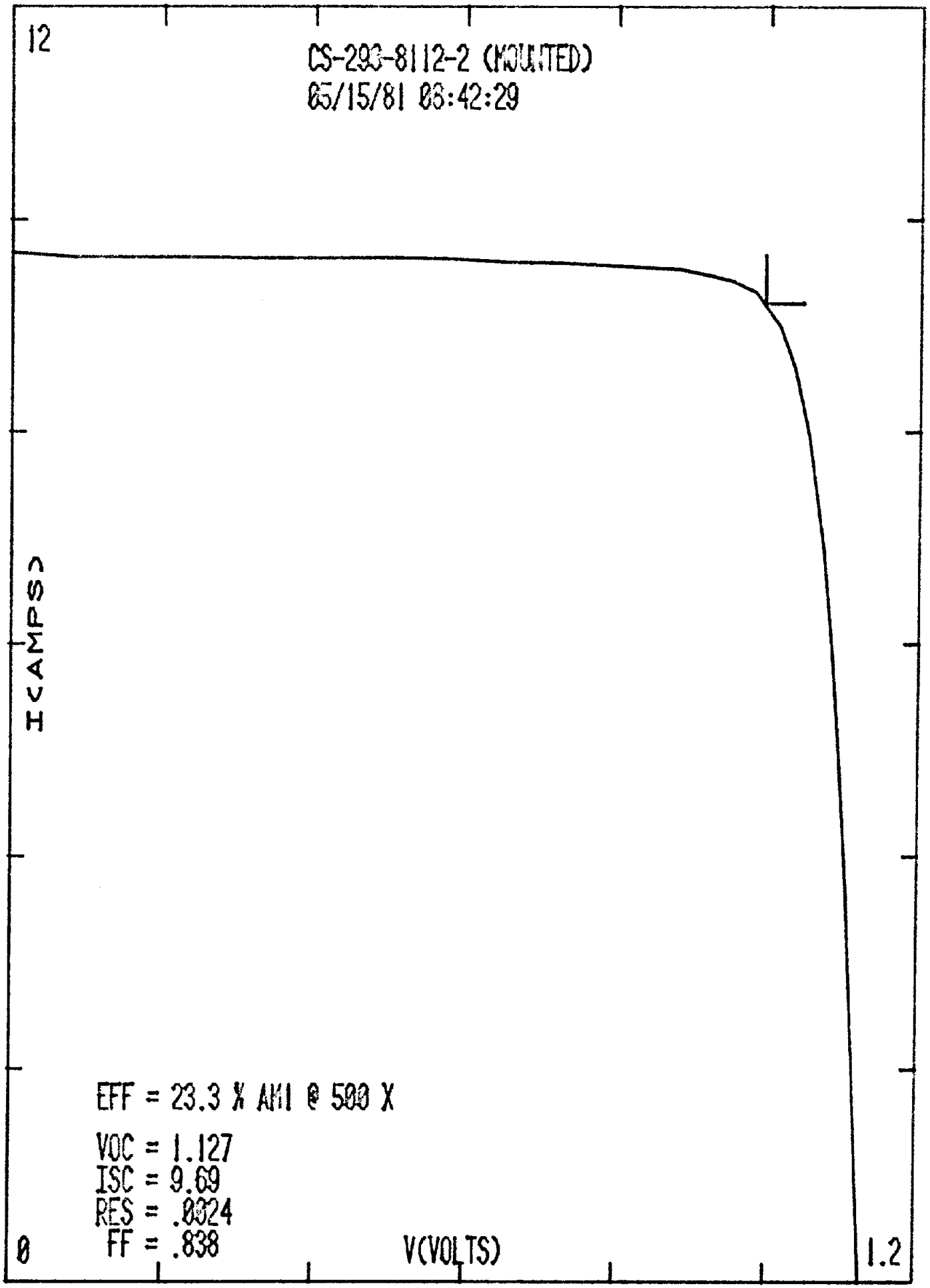
12
CS-290-8112-2 (MOUNTED)
05/15/81 08:42:29
I(AMPS)
EFF = 23.3 % AM1 @ 500 X
VOC = 1.127
ISC = 9.69
RES = .0024
FF = .838
0
V(VOLTS)
1.2

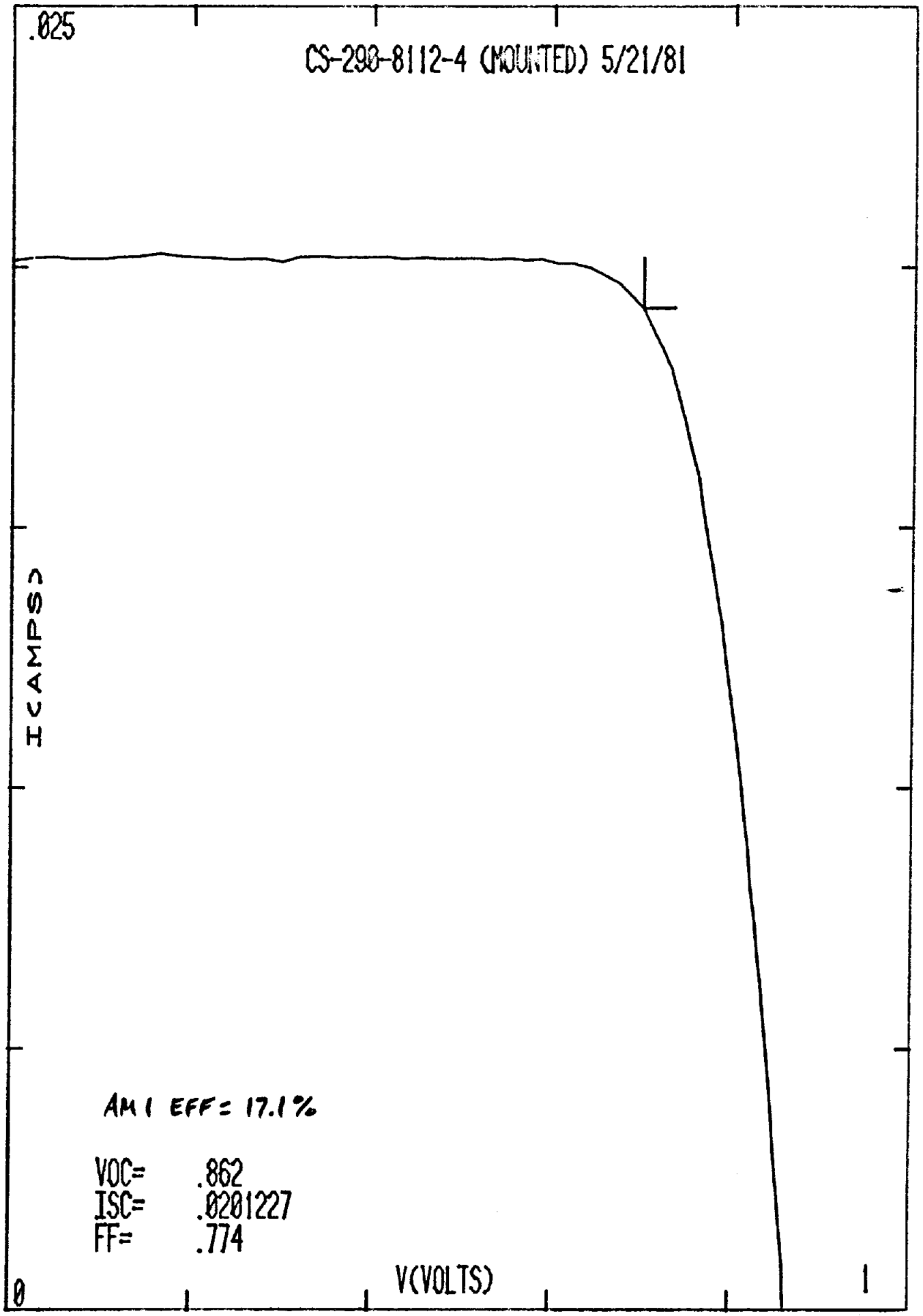
.025
CS-290-8112-4 (MOUNTED) 5/21/81
I(AMPS)
AM1 EFF= 17.1%
VOC= .862
ISC= .0201227
FF= .774
0
V(VOLTS)
1

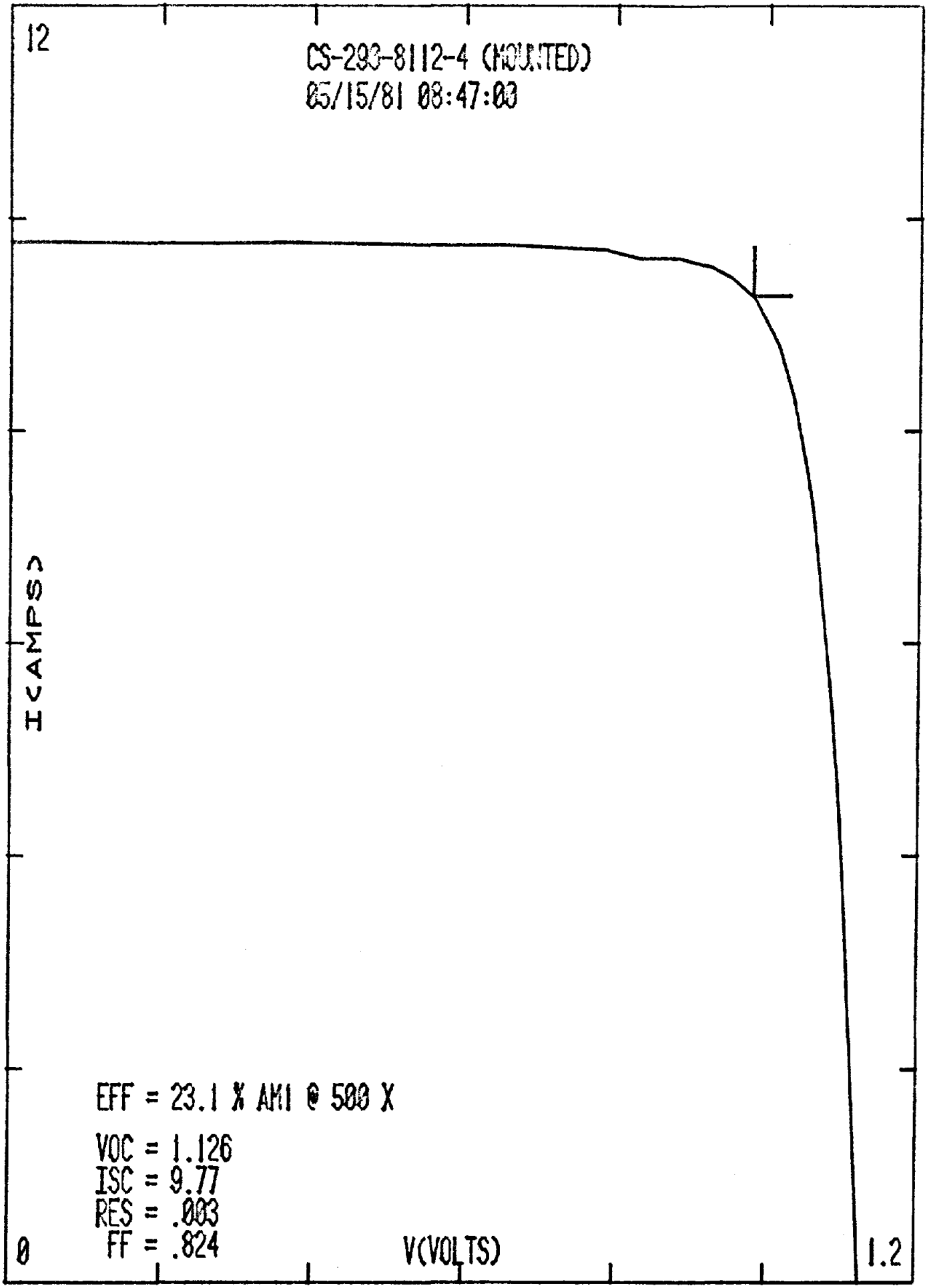
12
CS-290-8112-4 (MOUNTED)
05/15/81 08:47:00
I(AMPS)
EFF = 23.1 % AM1 @ 500 X
VOC = 1.126
ISC = 9.77
RES = .003
FF = .824
0
V(VOLTS)
1.2

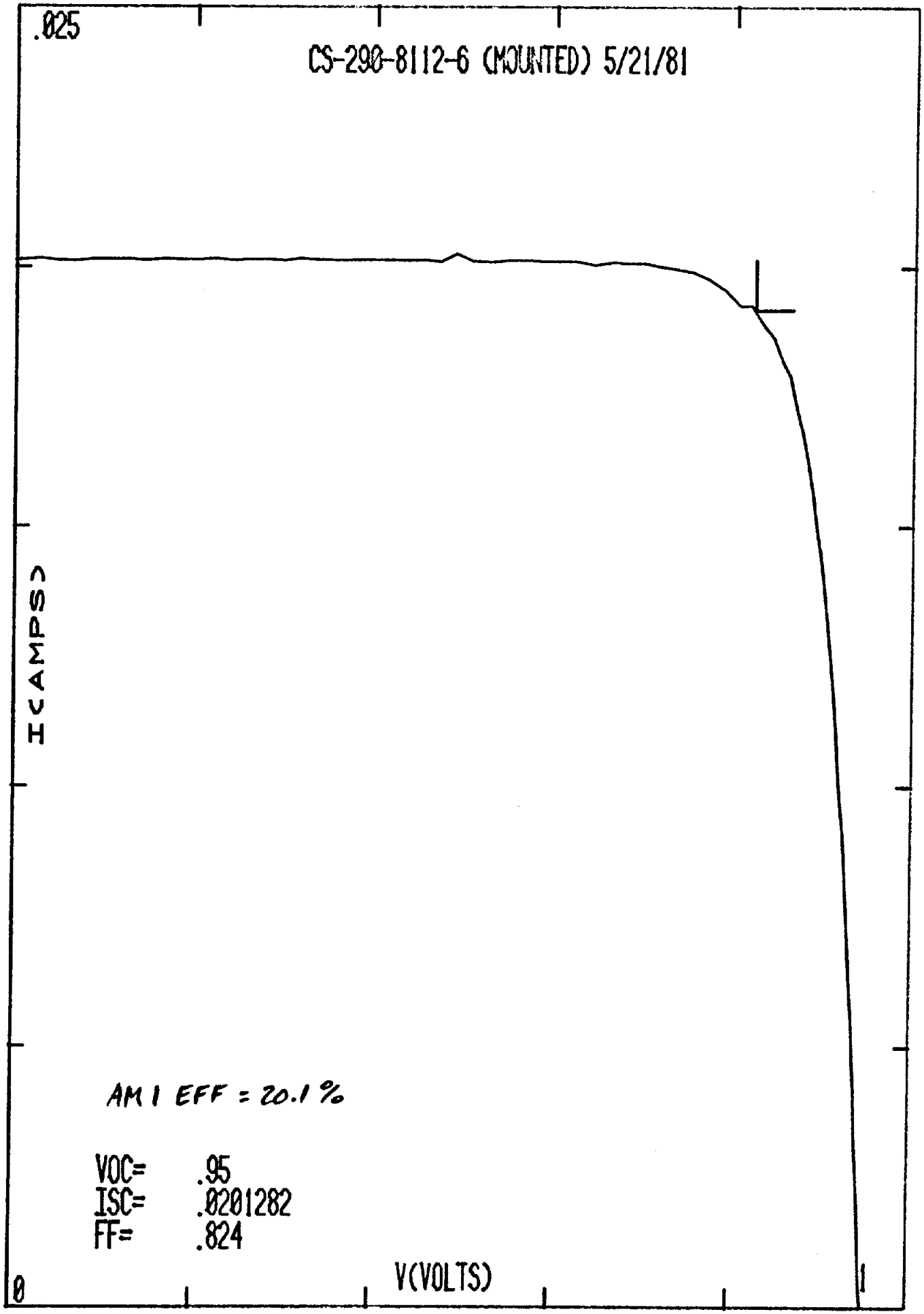
.025
CS-290-8112-6 (MOUNTED) 5/21/81
I(AMPS)
AM 1 EFF = 20.1 %
VOC= .95
ISC= .0201282
FF= .824
V(VOLTS)
0
1

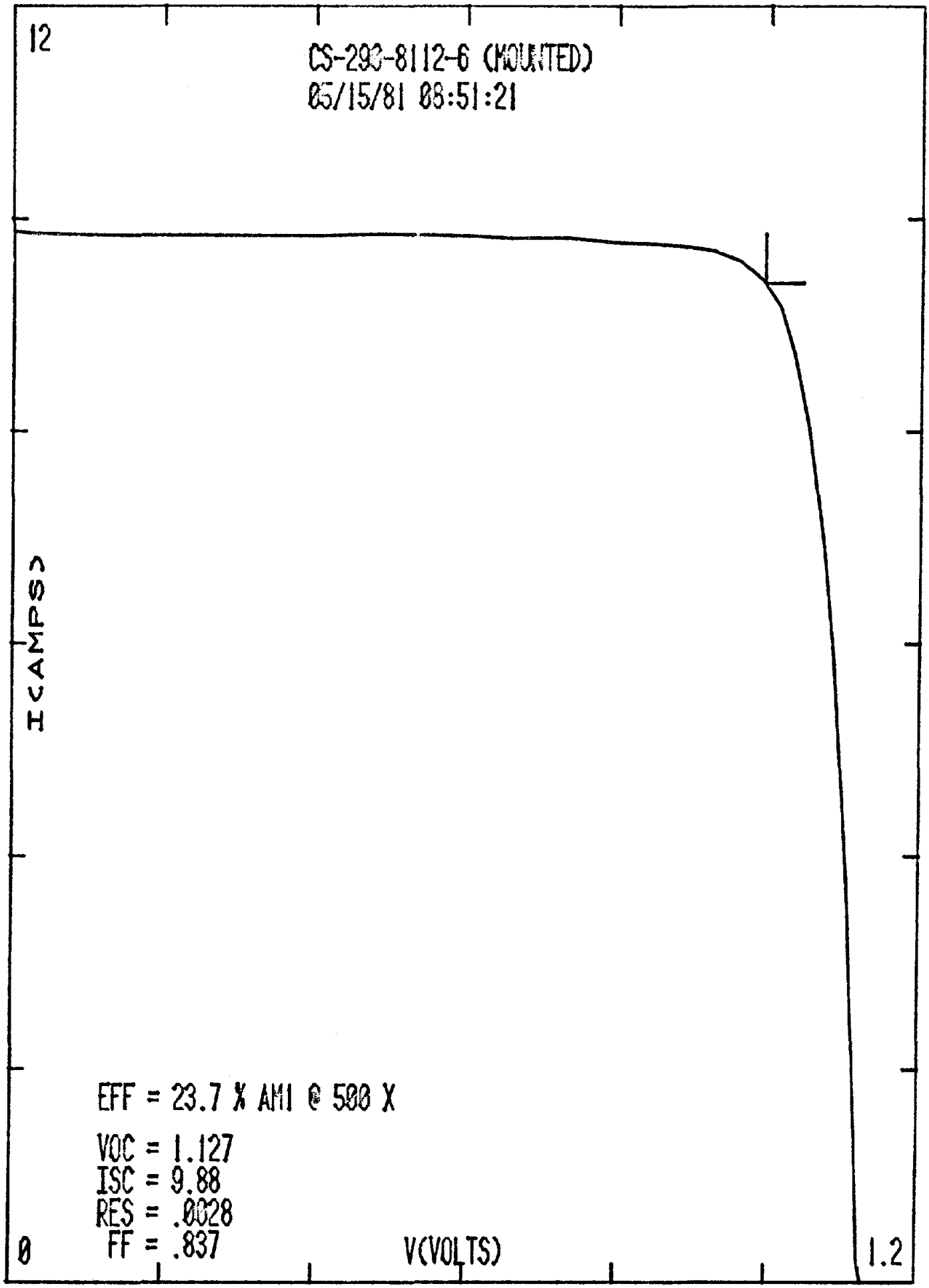
12
CS-290-8112-6 (MOUNTED)
05/15/81 08:51:21
I(AMPS)
EFF = 23.7 % AM1 @ 500 X
VOC = 1.127
ISC = 9.88
RES = .0028
FF = .837
0
V(VOLTS)
1.2

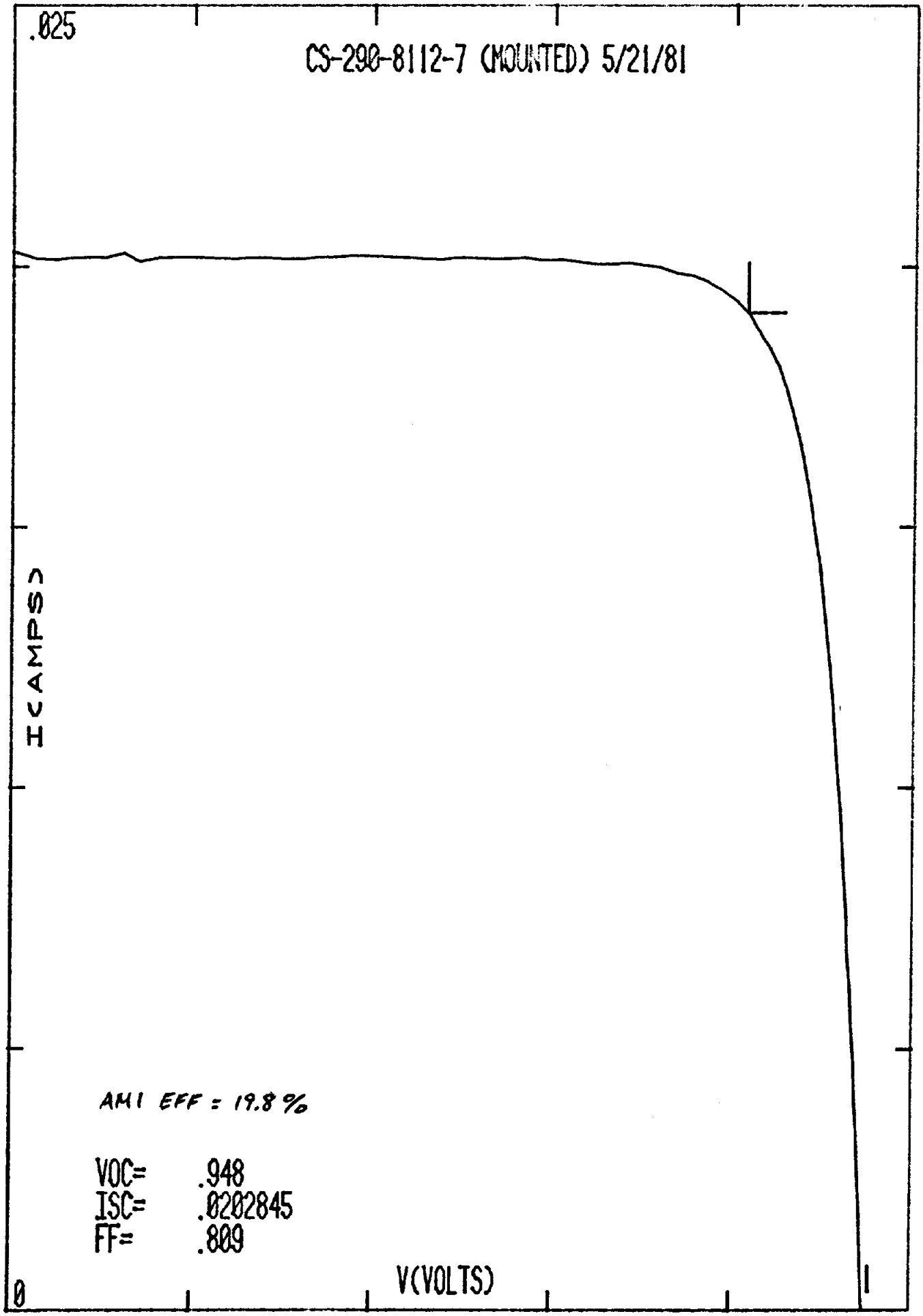
.025
CS-290-8112-7 (MOUNTED) 5/21/81
I(AMPS)
AM1 EFF = 19.8 %
VOC= .948
ISC= .0202845
FF= .809
V(VOLTS)
0
1

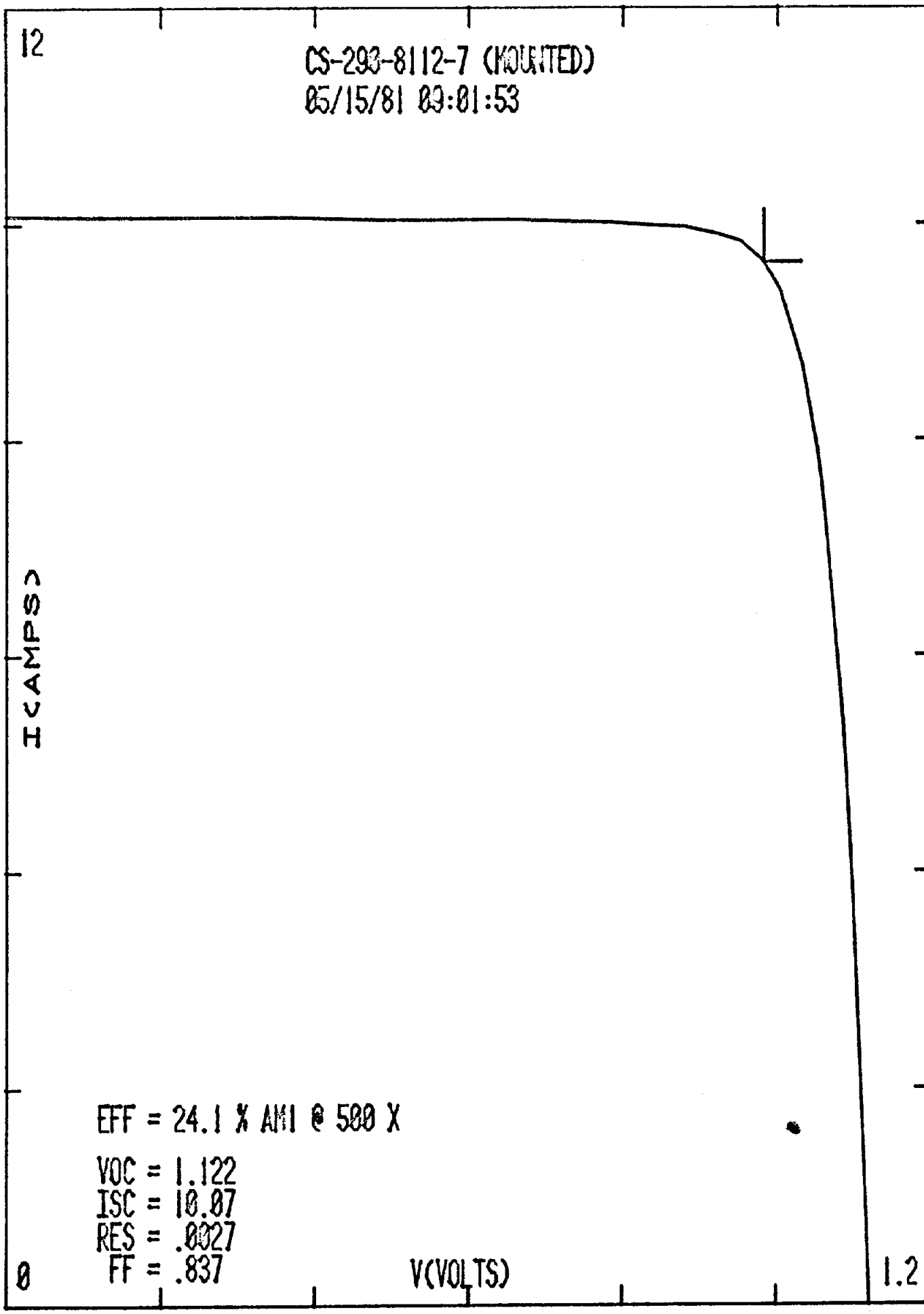
12
CS-293-8112-7 (MOUNTED)
05/15/81 09:01:53
I(AMPS)
EFF = 24.1 % AM1 @ 500 X
VOC = 1.122
ISC = 10.07
RES = .0027
FF = .837
0
V(VOLTS)
1.2

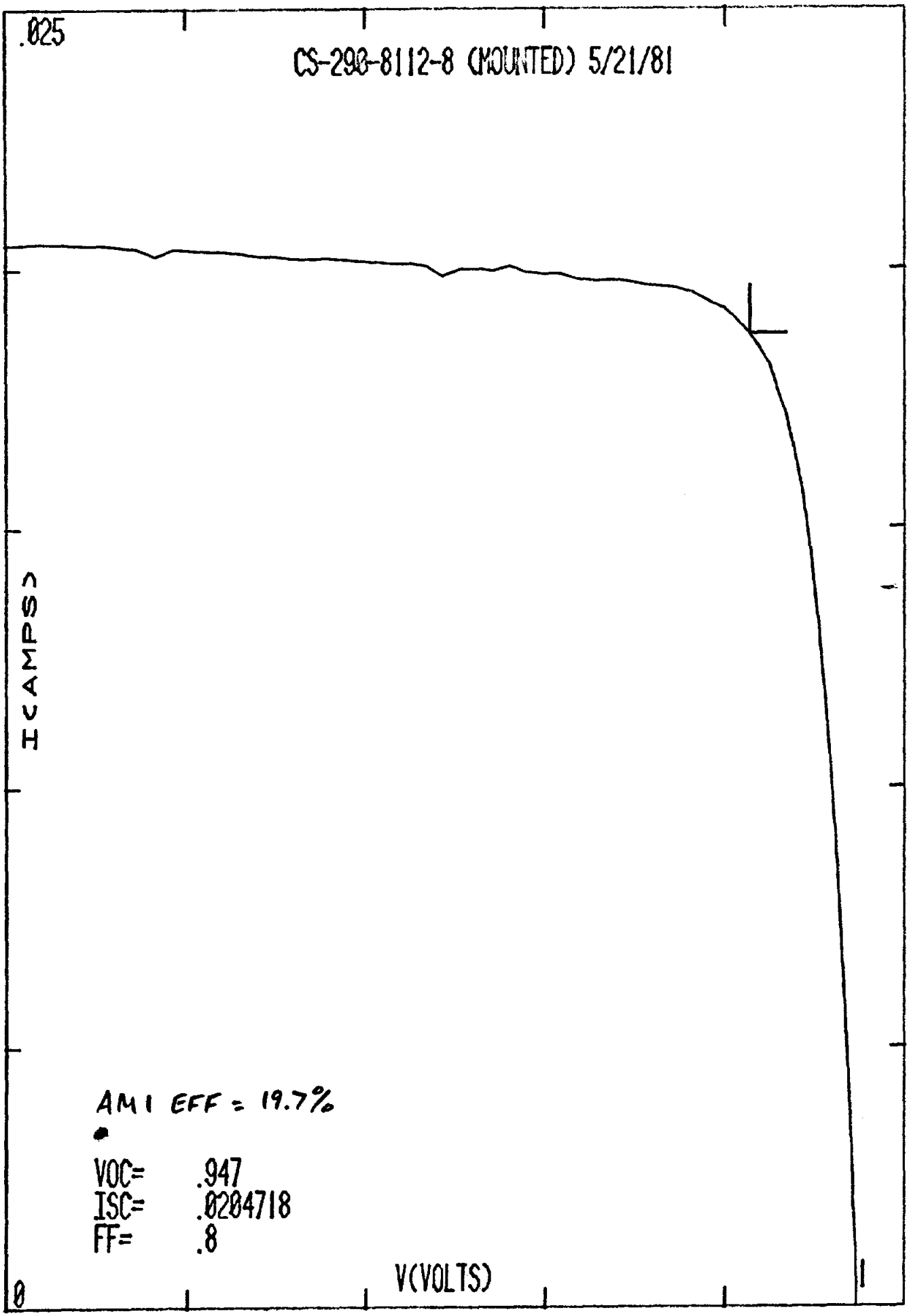
.025
CS-290-8112-8 (MOUNTED) 5/21/81
I(AMPS)
AM1 EFF = 19.7%
VOC= .947
ISC= .0204718
FF= .8
V(VOLTS)
0
1

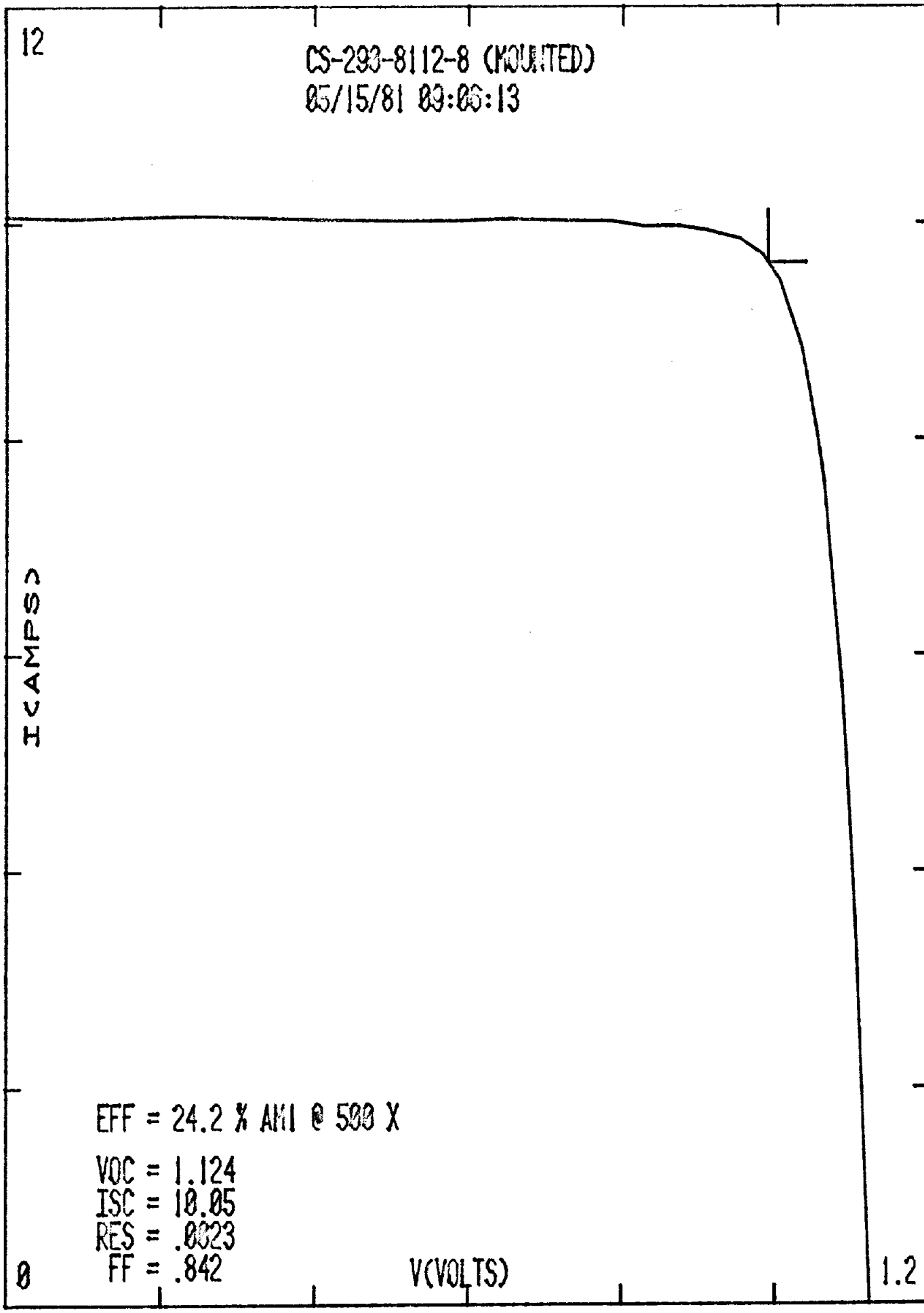
12
CS-293-8112-8 (MOUNTED)
05/15/81 09:06:13
I(AMPS)
EFF = 24.2 % AM1 @ 500 X
VOC = 1.124
ISC = 10.05
RES = .0023
FF = .842
0
V(VOLTS)
1.2

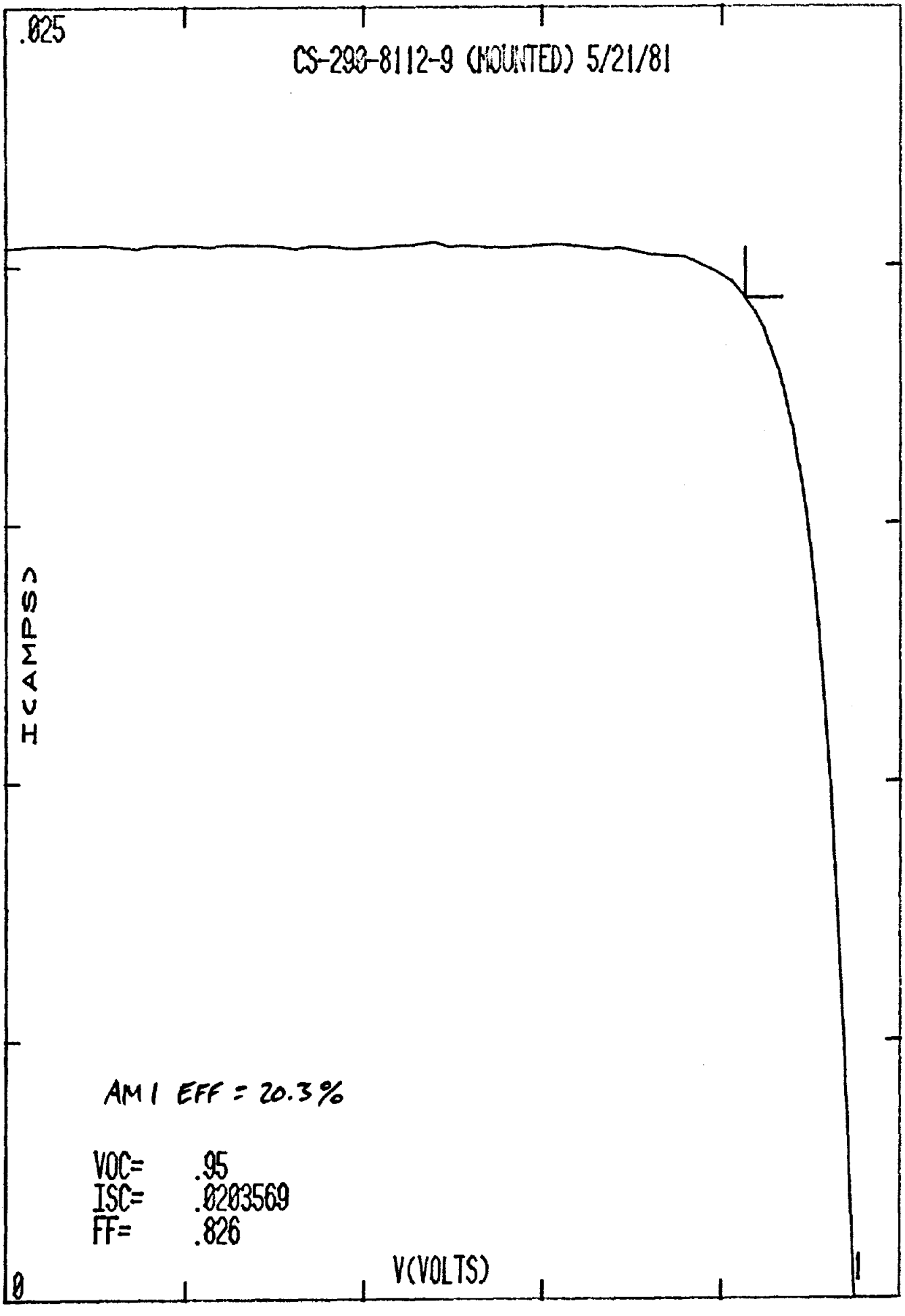
.025
CS-290-8112-9 (MOUNTED) 5/21/81
I(AMPS)
AM1 EFF = 20.3%
VOC= .95
ISC= .0203569
FF= .826
V(VOLTS)
0
1

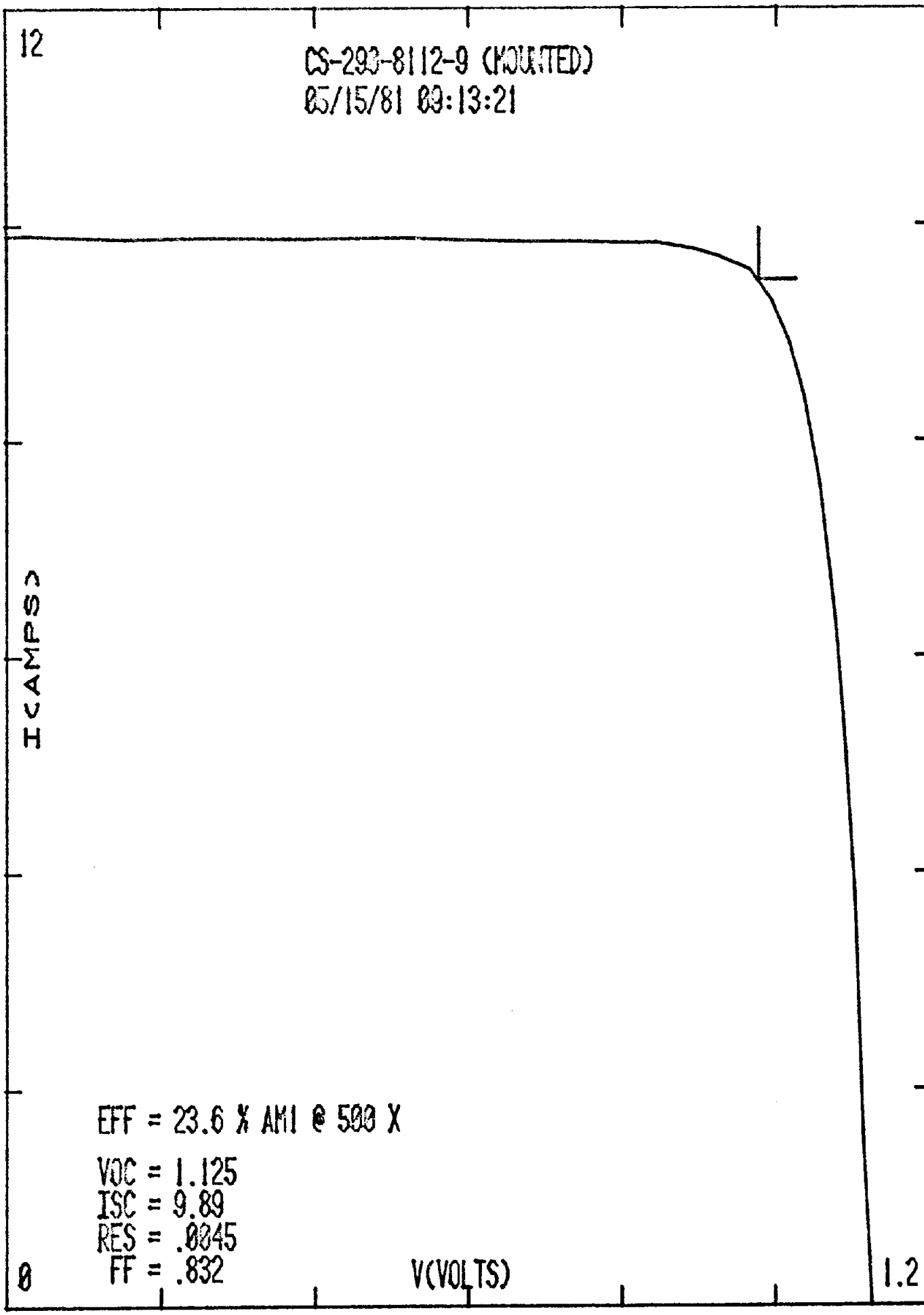
12
CS-293-8112-9 (MOUNTED)
05/15/81 09:13:21
I(AMPS)
EFF = 23.6 % AM1 @ 500 X
VOC = 1.125
ISC = 9.89
RES = .0045
FF = .832
0
V(VOLTS)
1.2

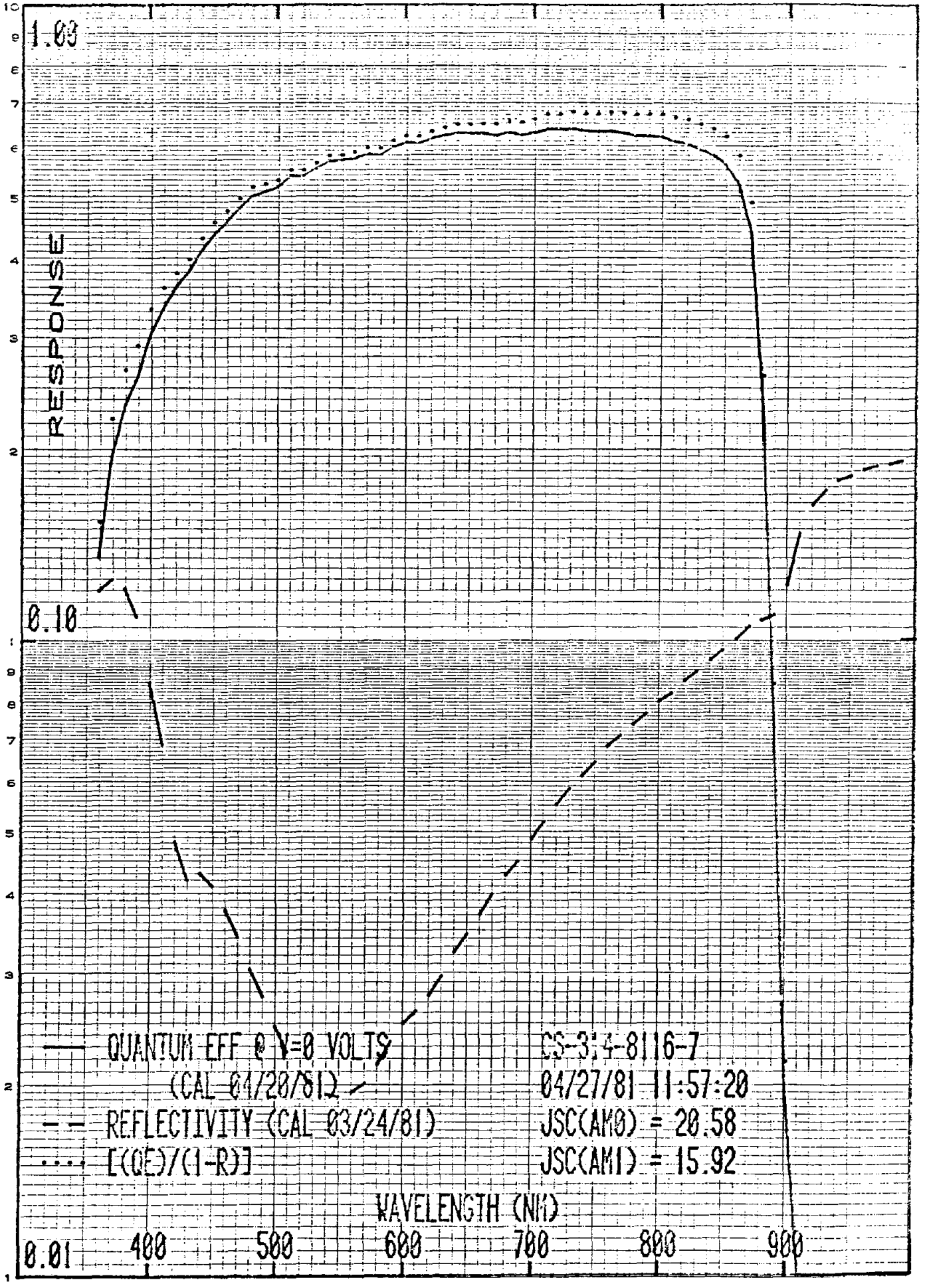
1.00
0.10
0.01
RESPONSE
WAVELENGTH (NM)
400
500
600
700
800
900
QUANTUM EFF @ V=0 VOLTS
(CAL 04/28/81)
REFLECTIVITY (CAL 03/24/81)
[(QE)/(1-R)]
CS-314-8116-7
04/27/81 11:57:20
JSC(AM0) = 20.58
JSC(AM1) = 15.92
DIETZGEN CORPORATION
MADE IN U.S.A.
NO. 340R-L210 DIETZGEN GRAPH PAPER
SEMI-LOGARITHMIC
2 CYCLES X 10 DIVISIONS PER INCH

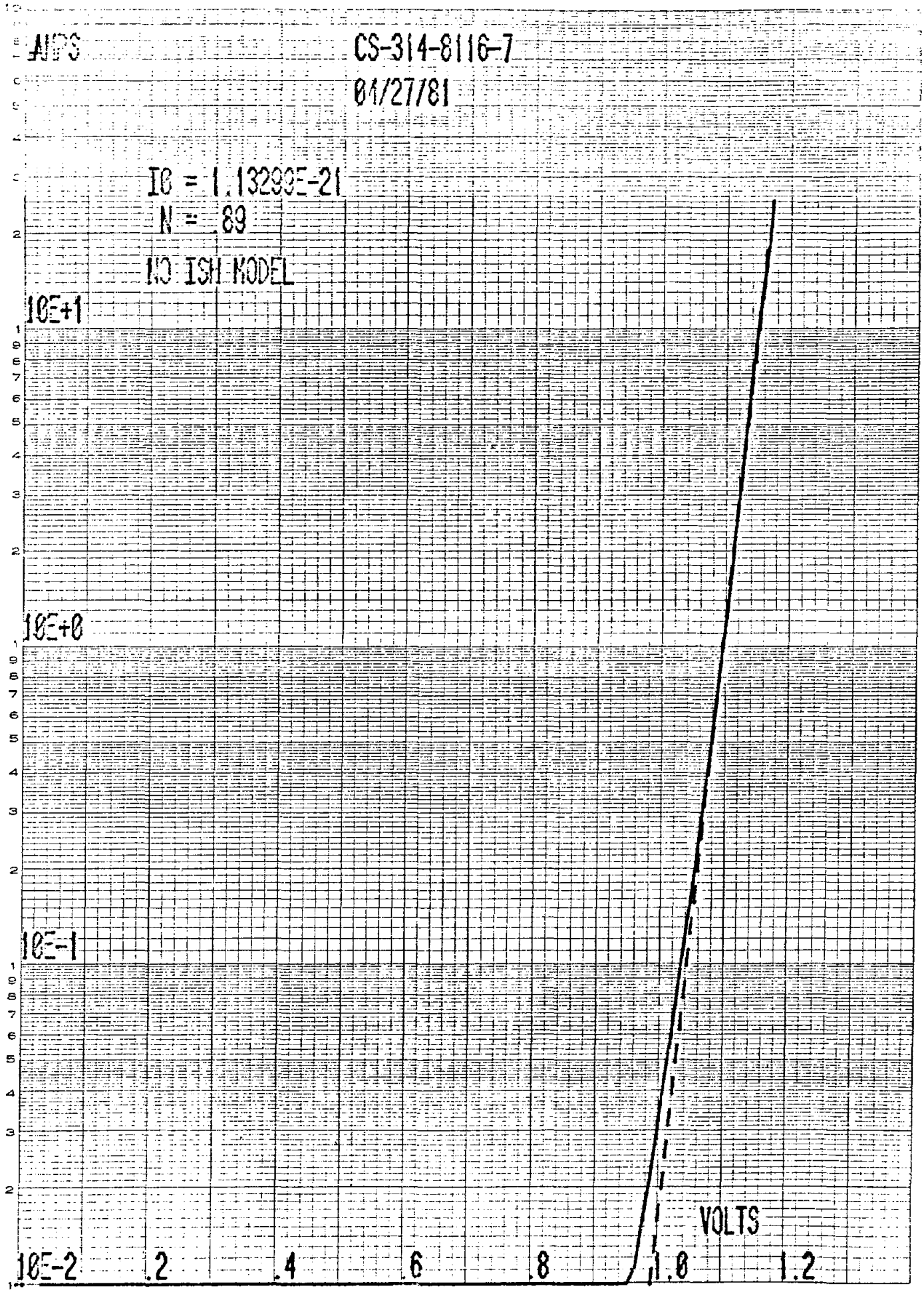

DIETZGEN CORPORATION
MADE IN U.S.A.
NO. 340R-L410 DIETZGEN GRAPH PAPER
SEMI-LOGARITHMIC
4 CYCLES X 10 DIVISIONS PER INCH

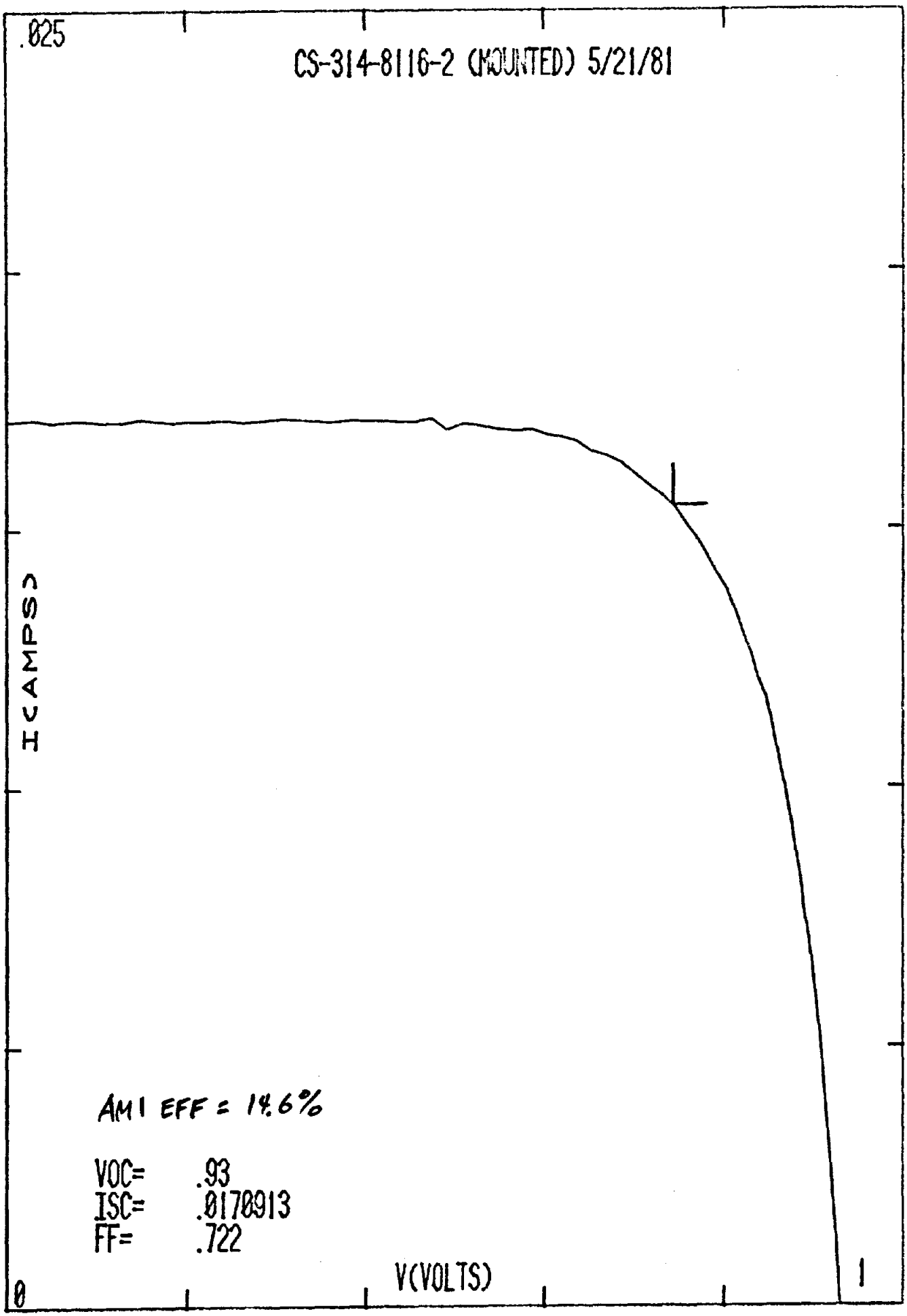
.025
CS-314-8116-2 (MOUNTED) 5/21/81
I(AMPS)
AM1 EFF = 14.6%
VOC= .93
ISC= .0170913
FF= .722
V(VOLTS)
0
1

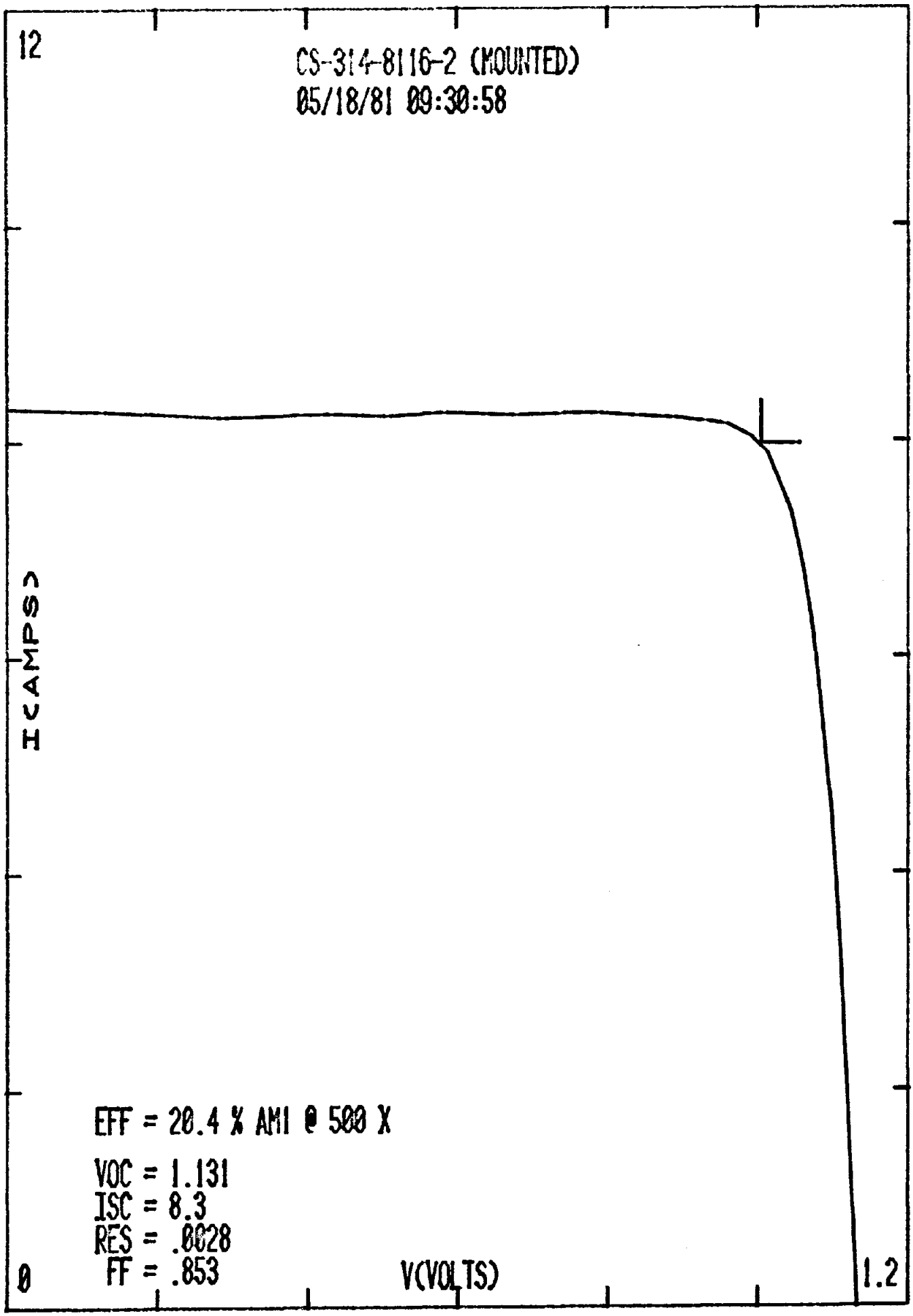
12
CS-314-8116-2 (MOUNTED)
05/18/81 09:30:58
I(AMPS)
EFF = 20.4 % AM1 @ 500 X
VOC = 1.131
ISC = 8.3
RES = .0028
FF = .853
0
V(VOLTS)
1.2

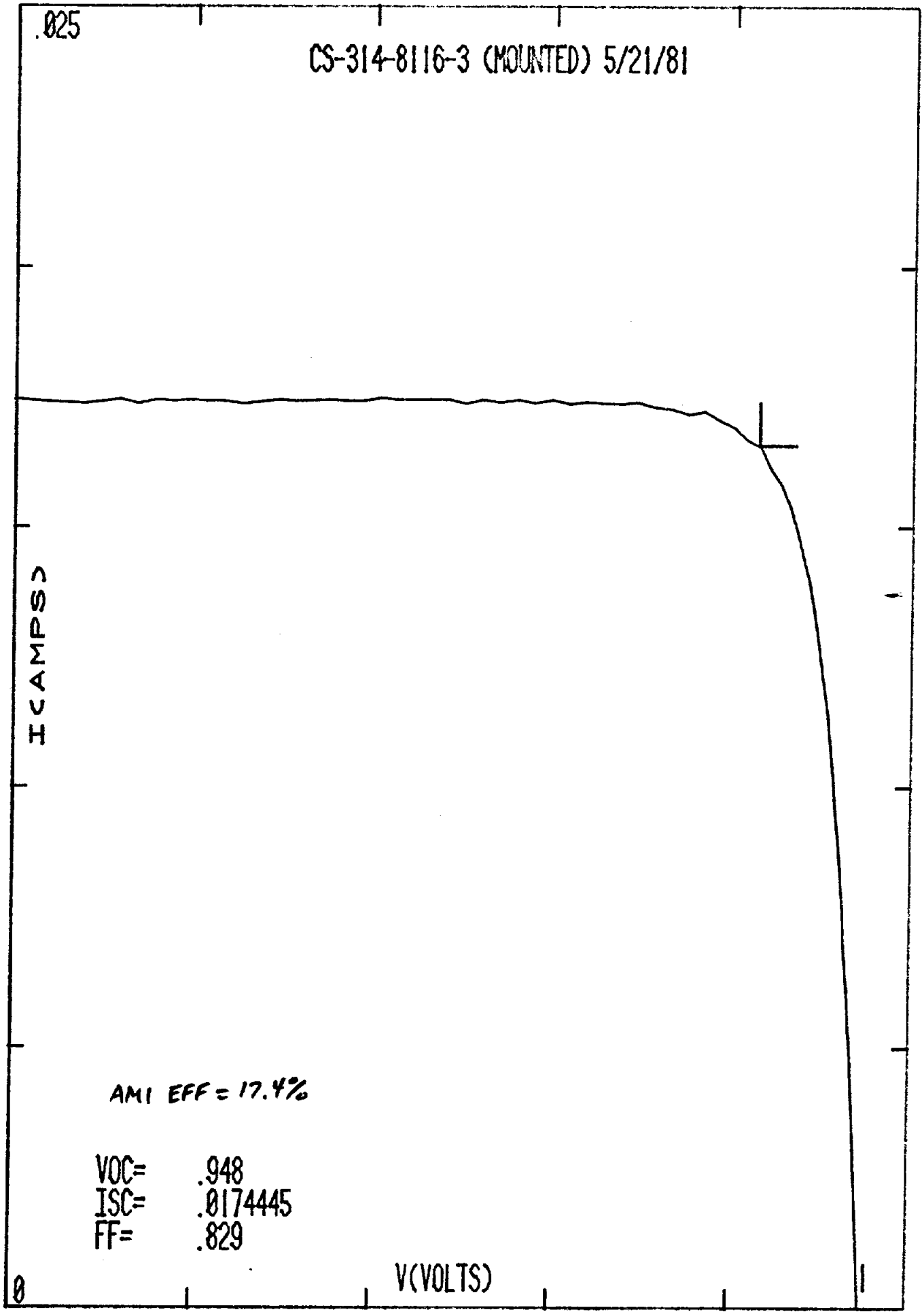
.025
CS-314-8116-3 (MOUNTED) 5/21/81
I(AMPS)
AM1 EFF = 17.4%
VOC= .948
ISC= .0174445
FF= .829
0
V(VOLTS)
1

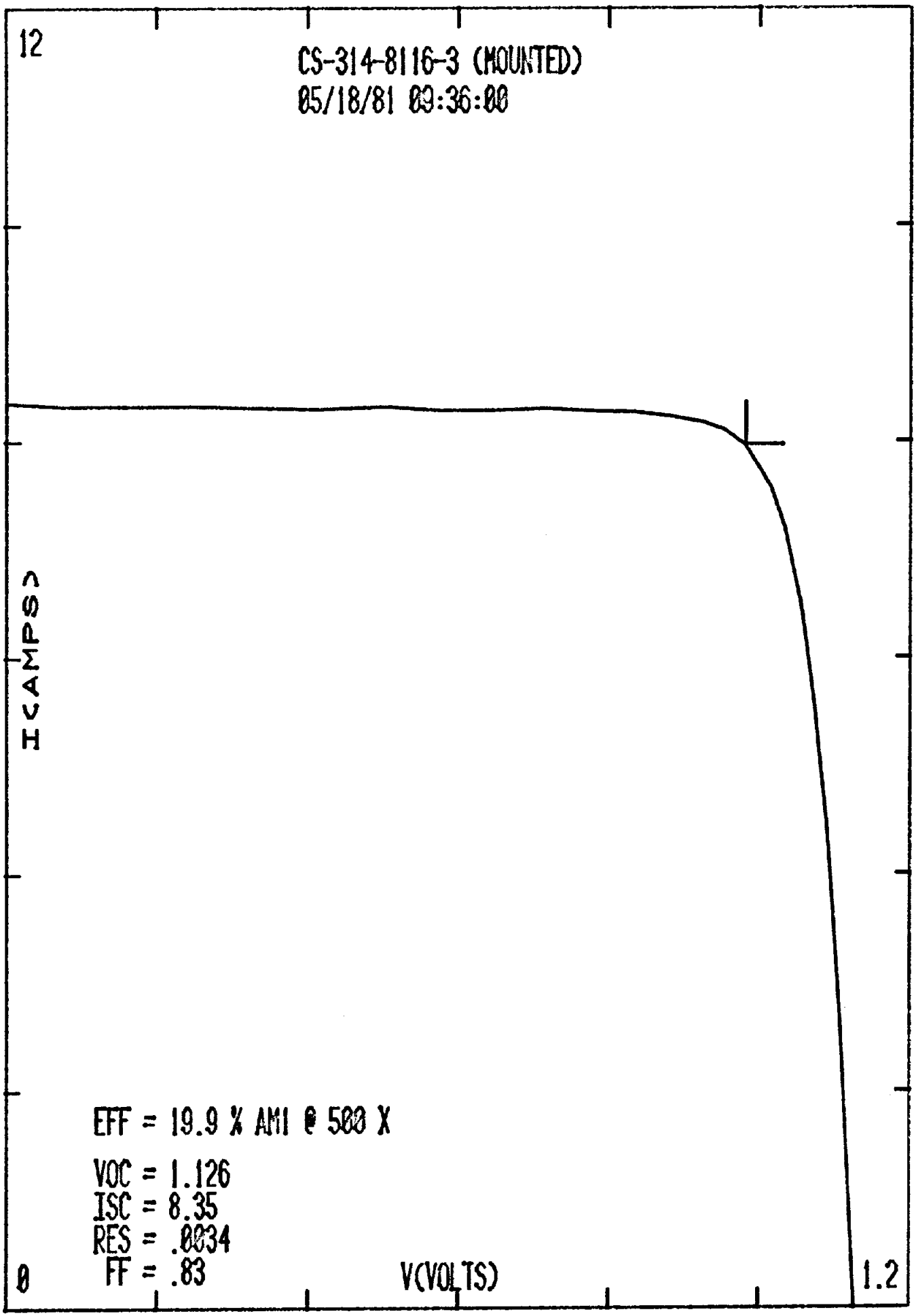
12
CS-314-8116-3 (MOUNTED)
05/18/81 09:36:00
I(AMPS)
EFF = 19.9 % AM1 @ 500 X
VOC = 1.126
ISC = 8.35
RES = .0034
FF = .83
0
V(VOLTS)
1.2

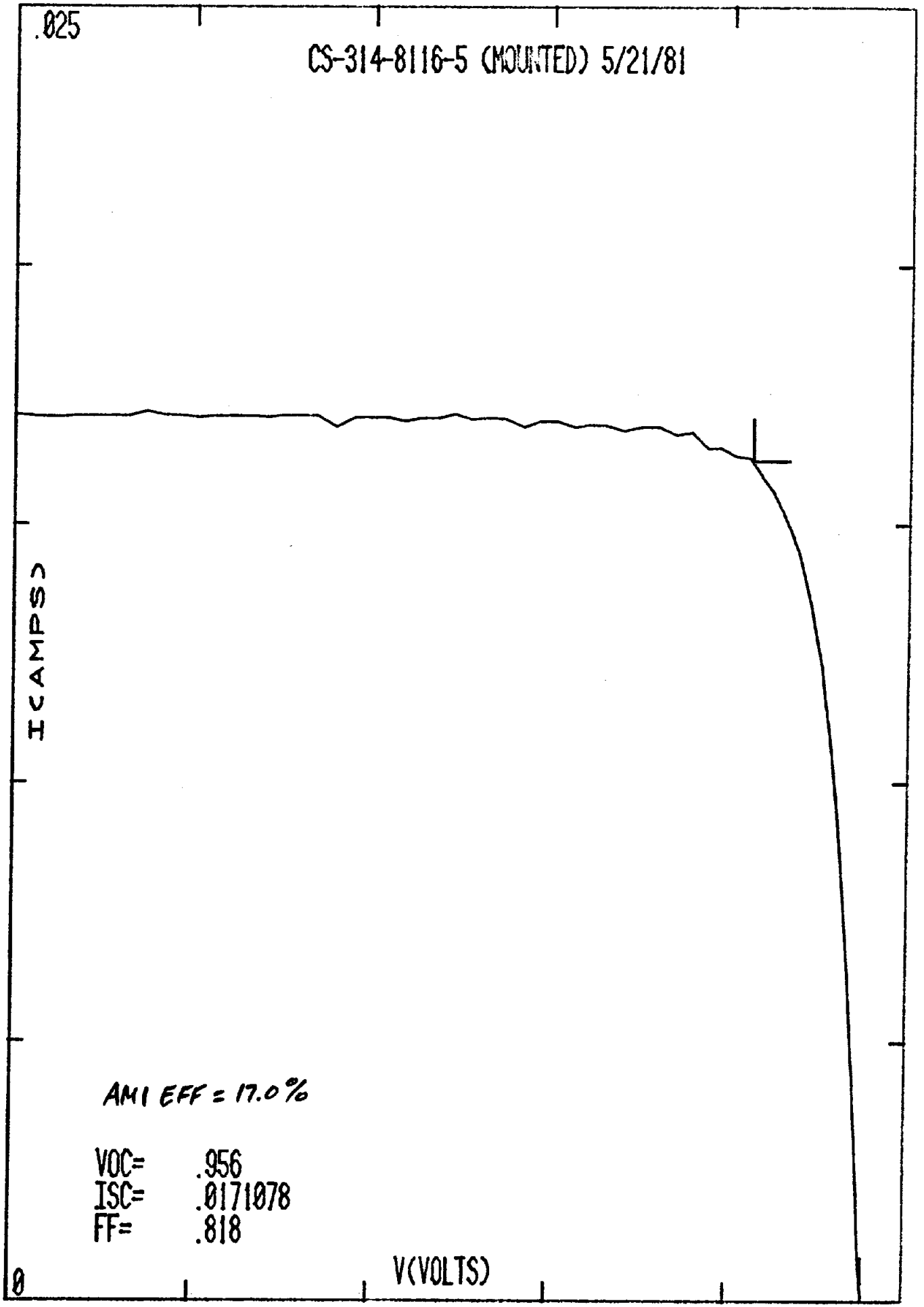
.025
CS-314-8116-5 (MOUNTED) 5/21/81
I(AMPS)
AM1 EFF = 17.0%
VOC= .956
ISC= .0171078
FF= .818
0
V(VOLTS)

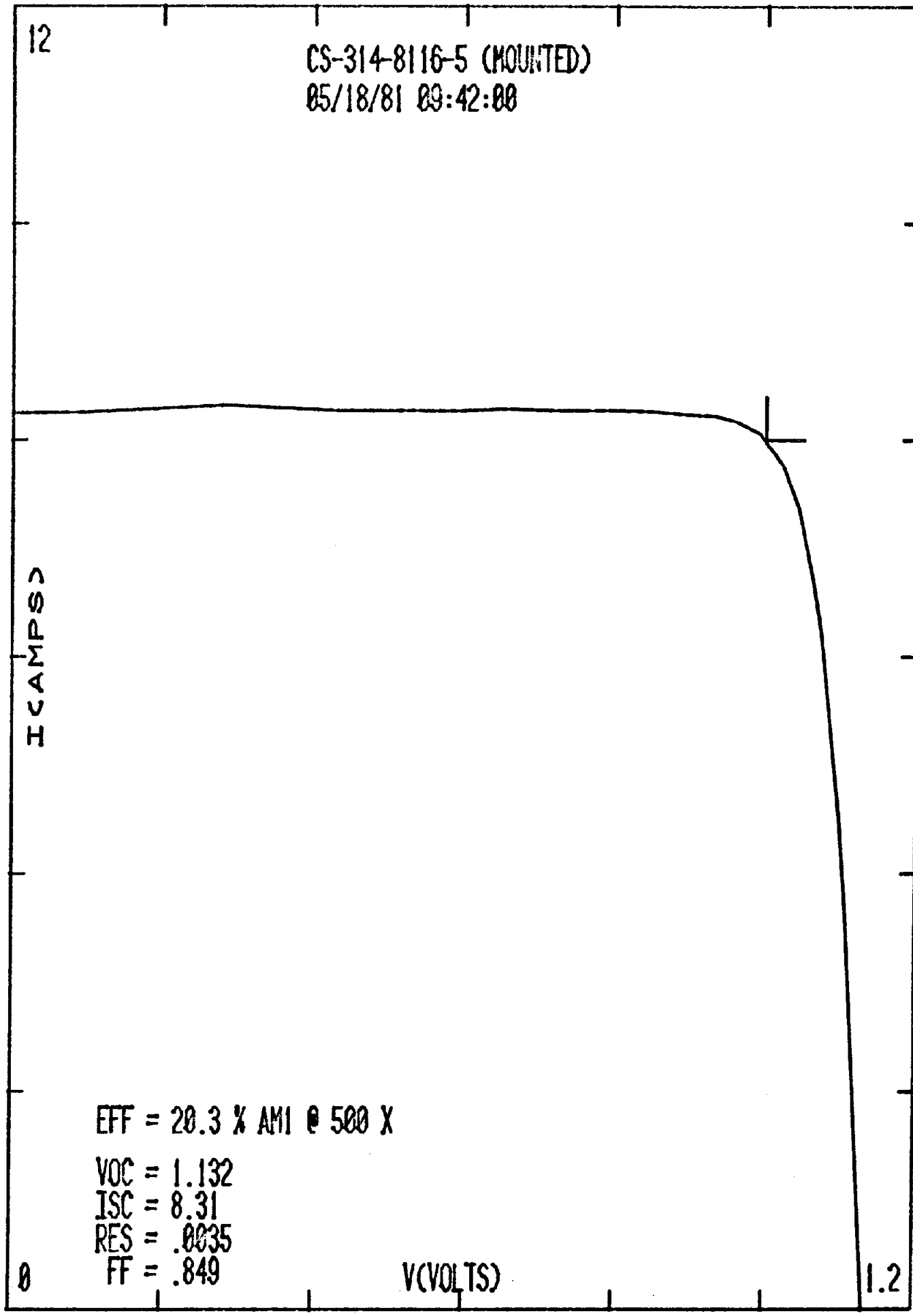
12
CS-314-8116-5 (MOUNTED)
05/18/81 09:42:00
I(AMPS)
EFF = 20.3 % AM1 @ 500 X
VOC = 1.132
ISC = 8.31
RES = .0035
FF = .849
0
V(VOLTS)
1.2

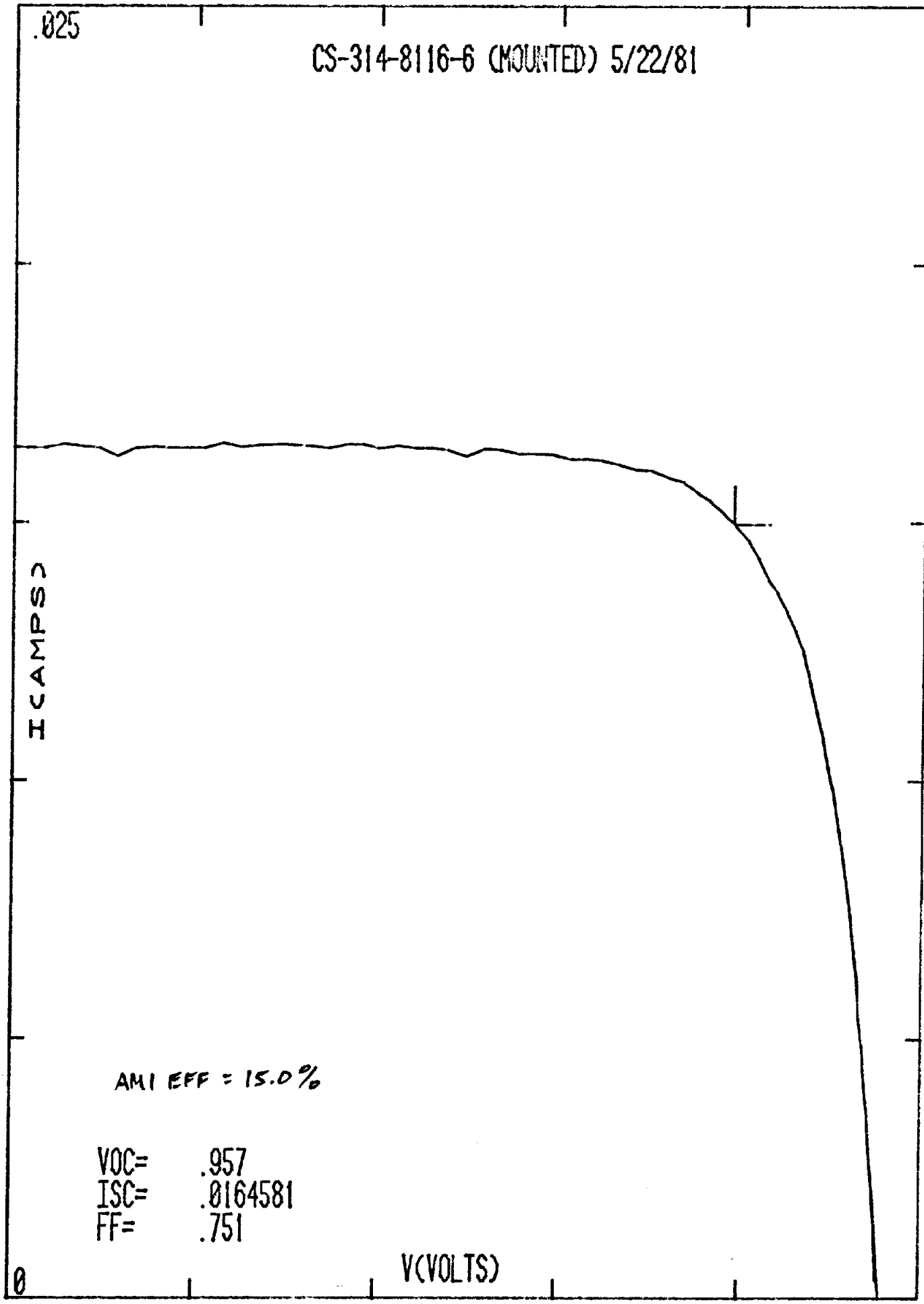
.025
CS-314-8116-6 (MOUNTED) 5/22/81
I(AMPS)
AMI EFF = 15.0%
VOC= .957
ISC= .0164581
FF= .751
0
V(VOLTS)

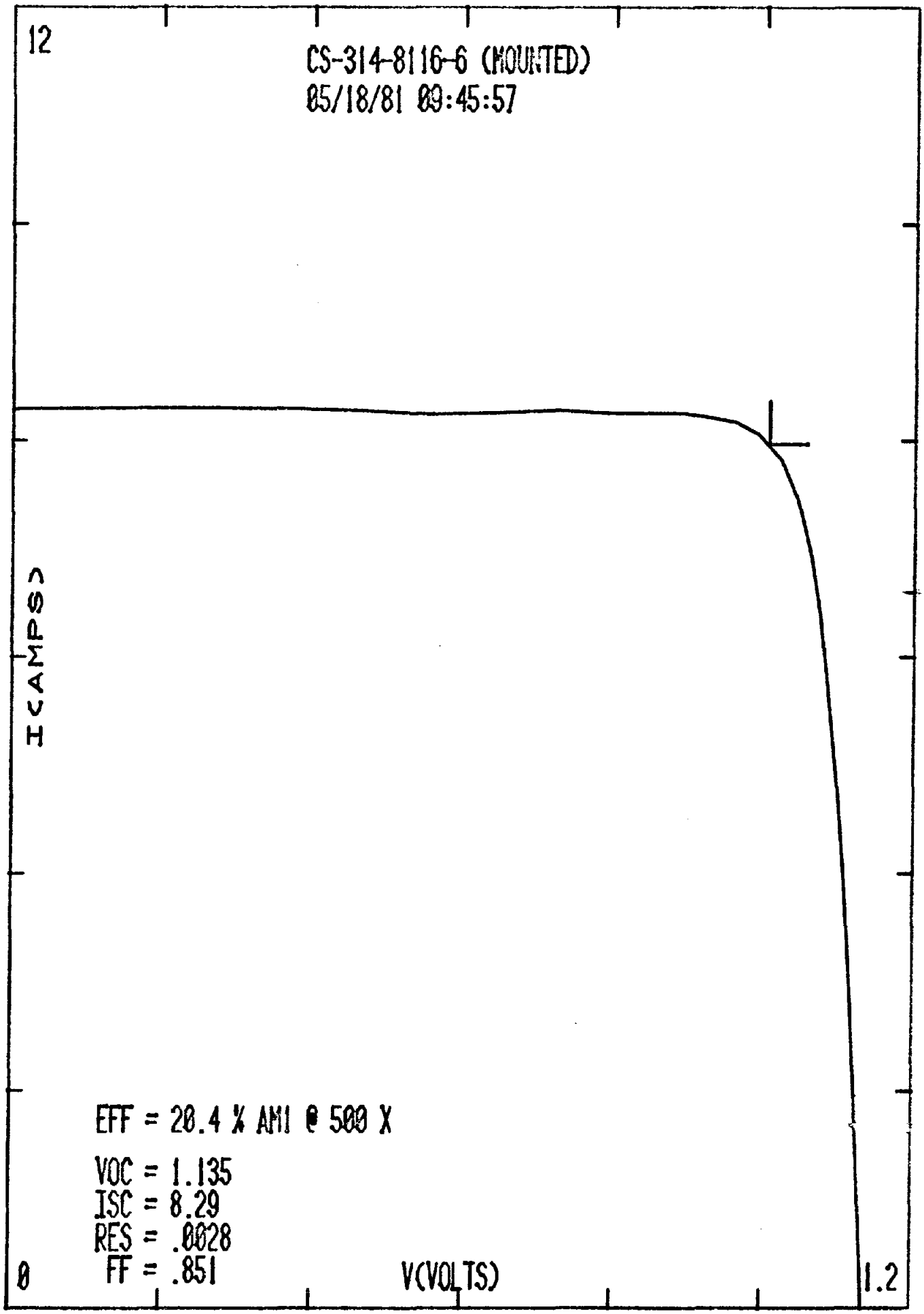
12
CS-314-8116-6 (MOUNTED)
05/18/81 09:45:57
I(AMPS)
EFF = 20.4 % AM1 @ 500 X
VOC = 1.135
ISC = 8.29
RES = .0028
FF = .851
0
V(VOLTS)
1.2

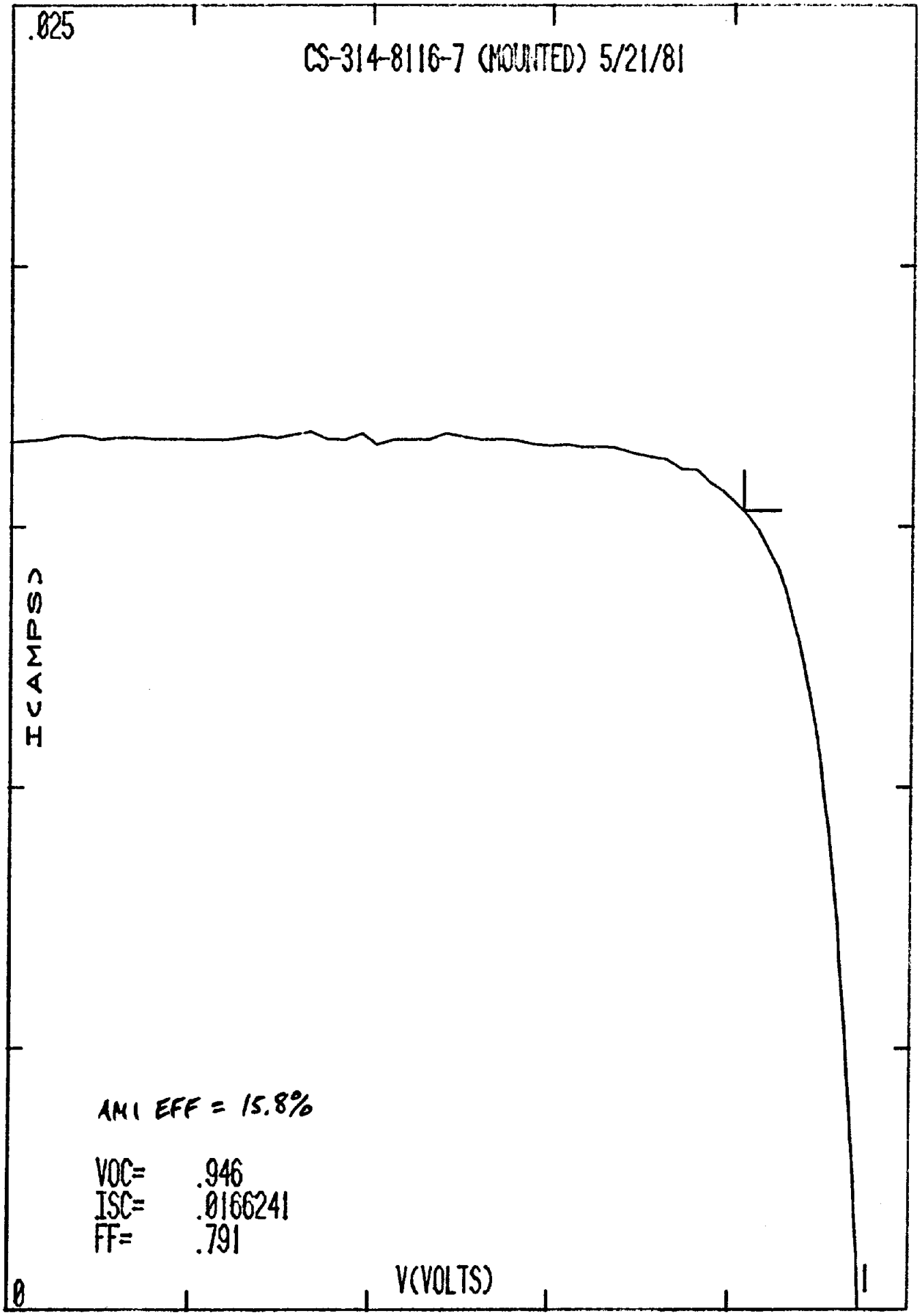
.025
CS-314-8116-7 (MOUNTED) 5/21/81
I(AMPS)
AM1 EFF = 15.8%
VOC= .946
ISC= .0166241
FF= .791
V(VOLTS)
0
1

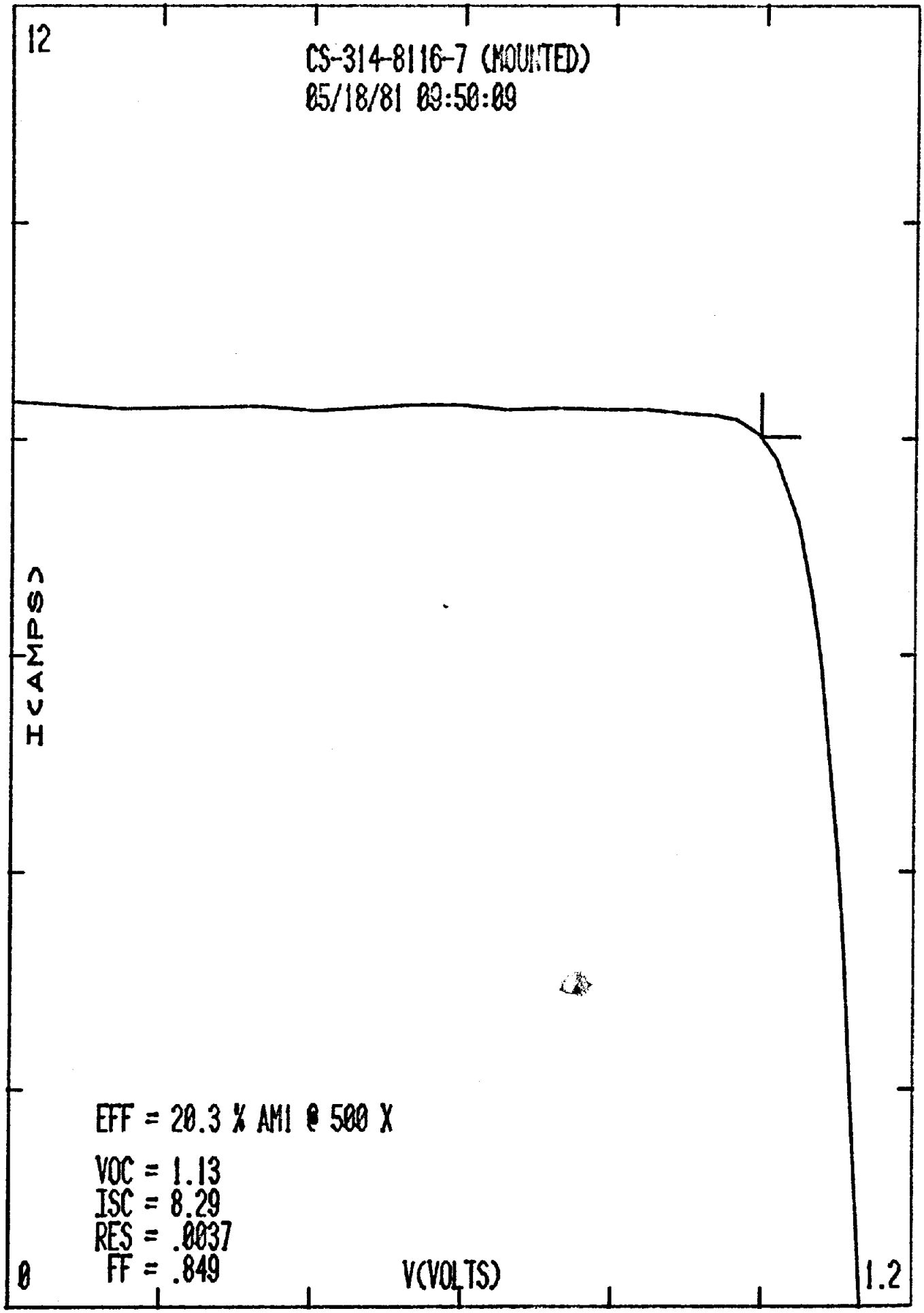
12
CS-314-8116-7 (MOUNTED)
05/18/81 09:50:09
I(AMPS)
EFF = 20.3 % AM1 @ 500 X
VOC = 1.13
ISC = 8.29
RES = .0037
FF = .849
0
V(VOLTS)
1.2

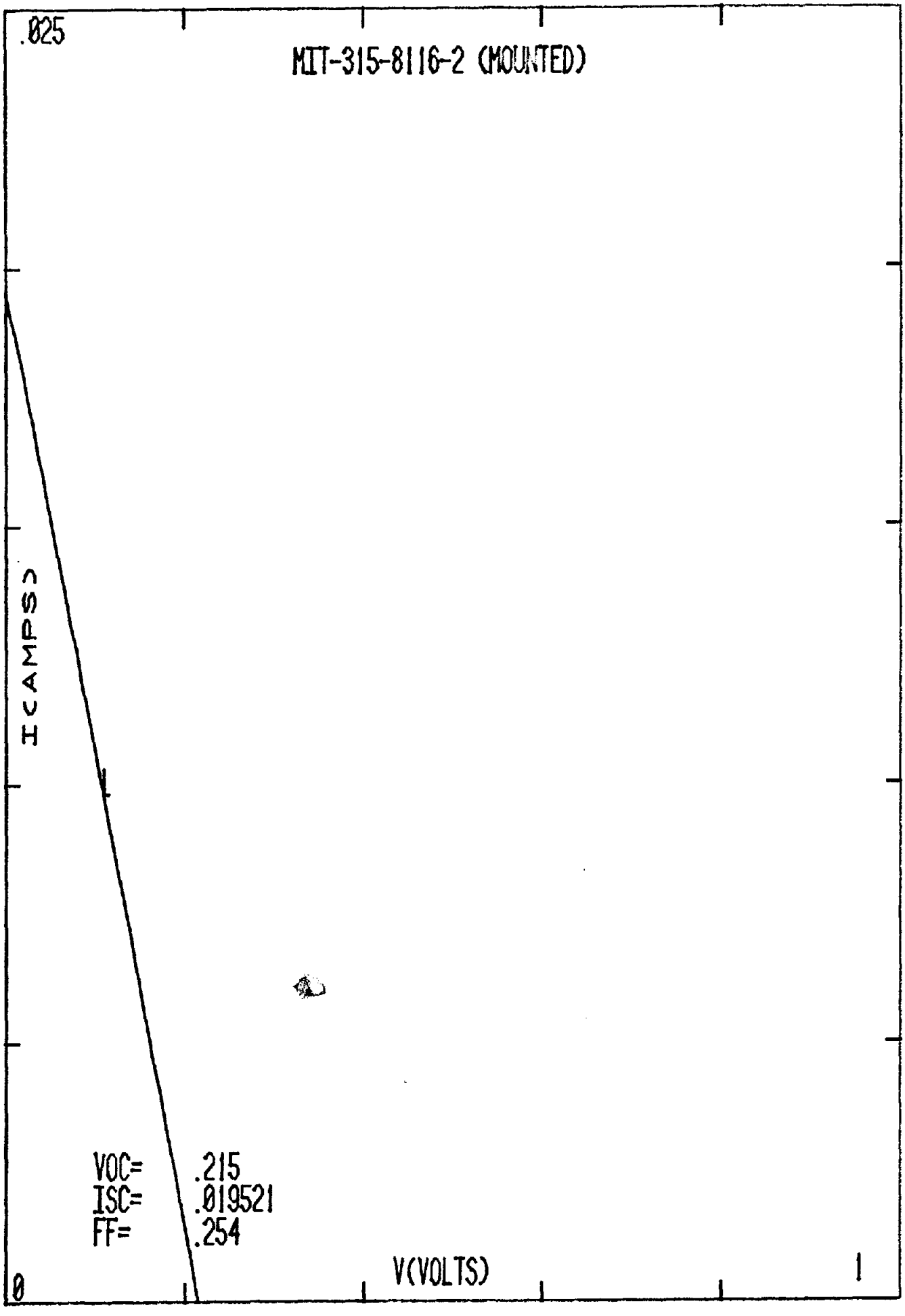
.025
MIT-315-8116-2 (MOUNTED)
I(AMPS)
VOC= .215
ISC= .019521
FF= .254
V(VOLTS)
0
1

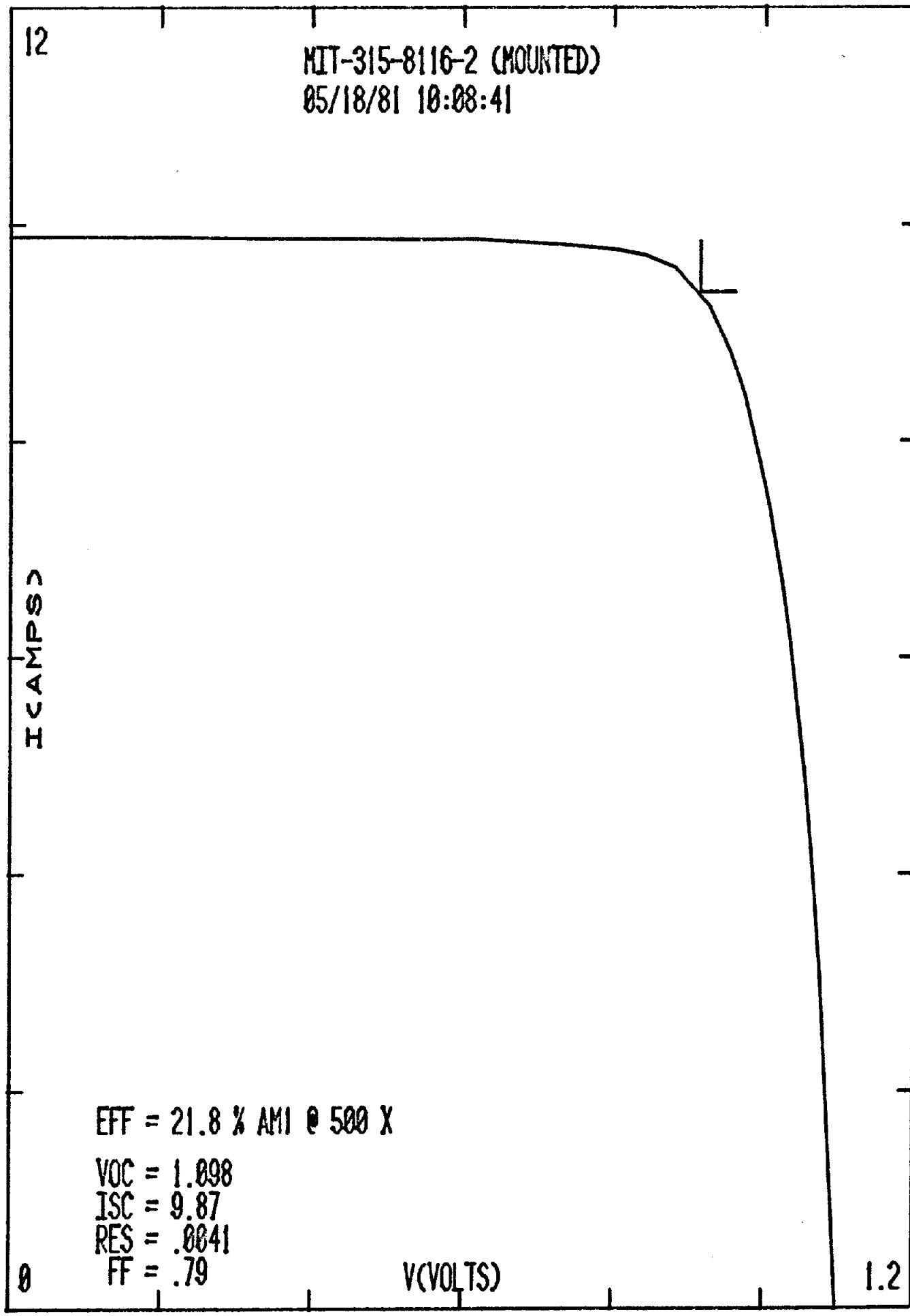
12
MIT-315-8116-2 (MOUNTED)
05/18/81 10:08:41
I(AMPS)
EFF = 21.8 % AM1 @ 500 X
VOC = 1.098
ISC = 9.87
RES = .0041
FF = .79
0
V(VOLTS)
1.2

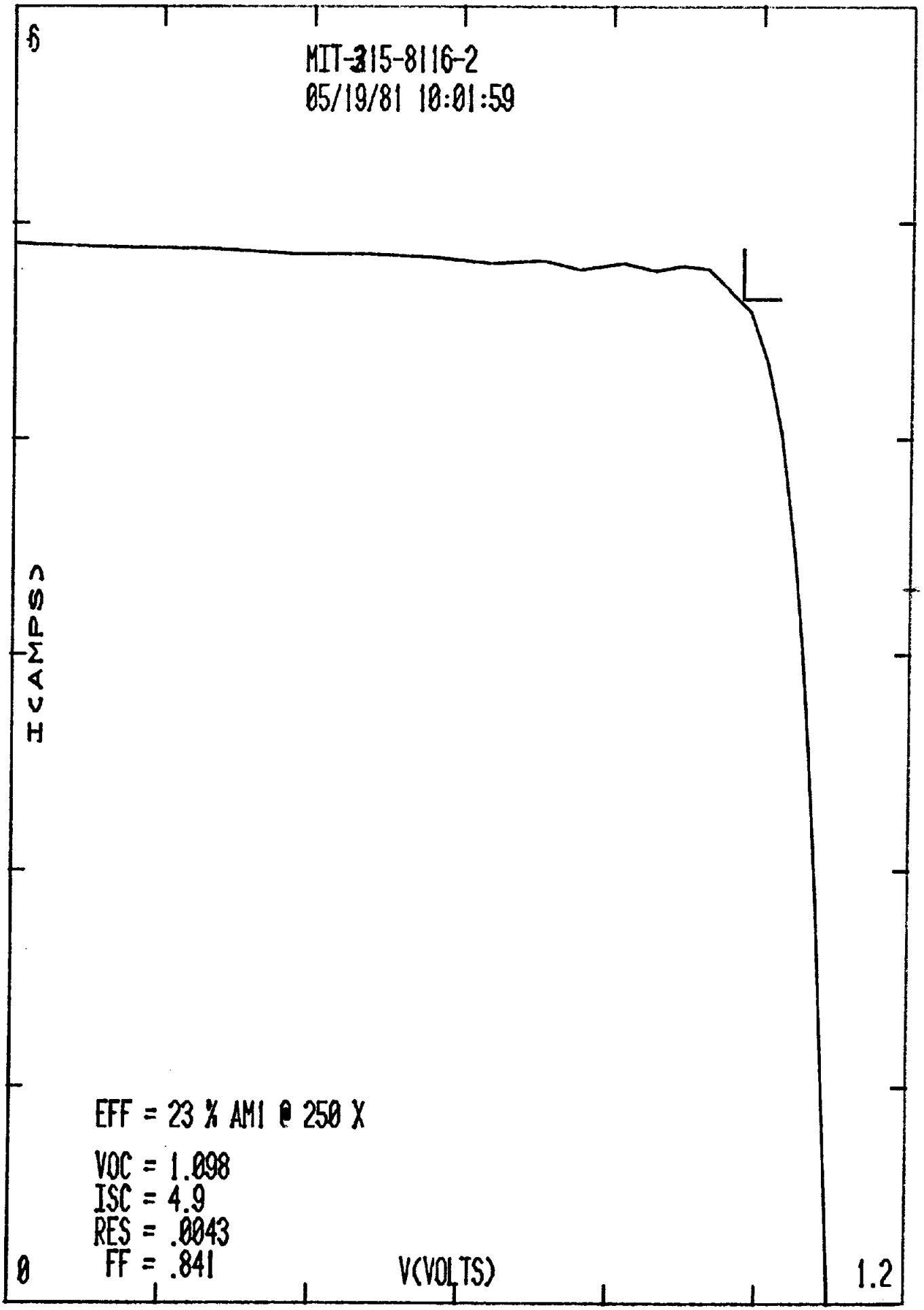
6
MIT-315-8116-2
05/19/81 10:01:59
I(AMPS)
EFF = 23 % AM1 @ 250 X
VOC = 1.098
ISC = 4.9
RES = .0043
FF = .841
0
V(VOLTS)
1.2

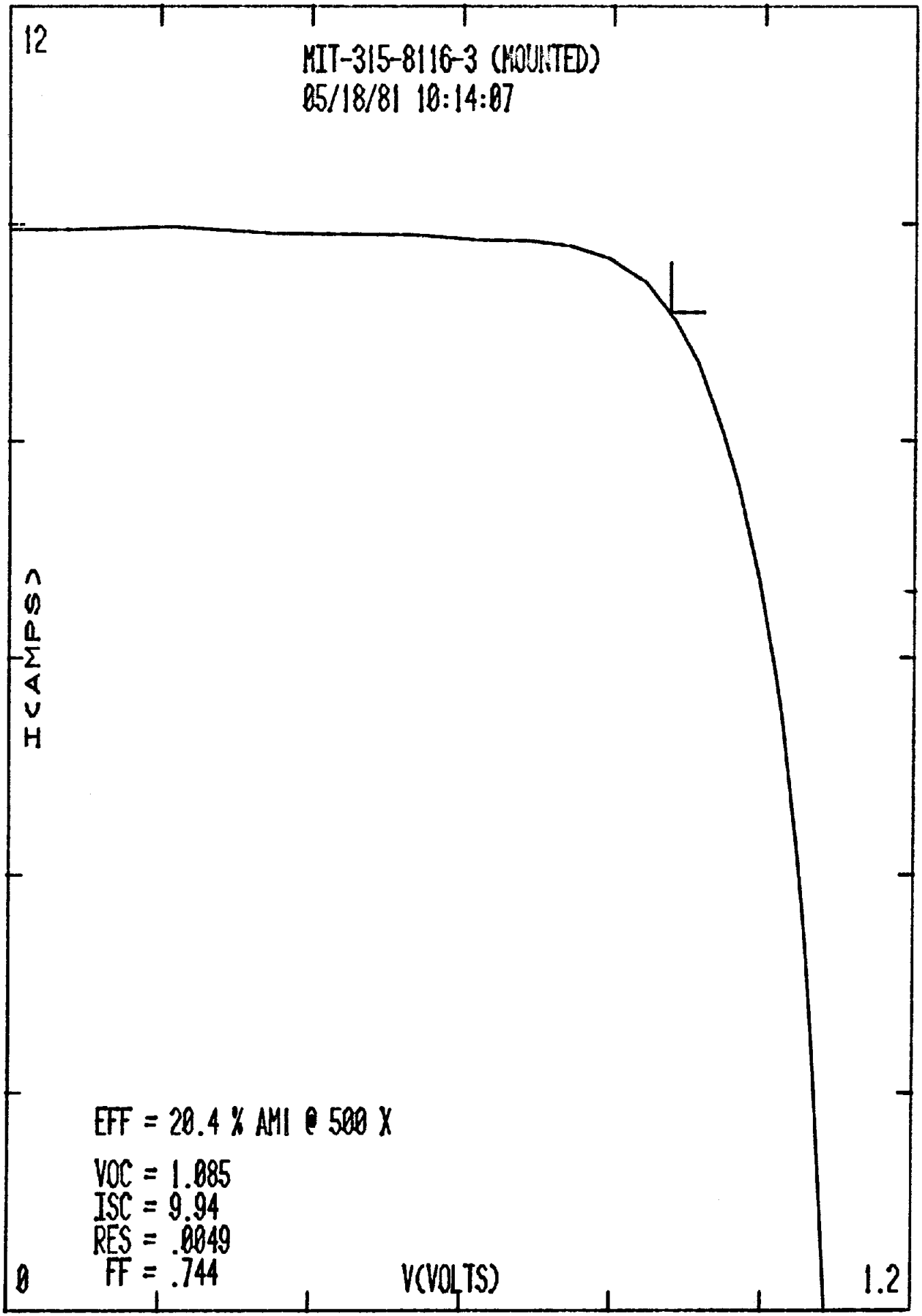
12
MIT-315-8116-3 (MOUNTED)
05/18/81 10:14:07
I(AMPS)
EFF = 20.4 % AMI @ 500 X
VOC = 1.085
ISC = 9.94
RES = .0049
FF = .744
0
V(VOLTS)
1.2

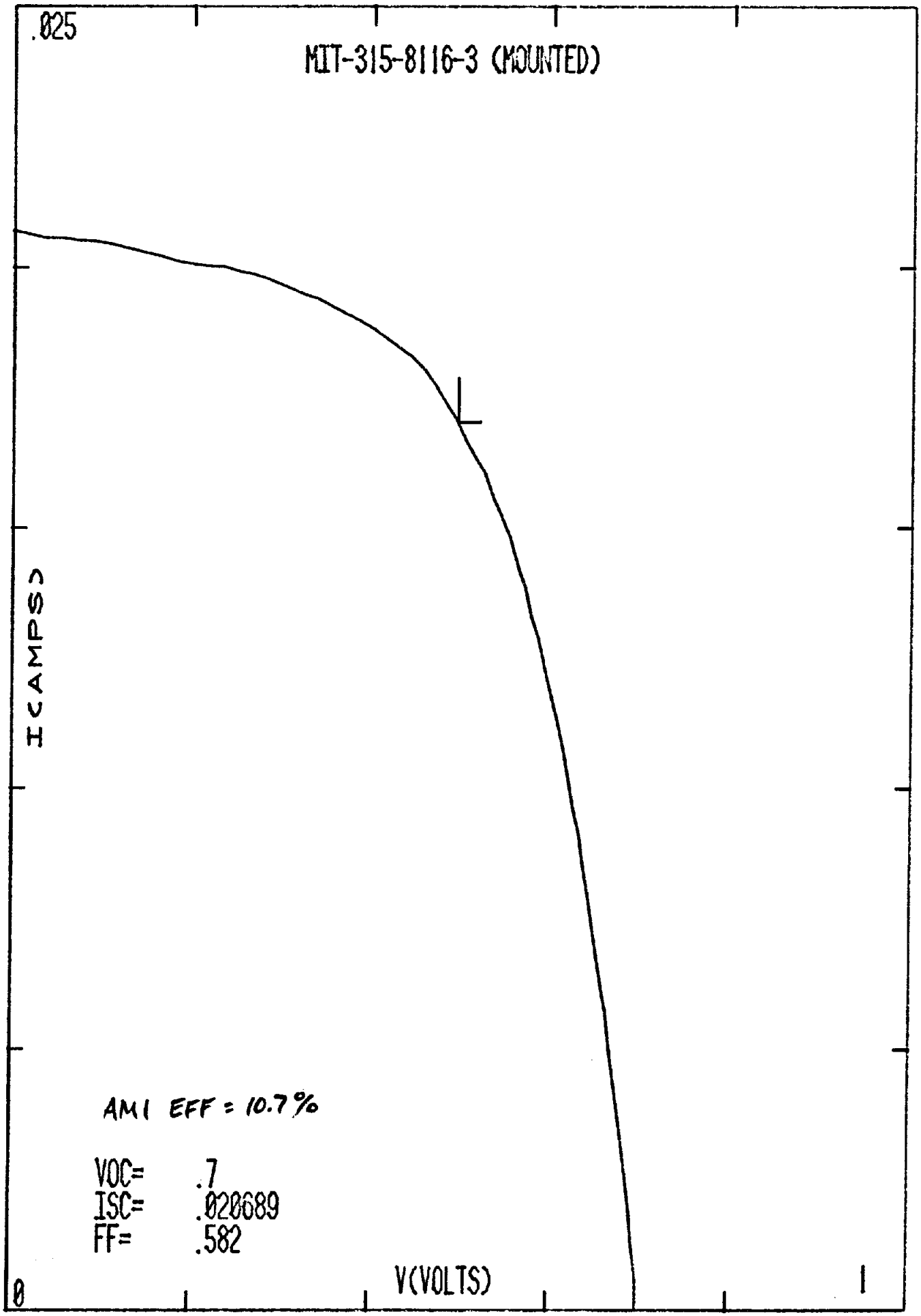
.025
MIT-315-8116-3 (MOUNTED)
I(AMPS)
AM1 EFF = 10.7%
VOC= .7
ISC= .020689
FF= .582
V(VOLTS)
0
1

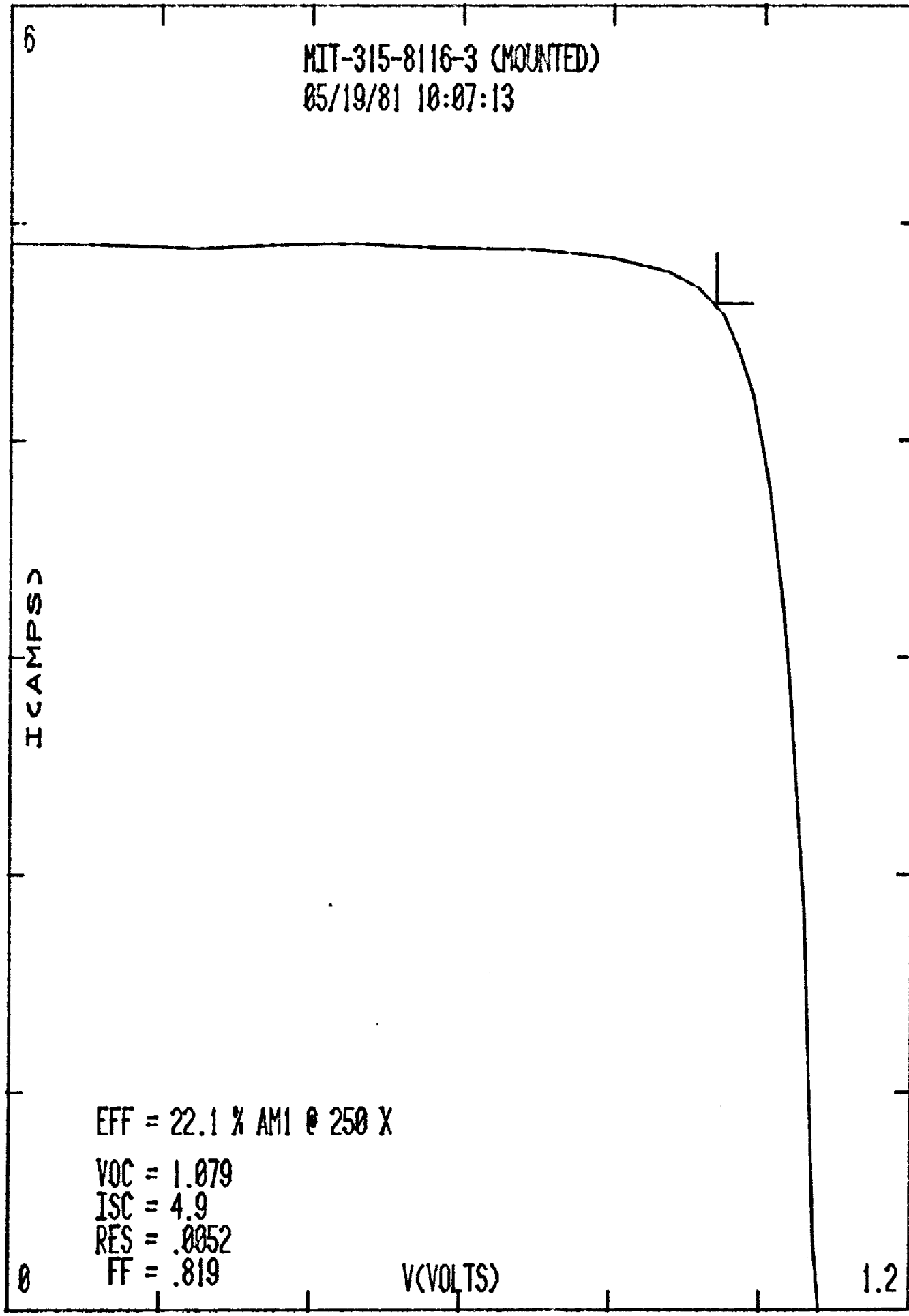
6
MIT-315-8116-3 (MOUNTED)
05/19/81 10:07:13
I(AMPS)
EFF = 22.1 % AM1 @ 250 X
VOC = 1.079
ISC = 4.9
RES = .0052
FF = .819
0
V(VOLTS)
1.2

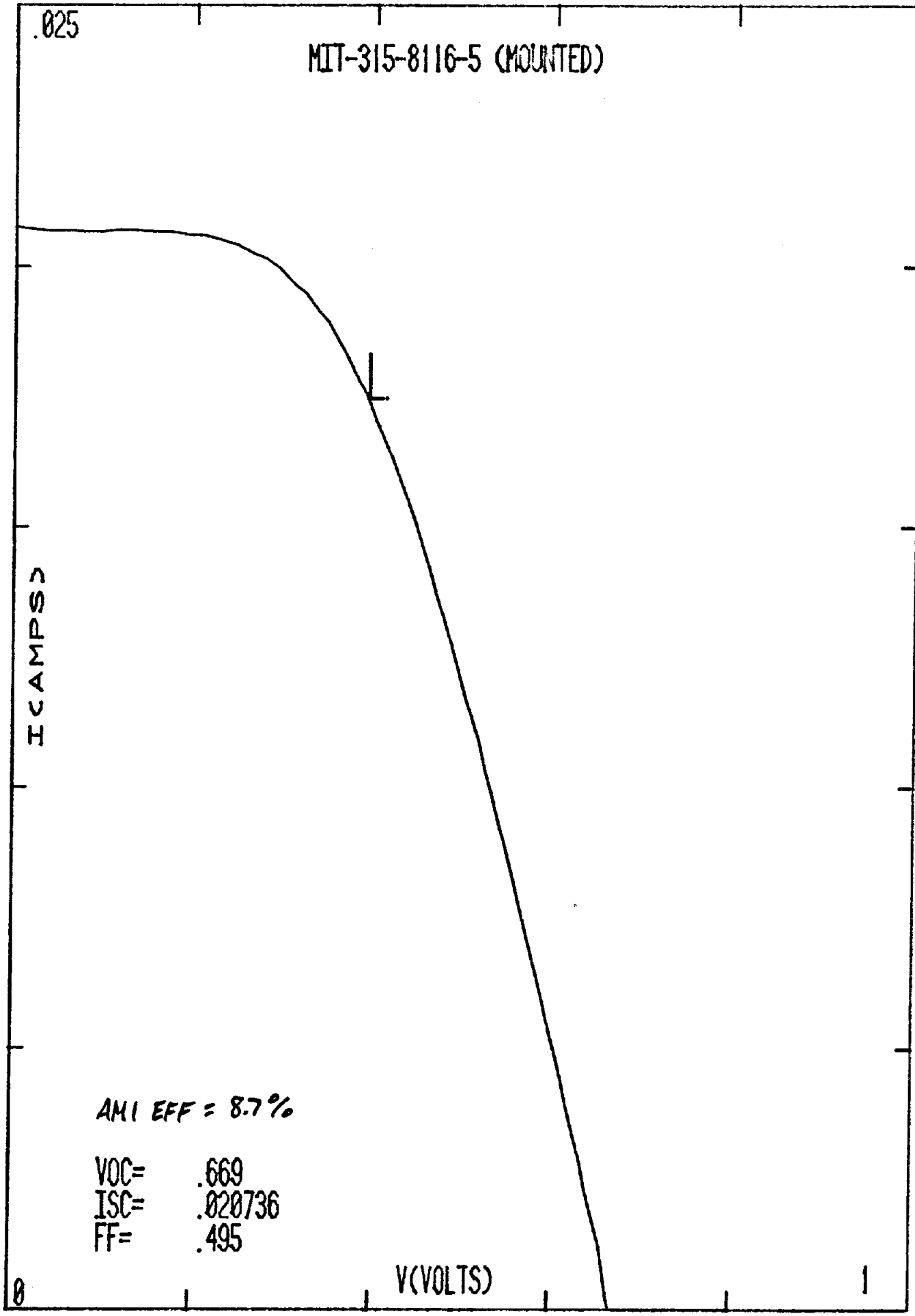
.025
MIT-315-8116-5 (MOUNTED)
I(AMPS)
AM1 EFF = 8.7%
VOC= .669
ISC= .020736
FF= .495
V(VOLTS)
0
1

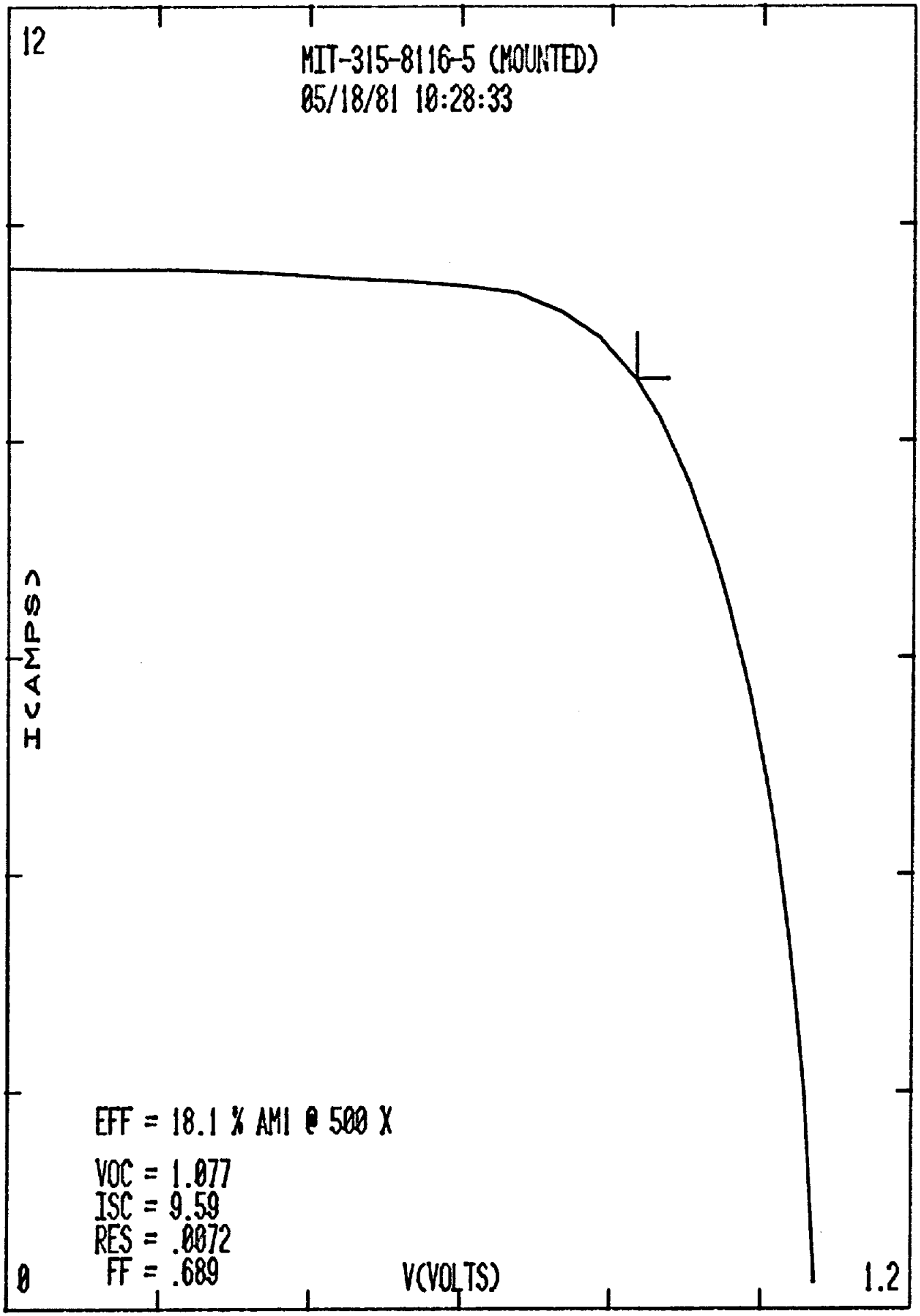
12
MIT-315-8116-5 (MOUNTED)
05/18/81 10:28:33
I(AMPS)
EFF = 18.1 % AMI @ 500 X
VOC = 1.077
ISC = 9.59
RES = .0072
FF = .689
0
V(VOLTS)
1.2

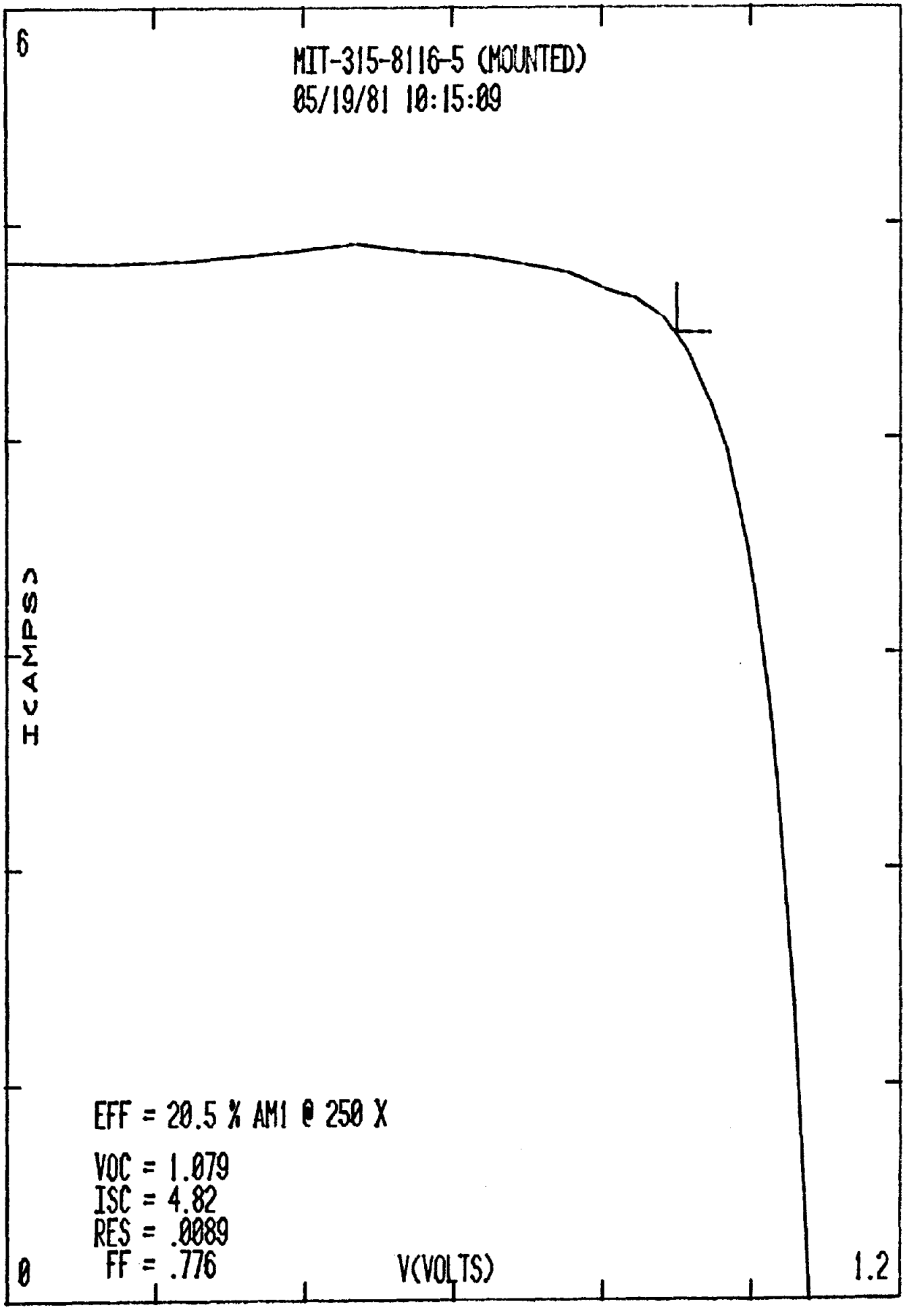
6
MIT-315-8116-5 (MOUNTED)
05/19/81 10:15:09
I(AMPS)
EFF = 20.5 % AM1 @ 250 X
VOC = 1.079
ISC = 4.82
RES = .0089
FF = .776
0
V(VOLTS)
1.2

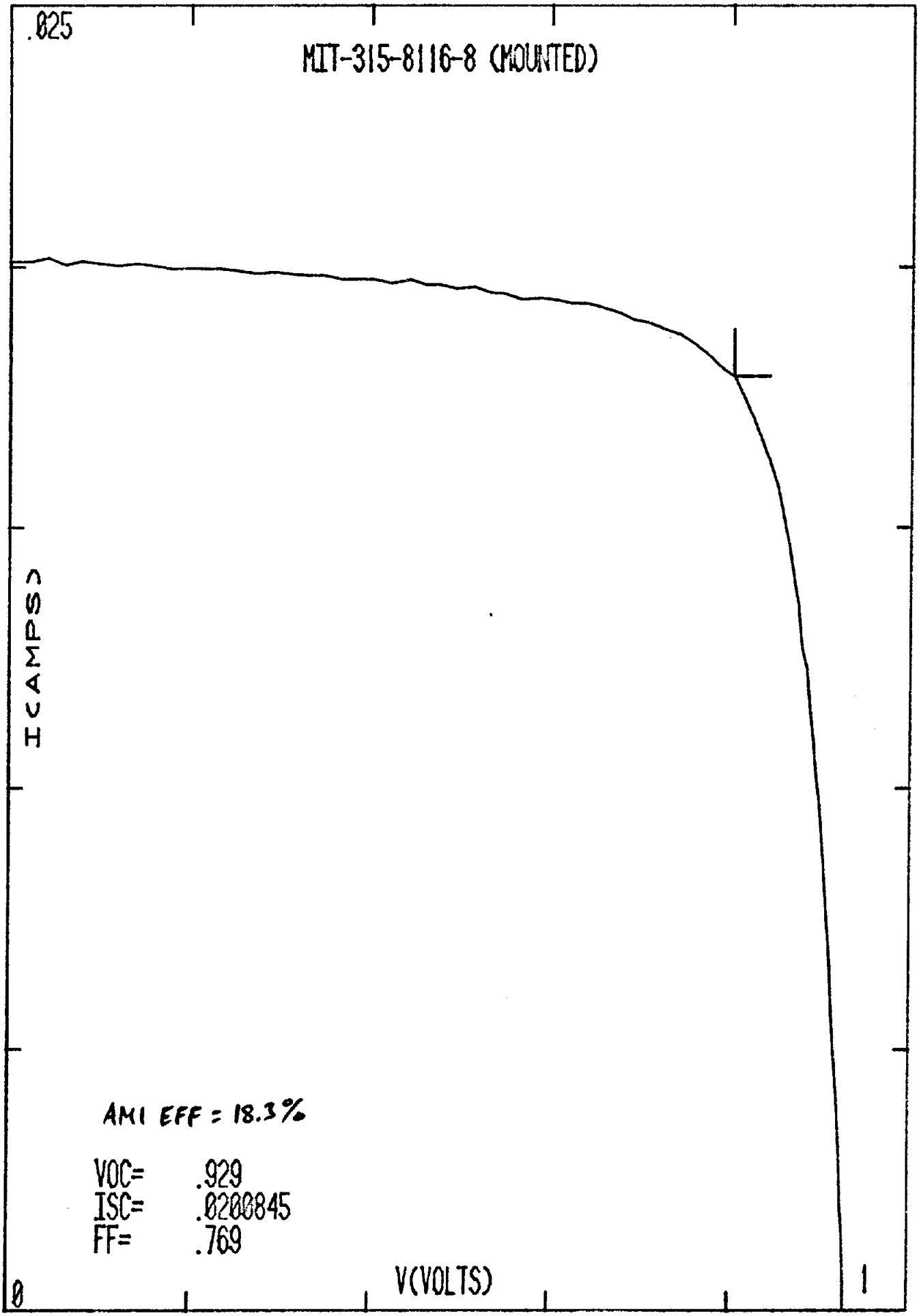
.025
MIT-315-8116-8 (MOUNTED)
I(AMPS)
AMI EFF = 18.3%
VOC= .929
ISC= .0200845
FF= .769
V(VOLTS)
0
1

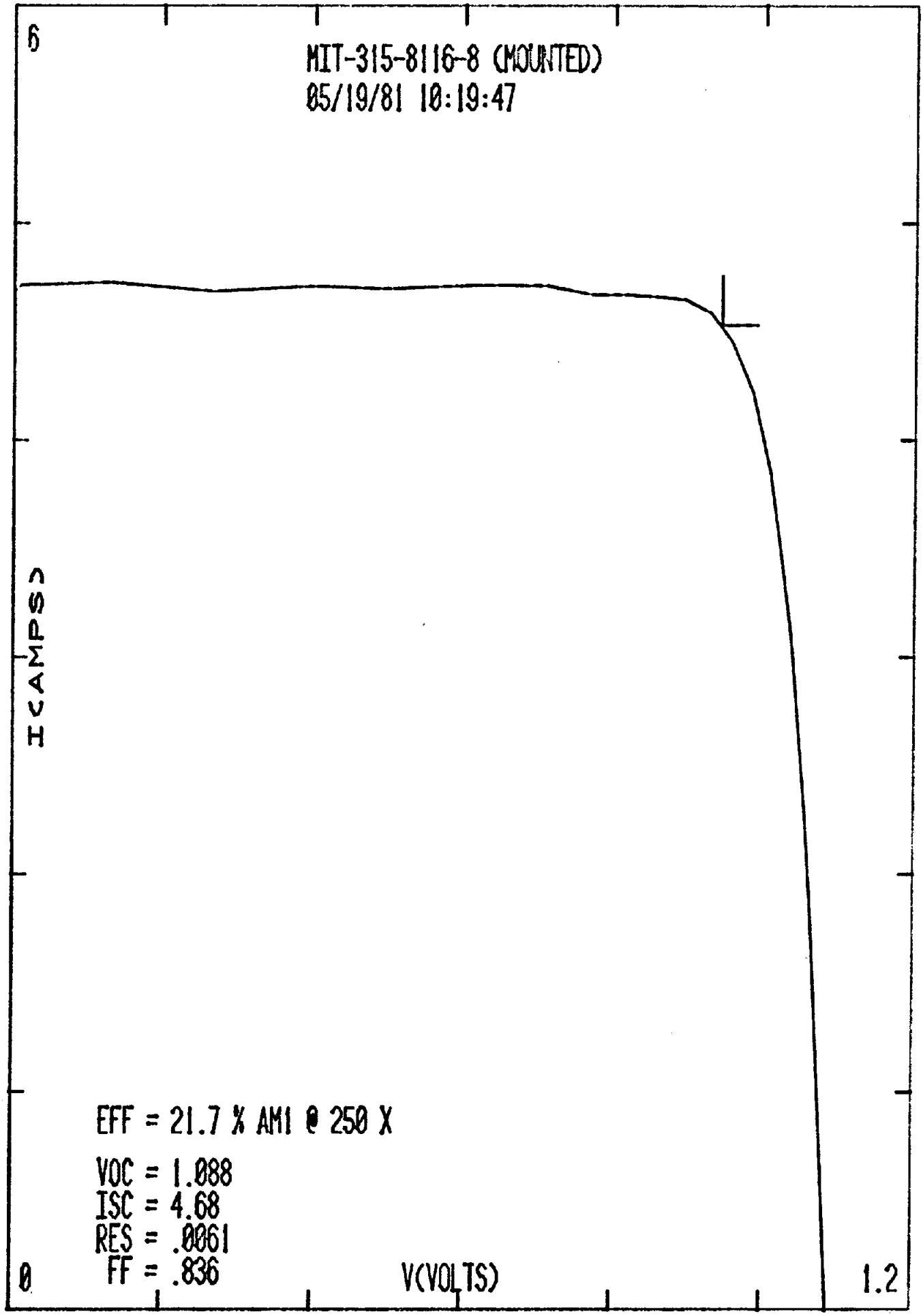
6
MIT-315-8116-8 (MOUNTED)
05/19/81 10:19:47
I(AMPS)
EFF = 21.7 % AM1 @ 250 X
VOC = 1.088
ISC = 4.68
RES = .0061
FF = .836
0
V(VOLTS)
1.2

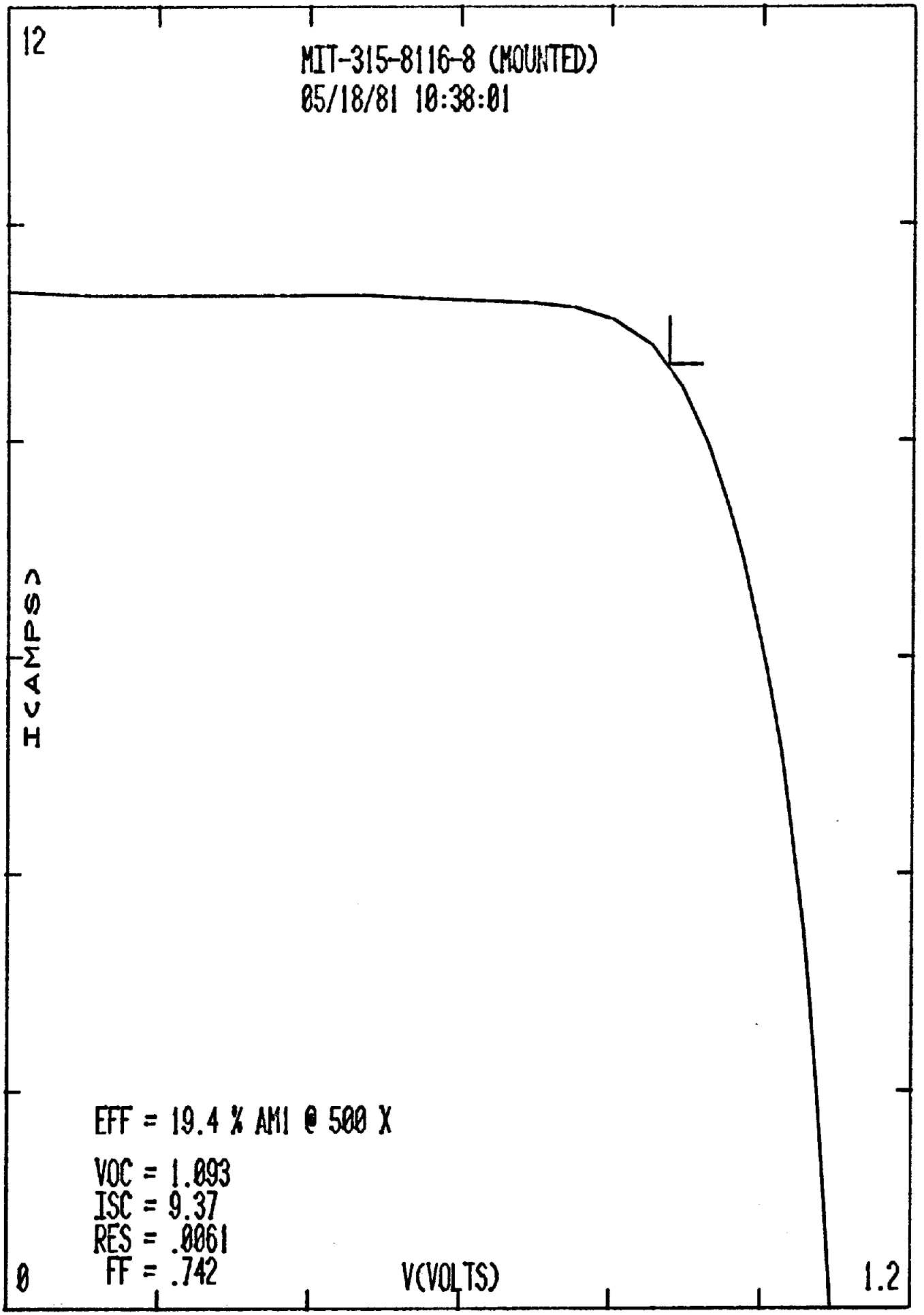
12
MIT-315-8116-8 (MOUNTED)
05/18/81 10:38:01
I(AMPS)
EFF = 19.4 % AM1 @ 500 X
VOC = 1.093
ISC = 9.37
RES = .0061
FF = .742
0
V(VOLTS)
1.2

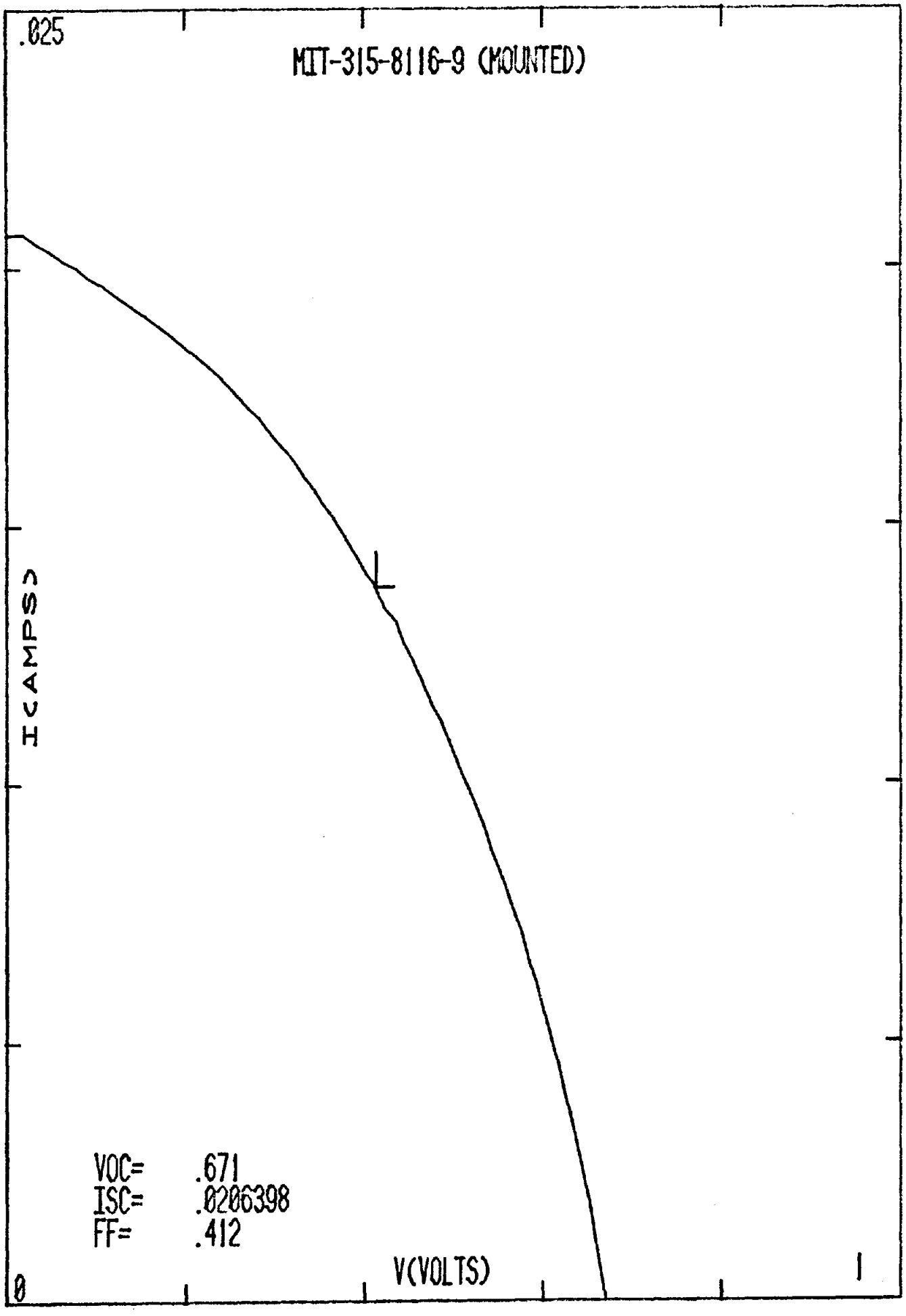
.025
MIT-315-8116-9 (MOUNTED)
I(AMPS)
VOC= .671
ISC= .0206398
FF= .412
V(VOLTS)
0
1

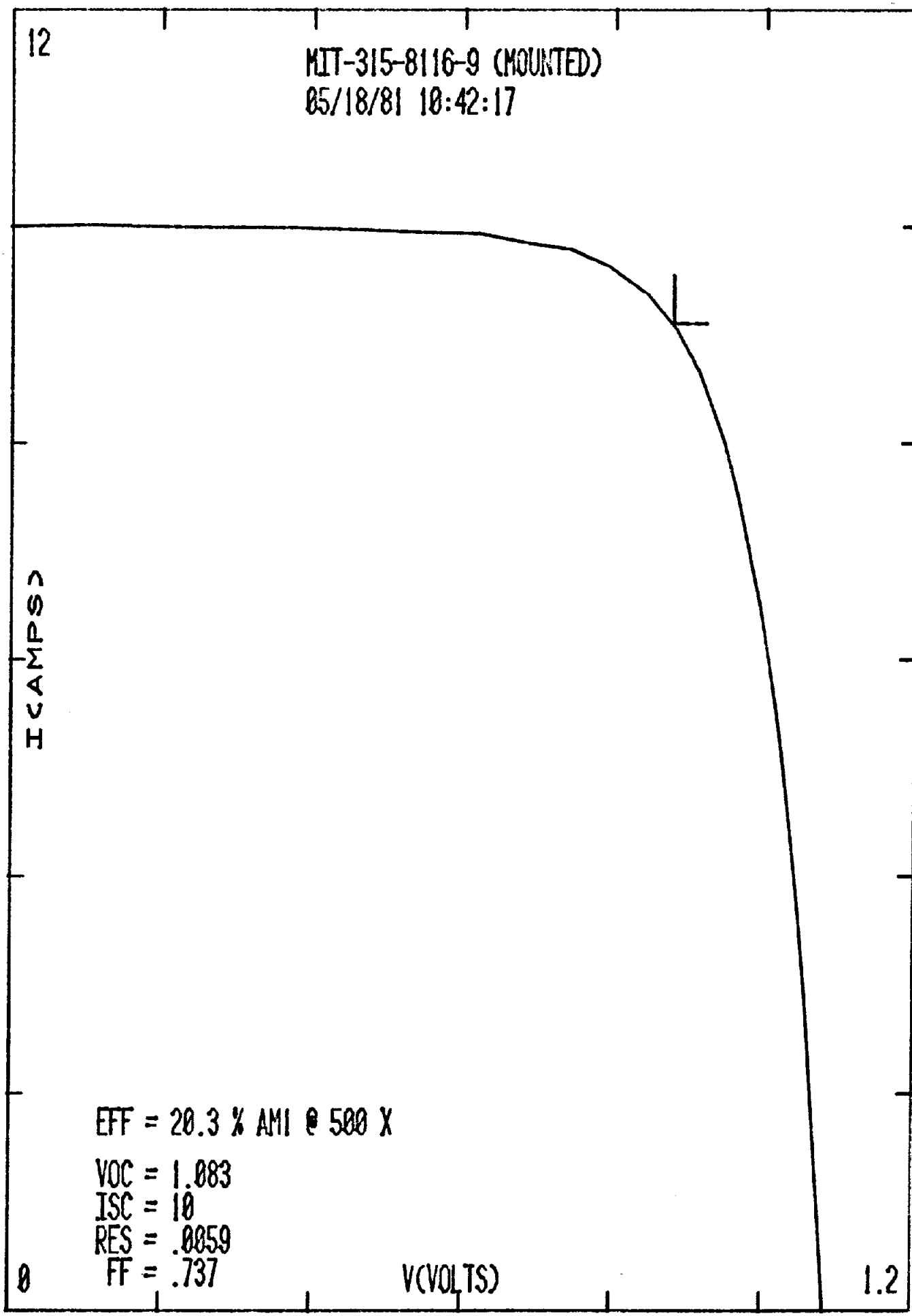
12
MIT-315-8116-9 (MOUNTED)
05/18/81 10:42:17
I(AMPS)
EFF = 20.3 % AM1 @ 500 X
VOC = 1.083
ISC = 10
RES = .0059
FF = .737
0
V(VOLTS)
1.2

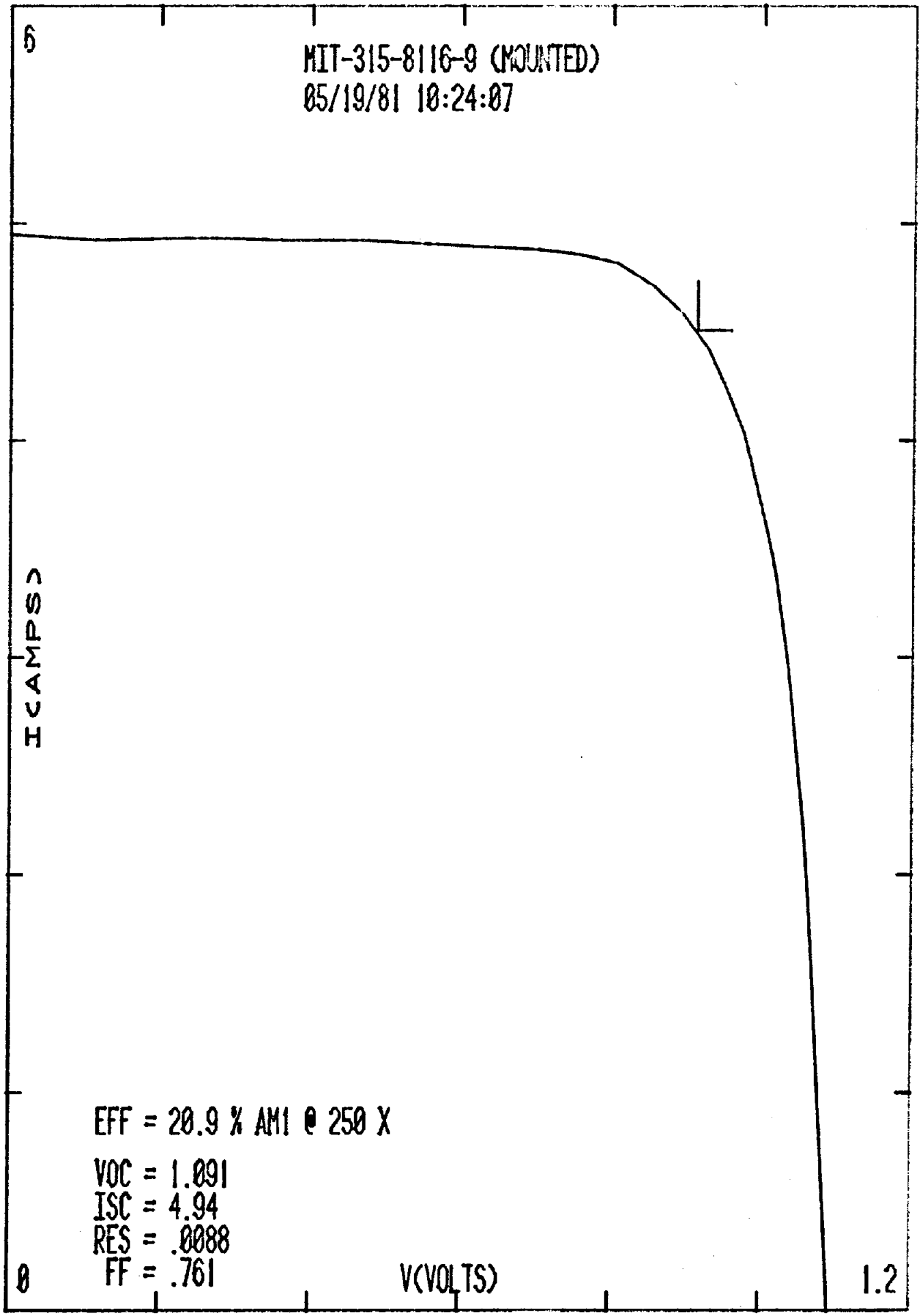
6
MIT-315-8116-9 (MOUNTED)
05/19/81 10:24:07
I(AMPS)
EFF = 20.9 % AM1 @ 250 X
VOC = 1.091
ISC = 4.94
RES = .0088
FF = .761
0
V(VOLTS)
1.2

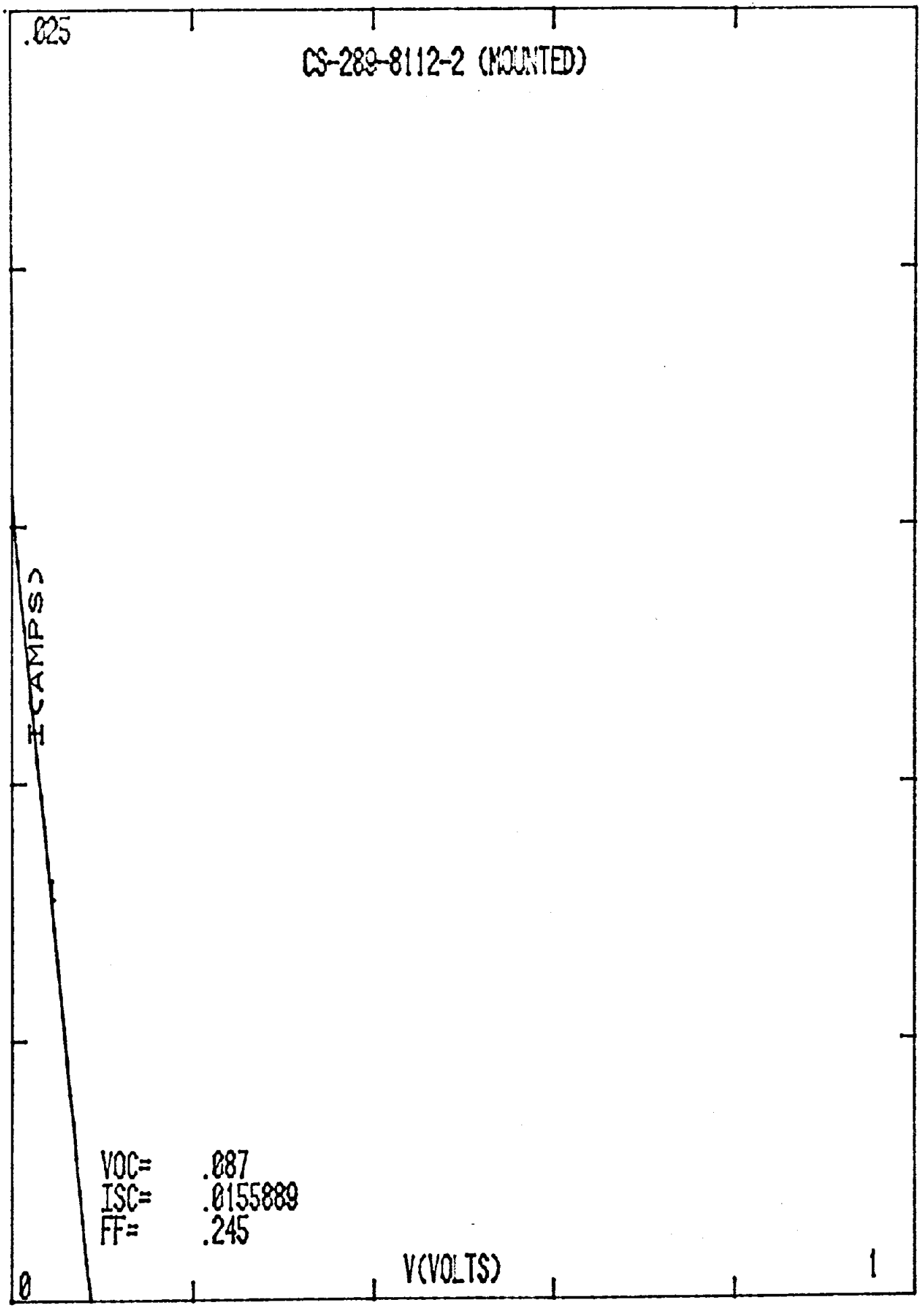
.025
CS-289-8112-2 (MOUNTED)
I(AMPS)
VOC= .087
ISC= .0155889
FF= .245
V(VOLTS)
0
1

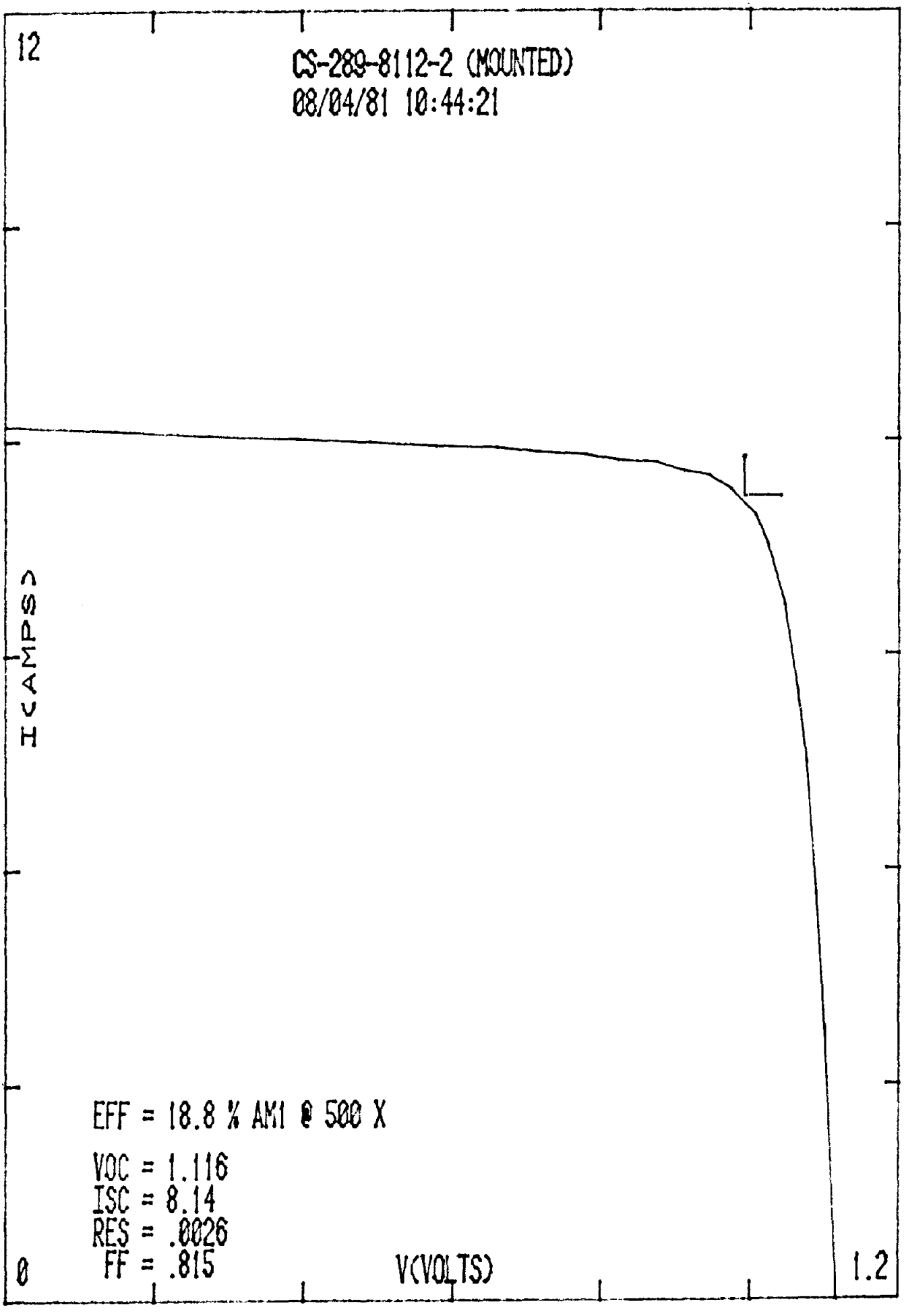
12
CS-289-8112-2 (MOUNTED)
08/04/81 10:44:21
I(AMPS)
EFF = 18.8 % AM1 @ 500 X
VOC = 1.116
ISC = 8.14
RES = .0026
FF = .815
0
V(VOLTS)
1.2

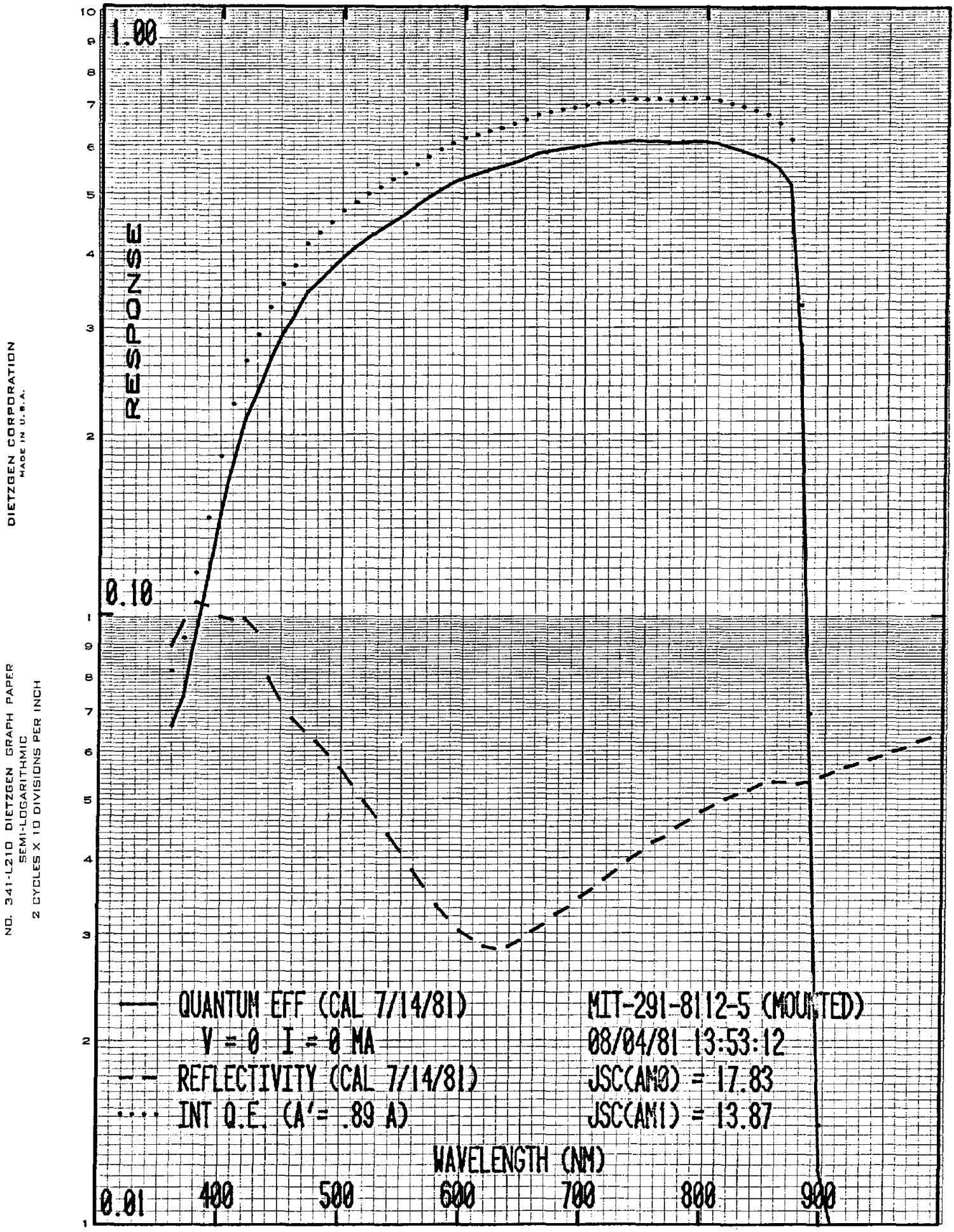
1.00
0.10
0.01
RESPONSE
WAVELENGTH (NM)
400
500
600
700
800
900
QUANTUM EFF (CAL 7/14/81)
V = 0 I = 0 MA
REFLECTIVITY (CAL 7/14/81)
INT Q.E. (A' = .89 A)
MIT-291-8112-5 (MOUNTED)
08/04/81 13:53:12
JSC(AM0) = 17.83
JSC(AM1) = 13.87
DIETZGEN CORPORATION
MADE IN U.S.A.
NO. 341-L210 DIETZGEN GRAPH PAPER
SEMI-LOGARITHMIC
2 CYCLES X 10 DIVISIONS PER INCH

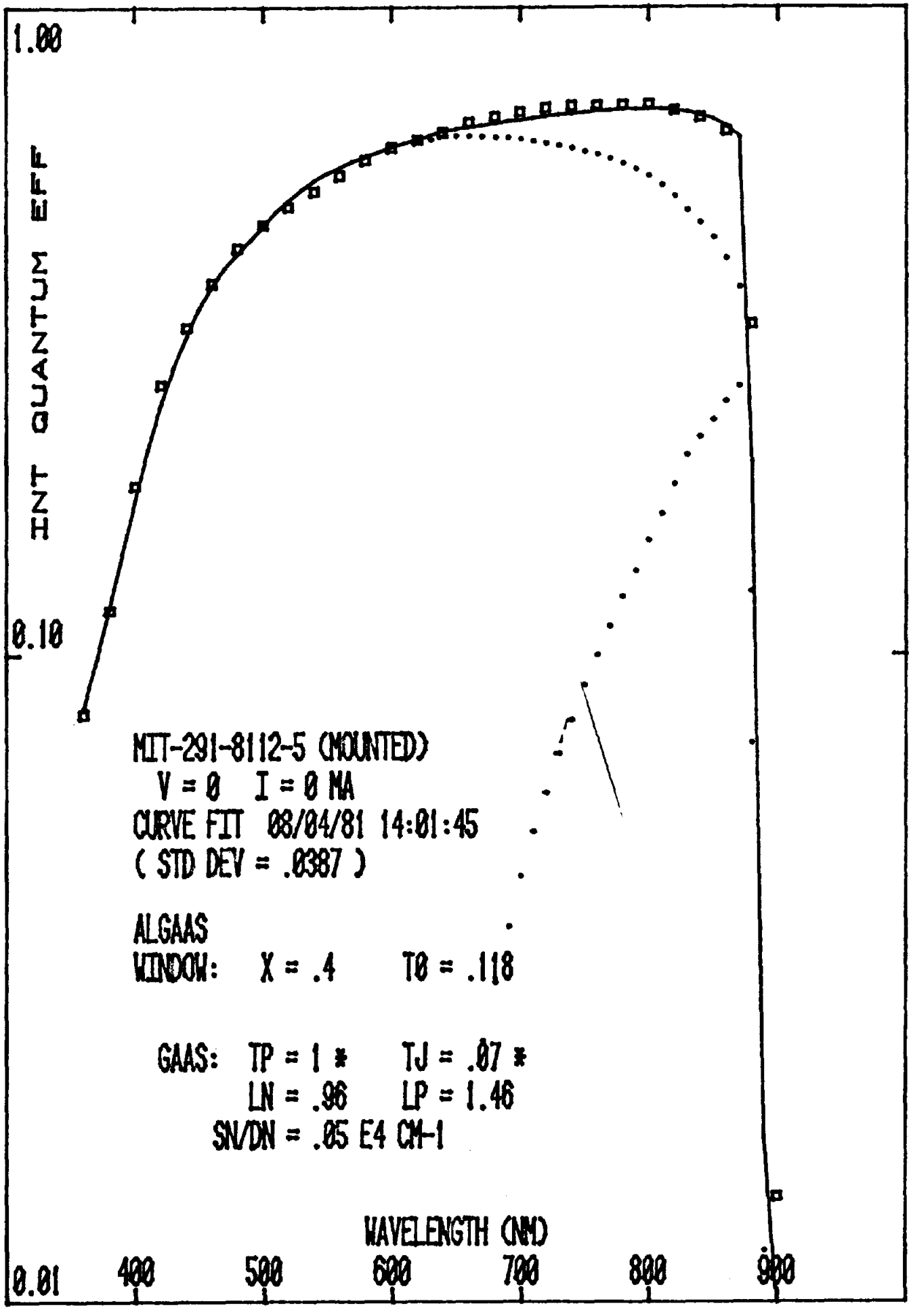
1.00
0.10
0.01
INT QUANTUM EFF
MIT-291-8112-5 (MOUNTED)
V = 0 I = 0 MA
CURVE FIT 08/04/81 14:01:45
(STD DEV = .0387)
ALGAAS
WINDOW: X = .4 T0 = .118
GAAS: TP = 1 * TJ = .07 *
LN = .96 LP = 1.46
SN/DN = .05 E4 CM-1
WAVELENGTH (NM)
400
500
600
700
800
900

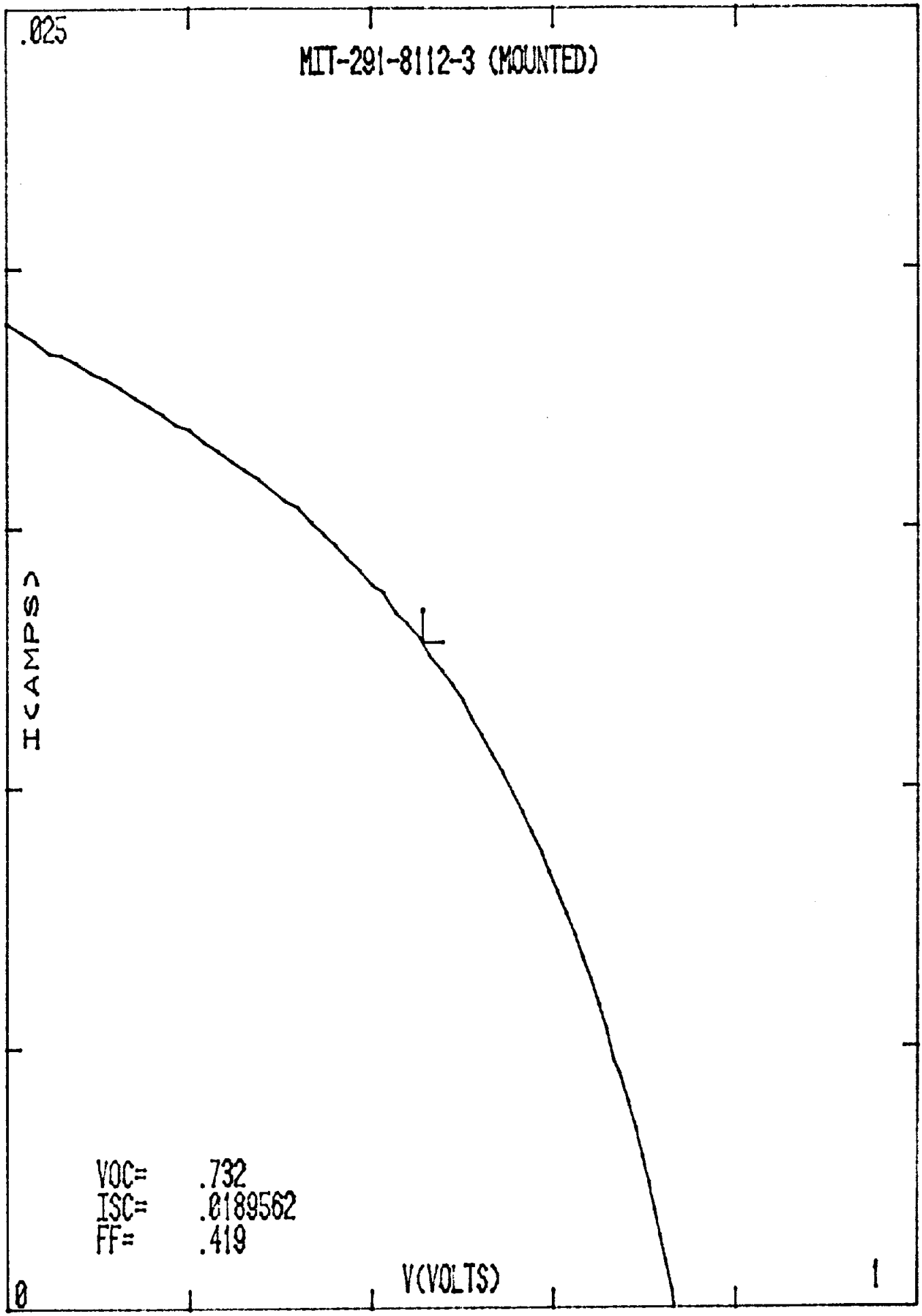
.025
MIT-291-8112-3 (MOUNTED)
I(AMPS)
VOC= .732
ISC= .0189562
FF= .419
V(VOLTS)
0
1

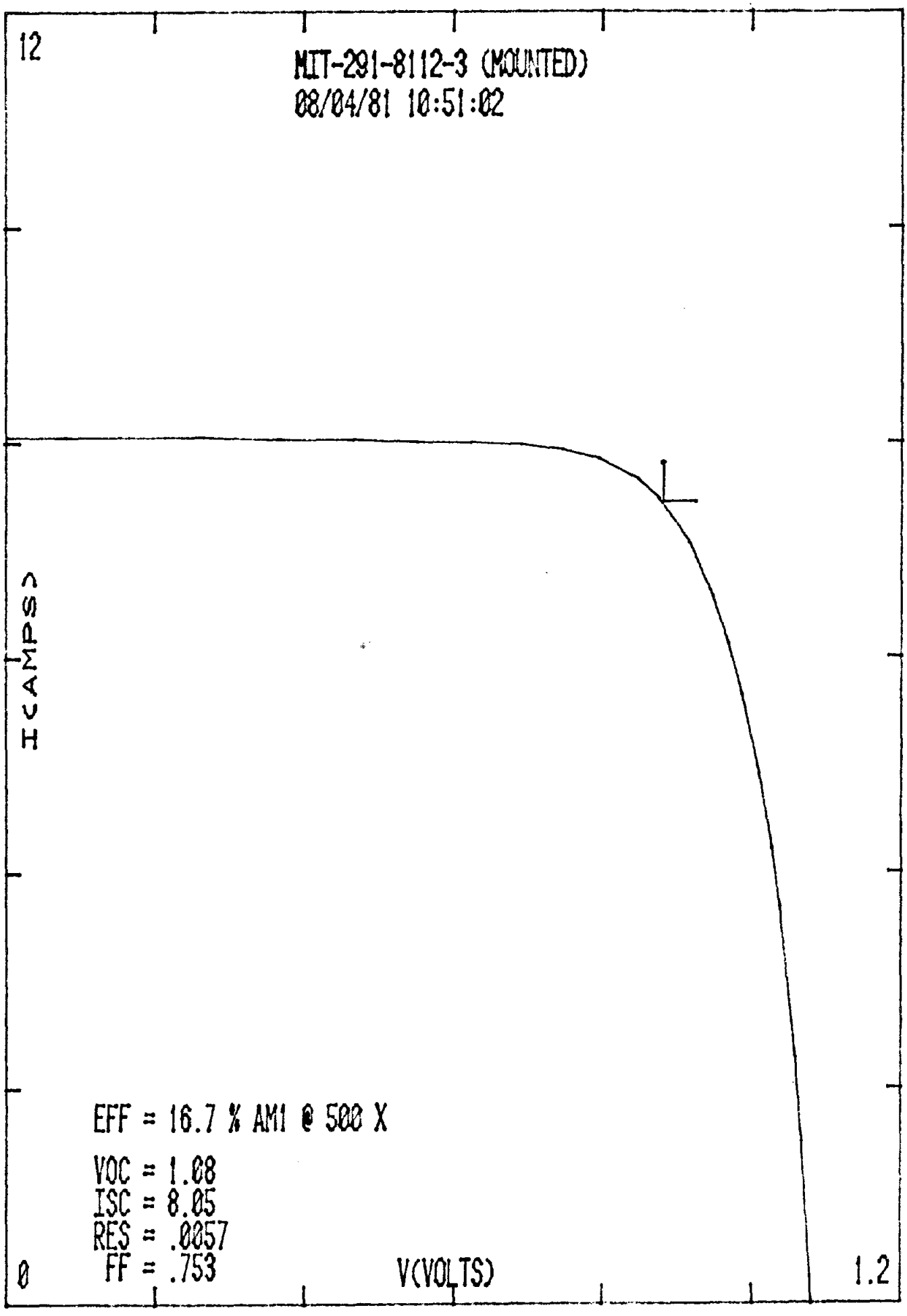
12
MIT-291-8112-3 (MOUNTED)
08/04/81 10:51:02
I(AMPS)
EFF = 16.7 % AM1 @ 500 X
VOC = 1.08
ISC = 8.05
RES = .0057
FF = .753
0
V(VOLTS)
1.2

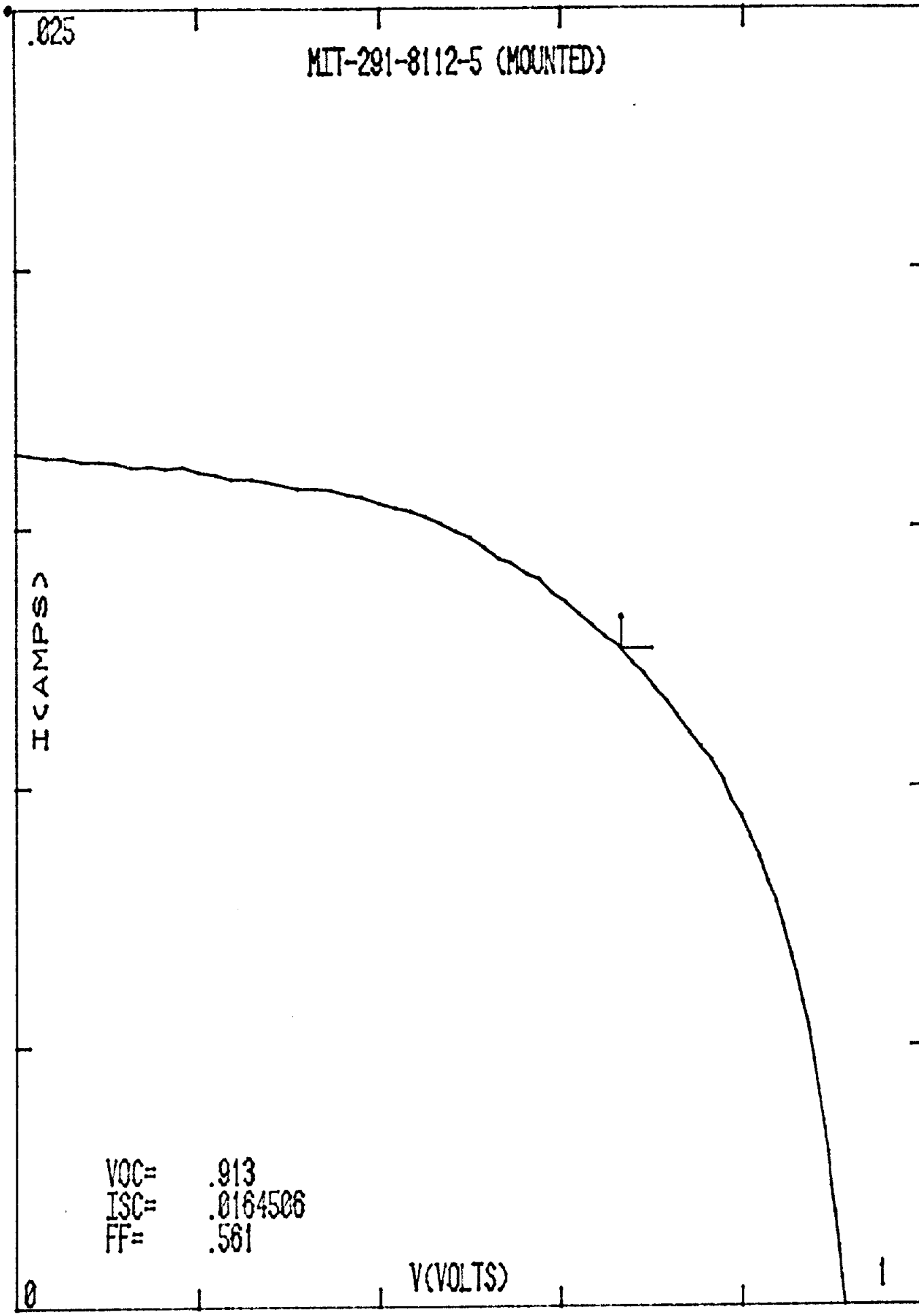
.025
MIT-291-8112-5 (MOUNTED)
I(AMPS)
VOC= .913
ISC= .0164506
FF= .561
V(VOLTS)
0
1

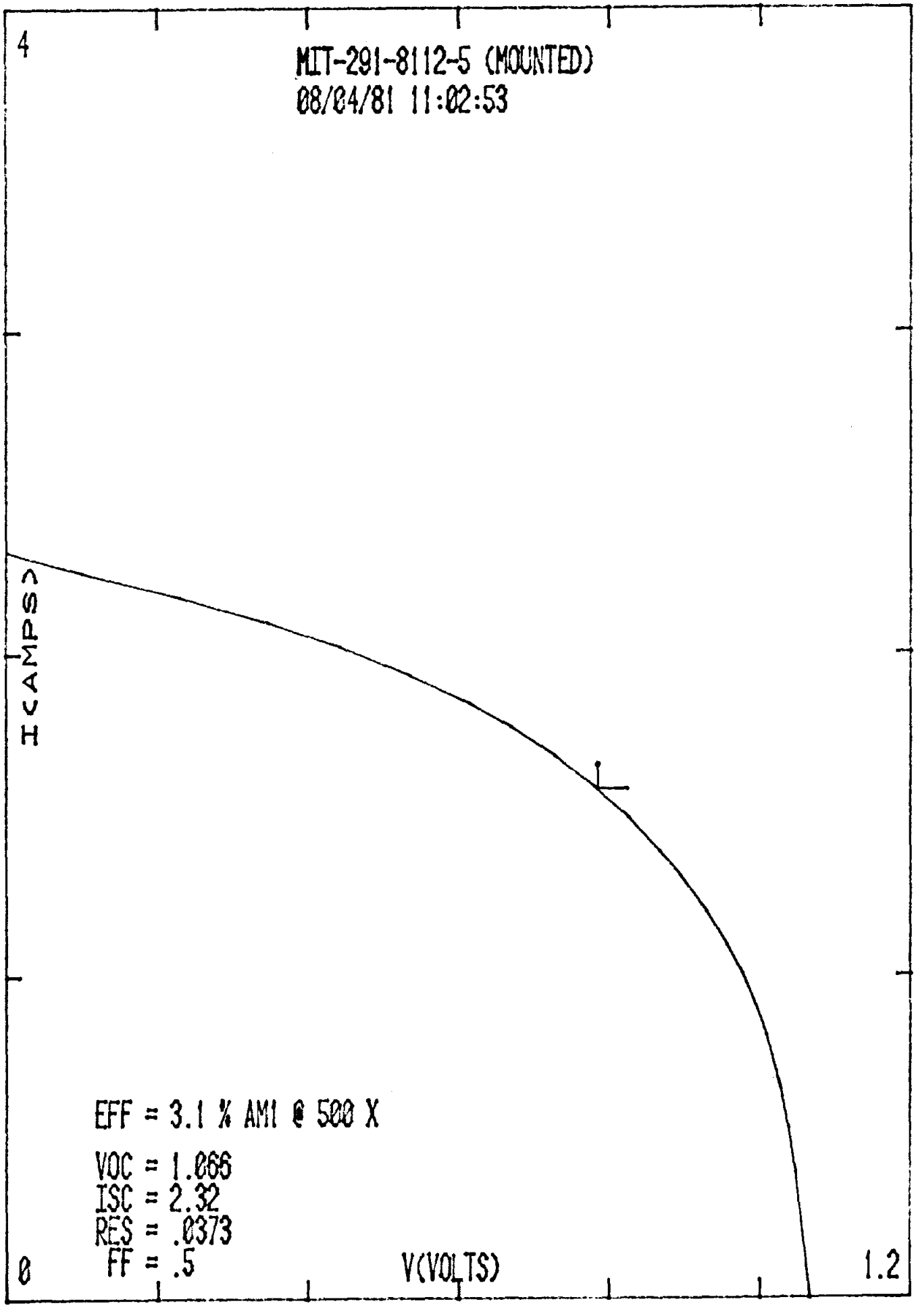
4
MIT-291-8112-5 (MOUNTED)
08/04/81 11:02:53
I(AMPS)
EFF = 3.1 % AM1 @ 500 X
VOC = 1.066
ISC = 2.32
RES = .0373
FF = .5
0
V(VOLTS)
1.2

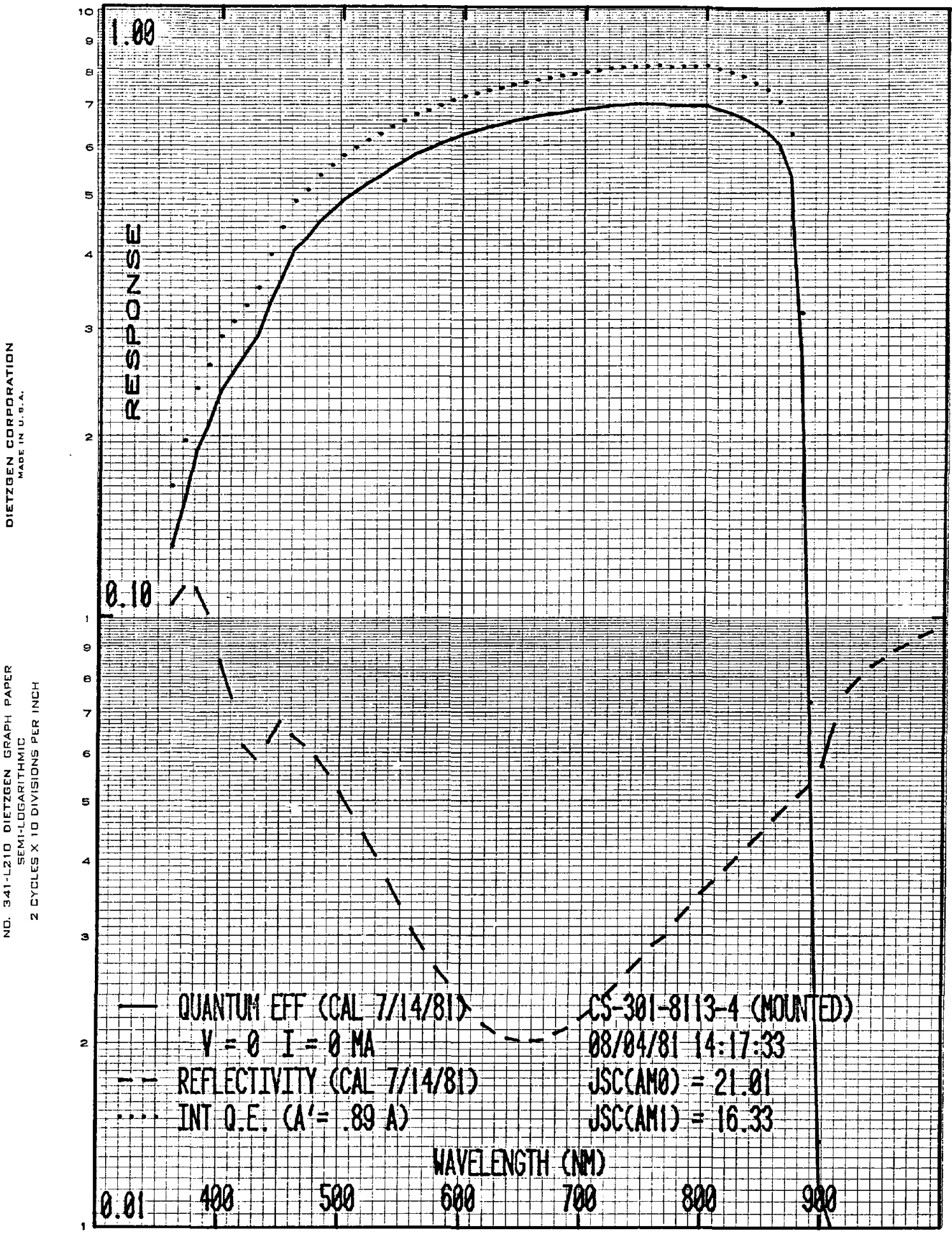
1.00
0.10
0.01
RESPONSE
WAVELENGTH (NM)
400
500
600
700
800
900
QUANTUM EFF (CAL 7/14/81)
V = 0 I = 0 MA
REFLECTIVITY (CAL 7/14/81)
INT Q.E. (A'= .89 A)
CS-301-8113-4 (MOUNTED)
08/04/81 14:17:33
JSC(AM0) = 21.01
JSC(AM1) = 16.33
DIETZGEN CORPORATION
MADE IN U.S.A.
NO. 341-L210 DIETZGEN GRAPH PAPER
SEMI-LOGARITHMIC
2 CYCLES X 10 DIVISIONS PER INCH

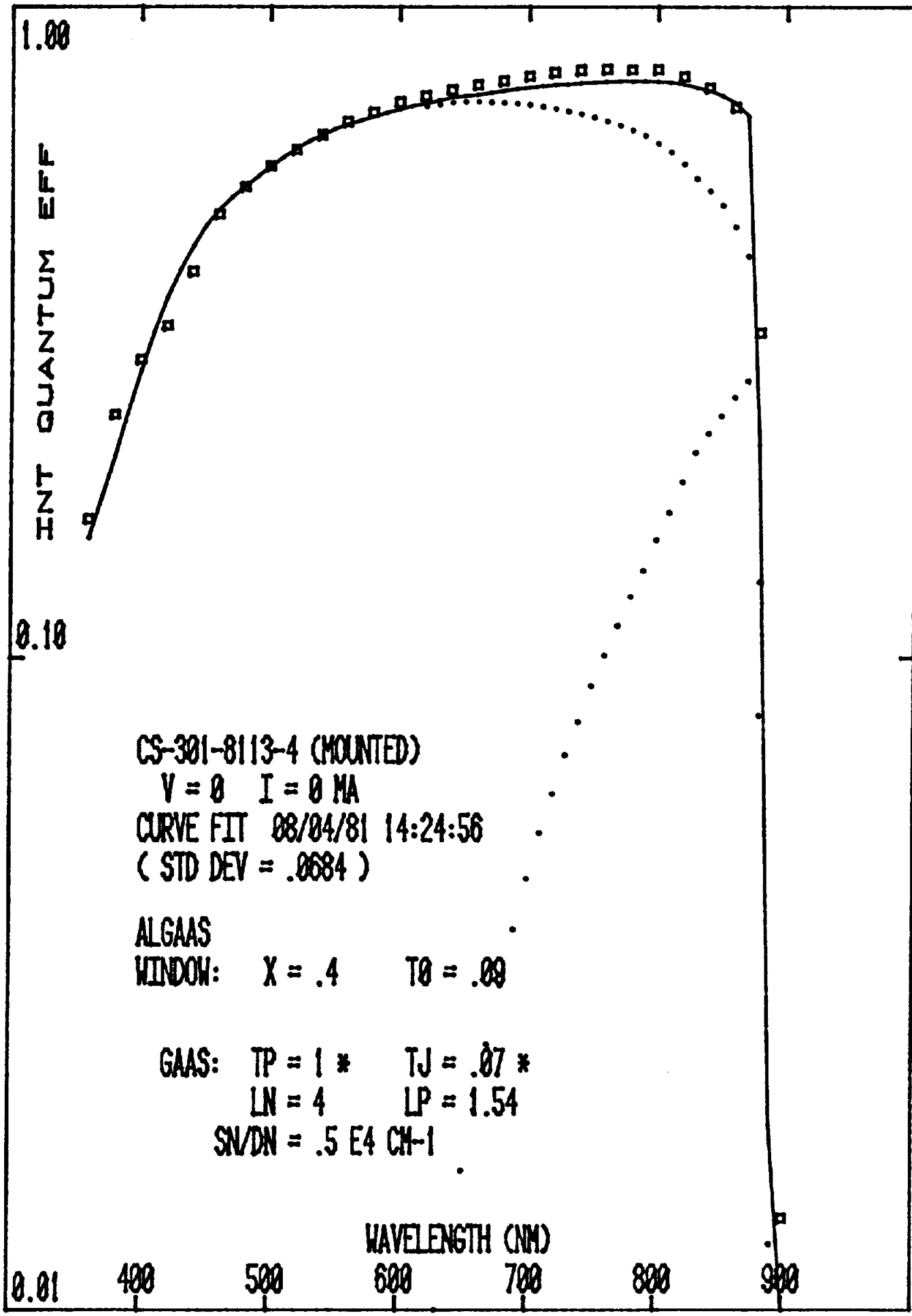
1.00
0.10
0.01
INT QUANTUM EFF
CS-301-8113-4 (MOUNTED)
V = 0 I = 0 MA
CURVE FIT 08/04/81 14:24:56
(STD DEV = .0684)
ALGAAS
WINDOW: X = .4 T0 = .09
GAAS: TP = 1 * TJ = .07 *
LN = 4 LP = 1.54
SN/DN = .5 E4 CM-1
WAVELENGTH (NM)
400
500
600
700
800
900

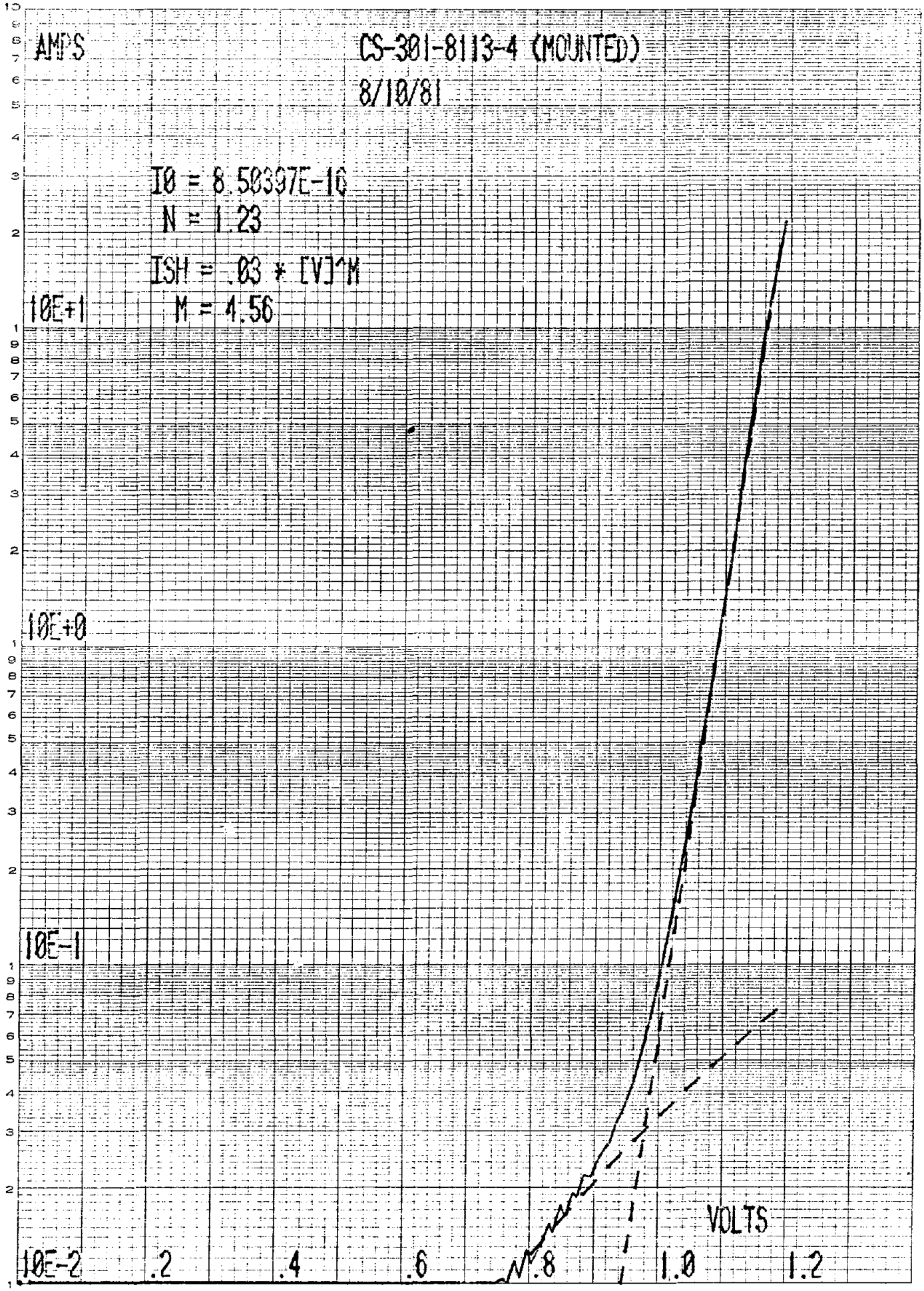

DIETZGEN CORPORATION
MADE IN U.S.A.
NO. 340R-L410 DIETZGEN GRAPH PAPER
SEMI-LOGARITHMIC
4 CYCLES X 10 DIVISIONS PER INCH

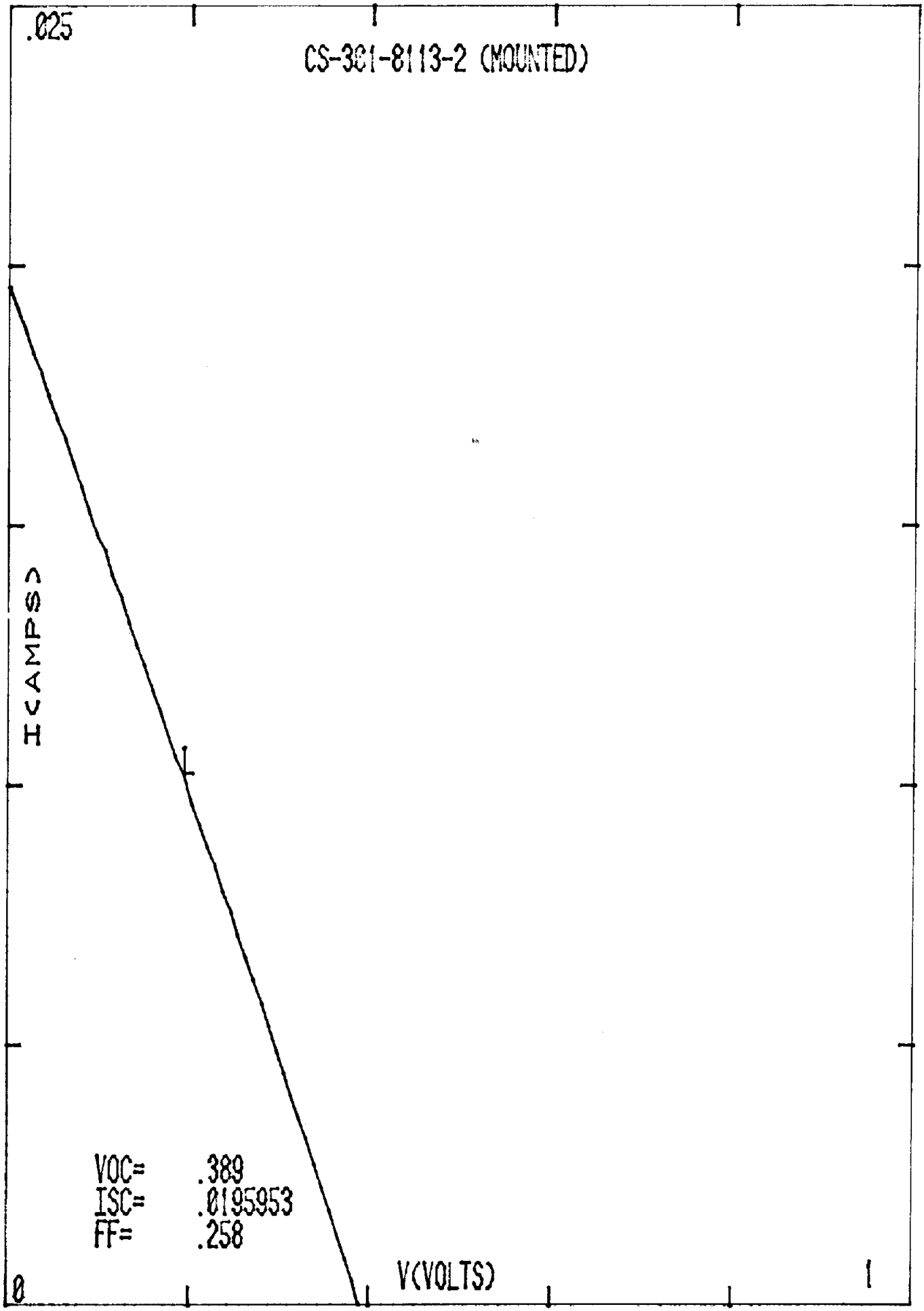
.025
CS-381-8113-2 (MOUNTED)
I(AMPS)
VOC= .389
ISC= .0195953
FF= .258
0
V(VOLTS)
1

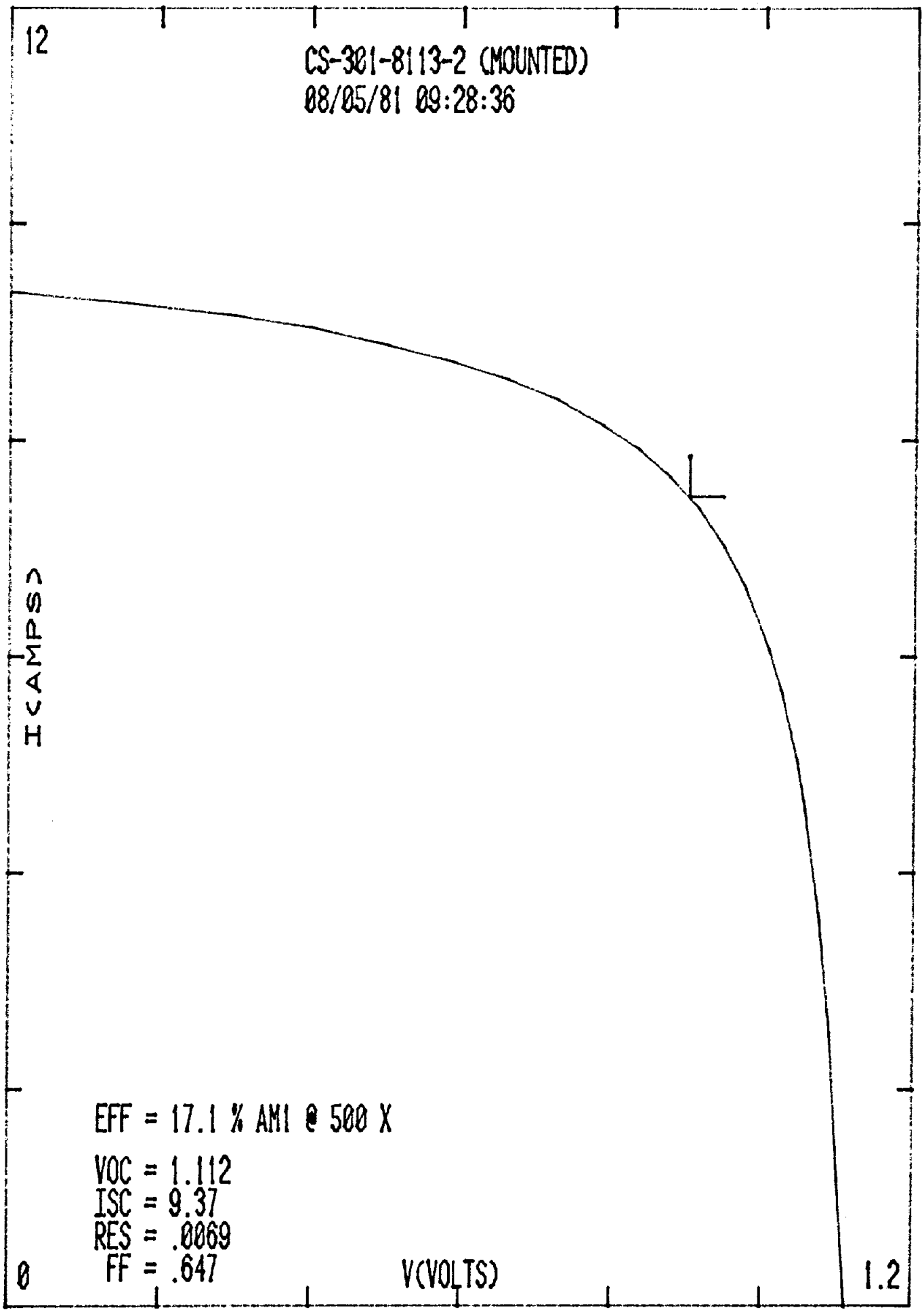
12
CS-301-8113-2 (MOUNTED)
08/05/81 09:28:36
I(AMPS)
EFF = 17.1 % AM1 @ 500 X
VOC = 1.112
ISC = 9.37
RES = .0069
FF = .647
0
V(VOLTS)
1.2

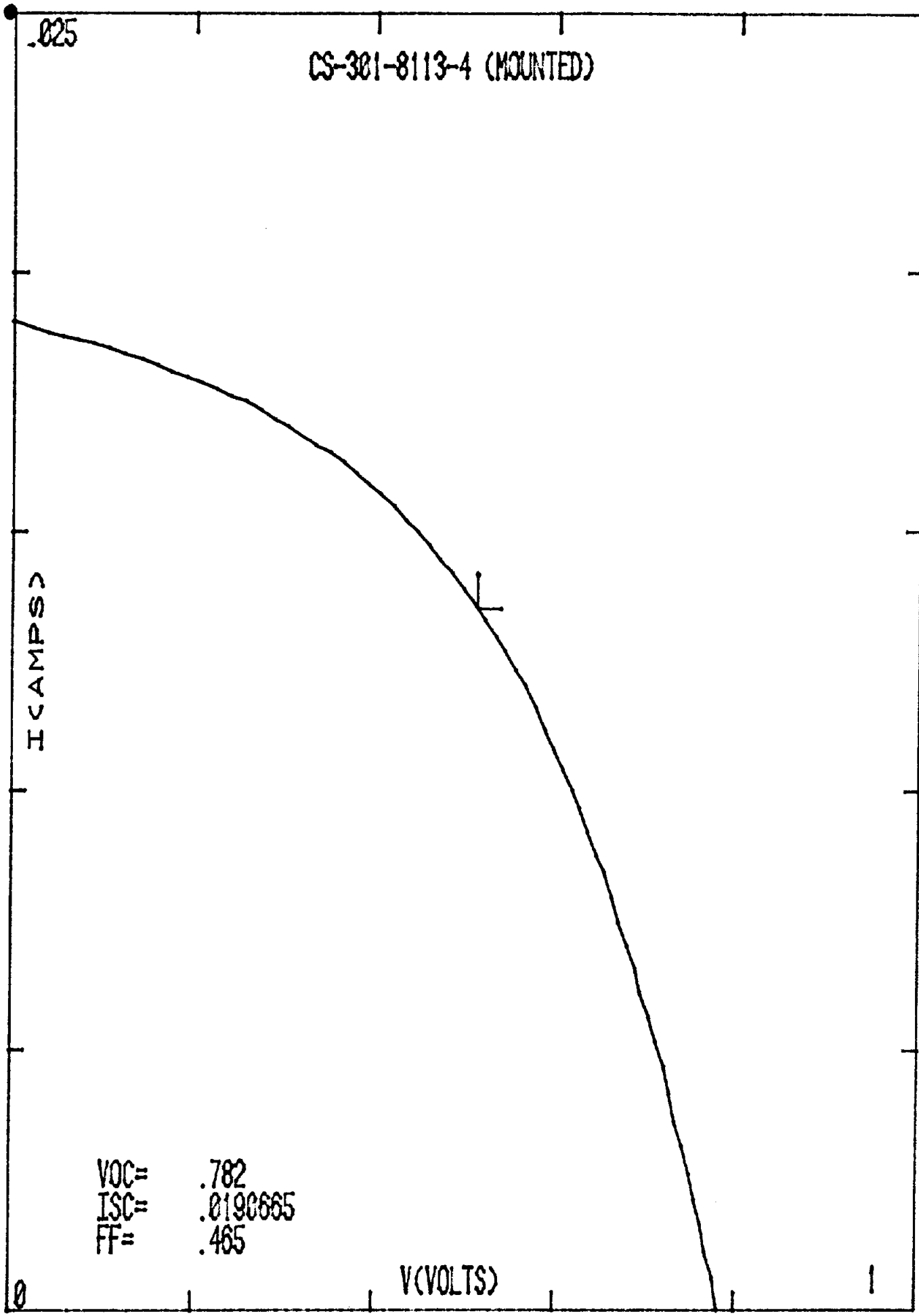
.025
CS-301-8113-4 (MOUNTED)
I(AMPS)
VOC= .782
ISC= .0190665
FF= .465
0
V(VOLTS)
1

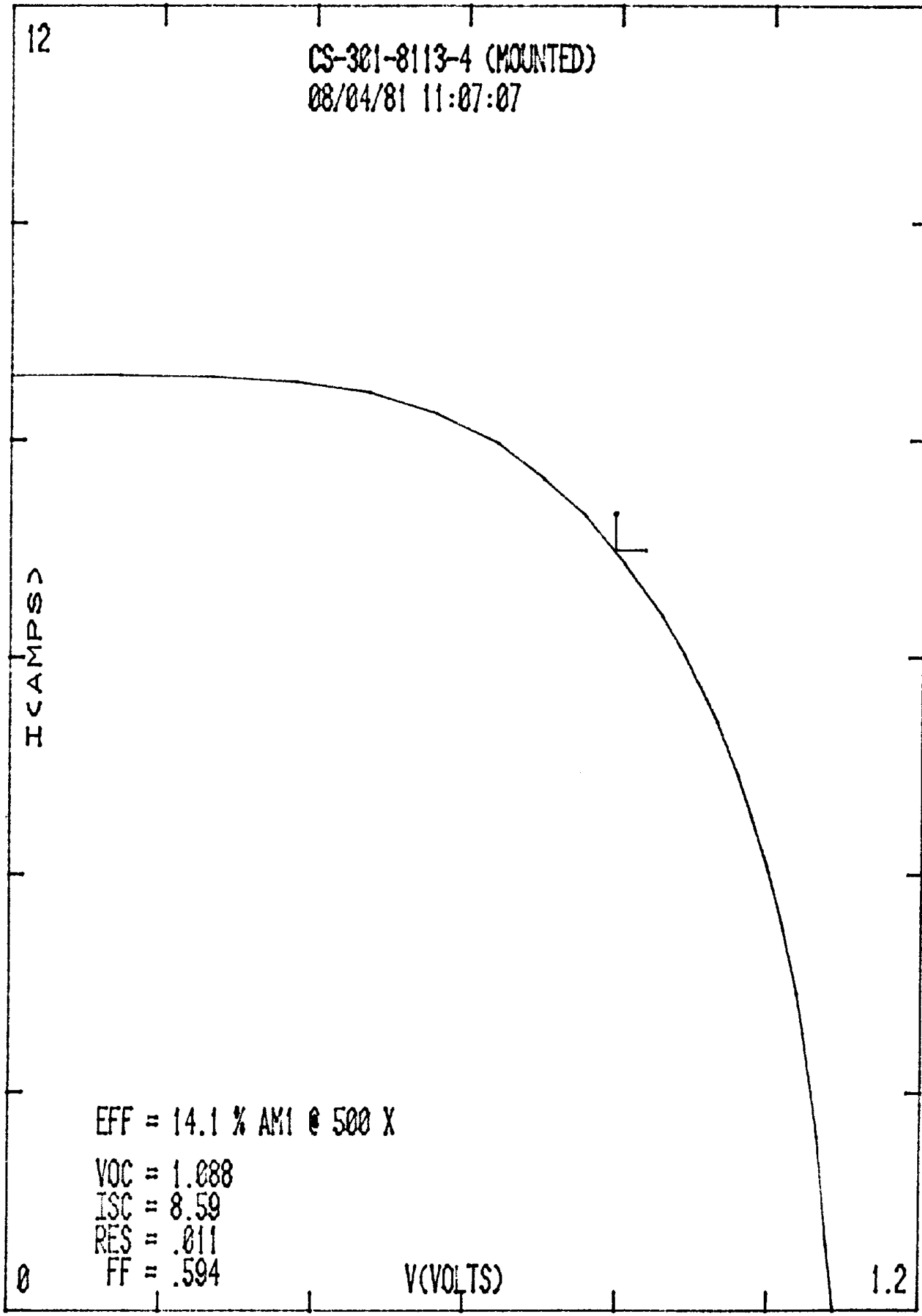
12
CS-301-8113-4 (MOUNTED)
08/04/81 11:07:07
I(AMPS)
EFF = 14.1 % AM1 @ 500 X
VOC = 1.088
ISC = 8.59
RES = .011
FF = .594
0
V(VOLTS)
1.2

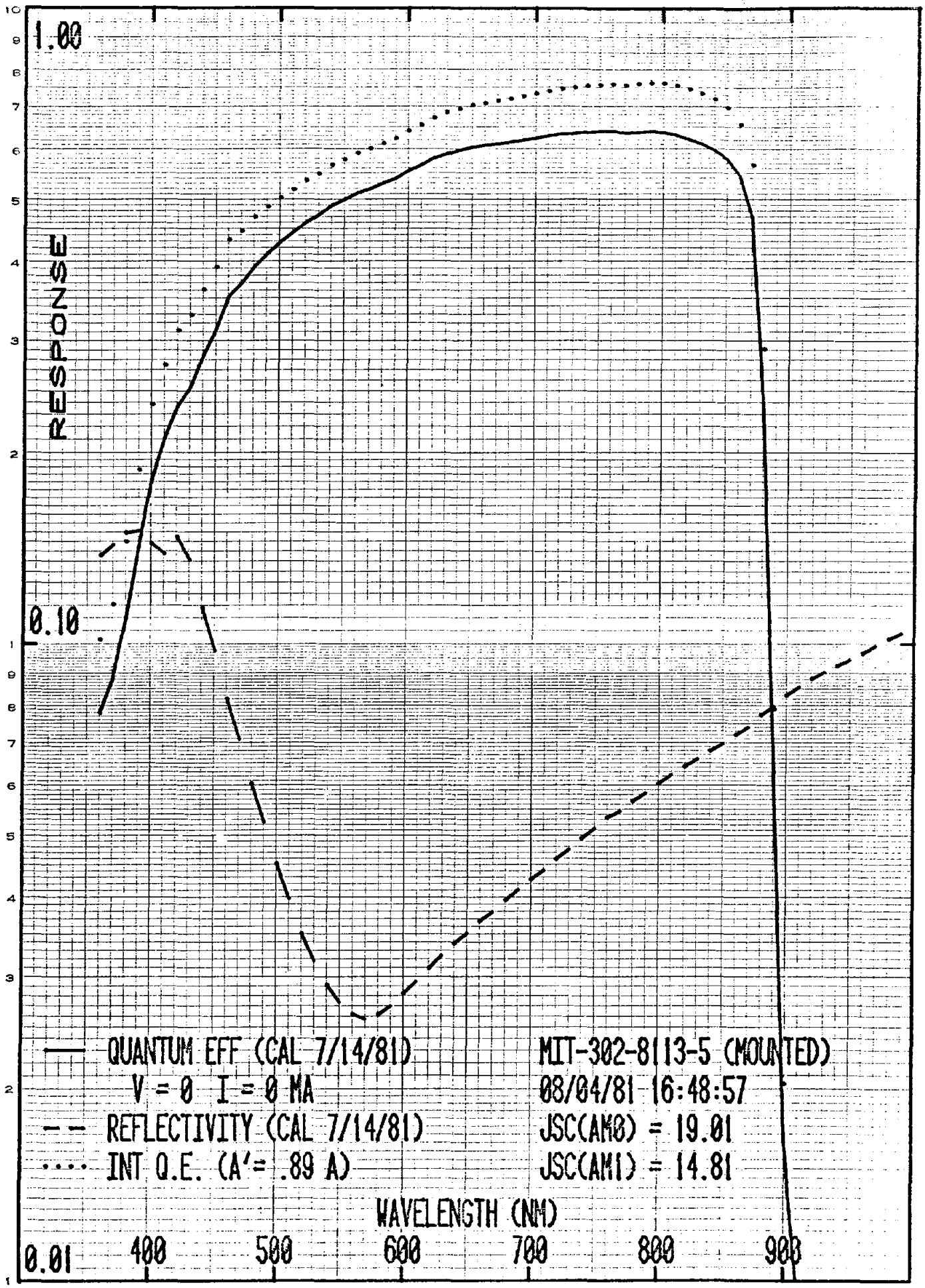

DIETZGEN CORPORATION
MADE IN U.S.A.
NO. 340R-L210 DIETZGEN GRAPH PAPER
SEMI-LOGARITHMIC
2 CYCLES X 10 DIVISIONS PER INCH

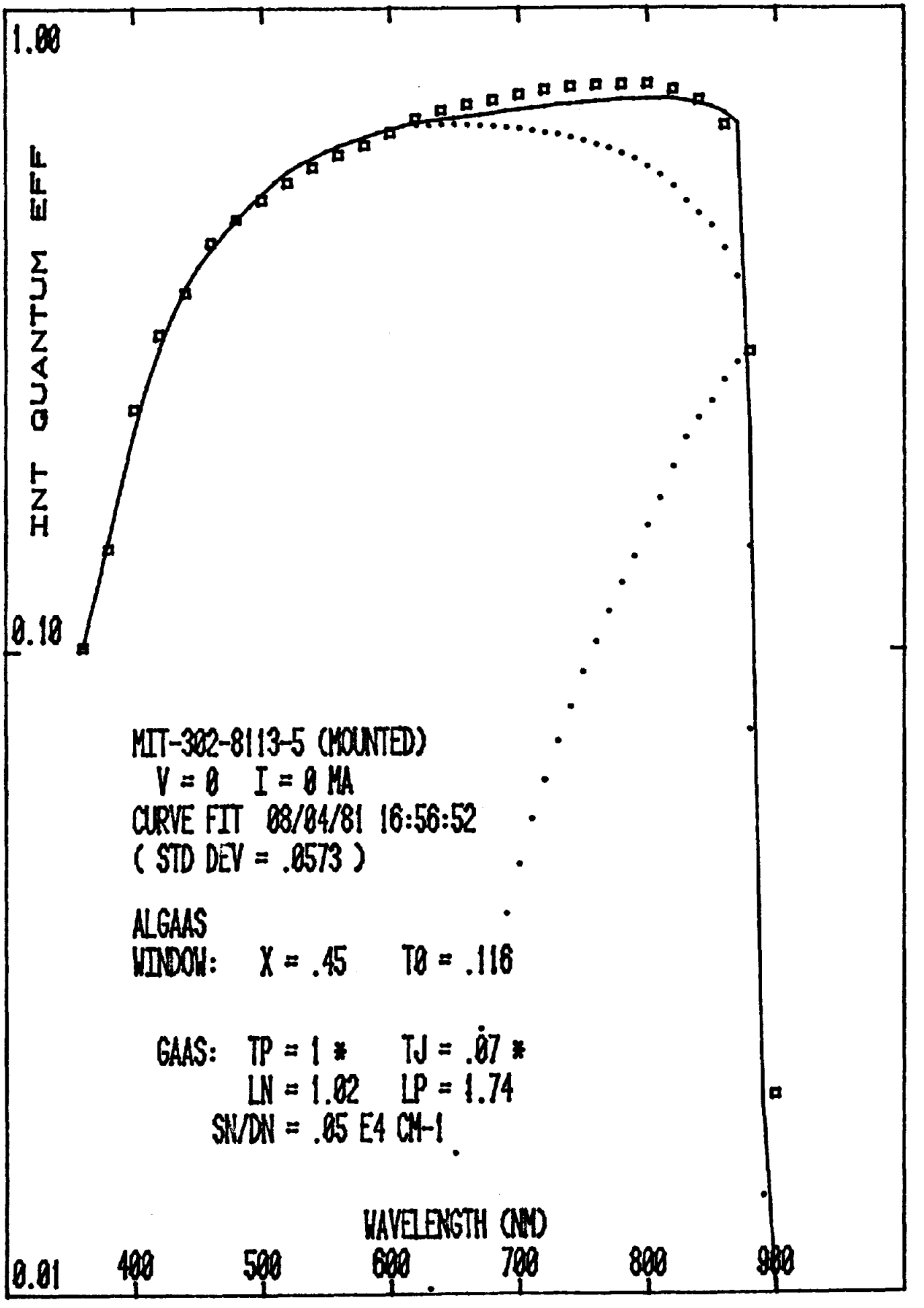
1.00
0.10
0.01
INT QUANTUM EFF
MIT-302-8113-5 (MOUNTED)
V = 0 I = 0 MA
CURVE FIT 08/04/81 16:56:52
(STD DEV = .0573)
ALGAAS
WINDOW: X = .45 T0 = .116
GAAS: TP = 1 * TJ = .07 *
LN = 1.02 LP = 1.74
SN/DN = .05 E4 CM-1
WAVELENGTH (NM)
400
500
600
700
800
900

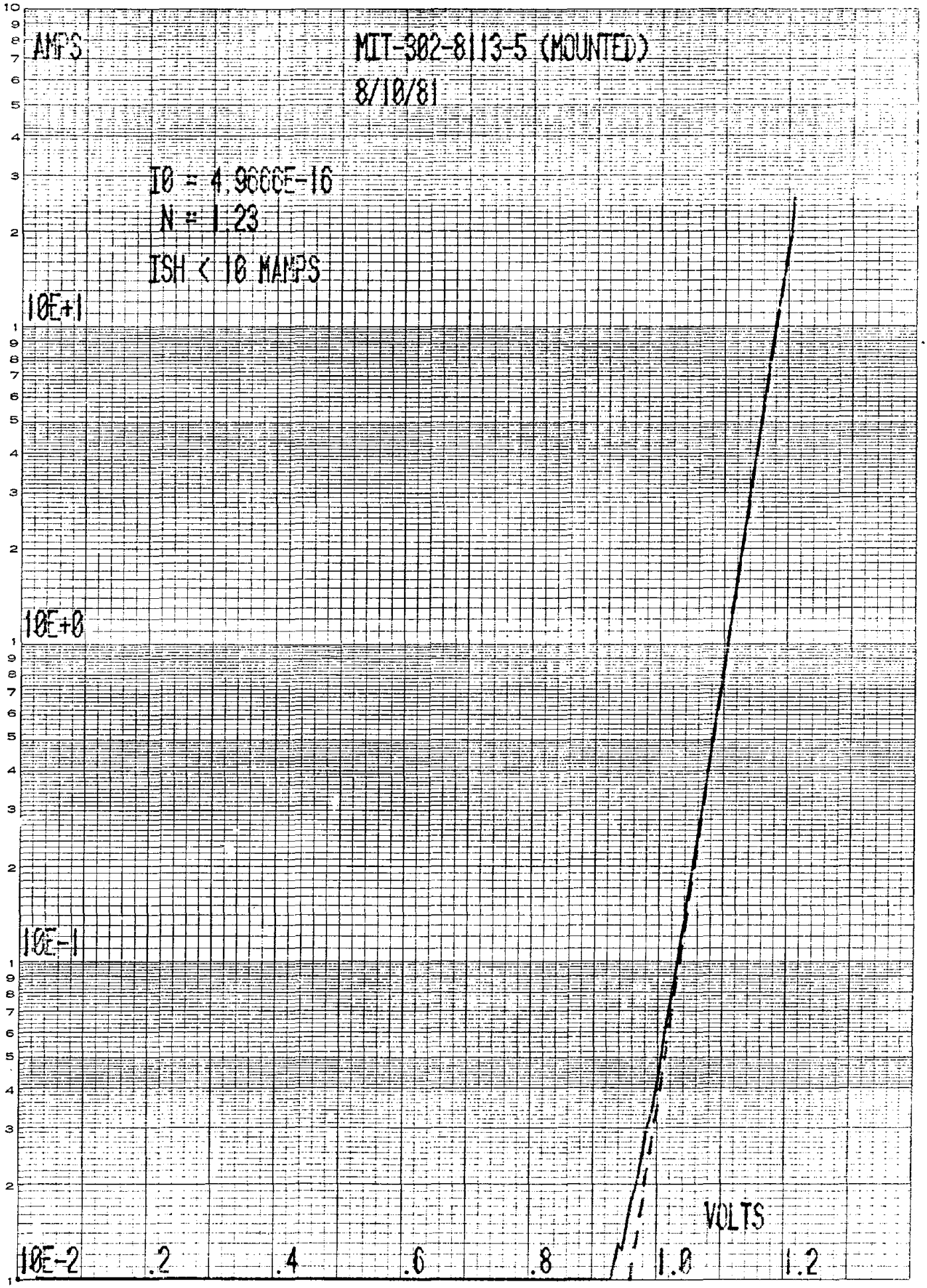

DIETZGEN CORPORATION
MADE IN U.S.A.
NO. 340R-L410 DIETZGEN GRAPH PAPER
SEMI-LOGARITHMIC
4 CYCLES X 10 DIVISIONS PER INCH

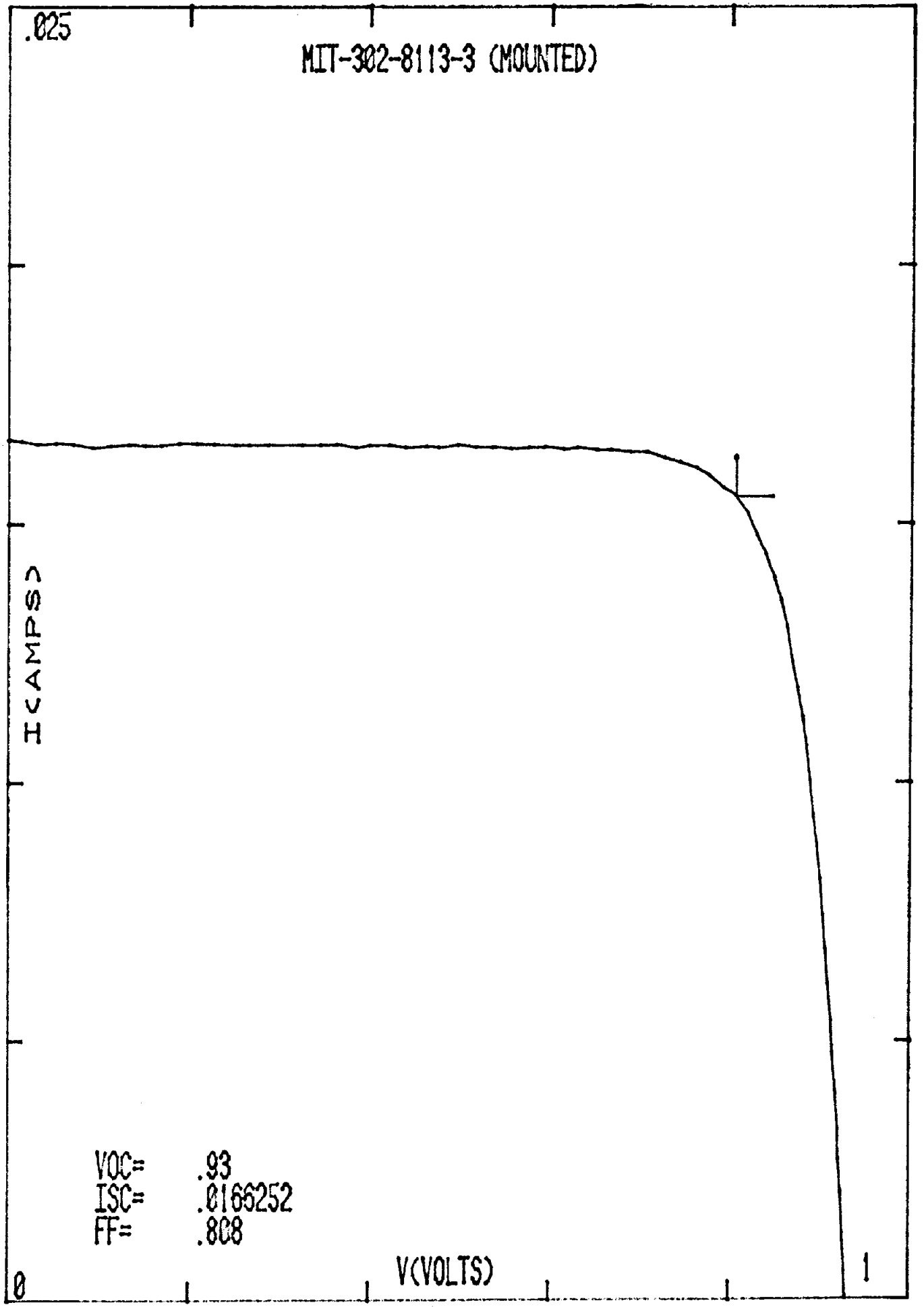
.025
MIT-302-8113-3 (MOUNTED)
I(AMPS)
VOC= .93
ISC= .0166252
FF= .808
V(VOLTS)
0
1

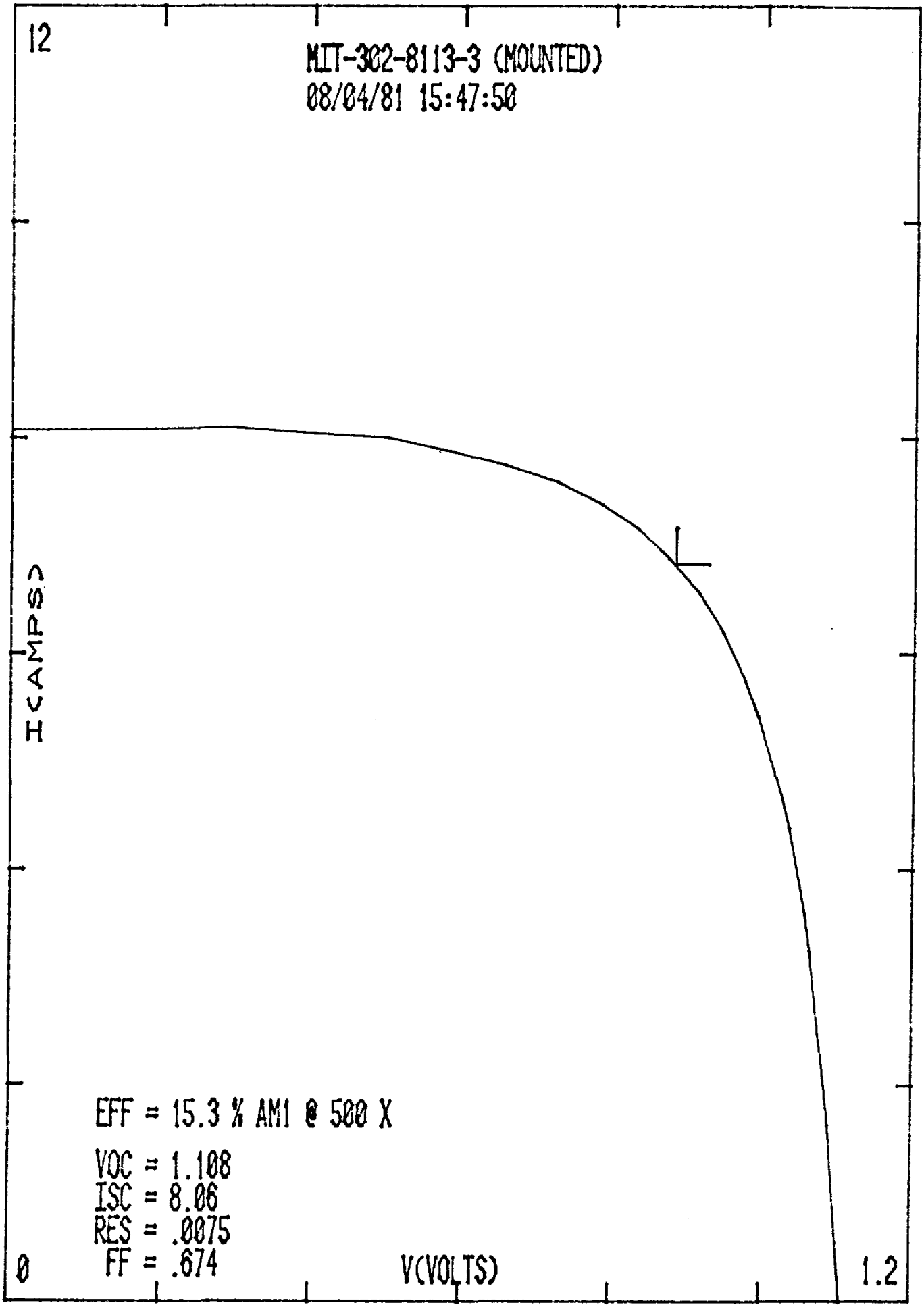
12
MIT-302-8113-3 (MOUNTED)
08/04/81 15:47:50
I(AMPS)
EFF = 15.3 % AM1 @ 500 X
VOC = 1.108
ISC = 8.06
RES = .0075
FF = .674
0
V(VOLTS)
1.2

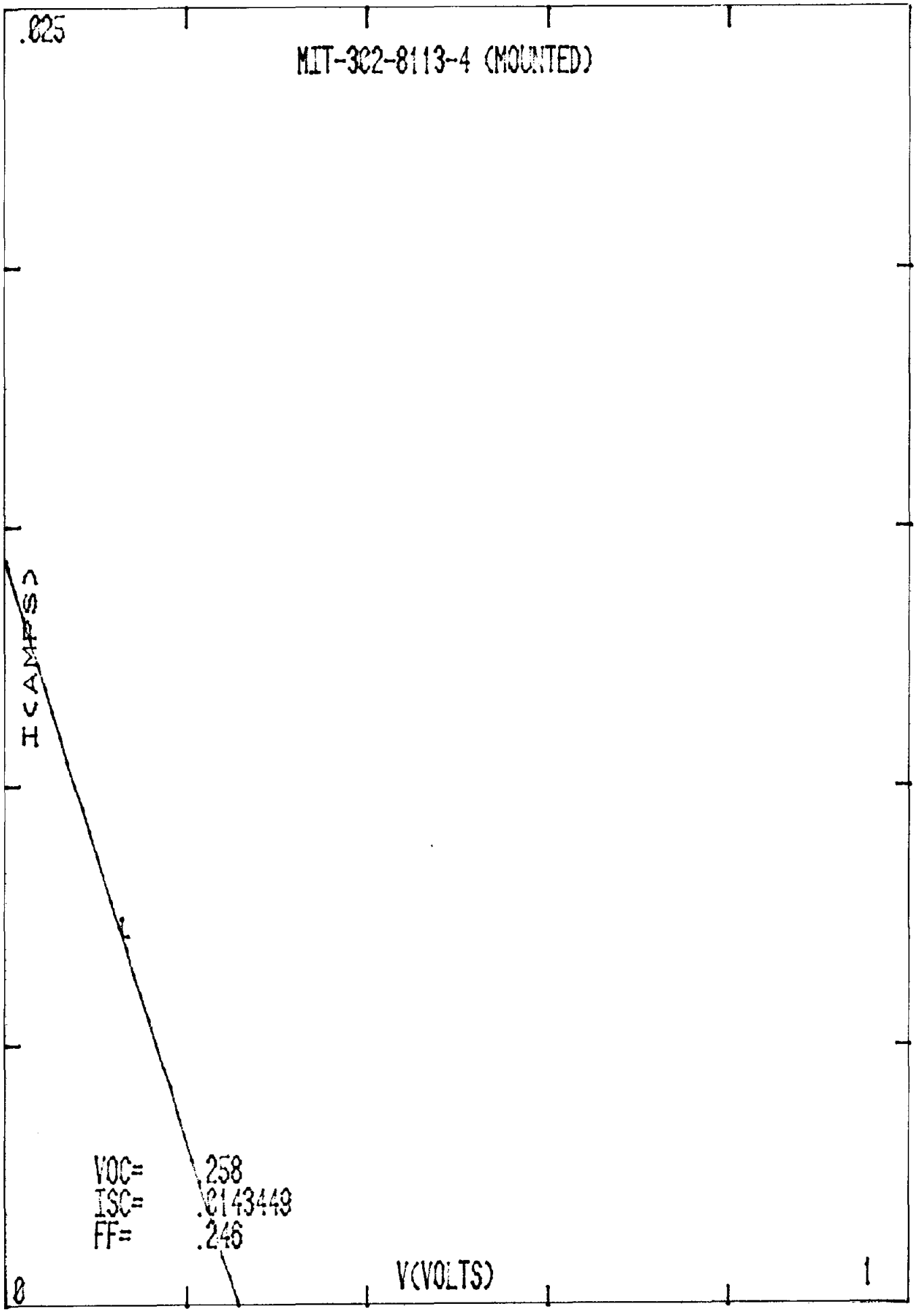
.025
MIT-302-8113-4 (MOUNTED)
I(AMPS)
VOC= .258
ISC= .0143449
FF= .246
V(VOLTS)
0
1

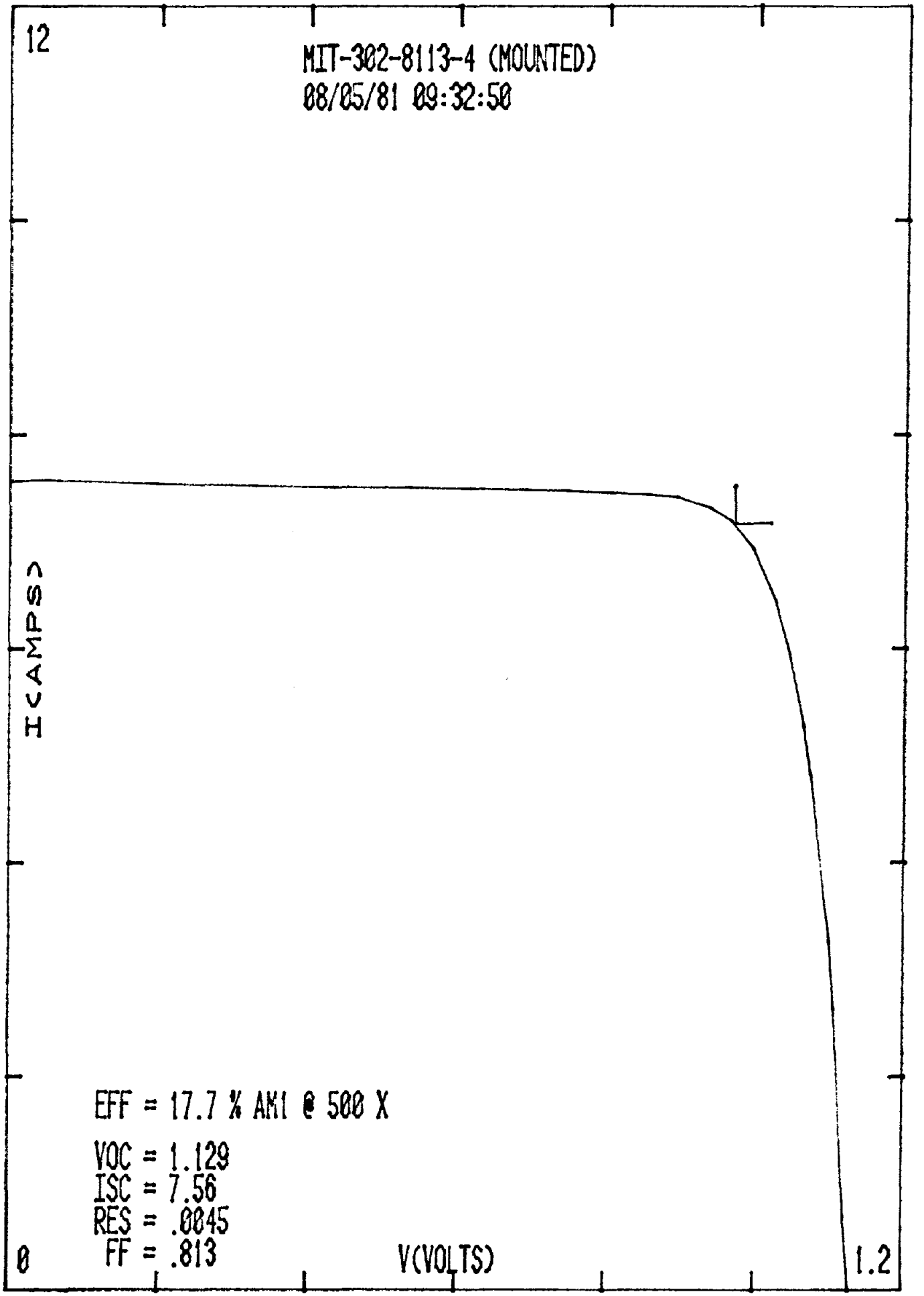
12
MIT-302-8113-4 (MOUNTED)
08/05/81 09:32:50
I(AMPS)
EFF = 17.7 % AM1 @ 500 X
VOC = 1.129
ISC = 7.56
RES = .0045
FF = .813
0
V(VOLTS)
1.2

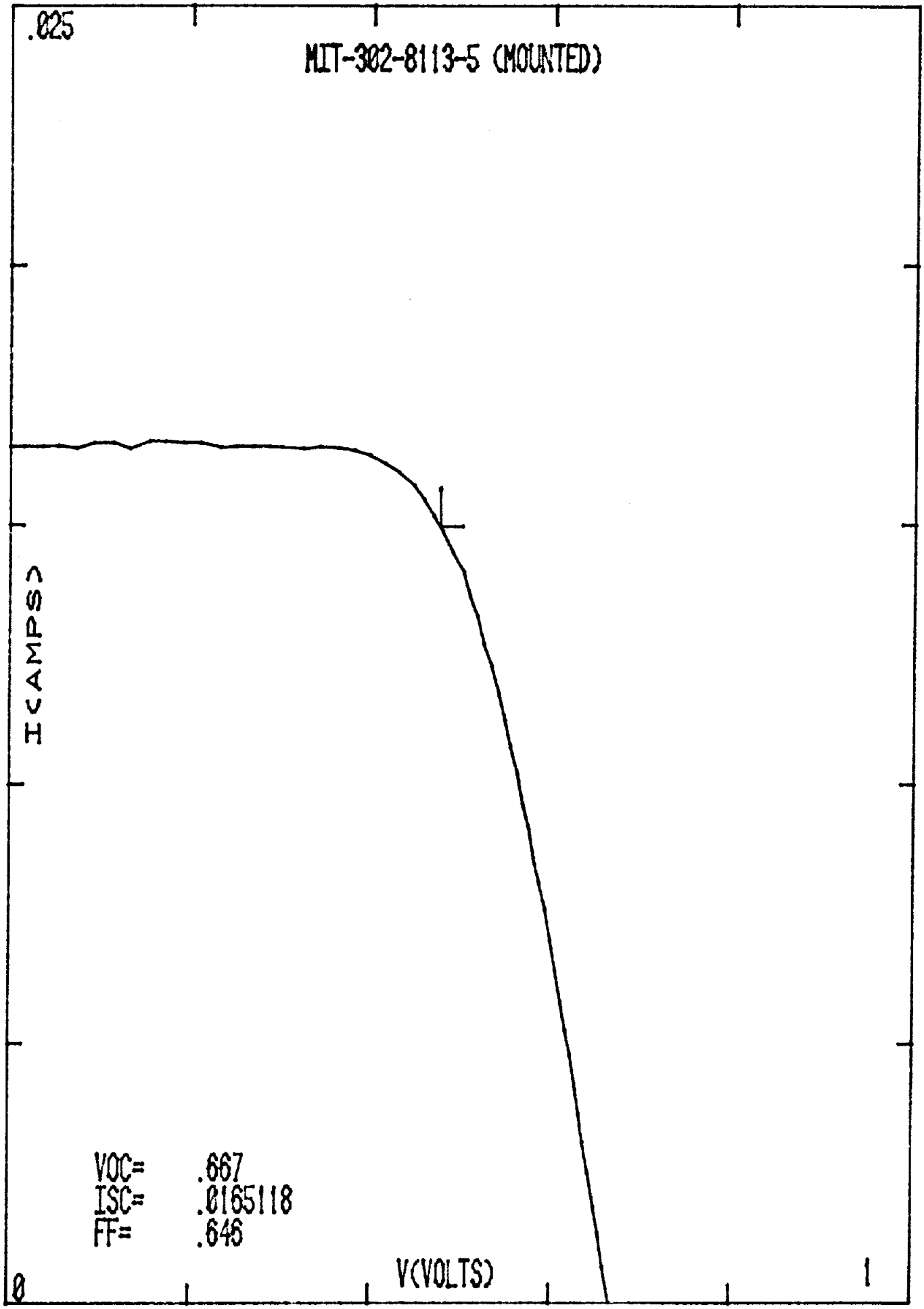
.025
MIT-302-8113-5 (MOUNTED)
I(AMPS)
VOC= .667
ISC= .0165118
FF= .646
V(VOLTS)
0
1

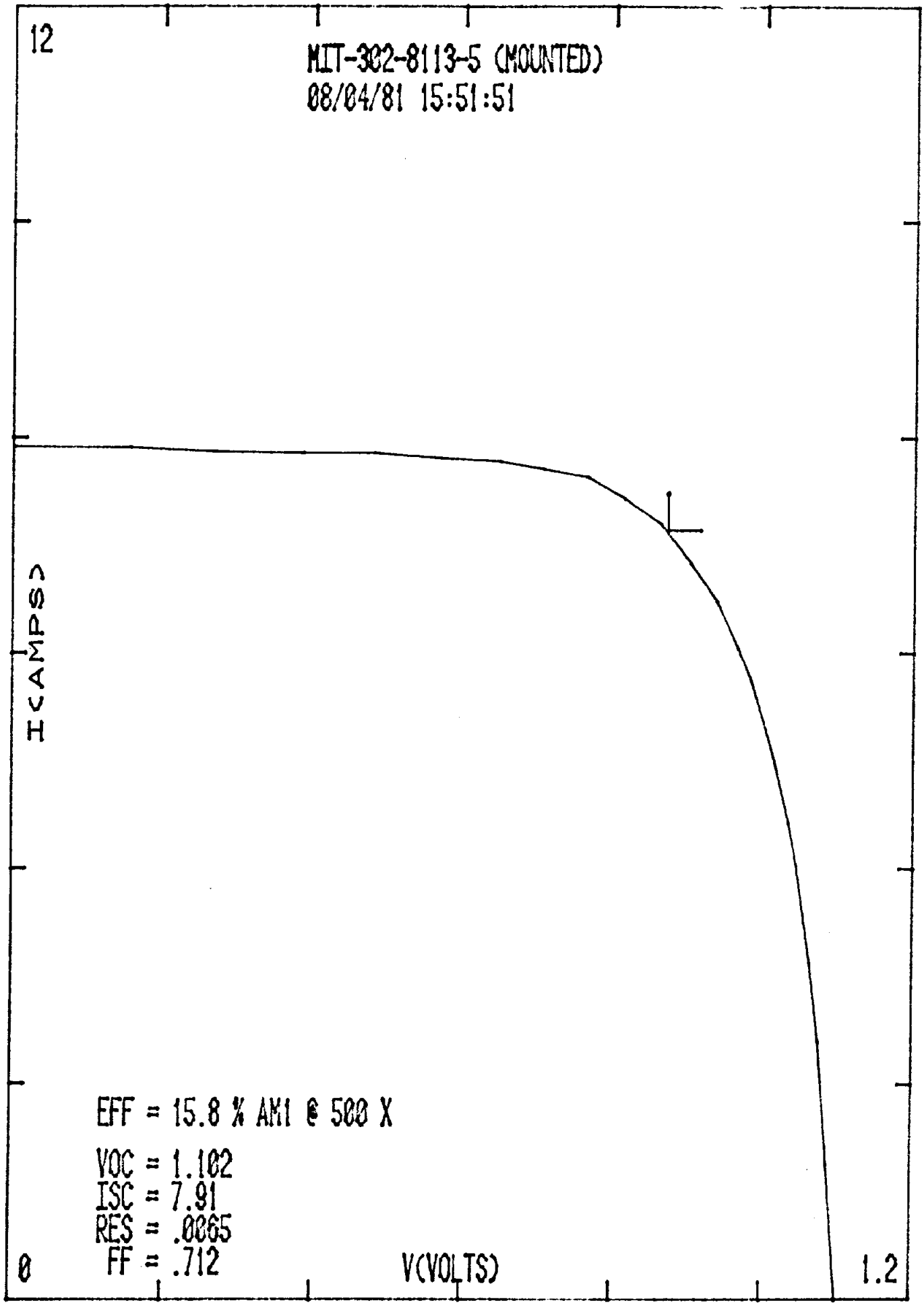
12
MIT-302-8113-5 (MOUNTED)
08/04/81 15:51:51
I(AMPS)
EFF = 15.8 % AM1 @ 500 X
VOC = 1.102
ISC = 7.91
RES = .0065
FF = .712
0
V(VOLTS)
1.2

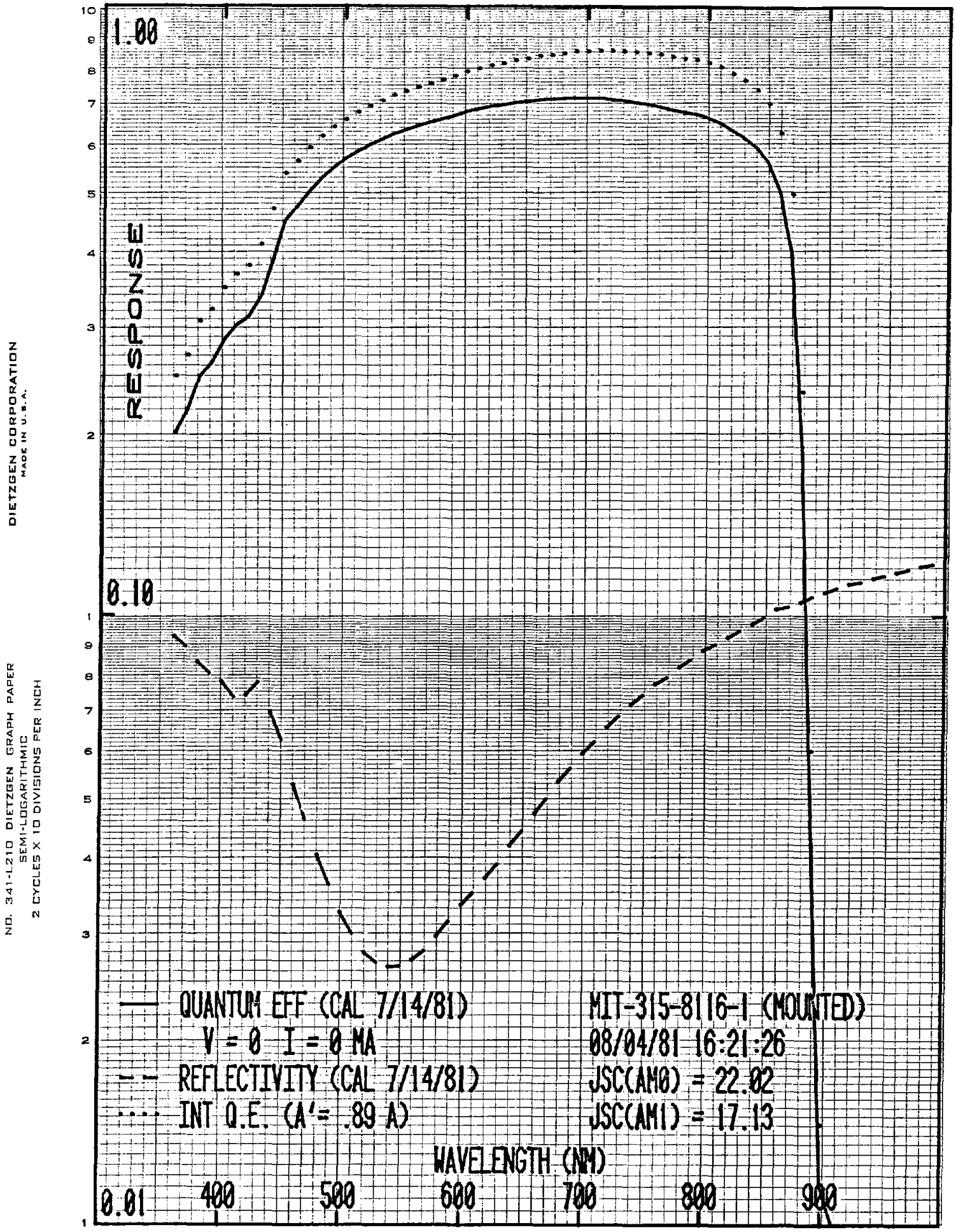
1.00
0.10
0.01
RESPONSE
400
500
600
700
800
900
WAVELENGTH (NM)
QUANTUM EFF (CAL 7/14/81)
V = 0 I = 0 MA
REFLECTIVITY (CAL 7/14/81)
INT Q.E. (A'= .89 A)
MIT-315-8116-1 (MOUNTED)
08/04/81 16:21:26
JSC(AM0) = 22.02
JSC(AM1) = 17.13
DIETZGEN CORPORATION
MADE IN U.S.A.
NO. 341-LZ10 DIETZGEN GRAPH PAPER
SEMI-LOGARITHMIC
2 CYCLES X 10 DIVISIONS PER INCH

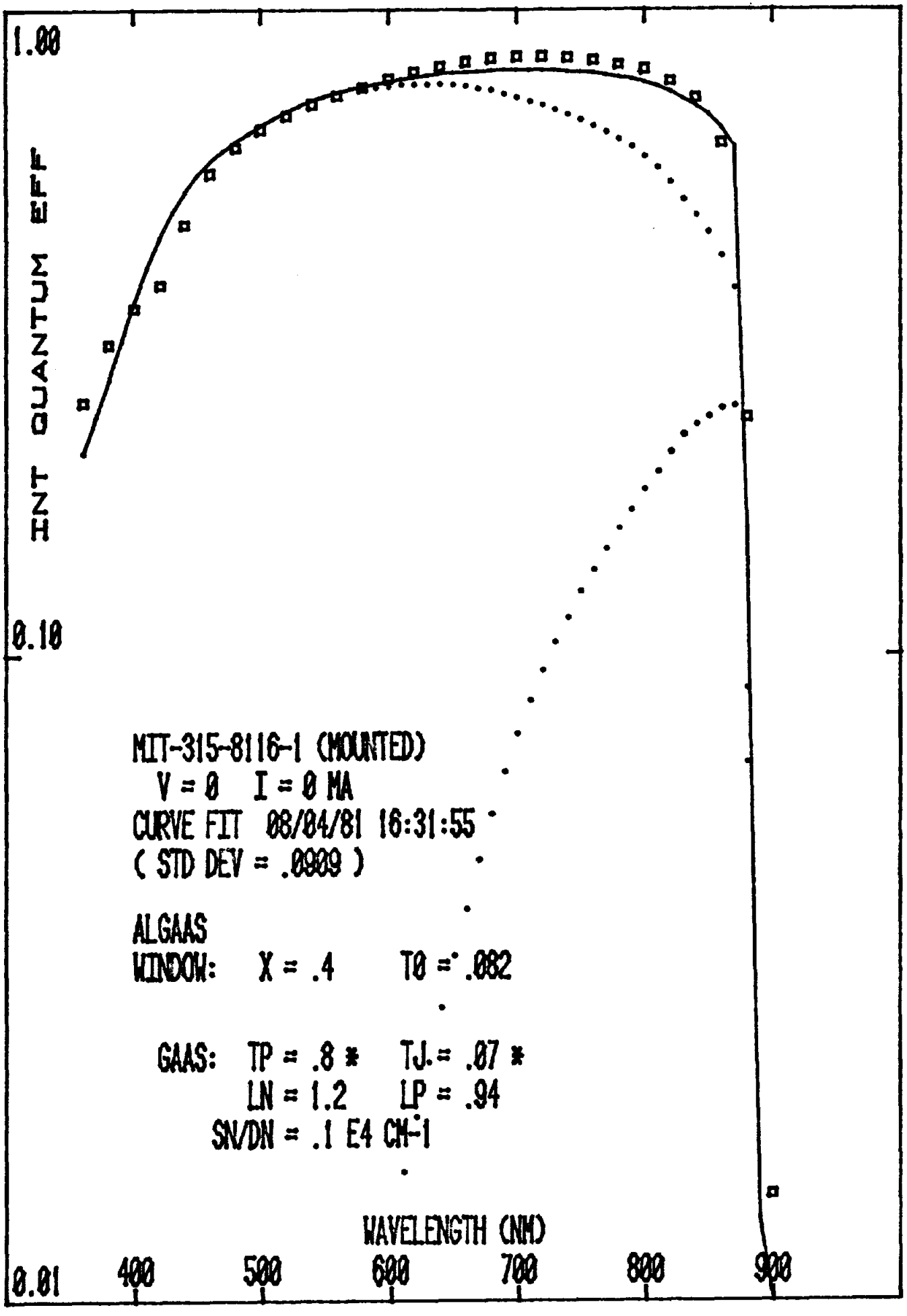
1.00
0.10
0.01
INT QUANTUM EFF
MIT-315-8116-1 (MOUNTED)
V = 0 I = 0 MA
CURVE FIT 08/04/81 16:31:55
(STD DEV = .0009)
ALGAAS
WINDOW: X = .4 T0 = .082
GAAS: TP = .8 * TJ = .07 *
LN = 1.2 LP = .94
SN/DN = .1 E4 CM-1
WAVELENGTH (NM)
400
500
600
700
800
900

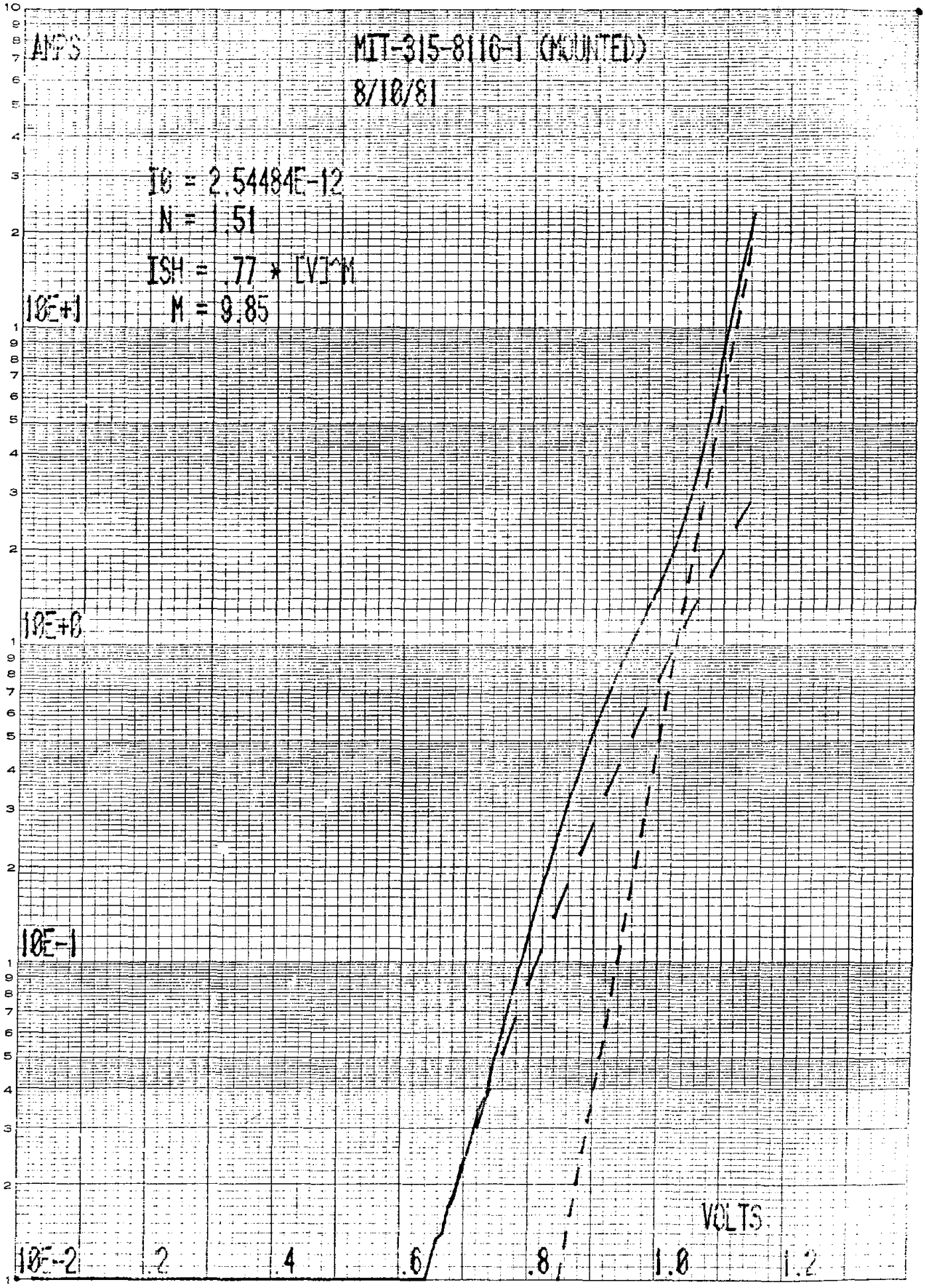

DIETZGEN CORPORATION
MADE IN U.S.A.
NO. 340R-L410 DIETZGEN GRAPH PAPER
SEMI-LOGARITHMIC
4 CYCLES X 10 DIVISIONS PER INCH

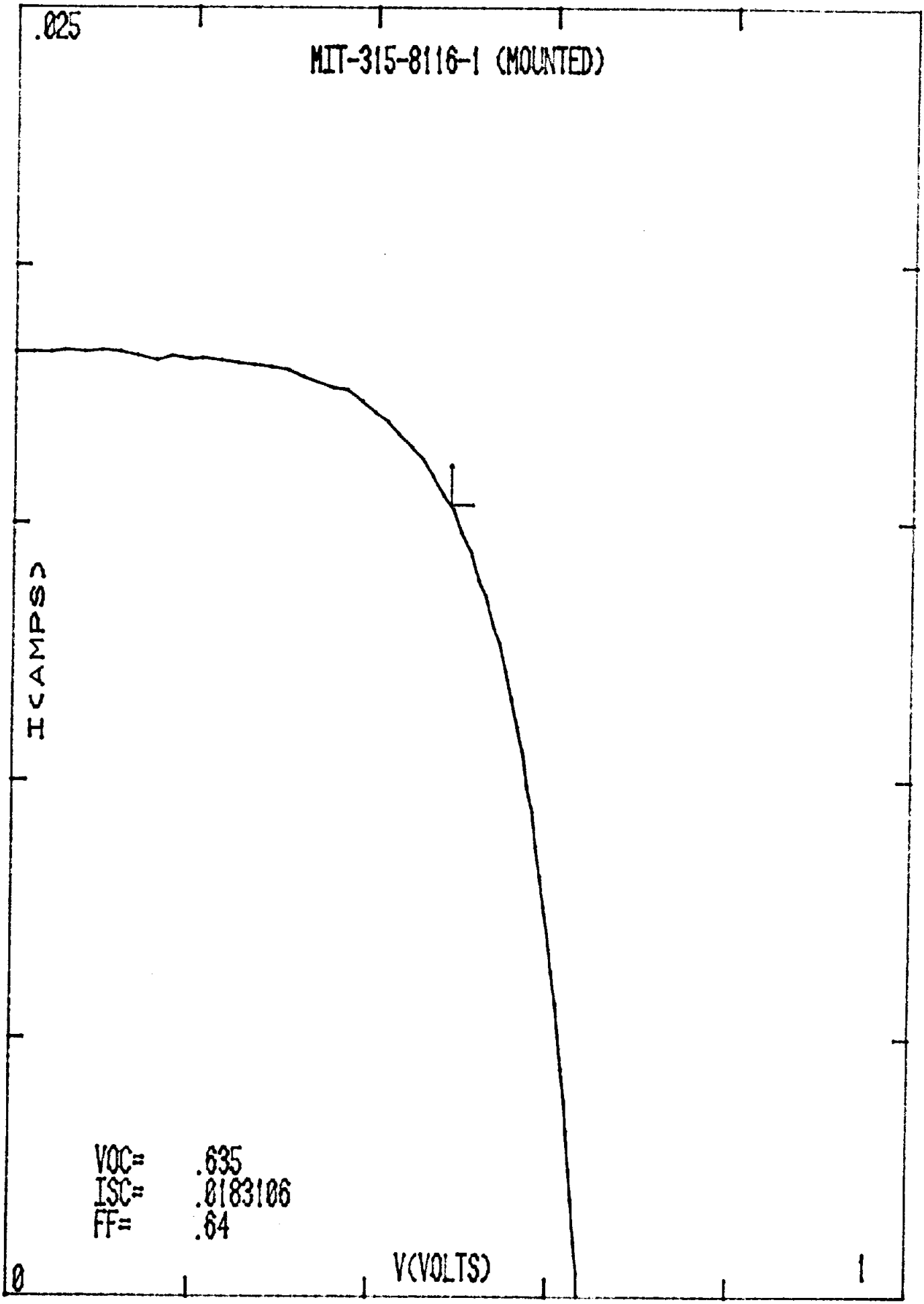
.025
MIT-315-8116-1 (MOUNTED)
I(AMPS)
VOC= .635
ISC= .0183106
FF= .64
0
V(VOLTS)
1

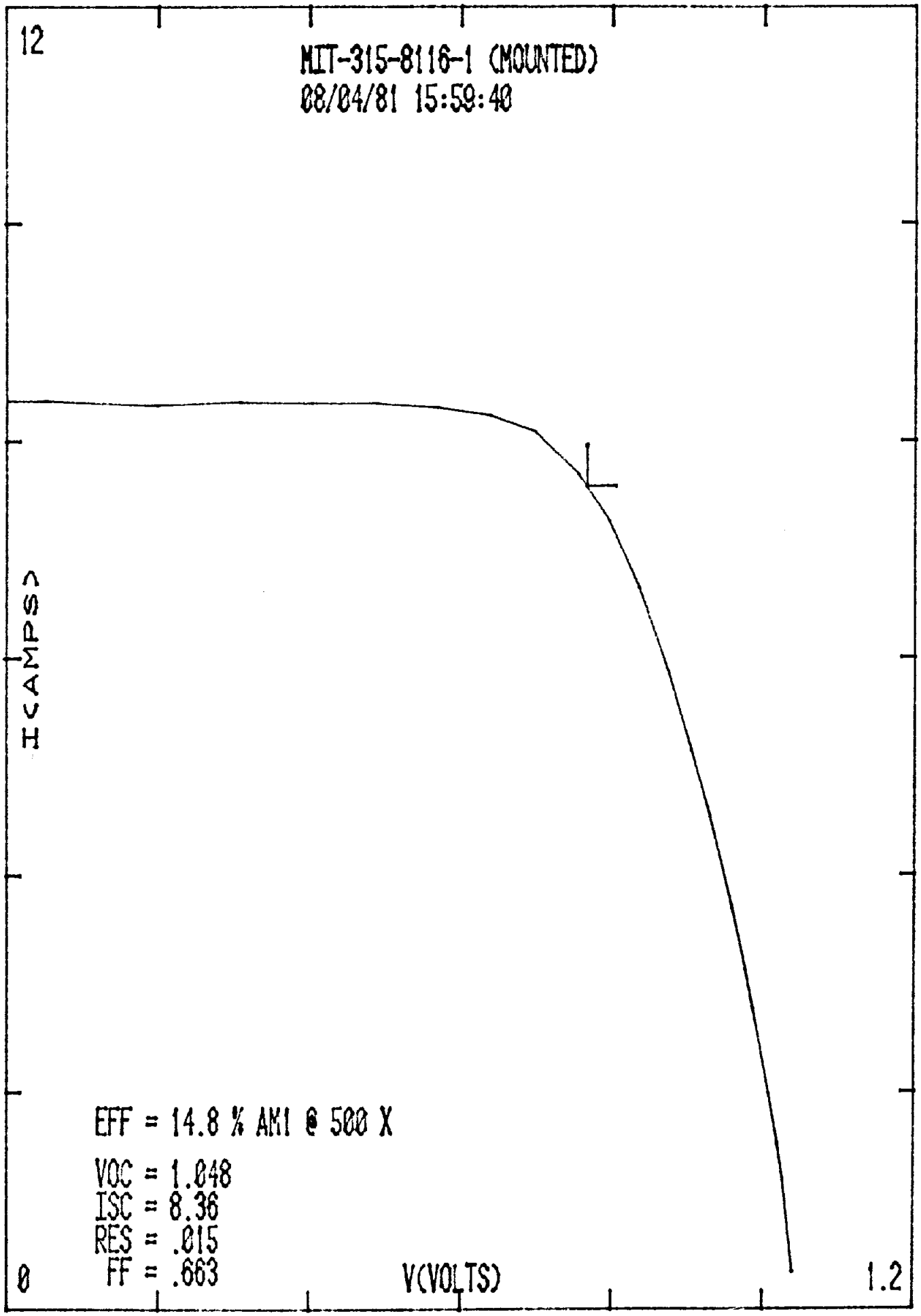
12
MIT-315-8116-1 (MOUNTED)
08/04/81 15:59:40
I(AMPS)
EFF = 14.8 % AM1 @ 500 X
VOC = 1.048
ISC = 8.36
RES = .015
FF = .663
0
V(VOLTS)
1.2

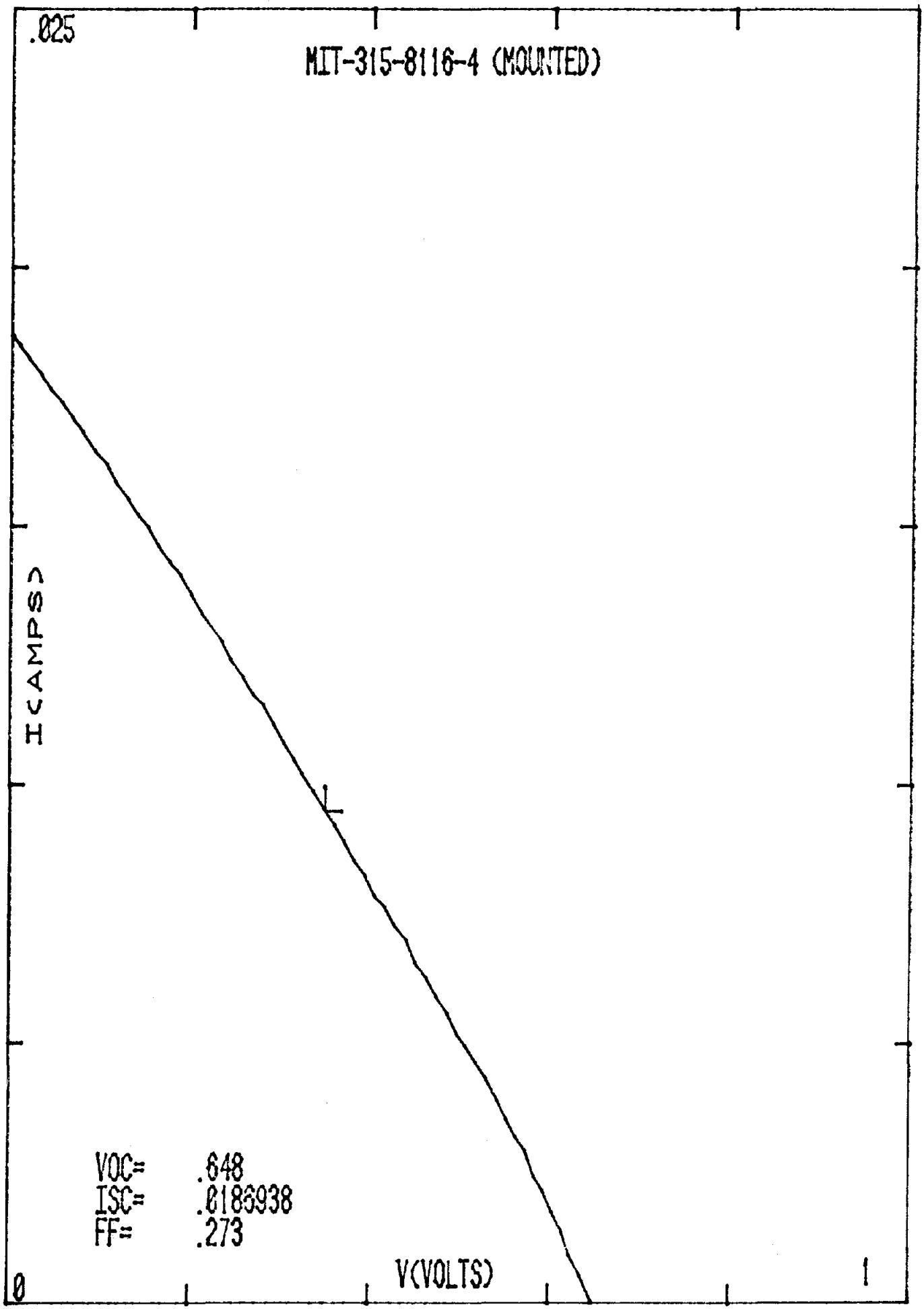
.025
MIT-315-8116-4 (MOUNTED)
I(AMPS)
VOC= .648
ISC= .0183938
FF= .273
0
V(VOLTS)
1

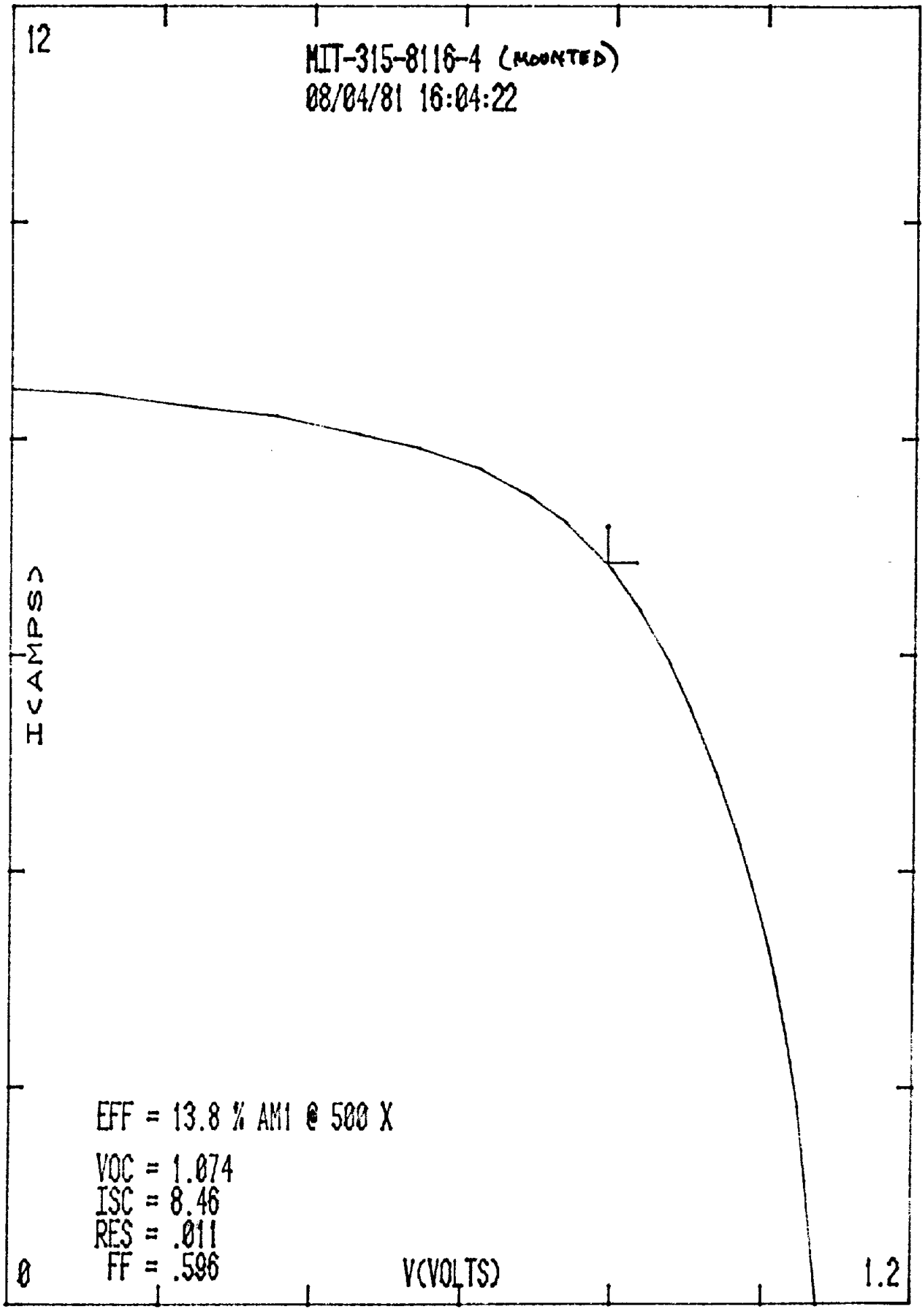
12
MIT-315-8116-4 (MOUNTED)
08/04/81 16:04:22
I(AMPS)
EFF = 13.8 % AM1 @ 500 X
VOC = 1.074
ISC = 8.46
RES = .011
FF = .596
0
V(VOLTS)
1.2

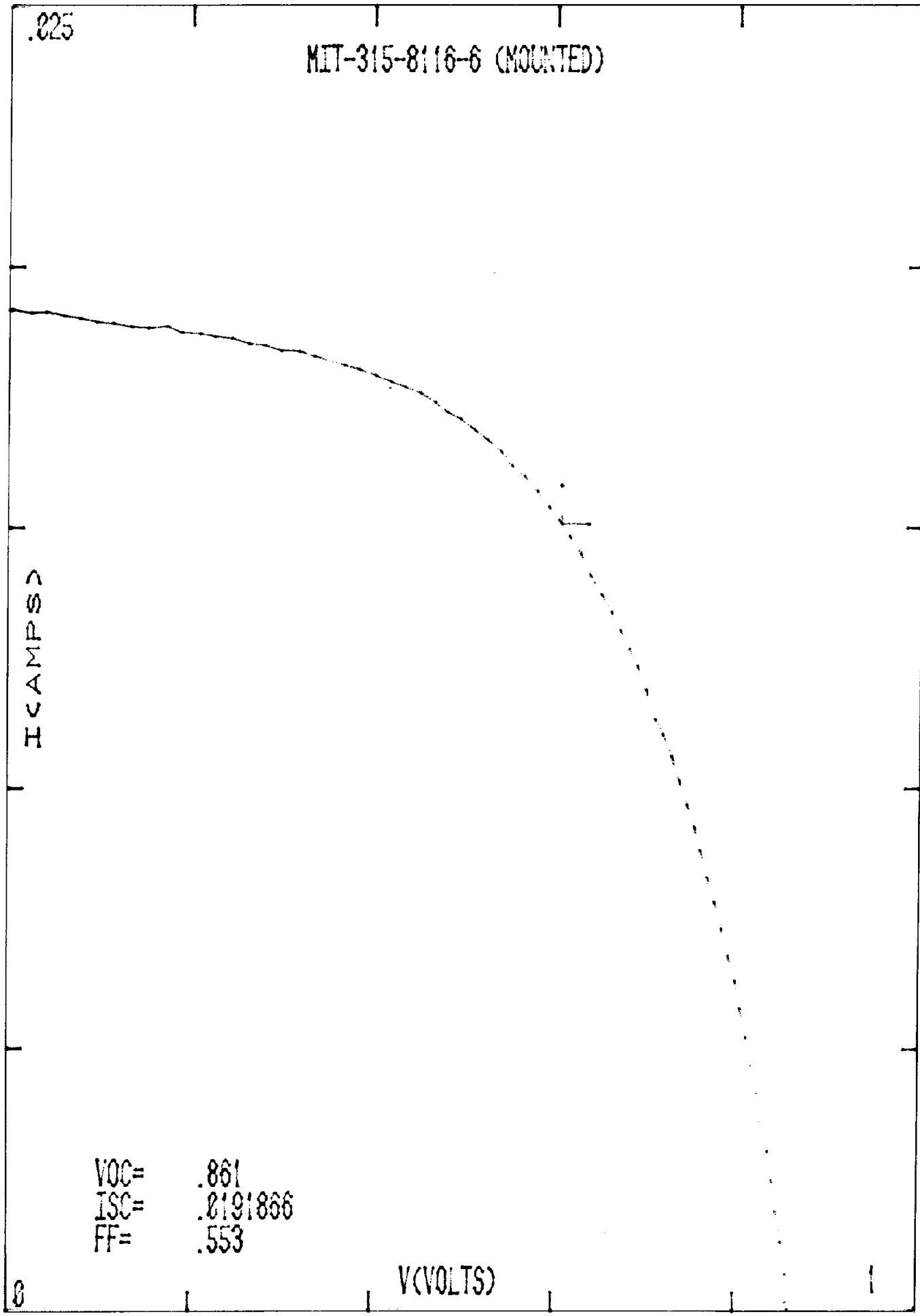
.025
MIT-315-8116-6 (MOUNTED)
I(AMPS)
VOC= .861
ISC= .0191866
FF= .553
V(VOLTS)
0
1

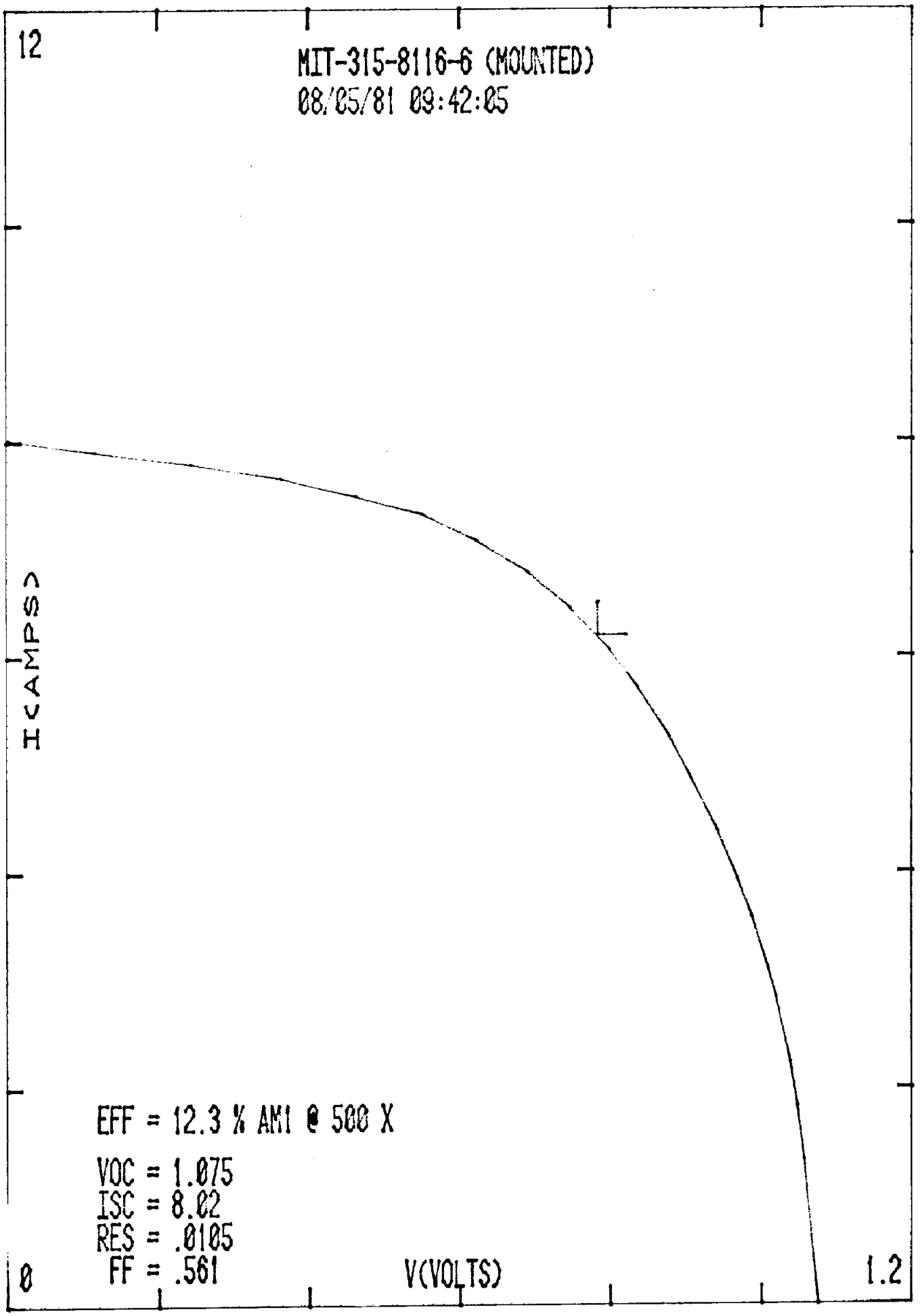
12
MIT-315-8116-6 (MOUNTED)
08/05/81 09:42:05
I(AMPS)
EFF = 12.3 % AM1 @ 500 X
VOC = 1.075
ISC = 8.02
RES = .0105
FF = .561
0
V(VOLTS)
1.2

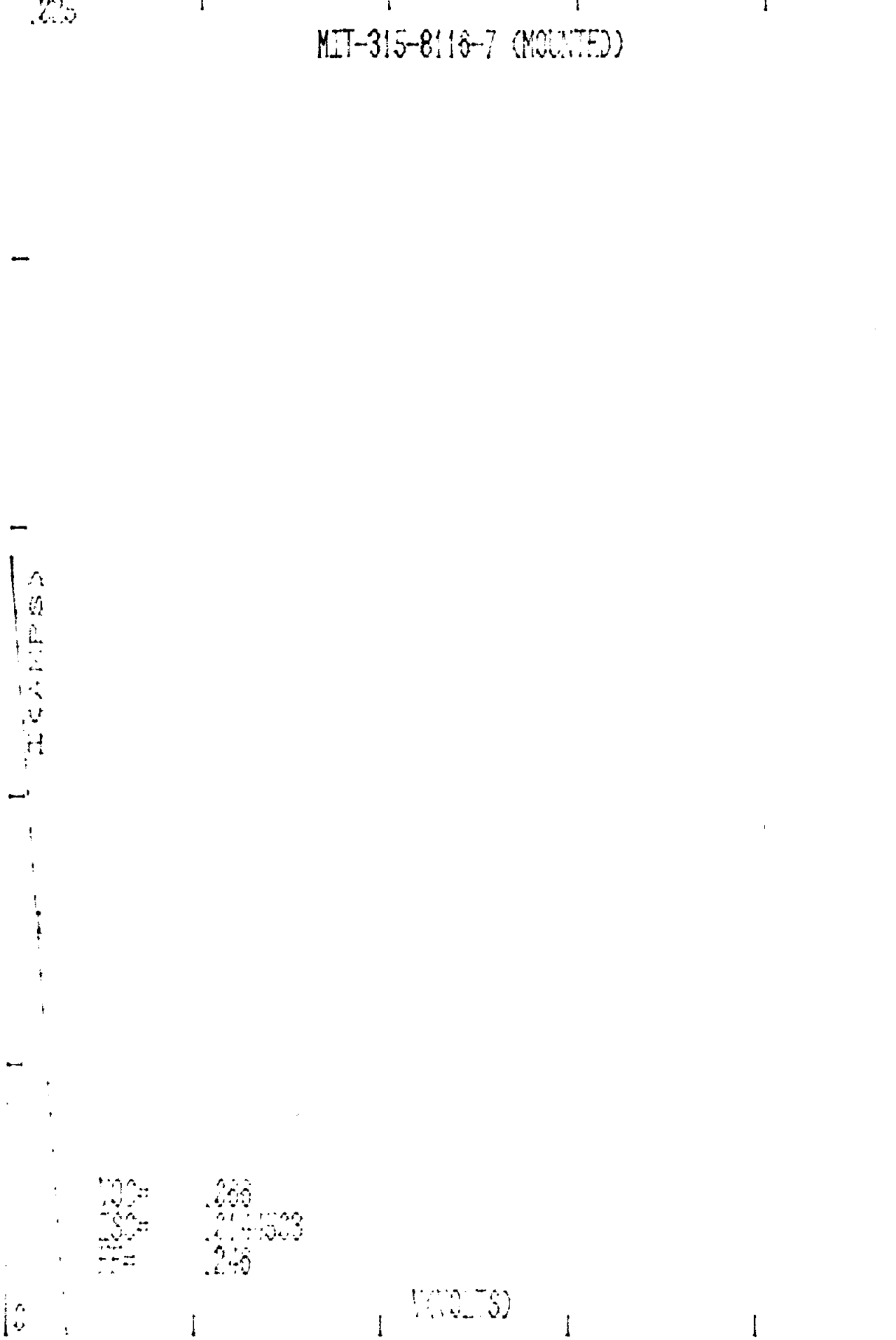
.225
MIT-315-8118-7 (MOUNTED)
.400
.245
0

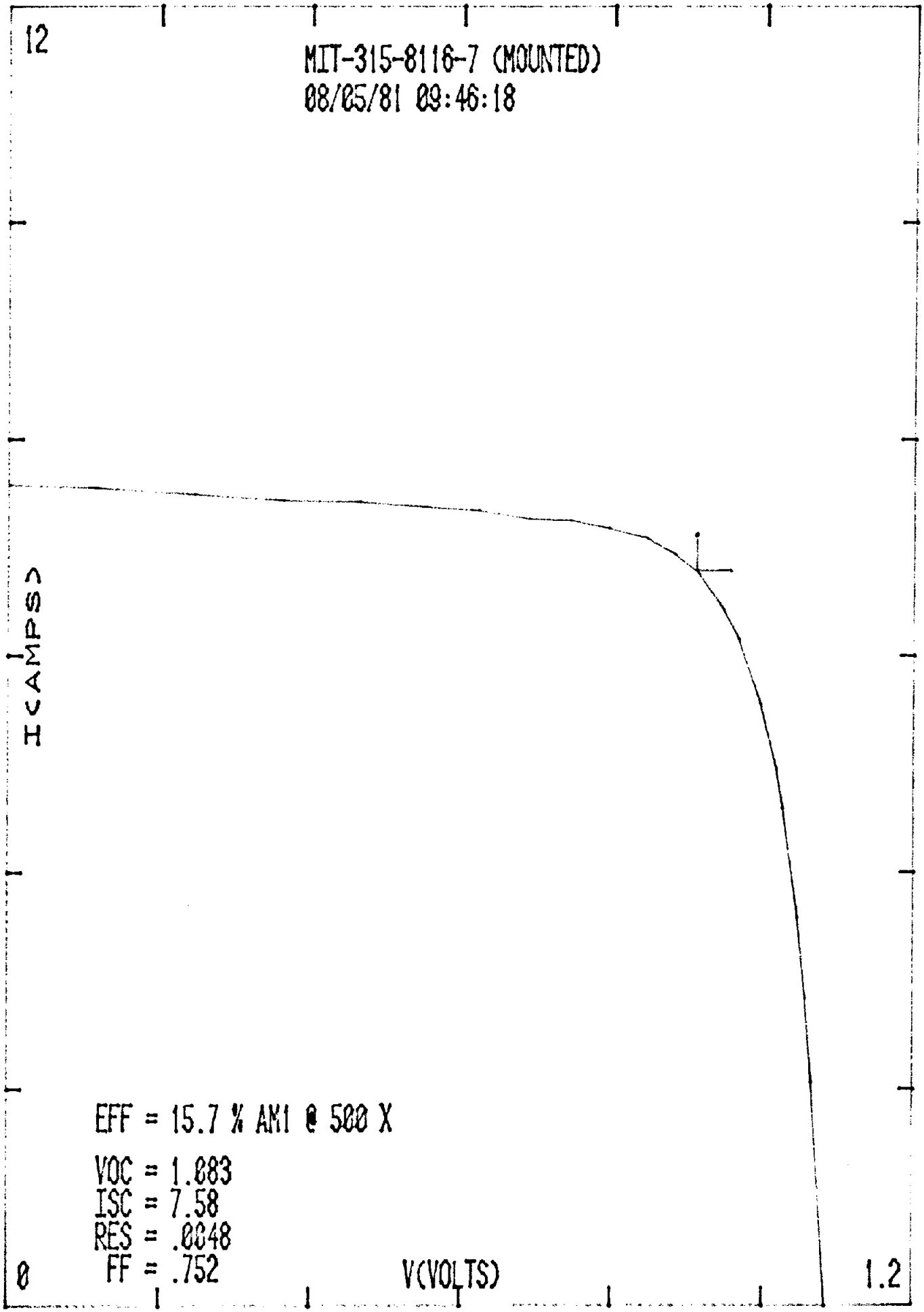
12
MIT-315-8116-7 (MOUNTED)
08/05/81 09:46:18
I(AMPS)
EFF = 15.7 % AM1 @ 500 X
VOC = 1.083
ISC = 7.58
RES = .0048
FF = .752
0
V(VOLTS)
1.2

APPENDIX 3

THE EFFECT OF DISTRIBUTED SHEET RESISTANCE ON THE PERFORMANCE OF SOLAR CELLS

THE EFFECT OF DISTRIBUTED SHEET RESISTANCE ON THE PERFORMANCE OF SOLAR CELLS

J. R. Oliver
Rockwell International
Microelectronics Research and Development Center
Thousand Oaks, California 91360

ABSTRACT

Illuminated and dark current-voltage (I-V) characteristics of solar cells with one- and two-dimensional distributed sheet resistance networks are presented for a wide range of operating conditions. The models take into account the effect of depletion width variation with voltage, as well as the shunting behavior of the diode region beneath the contact metallization. The value of the equivalent series resistance, R_{eq}, as derived from the slope of the light I-V curve near the open circuit voltage V_{oc}, is shown to be substantially affected by the metallization area and the level of the photogenerated current I_{ph}. It is shown that for values of the sheet resistance, R_s, such that $I_{ph}R_s < 0.1$ volt, a lumped equivalent series resistance model with $R_{eq} = R_s/3$ is a reasonable approximation for solar cell design and evaluation.

Theoretical and experimental data for radial concentrator solar cells show that the "photoconductive shunt" phenomenon at high concentration is actually due to excessive sheet resistance, in spite of low measured values for R_{eq}. Computed data for R_s/R_{eq}, fill factor, and short circuit current are presented as functions of $I_{ph}R_s$ and the metallization area.

Preprint - submitted to IEEE Transactions on Electron Devices

THE EFFECT OF DISTRIBUTED SHEET RESISTANCE ON THE PERFORMANCE OF SOLAR CELLS

J. R. Oliver
Rockwell International
Microelectronics Research and Development Center
Thousand Oaks, California 91360

During the course of testing and evaluation of AlGaAs/GaAs concentrator solar cells, occasionally a substantial reduction in cell fill factor and efficiency has been observed with concentrations greater than 100 SUNs. An example of this is shown in Fig. 1 for cell current-voltage (I-V) curves taken at 1 SUN AM1 (dc) and 500 SUNs (xenon flash) simulated illumination using computer controlled test equipment. In this particular example, the 1 SUN I-V curve shows good open circuit voltage, V_{oc}, and short circuit current, I_{sc}, with an excellent fill factor of 0.819 and good efficiency (21.1%). However, at 500 SUNs the I-V curve has "softened" considerably, with a substantial non-zero slope of the curve near V = 0, suggesting that some kind of shunt leakage effect is occurring. Furthermore, evaluation of the cell equivalent series resistance from the slope of the I-V curve at V_{oc}, given by[1,2]

$$R_{eq} \cong -(dV/dI)_{V_{oc}} - nkT/eI_{sc} \qquad (1)$$

where n is the diode quality factor, k is Boltzman's constant, and T is the temperature, gives a value of R_{eq} = 9.8 mΩ, a resistance far too small to account for the drastic reduction in cell efficiency at 500 SUNs. In addition, dark I-V characteristics for this cell show nearly ideal diode performance, with insignificant shunt leakage and little evidence of series resistance problems at high currents.

There are several possible explanations for the kind of result presented in Fig. 1(b). One possibility is that the solar cell collection efficiency decreases with forward bias as a result of decreasing depletion layer width. Since the large majority of photo-generated carriers in AlGaAs/GaAs solar cells are generated in the surface p (or n) layer as a result of the high ($>10^4$ cm^{-1}) optical absorption coefficient of GaAs, cell collection

efficiency is primarily determined by the ability of these carriers to diffuse through the neutral p-layer to the depletion region. Collection efficiency is therefore a function of both the minority carrier diffusion length and the junction depth[3]. For cells with a proportionately large p-layer depletion width, W_{depl}, the junction depth will increase as W_{depl} decreases with forward bias. Therefore, cells with a low minority carrier diffusion length will show decreasing collection efficiency under forward bias conditions. This effect, however, can be expected to be present or even enhanced at low light intensities, in contradiction to the kind of results depicted in Fig. 1. Furthermore, spectral response measurements[4] on these cells frequently show excellent internal quantum efficiencies (>0.95 maximum) with electron diffusion lengths up to ~4 μm as determined by spectral response least-squares curve-fitting, a value much larger than the nominal 1 μm p-layer thickness.

Another possibility is the effect of an intensity-dependent recombination velocity at the AlGaAs/GaAs interface, or alternatively at the p-layer surface for cells without an AlGaAs window layer. The presence of a large number of interface states can cause significant band bending near the interface and effectively trap any short wavelength generated minority carriers (the so-called "dead zone" problem)[5]. A compelling argument against this effect is that I-V curves identical to the type shown in Fig. 1(b) can be obtained with long wavelength (>700 nm) illumination for equal values of I_{sc}. Furthermore, interfacial recombination, in general, tends to decrease rather than increase with higher illumination. Photoconductive edge leakage can also be discounted, as edge masking has no effect on the I-V characteristic at high illumination intensities.

The type of results depicted in Fig. 1 phenomenologically suggests a "photoconductive shunt", although it is difficult to conceive of a physical mechanism that would produce such an effect. It will be shown, however, that such a characteristic can be adequately described by taking account of the distributed nature of the series sheet resistance. The shunting effect, as described here, is actually due to the excess forward biasing of the p-n junction in regions distant from the front-surface contact metallization. In the model to be described, we will examine both one- and two-dimensional sheet

resistance effects for the dark and light I-V characteristics of solar cells, including the influence of the contact metallization and the variation in sheet resistance with depletion layer width. The computed results apply generally to all types of solar cells, including Si cells and cells operated over a wide range of illumination intensities.

DISTRIBUTED SHEET RESISTANCE MODEL

The effects of a distributed sheet resistance network on the performance of solar cells has been examined by several authors[6-9]. It has been shown[10,11] that for low values of $I_{ph}R_s$, where I_{ph} is the total photogenerated current and R_s is the series sheet resistance, a single lumped series resistance model can give a fair approximation to a more elaborate distributed network. However, for high values of photocurrent and/or sheet resistance, a lumped series reistance model is no longer adequate. A more realistic one-dimensional distributed network can be modeled as shown in Fig. 2. The active area of the device is broken down into m cells, each generating a current I_{ph}/m with a sheet resistance R_s/m. This network is shunted by the diode region underneath the contact metallization with a fractional area A = A(metal)/A(total). The inclusion of the contact diode region, which includes the grid metallization plus contact (bus) pads, is of particular importance since this region can comprise up to 45% of the total diode surface area in the case of radial concentrator cells, and 10-20% of the surface area for rectangular cells. The contact resistance, R_c, is composed of two parts, as shown in Fig. 2: the resistance R_{c1} for contact to the active area of the cell, and R_{c2} for contact to the diode region beneath the metallization. In general, $R_{c1} \neq R_{c2}$, as these resistances will be a function of the both gridline and bus metallization areas. The metallization resistance, R_m, which is primarily due to the fine gridlines, has not been included in Fig. 1 since it is a distributed resistance effect analogous to the sheet resistance, and therefore difficult to model without substantial complexity. However, unlike the sheet and contact resistances, which are affected by cell growth conditions and processing variables, the metallization resistance is primarily governed by the design of the contact geometry and the metallization thickness. It will be assumed for the purposes

of this paper that the contact metallization has been properly designed to minimize R_m, so that it can be ignored. Likewise, base resistance effects due to substrate resistivity and backside contacting will also be ignored.

The non-linear nature of the network in Fig. 2 requires the use of numerical computer techniques for the generation of I-V curves. Since identical curves can be generated for differing values of I_{ph} and R_s so long as the product $I_{ph}R_s$ remains the same, I-V curves are specified in terms of the latter. Briefly, values for $I_{ph}R_s$, the diode quality factor n, and the fractional metallization area A are initially specified. The p-n junction diode characteristic is specified by a diode voltage V_d @ I_{ph} through the relation

$$I_{ph} = (1 - A)I_o[\exp(eV_d/nkT) - 1] \qquad (2)$$

where I_o is the saturation current for the entire diode area. Equation (2) is the usual diode equation which takes into account the fractional reduction A of the cell active area due to the contact metallization. The saturation currents for the active area segments and the region underneath the contact metallization are therefore given by $(1-A)I_o/m$ and AI_o, respectively. The specification of the diode voltage V_d rather than I_o removes the complexity of attempting to specify I_o for different values of n, and furthermore, it is a parameter which is closely related to V_{oc}.

The contact resistances R_{c1} and R_{c2} will be assumed to be sufficiently small compared to R_s so that they can be ignored for the purposes of this paper. Light I-V curves are simulated on the computer by assuming a cell output voltage, V, and a normalized current I/I_{ph}, and then computing the voltage and current at each node of Fig. 2, going from right to left. If the voltage at the kth node is greater than V_d, or if the current is greater than $I_{ph}(m-k)/m$, the current is reduced by a small increment $\Delta I/I_{ph}$, and the process is repeated. When the mth node is finally reached, the current I at V has been determined, and the next output voltage step is taken.

A family of current-voltage curves for V_d = 1.15 volts, A = 0.2, n = 1 and $I_{ph}R_s$ = 0-5 are shown in Fig. 3(a). Curves for the same set of parameters with n = 2 are shown for comparison in Fig. 3(b). Note that the curves at the extremes of high and low generation current bear a striking resemblance to the experimental curves shown in Fig. 1. Of particular interest is the de-

creasing value of I_{sc}/I_{ph} and the non-zero slope of the I-V curves near I_{sc} for values of $I_{ph}R_s > 1$ volt. Nevertheless, the curves become quite steep near V_{oc} implying a low apparent series resistance. Figure 4 shows the relationship between the equivalent sheet resistance R_{eq}, as determined from Eq. (1), and R_s for several values of the fractional metallization area A. It is seen that $R_{eq} < R_s$ for all values of I_{ph}, with the difference becoming greater as I_{ph} is increased. Furthermore, the metallization area has a significant influence on the value of R_{eq}. This is not unexpected upon close inspection of the model given in Fig. 2, since the dynamic resistance of the metallization diode appears in parallel with the net series resistance of the active region. In effect, the current shunting behavior of the diode region underneath the contact metallization cuts off the I-V characteristic at an open circuit voltage smaller than what would be expected when A = 0, thereby steepening the I-V characteristic near V_{oc} and reducing the value of R_{eq}. At low currents, the reduction in V_{oc} can be given approximately by $V_{oc} = V_d + [(nkT/e) \ln(1-A)]$ using Eq. (2). At higher currents, the reduction in V_{oc} is even greater because of the additional voltage drop across the distributed sheet resistance network.

It is of interest to compare the results of Fig. 4 with the equivalent lumped series resistance, R^p_{eq}, derived from the ohmic power loss in the active region[12]. Consider a rectangular active region segment of length L bounded by two gridlines separated by a distance ℓ. The incremental sheet resistance normal to the gridlines for a resistivity ρ is given by

$$dR_s = \rho dx/Lt_p \tag{3}$$

where t_p is the neutral p (or n) layer thickness and x is the distance from the mid-point between the two gridlines. For a generation current density of $J_{ph} = I_{ph}/(L\ell)$, the current flowing toward either gridline from a region x wide is simply given by

$$I = J_{ph}Lx \tag{4}$$

so that the total power loss is given by

$$I_{ph}R^p_{eq} = 2\int_0^{\ell/2}(J^2_{ph}L\rho/t_p)x^2dx \;=\; J^2_{ph}(\rho\ell^3L/12t_p). \qquad (5)$$

Therefore, from Eq. (5), we have

$$I_{ph}R^p_{eq} = J_{ph}(\rho\ell^2/12t_p). \qquad (6)$$

This is to be compared with the value of $I_{ph}R_s$ given by

$$I_{ph}R_s = \int_0^{\ell/2}(J_{ph}\rho/t_p)xdx \;=\; J_{ph}(\rho\ell^2/4t_p). \qquad (7)$$

Comparing Eqs. (6) and (7) then, we have $R_s/R^p_{eq} = 3$, in agreement with the computed asymptotic ($I_{ph}R_{eq} \ll 1$) value in Fig. 4 for A = 0. Hence, the experimentally determined value of R_{eq} using Eq. (2) in an accurate measure of the lumped equivalent power resistance as long as the fractional metallization area and the total generated current are low. This is not surprising, for at low currents a lumped equivalent series resistance model is a reaonable approximation to the distributed network of Fig. 2, as discussed earlier[10,11]. However, for A>0 and/or large values of I_{ph}, the value of the sheet resistance must be determined from measured values of R_{eq} using the results of Fig. 4. These results strongly bring to question the interpretation of the derivative I-V series resistance measurement techniques presented by Chaffin and Osbourn[1] and Cape et al.[2] when applied at high illumination intensities. This problem will be discussed in further detail in a companion paper[13].

The dark current-forward voltage characteristic of the equivalent circuit in Fig. 2 can be numerically calculated by computer in a manner similar to that outlined earlier. In this case, the generation currents I_{ph}/m in Fig. 2 are all zero, and I_{ph} in Eq. (2) is replaced by the maximum forward dark current I_{max}. The normalized dark I-V characteristic for $I_{max}R_s = 10$, A = 0.2, $V_d = 1.15$ and n = 1 is shown in Fig. 5. It can be seen that the effect of the distributed sheet resistance is barely detectable even at high currents; this is because the bulk of the injected dark current is conducted by the diode region underneath the metallization in parallel with the distributed resistance network. The difference between the diode voltage V_d (Eq. (2)) and V_{max}

at high values of I_{max} is a function of the metallization to active area ratio and is approximately given by $V_{max} \cong V_d - (nkT/e)\ell n(A/1-A)$. Hence, for A = 0.2, V_{max} = 1.185 volts. The actual value is slightly less at 1.182 volts because of the small additional current conducted by the distributed sheet resistance network. The I-V characteristic for the same network with A = 0 is shown in Fig. 5 for comparison. Also shown is the curve for A = 0 with a lumped equivalent series resistance $R^p_{eq} = R_s/3$ (cf. Eqs. (6) and (7)). It can be seen that the lumped equivalent model is a reasonable representation of the distributed network only for values of $I/I_{max} < 10^{-2}$, or $IR^p_{eq} < 0.03$.

DEPLETION WIDTH MODULATION

In addition to the foregoing, for lightly doped surface layers or for solar cells with shallow p-n junctions, the modulation of the depletion width with voltage can also have a significant effect on the I-V characteristics. This is because the neutral surface layer thickness (i.e., junction depth) will change with voltage-controlled variations of the p-layer depletion width, W_{depl}. Because of the wide variety of doping concentrations and p-layer thicknesses possible in actual solar cells, it is preferable from a computational standpoint to specify a normalized depletion width $W_p = W_{depl}/W$, where W is the total thickness of the p-layer. A similar analysis can also be applied to n-on-p solar cells. Using the depletion approximately for uniform doping[14], W_p will change with voltage as

$$W_p(V) = W_{po}[(V_j - V)/V_j)]^{\frac{1}{2}} \tag{8}$$

where W_{po} is the value of W_p at V = 0 and V_j is the diffusion potential of the p-n junction. Since the junction depth $t_p = W(1-W_p)$, each element of the distributed sheet resistance network will have a depletion width dependence given by

$$[R_s(V_k)/m]\Big|_k = (R_s/m)[(1 - W_{po})/(1 - W_p(V_k))] \tag{9}$$

where R_s is the value of the sheet resistance at zero bias and V_k is the voltage at the kth node in Fig. 2.

Computer plots of the light I-V characteristics for a GaAs cell (V_j = 1.42 volts) with W_{po} = 0 and W_{po} = 0.5 are shown in Fig. 6 for a value of $I_{ph}R_s$ = 2 volts. All other parameters are the same as those given in Fig. 3. It can be seen that the W_{po} = 0.5 curve tends to "fill out" the characteristic with a corresponding higher fill factor (0.476 vs. 0.40). The equivalent sheet resistance is also lower for this curve ($I_{ph}R_{eq}$ = 0.097 vs. 0.132) as a result of the steeper slope of the characteristic near V_{oc}. The general reduction of R_{eq} is shown in the dotted curve of Fig. 4 for W_{po} = 0.5.

Also shown in Fig. 6 is the light I-V curve for a lumped equivalent sheet resistance given by $I_{ph}R^p_{eq} = I_{ph}R_s/3$ and W_{po} = 0. Although the fill factor (0.414) is comparable to that for the distributed sheet resistance case, the overall shape of the curve is substantially different. A general comparison of fill factors and I_{sc} values for the lumped and distributed models is shown in Fig. 7. The fill factor is only slightly enhanced for $A>0$ as a result of the slight reduction in V_{oc}. However, a far more significant change in fill factor and I_{sc} occurs for moderate values of the normalized depletion width W_{po}.

TWO-DIMENSIONAL MODEL

The preceding analysis has considered the distributed sheet resistance as a one-dimensional problem. Such an analysis is perfectly adequate for rectangular cells having parallel gridlines and uniform illumination, since each of the m incremental elements in Fig. 2 will lie along equipotential lines parallel to the gridlines. However, this is not the situation for concentrator cells having a radial contact geometry. In this case, the high intensity illumination is generally non-uniform and the gridline spacing is a linear function of radius. Here a two-dimensional analysis must be used, even if the illumination is assumed to be uniform over the entire cell active area. For uniform illumination, paralleled sheet resistance networks of the type shown in Fig. 2 are used in which the incremental values of R_s/m, I_{ph}/m, and diode area (or saturation current) are linear functions of the contact spacing, ℓ. The kth nodes of adjacent networks are interconnected by incremental sheet resistance elements, R'_s. However, for cell geometries where the contact spacing vs. length

ratio $\ell/L \ll 1$, the elements R_s' may be deleted so that the paralleled networks can be evaluated independently of each other. The paralleled networks are terminated by a single metallization diode of fractional area A, as before, where once again the contact resistances R_{c1} and R_{c2} are ignored.

Present radial cell geometry design favors radial gridlines intersected by concentric lines spaced at radii r/2, r/4, r/8, etc.[15]. The number of radial lines in each concentric ring is adjusted so that the average gridline spacing is constant for all rings. Hence, the ratio of minimum to maximum line spacing is given by $t_f = 0.5$. Figure 8 shows a computer-generated family of light I-V curves for this case with $V_d = 1.15$ volts, $n = 1$, $W_{po} = 0$, and $I_{ph}R_s = 0$-5 volts. The metallization area is A = 0.4 for Fig. 8, appropriate to a rectangular bus region circumscribing the circular active area. A comparison of Figs. 3 and 8 shows that the radial geometry causes a slight "softening" of the I-V characteristics, particularly for values of $I_{ph}R_s$ near 1. For example, the $I_{ph}R_s = 0.5$ volt curves in Figs. 3 and 8 have fill factors of 0.735 and 0.699, respectively. This "softening" characteristic becomes dramatically worse, however, for V-shaped active regions with $t_f = 0$ (no concentric grid lines), for which the fill factor is only 0.580 in the present example. Such a geometry is clearly not desirable for radial cell design.

The equivalent sheet resistances R_{eq} (Eq. (2)) for the two-dimensional example of Fig. 8 are essentially the same as those for Fig. 3, save for the difference in the metallization areas for the two cases. Therefore, the results shown in Fig. 4 are also applicable to the two-dimensional model. Figure 9 graphically shows the two-dimensional voltgae profile of the active region for a radial geometry with $t_f = 0.5$ and $I_{ph}R_s = 2$ volts. The nonlinearity of the cell voltage as a function of both radius and distance from the contact is clearly evident. In the regions where the voltage approaches the open circuit diode voltage, V_d, virtually all of the photogenerated current is cut off by the forward biased diode[6,9]. This is particularly evident in Fig. 9(b) for a terminal voltage of 0.74 volts (the maximum power point) where only 60.7% of the photocurrent is collected at the contact.

EXPERIMENTAL

Consider now a series of Rockwell International AlGaAs/GaAs concentrator solar cells, N7/M-186, grown at 655°C by the MO-CVD process[16]. These are 1 cm diameter radial geometry cells designed to operate at 400-600 SUNs intensity. This series of cells shows excellent spectral response (maximum internal quantum efficiency of 0.96) with fill factors of ~0.84 and efficiencies of 21-22% at 70 SUNs intensity. However, at higher intensities the cell I-V characteristics are considerably softened, much in the same manner as shown in Fig. 1, with efficiencies of only 13-14% at 500 SUNs. Nevertheless, the apparent equivalent sheet resistance is in the range of only 4.5-7 milliohms.

Accurate capacitance-voltage measurements on such large area cells are difficult because of low-level leakage currents. However, capacitance measurements on the lowest leakage cells show a total depletion width of 0.275 μm, a value substantially larger than targeted and indicative of abnormally low doping. The question remains whether the doping levels are low in the surface p-layer or in the underlying n-layer. If the doping is low in the n-type epilayer, the attendant increase in resistivity is not expected to affect cell performance because of the large area and small thickness of the epilayer (10 μm on an n^+ substrate). Hence, assuming instead that the n-layer is nominally doped to $N_D = 4 \times 10^{17}$ cm^{-3}, then the depletion width in the p-layer is $W_{depl} = 0.255$ μm with $N_A = 2.85 \times 10^{16}$ cm^{-3}. This low doping level corresponds to a resistivity $\rho = 0.55$ ohm-cm for a hole mobility of 400 cm^2/V-sec at room temperature.

Measurements on cell N7/M-186-3 show a maximum photocurrent I_{ph} = 15.65 amps at 750 SUNs illumination for moderate reverse bias in the range of -1 to -3 volts. This corresponds to a current density of J_{ph} = 22.05 amps/cm^2 for an active cell area, less 10% gridline obscuration, of 0.71 cm^2. From Eq. (7) then, for a nominal junction depth $t_p = 1.0$ μm and an average finger spacing of $\ell = 0.83$ μm, we have

$$I_{ph}R_s = 2.10 \text{ volts @ 750 SUNs}$$

$$W_{po} = W_{depl}/W = 0.203.$$

Computed curves for 750, 500, and 250 SUNs illumination are compared with normalized I/I_{ph} I-V data for this cell in Fig. 10. Best fit to the data is achieved with $W_{po} = 0.2$ and $I_{ph}R_s = 1.9$ at 750 SUNs, in excellent agreement with the computed values given above. These curves were computed with a metallization coverage (gridline + bus) of 42% of the total wafer area and a min/max gridline separation ratio of 0.5 appropriate to our radial cell geometry. The value for R_{eq}, derived from the slope of the computed I-V curve at V_{oc}, is 6.0 mΩ, in good agreement with the experimentally measured value of 4.8 mΩ. It should be noted that the computed equivalent sheet resistance is a factor of 20 smaller than the value of R_s.

Figure 11 shows the computed and measured normalized dark I-V characteristics for the same cell with a reference current $I_{max} = 15.65$ amps. It is seen that the effect of the series sheet resistance is essentially undetectable even at high currents. Also shown in the dotted curve is the computed "apparent" junction current $(1 - I/I_{ph})$ taken from the 750 SUNs data of Fig. 10. The latter deviates substantially from the actual dark I-V characteristic, and looks very much like cell shunt leakage -- hence the name "photoconductive shunt". The excellent agreement between the computed and measured curves in Figs. 10 and 11 strongly suggests, however, that this effect is actually due to the distributed two-dimensional nature of current generation and surface layer sheet resistance in the active region.

SUMMARY

The foregoing analysis shows that many of the "soft" light I-V characteristics of solar cells can be attributed to excessively high surface layer sheet resistance, this in spite of apparently contradictory low equivalent series resistance values deduced from derivative light I-V measurements or near-ideal dark I-V data. These I-V characteristics give the appearance of a "photoconductive shunt" phenomena at moderate to high illumination intensities, when in fact the shunting behavior is due to the progressive forward biasing of the p-n junction in regions away from the contact metallization. In general, high sheet resistance results in driving up the operating voltage in regions far away from the contact gridlines, and can even cut off the current

contributions from those regions where the local operating voltage approaches V_d[6,9]. When the $I_{ph}R_s$ product becomes large, the self-biasing of the p-n junction can cut off a substantial portion of the total photogenerated current, resulting in poor fill factors and a sublinear dependence of I_{sc} on illumination intensity. This type of effect has been observed for linear arrays as well as individual AlGaAs/GaAs solar cells[17,18].

It should be emphasized that sheet resistance considerations need not be confined to the performance of concentrator solar cells. For example, it is possible that a significant degradation in cell performance can occur when scaling up cell area from small test mesas. Such an effect can be explained by localized defects which provide low resistance shunting paths in the large area cell. However, we have seen that apparent shunting behavior may also be attributed to excessive sheet resistance. Since, from Eq. (7), the ohmic sheet resistance loss is proportional to the square of the contact gridline separation, the series sheet resistance in a large area cell may be drastically larger than for a small test mesa, and therefore show degraded performance in comparison with the latter. This may be checked by examining cell I-V characteristics at progressively higher illumination intensities, since sheet resistance problems will appear as a decline in cell performance at higher light levels, whereas a cell with localized shunting defects will instead show a progressive improvement. A further check can be provided by dark I-V characteristics, since shunt leakage paths will show significant deviations from a near-ideal diode characteristic.

The fact that solar cells should be fully tested at actual operating illumination intensities with at least either dc or flash solar simulation is obvious. However, the analysis presented here shows that derivative light I-V measurements of the equivalent series resistance at high light intensities do not properly represent the true value of R_s in the absence of appropriate correction factors (cf. Fig. 4). The difference between the measured value of R_{eq} at V_{oc} and the actual value of R_s is due to the distributed nature of the sheet resistance and the current shunting effect of the diode region beneath the contacts. The latter has usually been ignored in the analysis of solar cell characteristics, yet it has a significant effect on the slope of the light I-V characteristic near V_{oc}. Furthermore, dark I-V characteristics for cells with low contact resistance will show near-ideal diode behavior even though

the sheet resistance may be large. Hence, dark I-V characteristics cannot be expected to reveal sheet resistance problems, even at very high current levels, although they can indicate the presence of significant contact resistance problems. The combined effects of sheet and contact resistance, and effective methods for their measurement, will be considered in much greater detail in a companion paper[13].

Although a single lumped equivalent sheet resistance model is totally inadequate to describe the light I-V characteristics of a solar cell with $I_{ph}R_s > 1$ volt, such a model can still be reasonably applied at lower levels. Under the latter conditions, the lumped equivalent power resistance R^p_{eq} of Eq. (6) is a reasonably accurate representation of the distributed sheet resistance with $R^p_{eq} = R_s/3$. Since clearly one does not wish to intentionally design solar cells with excessively high sheet resistance, the lumped equivalent model can still be deemed adequate for most design purposes. In general, cell design should require that the value of $I_{ph}R_s$ be kept below 0.1 volt for good efficiency.

The analysis presented here shows that a two-dimensional distributed sheet resistance model must be used to adequately represent the I-V characteristics of radial cells. Furthermore, the influence of the depletion width variation with voltage must also be considered for lightly doped and/or thin surface layers. The moderate improvement in cell fill factor when this is taken into account presents interesting possibilities for the design of low concentration solar cells, particularly those for space applications where radiation hardening requires relatively thin surface layers[18].

Although the data presented is representative of GaAs concentrator solar cells, a similar analysis of cells in other materials such as Si can be obtained by merely shifting the I-V curves up or down in voltage, as required. The curves for I_{sc} and fill factor in Fig. 7 will be correspondingly affected by the value of V_{oc}. The calculation of the equivalent series resistance from the slope of the light I-V curve at V_{oc} as in Fig. 4 applies to all materials, as R_{eq} is virtually unaffected by the value of V_{oc}.

ACKNOWLEDGEMENTS

The author would like to thank Dr. John Cape and Dr. Stan Zehr for their many useful discussions and comments. This work was supported in part by Sandia National Laboratories under Contract No. 49-1792.

REFERENCES

1. R. J. Chaffin and G. C. Osbourn, "Measurement of concentrator solar cell series resistance by flash testing", Appl. Phys. Lett., vol. 37, p. 637, 1980.

2. J. A. Cape, J. R. Oliver and R. J. Chaffin, "A simplified flashlamp technique for solar cell series resistance measurements", Solar Cells, vol. 3, p. 215, 1981.

3. H. J. Hovel and J. M. Woodall, "Theoretical and experimental calculations of $Ga_{1-x}Al_xAs$-GaAs solar cells", Proceedings of 10th IEEE Photovoltaic Specialists Conference, p. 25, 1973.

4. J. A. Cape, J. R. Oliver, D. L. Miller and M. D. Paul, "Automated measurement system for solar cell optical characterization studies of GaAs and multijunction cascade cells", Proceedings of 15th IEEE Photovoltaic Specialists Conference, p. 1195, 1981.

5. H. J. Hovel, "Solar Cells", in Semiconductors and Semimetals, v. 11, pp. 15-20, 1975.

6. J. J. Wysocki, "The effect of series resistance on photovoltaic solar energy conversion", RCA Review, p. 57, 1961.

7. C. R. Fang and J. R. Hauser, "A two-dimensional analysis of sheet resistance and contact resistance effects in solar cells", Proceedings of 13th IEEE Photovoltaic Specialists Conference, p. 1306, 1978.

8. J. L. Boone and T. P. Van Doren, "Solar-cell design based on a distributed diode analysis", IEEE Trans. Electron Devices, v. 25, p. 767, 1978.

9. J. E. Mahan and G. M. Smirnov, "A new perspective on distributed series resistance effects in photovoltaic devices", Proceedings of 14th IEEE Photovoltaic Specialists Conference, p. 612, 1980.

10. R. T. Otterbein, D. L. Evans and W. A. Facinelli, "A modified single diode model for high illumination solar cells for simulation work", Proceedings of 13th IEEE Photovoltaic Specialists Conference, p. 1074, 1978.

11. R. T. Otterbein and D. L. Evans, "Two modified single diode models for simulating solar cells with distributed series resistance", Proceedings of 14th IEEE Photovoltaic Specialists Conference, p. 574, 1980.

12. J. Ewan, R. C. Knechtli, R. Loo and G. S. Kamath, "GaAs solar cells for high solar concentration applications", Proceedings of 13th IEEE Photovoltaic Specialists Conference, p. 941, 1978.

13. J. R. Oliver, "Solar cell contact and sheet resistance measurements", to be published.

14. S. Wang, Solid State Electronics (New York: McGraw Hill), pp. 313-317, 1966.

15. R. Sahai, D. D. Edwall and J. S. Harris, Jr., "High efficiency AlGaAs/GaAs concentrator solar cell development", Proceedings of 13th IEEE Photovoltaic Specialists Conference, p. 946, 1978.

16. J. A. Cape, J. R. Oliver and S. W. Zehr, "Efficiency improvement study for GaAs solar cells", Final Report for Sandia National Laboratories under Contract #49-1792, 1982.

17. J. J. Wiczer, J. A. Cape and J. S. Harris, Jr., "Gallium arsenide photovoltaic dense array for concentrator applications", SPIE, vol. 248, p. 114, 1980.

18. R. Loos, G. S. Kamath and R. C. Knechtli, "Radiation damage in GaAs solar cells", Proceedings of 14th IEEE Photovoltaic Specialists Conference, p. 1090, 1980.

FIGURE CAPTIONS

Fig. 1. I-V curves for an AlGaAs/GaAs concentrator cell at (a) 1 SUN and (b) 500 SUNs simulated illumination.

Fig. 2. Solar cell distributed sheet resistance network comprised of m elements. The network is terminated by the contact metallization diode region of normalized area A. R_{c1} and R_{c2} are contact resistances.

Fig. 3. Computed light I-V curves for V_d = 1.15 volts, A = 0.2 and $I_{ph}R_s$ = 0-5 volts for a 40 segment distributed network: (a) diode quality factor n = 1, (b) n = 2.

Fig. 4. Relationship between R_{eq} and R_s as a function of $I_{ph}R_{eq}$ and the metallization area A for n = 1. The lower dashed curve is for A = 0 and n = 2. Upper dashed curve is for A = 0.4 and W_{po} = 0.5 (see text).

Fig. 5. Computed dark I-V curves for V_d = 1.15 volts, n = 1, $I_{max}R_s$ = 10 volts and A = 0, 0.2 for a 40 segment distributed network. The dashed curve is for a lumped equivalent sheet resistance with $I_{max}R^p_{eq}$ = 3.33 and A = 0.

Fig. 6. Computed light I-V curves for the same conditions as in Fig. 3(a) with $I_{ph}R_s$ = 2 and a normalized depletion width W_{po} = 0, 0.5. The dashed curve is for a lumped equivalent sheet resistance with $I_{ph}R^p_{eq}$ = 0.667 and W_{po} = 0.

Fig. 7. Comparison of fill factors and short circuit currents for the lumped and distributed sheet resistance models with V_d = 1.15 volts, n = 1 and A = 0. The dashed curves are for the distributed model with W_{po} = 0.5.

Fig. 8. Computed light I-V curves for a two-dimensional distributed sheet resistance model with a radial finger separation ratio $t_f = 0.5$ and $W_{po} = 0$. All other parameters are the same as in Fig. 3(a).

Fig. 9. Computed two-dimensional voltage profile of the active region for a radial cell with $t_f = 0.5$, $V_d = 1.15$ volts, $n = 1$ and $I_{ph}R_s = 2$ volts. (a) Cell terminal voltage $V = 0$, (b) $V = 0.74$ volts (maximum power point).

Fig. 10. Computed and measured (N7/M-186-3) normalized light I-V curves for a radial cell with $t_f = 0.5$, $A = 0.42$, $n = 1$ and $W_{po} = 0.2$ at 750, 500 and 250 SUNs illumination. $I_{ph}R_s = 1.9$ volts and $V_d = 1.06$ volts at 750 SUNs for the computed data. Note the good agreement with the measured data taken with xenon flash illumination.

Fig. 11. Computed and measured (N7/M-186-3) normalized dark I-V curves for the same parameters of Fig. 10 with $I_{max} = 15.65$ amps. The tail in the measured curve is due to low level cell leakage. The dotted curve is the equivalent normalized junction current from the computed 750 SUNs curve in Fig. 10.

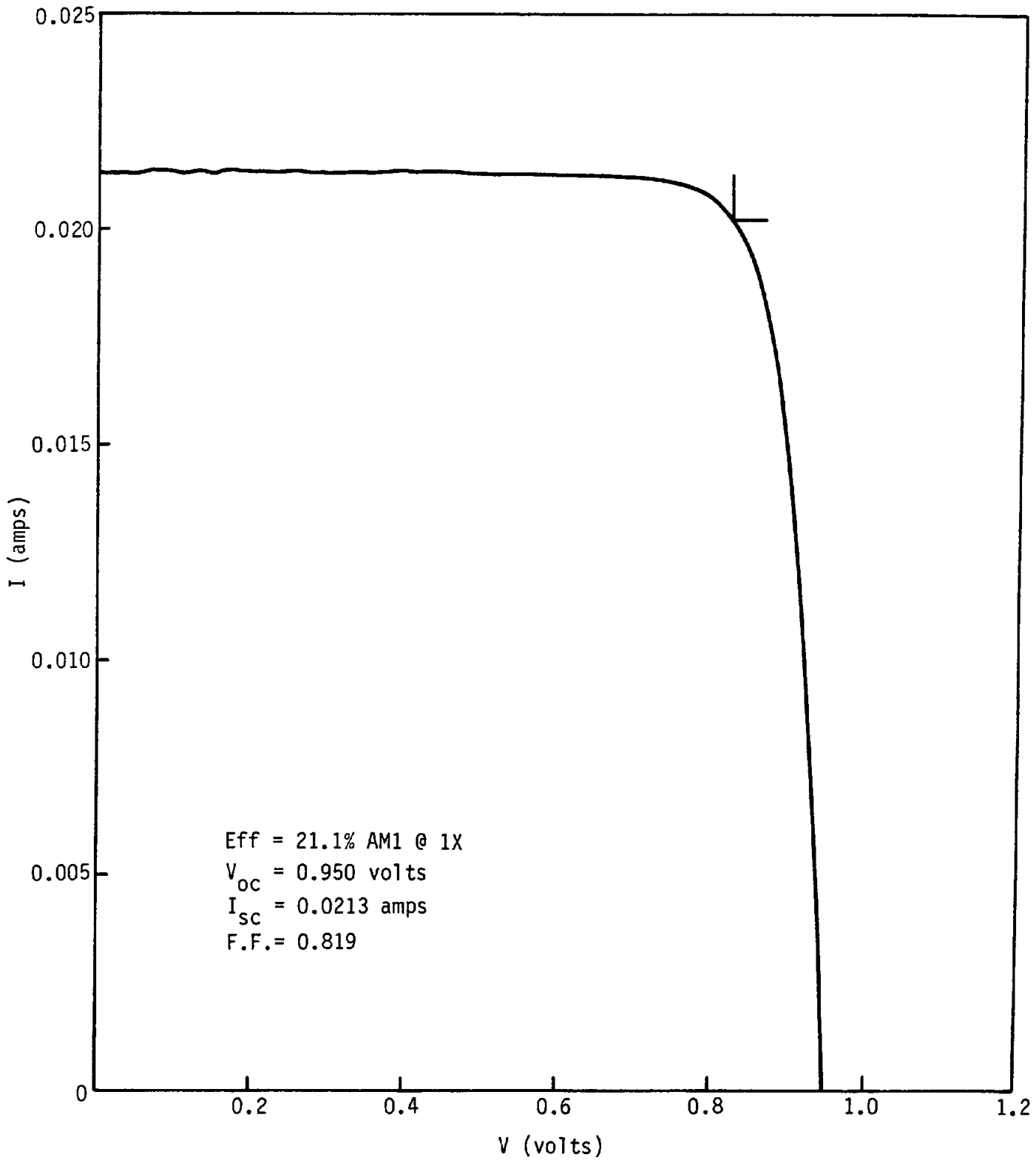
0.025
0.020
0.015
0.010
0.005
0
I (amps)
0.2
0.4
0.6
0.8
1.0
1.2
V (volts)
Eff = 21.1% AM1 @ 1X
V_{oc} = 0.950 volts
I_{sc} = 0.0213 amps
F.F.= 0.819

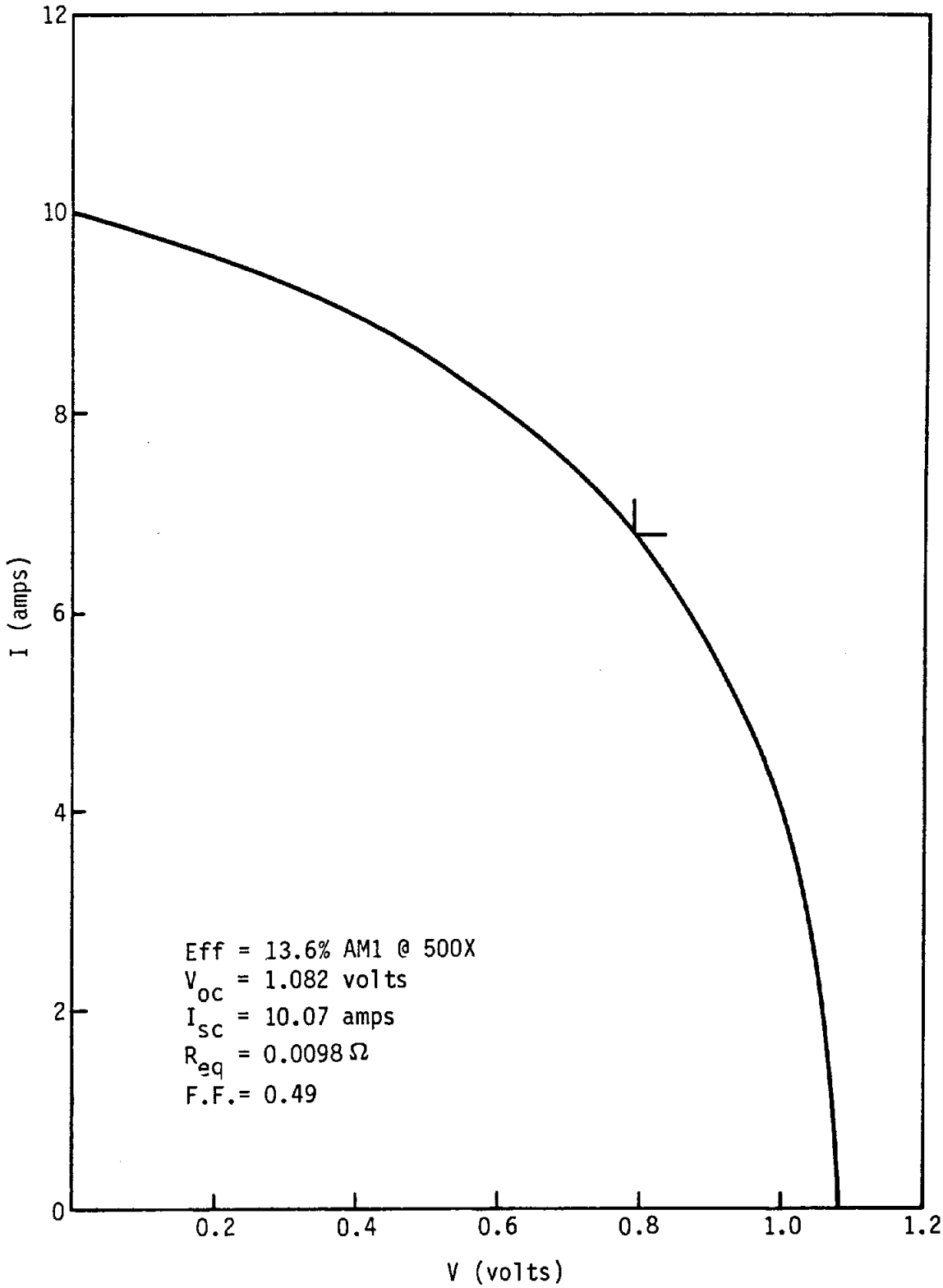
12
10
8
6
4
2
0
I (amps)
0.2
0.4
0.6
0.8
1.0
1.2
V (volts)
Eff = 13.6% AM1 @ 500X
V_{oc} = 1.082 volts
I_{sc} = 10.07 amps
R_{eq} = 0.0098 Ω
F.F.= 0.49

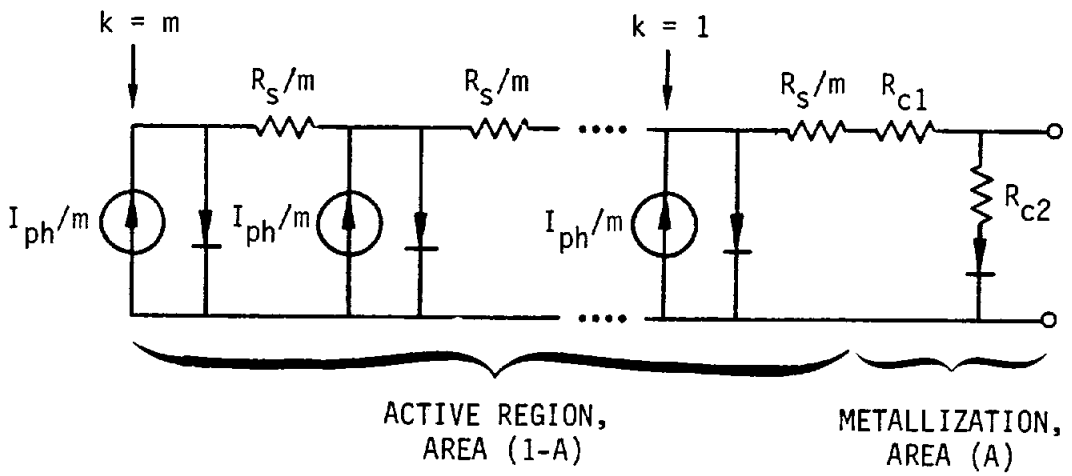
k = m
k = 1
R_s/m
R_s/m
R_s/m
R_{c1}
I_{ph}/m
I_{ph}/m
I_{ph}/m
R_{c2}
ACTIVE REGION,
AREA (1-A)
METALLIZATION,
AREA (A)

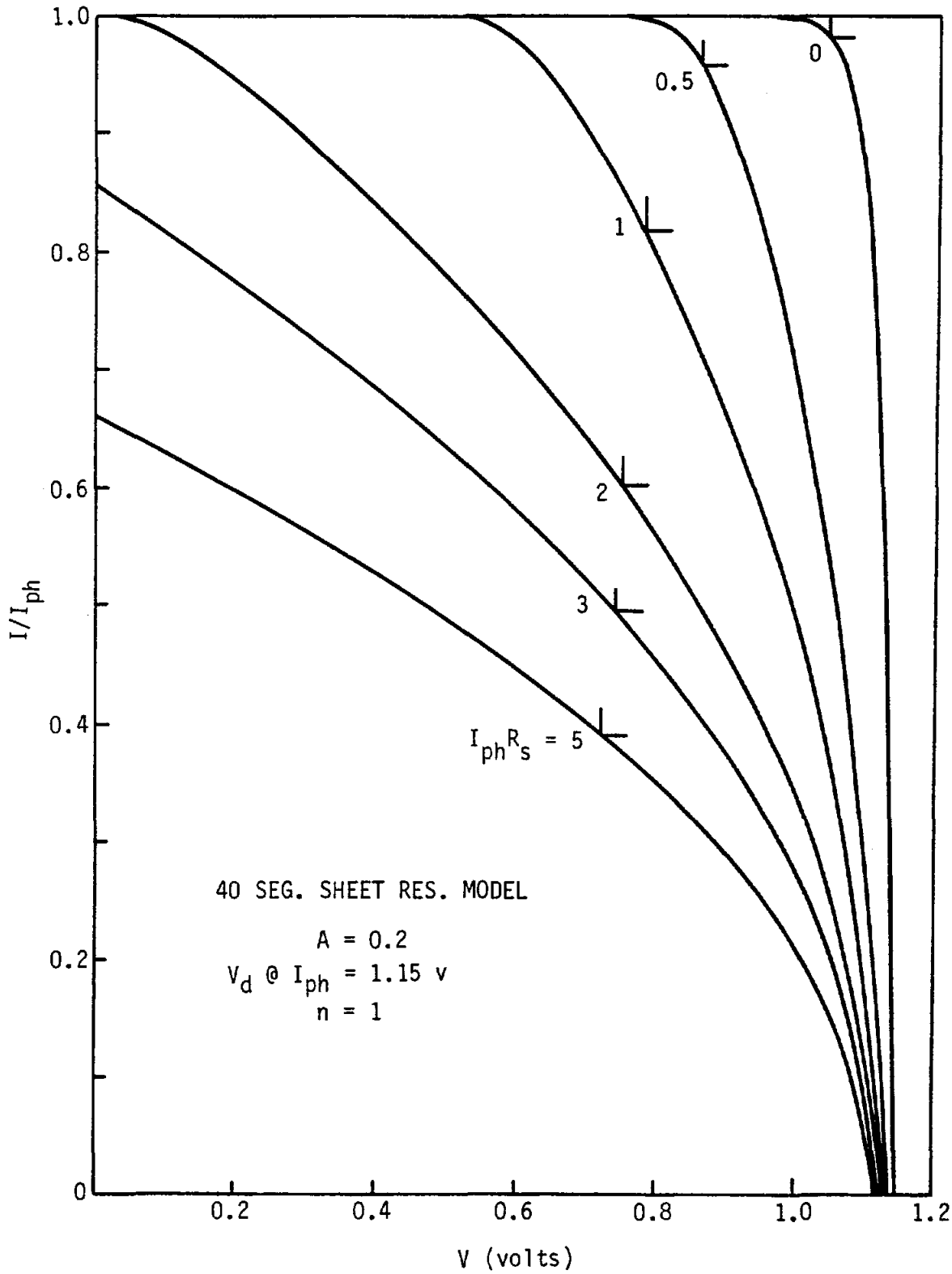
1.0
0.8
0.6
0.4
0.2
0
I/I_ph
0.2
0.4
0.6
0.8
1.0
1.2
V (volts)
0
0.5
1
2
3
I_ph R_s = 5
40 SEG. SHEET RES. MODEL
A = 0.2
V_d @ I_ph = 1.15 v
n = 1

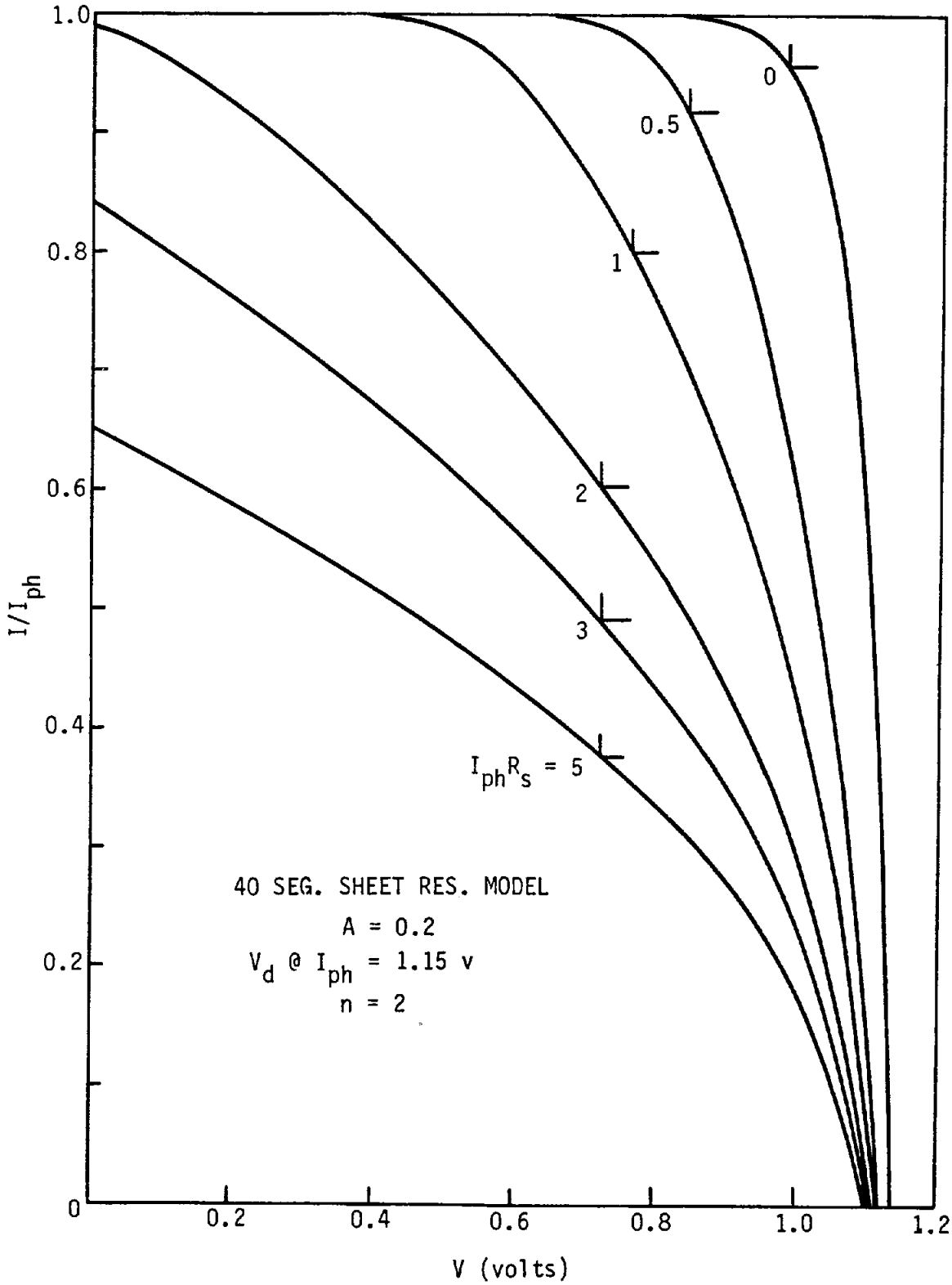
1.0
0.8
0.6
0.4
0.2
0
I/I_{ph}
0.2
0.4
0.6
0.8
1.0
1.2
V (volts)
0
0.5
1
2
3
$I_{ph}R_s$ = 5
40 SEG. SHEET RES. MODEL
A = 0.2
V_d @ I_{ph} = 1.15 v
n = 2

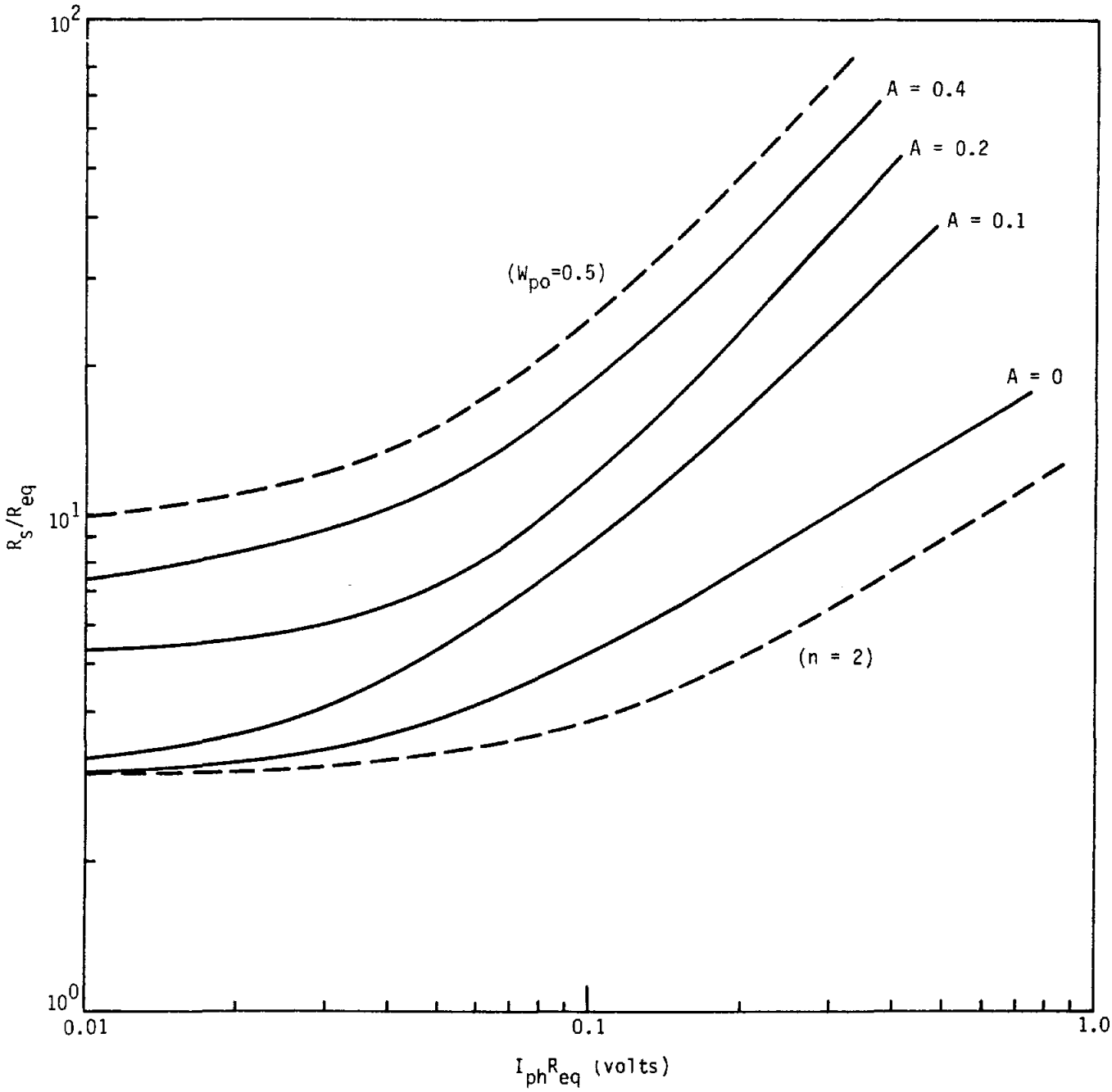
10^2
10^1
10^0
R_s/R_{eq}
A = 0.4
A = 0.2
A = 0.1
A = 0
(W_{po}=0.5)
(n = 2)
0.01
0.1
1.0
$I_{ph}R_{eq}$ (volts)

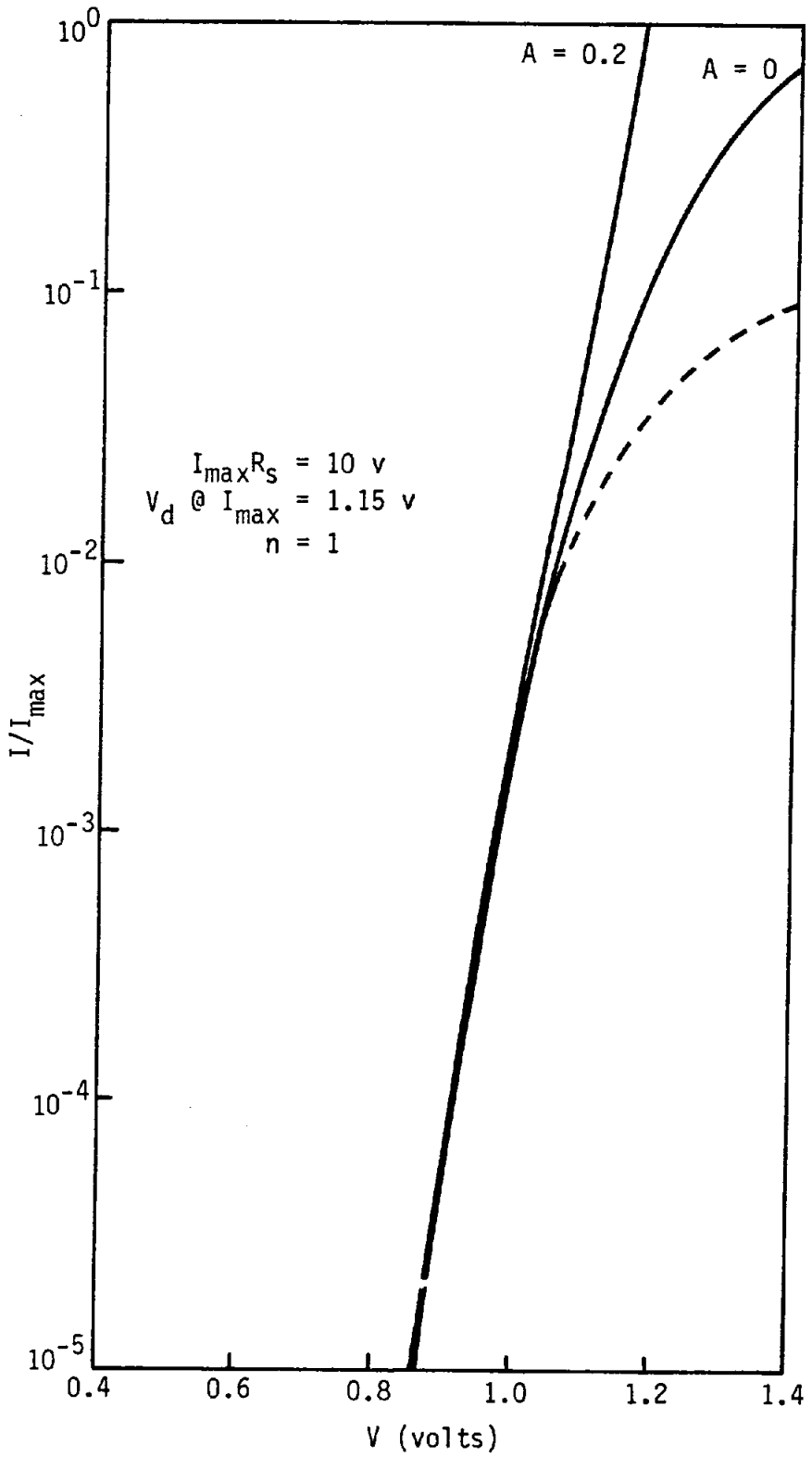
A = 0.2
A = 0
$I_{max}R_s$ = 10 v
V_d @ I_{max} = 1.15 v
n = 1
10^0
10^{-1}
10^{-2}
10^{-3}
10^{-4}
10^{-5}
I/I_{max}
0.4
0.6
0.8
1.0
1.2
1.4
V (volts)

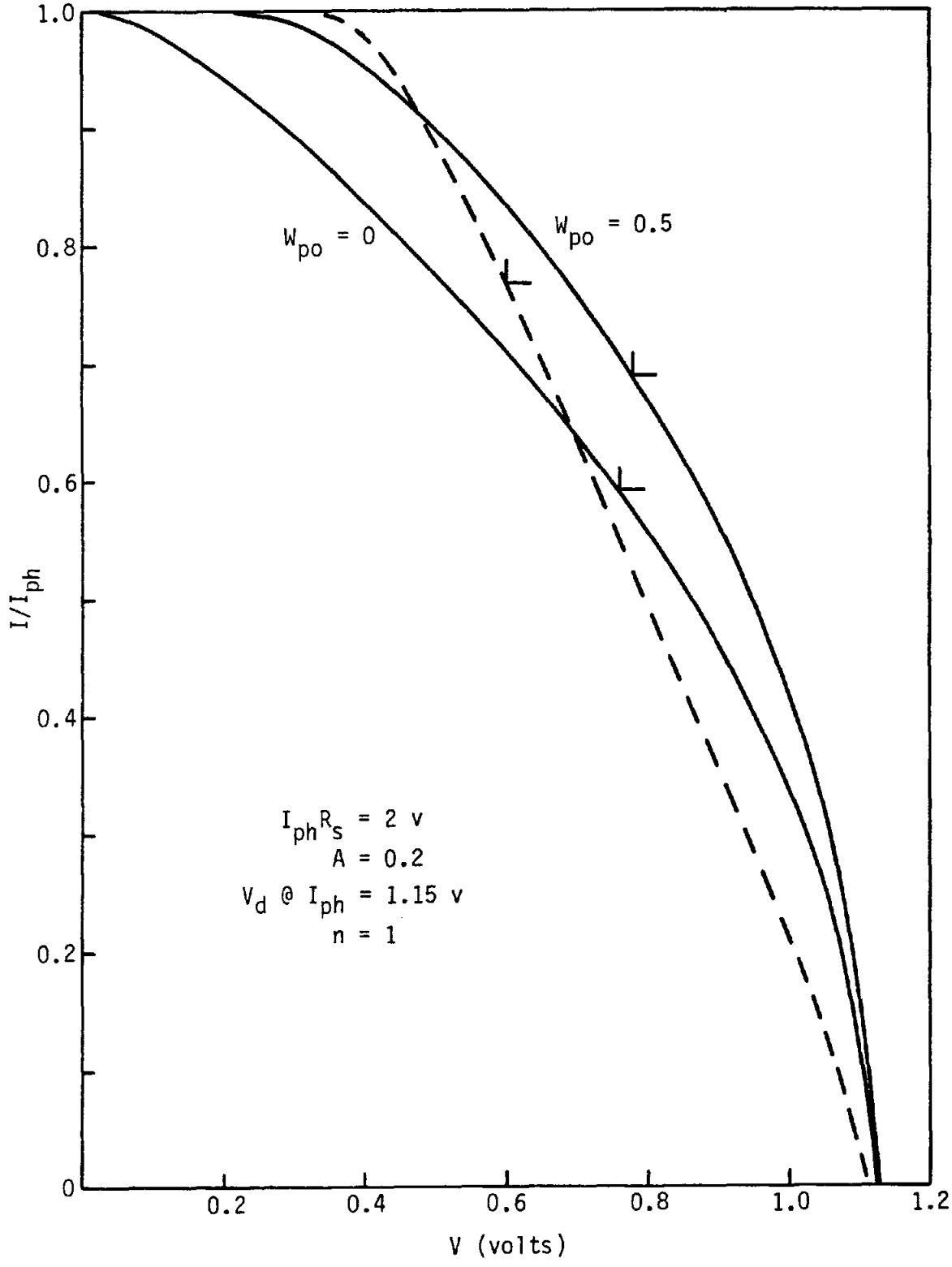
1.0
0.8
0.6
0.4
0.2
0
I/I_ph
W_po = 0
W_po = 0.5
I_ph R_s = 2 v
A = 0.2
V_d @ I_ph = 1.15 v
n = 1
0.2
0.4
0.6
0.8
1.0
1.2
V (volts)

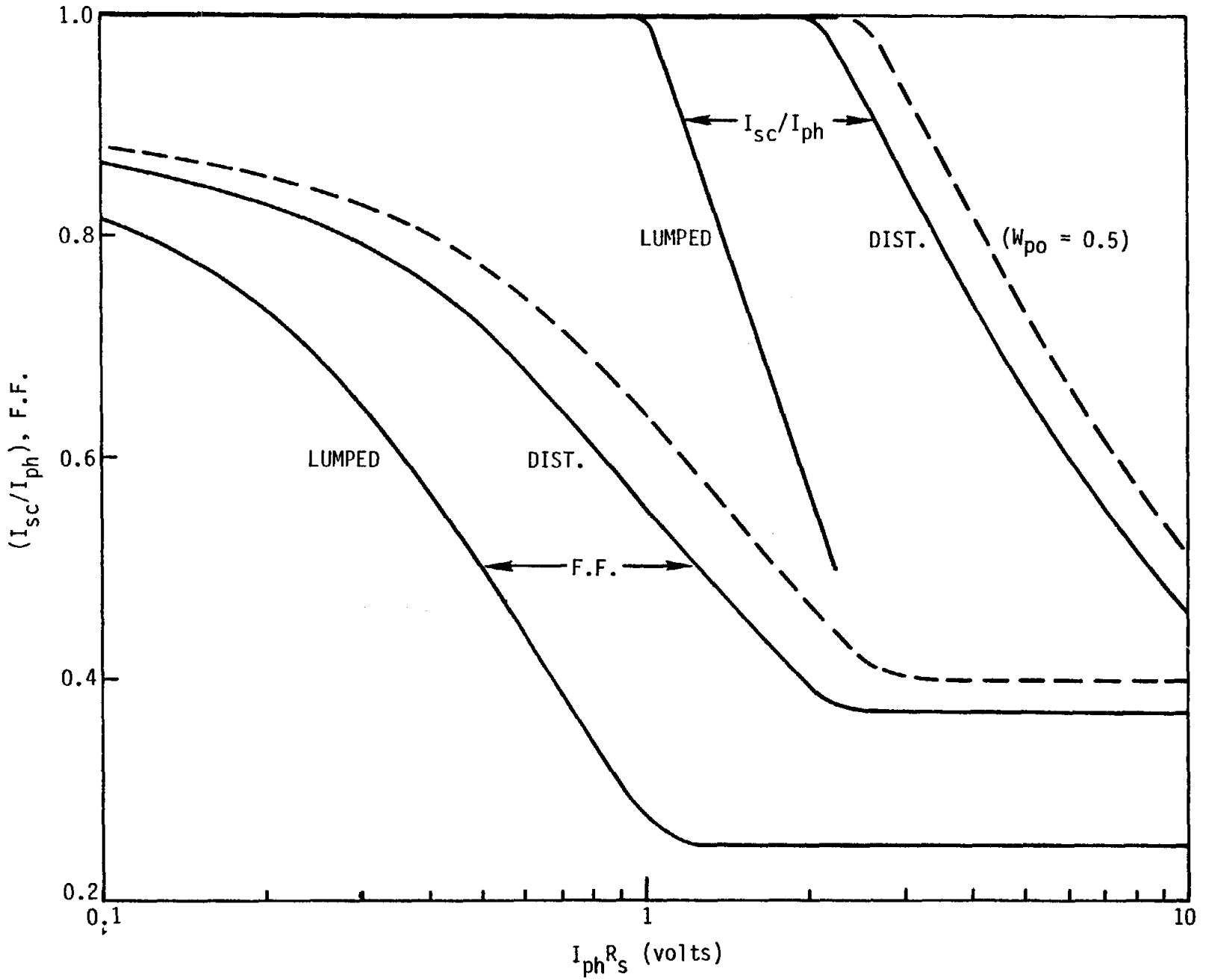
1.0
0.8
0.6
0.4
0.2
0.1
1
10
(I_{sc}/I_{ph}), F.F.
$I_{ph}R_s$ (volts)
I_{sc}/I_{ph}
LUMPED
DIST.
(W_{po} = 0.5)
LUMPED
DIST.
F.F.

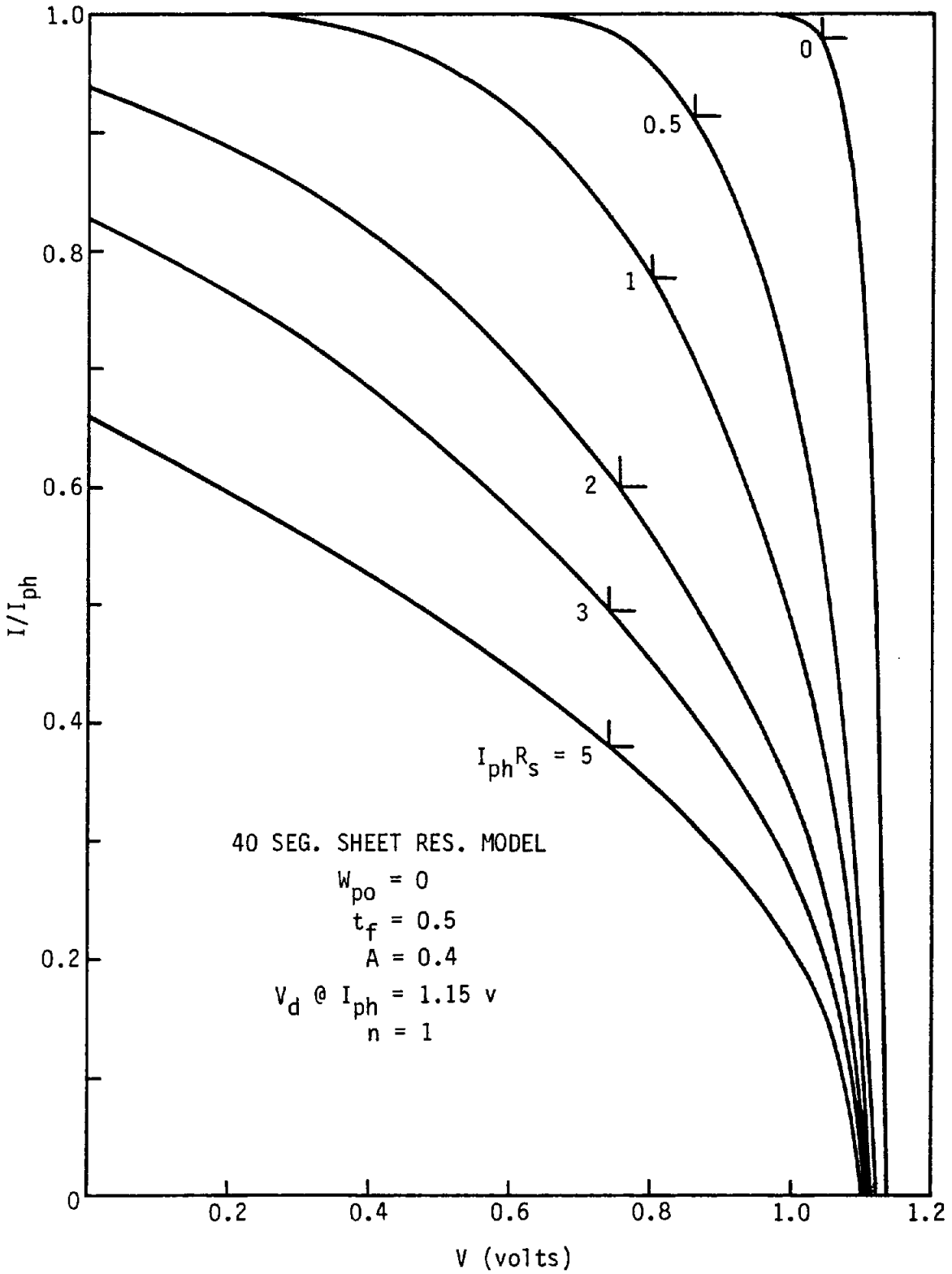
1.0
0.8
0.6
0.4
0.2
0
0.2
0.4
0.6
0.8
1.0
1.2
I/I_ph
V (volts)
0
0.5
1
2
3
I_ph R_s = 5
40 SEG. SHEET RES. MODEL
W_po = 0
t_f = 0.5
A = 0.4
V_d @ I_ph = 1.15 v
n = 1

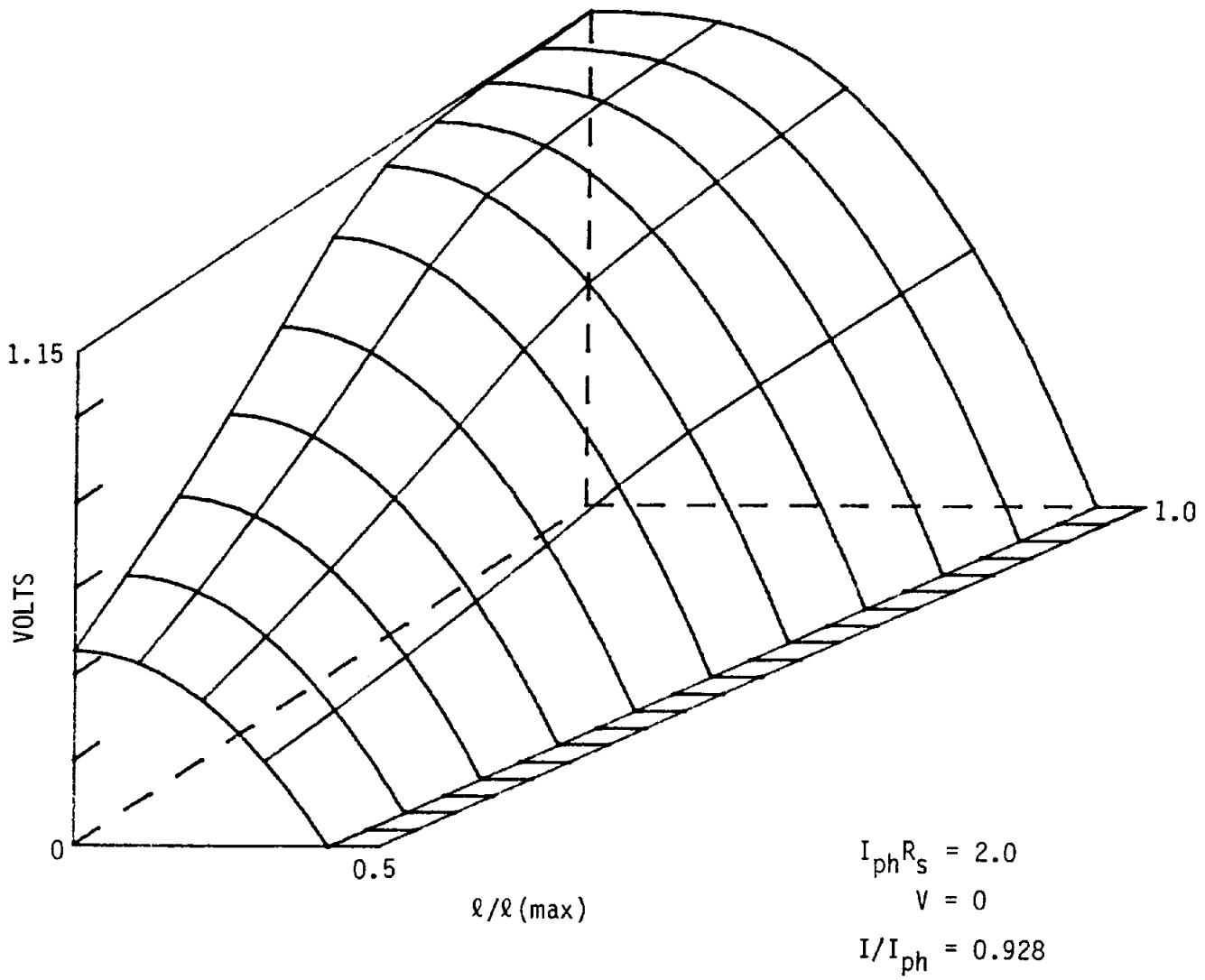
1.15
VOLTS
0
0.5
ℓ/ℓ(max)
1.0
$I_{ph}R_s$ = 2.0
V = 0
I/I_{ph} = 0.928

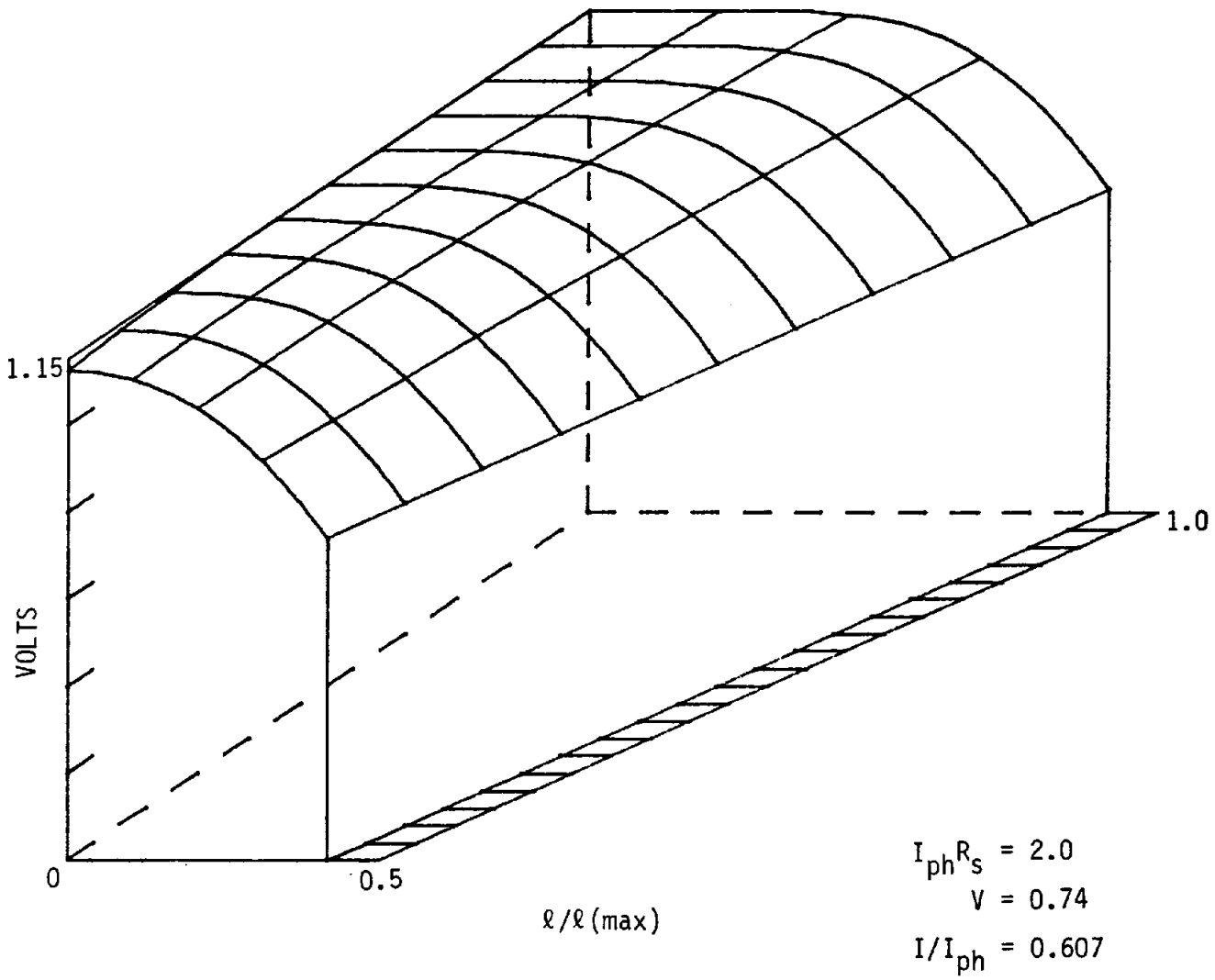
1.15
VOLTS
0
0.5
1.0
ℓ/ℓ(max)
$I_{ph}R_s$ = 2.0
V = 0.74
I/I_{ph} = 0.607

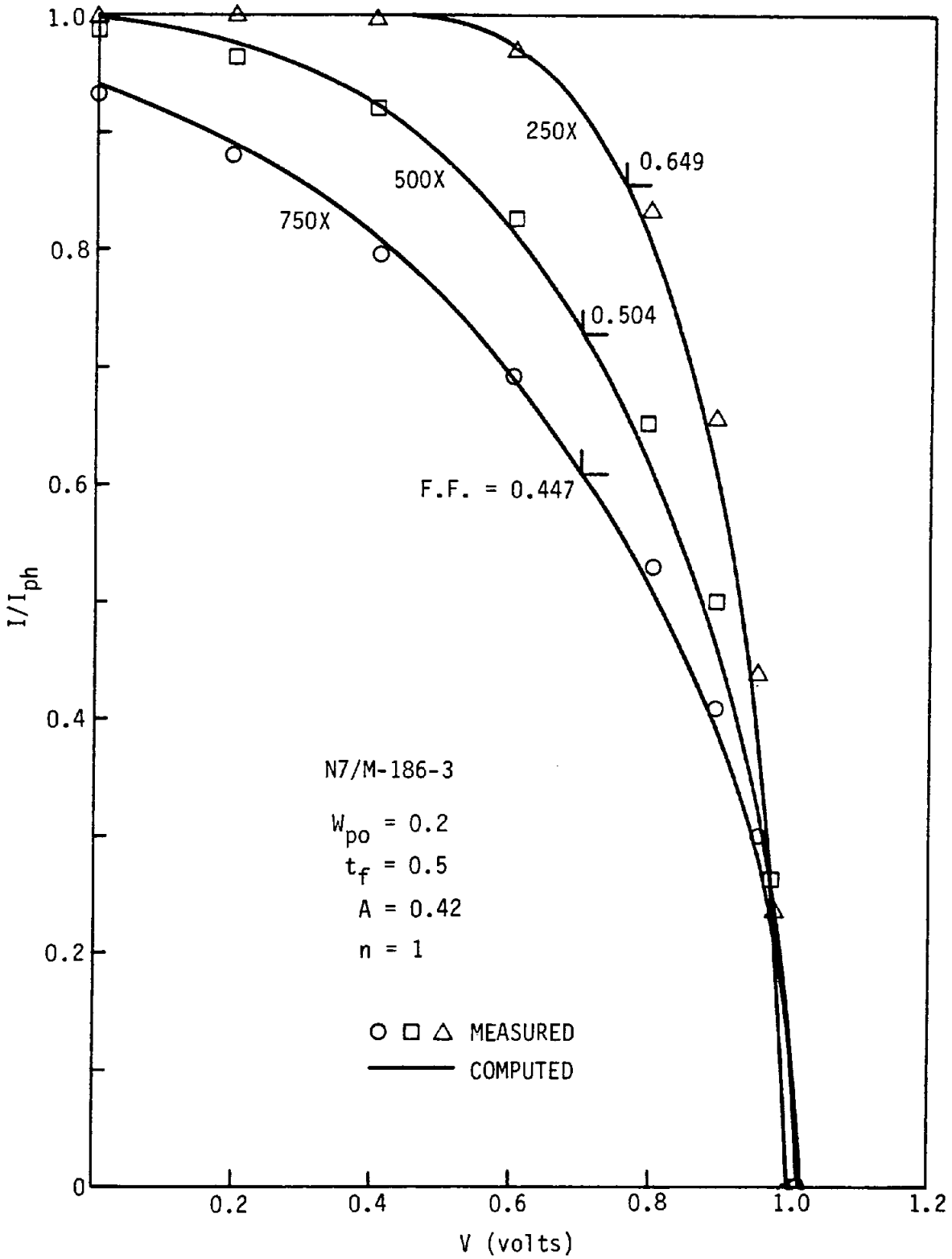
1.0
0.8
0.6
0.4
0.2
0
0.2
0.4
0.6
0.8
1.0
1.2
I/I_ph
V (volts)
250X
500X
750X
0.649
0.504
F.F. = 0.447
N7/M-186-3
W_po = 0.2
t_f = 0.5
A = 0.42
n = 1
MEASURED
COMPUTED

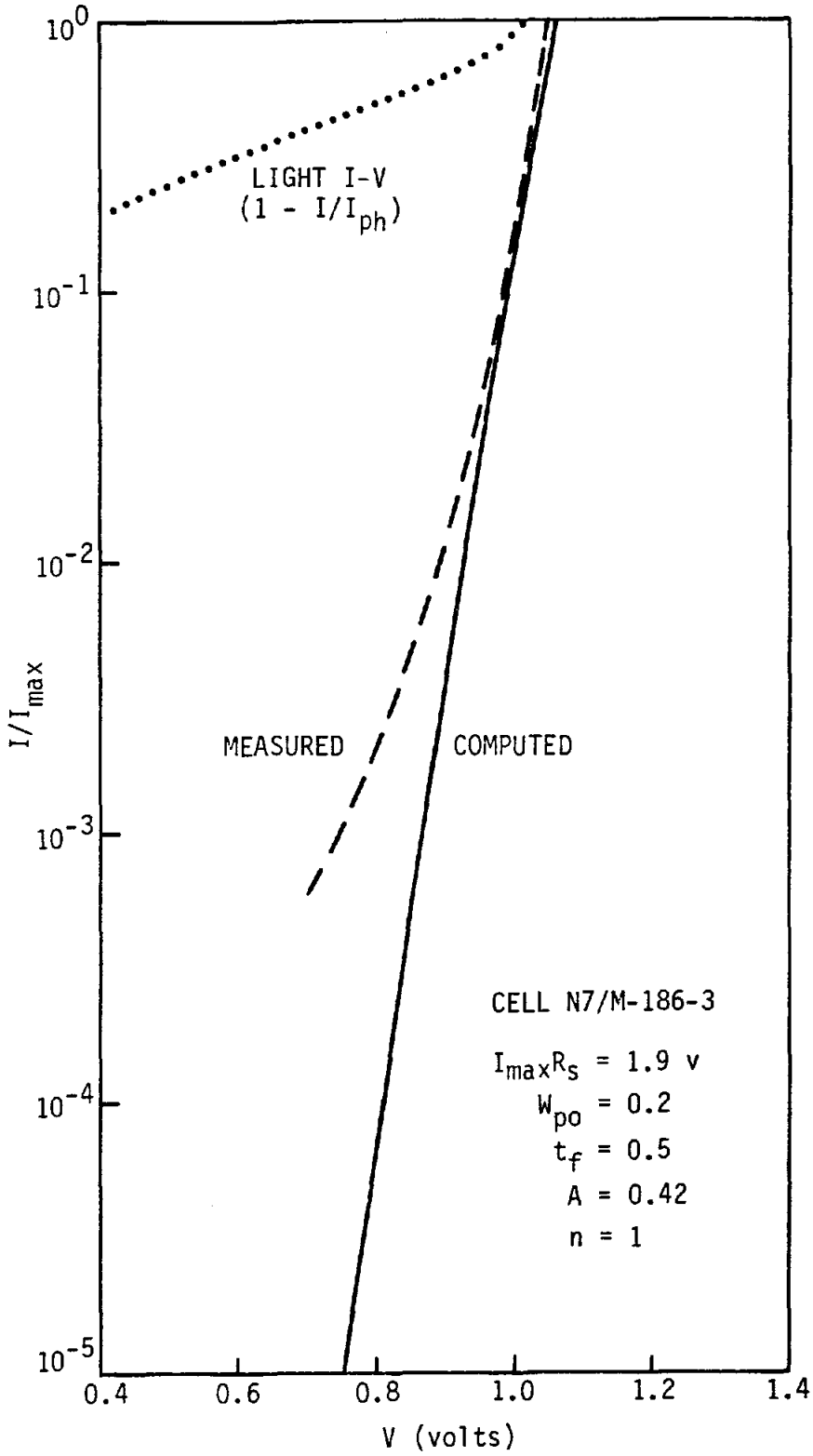
10^0
10^{-1}
10^{-2}
10^{-3}
10^{-4}
10^{-5}
I/I_{max}
LIGHT I-V
$(1 - I/I_{ph})$
MEASURED
COMPUTED
CELL N7/M-186-3
$I_{max}R_s$ = 1.9 v
W_{po} = 0.2
t_f = 0.5
A = 0.42
n = 1
0.4
0.6
0.8
1.0
1.2
1.4
V (volts)

DISTRIBUTION LIST

Acurex Corporation (2)
George Sutton
Bob Spencer
485 Clyde Avenue
Mountain View, CA 94042

Aerospace Corporation
Attn: Ed Simburger
2350 El Segundo Blvd.
El Segundo, CA 90266

Applied Solar Energy Corp. (3)
Attn: Steve Olah
Frank Ho
Ken Ling
15251 E. Don Julian Road
City of Industry, CA 91746

Arizona State University (2)
Attn: Charles Backus
Robert Sanderson
College of Engineering
Tempe, AZ 85261

Battelle
Attn: Don Carmichael
505 King Avenue
Columbus, OH 43201

BDM Corporation (3)
Attn: Tim Lambarski
Wayne Kauffman
Bill Schwinkendorf
1801 Randolph Road SE
Albuquerque, NM 87111

Chevron Research (2)
Attn: John Cape
R. Creek
576 Standard Avenue
Richmond, CA 94802

Cyro Industries
697 Route 46
Clifton, NJ 07015

U. S. Dept. of Energy (2)
ALO
Attn James Morley
Ethan Walker
P. O. Box 5400
Albuquerque, NM 87115

U. S. Dept. of Energy (7)
Division of PV Energy Systems
Attn: M. B. Prince (5)
L. A. Barrett
A. Scollaro
1000 Independence Ave. SW
Washington, DC 20585

E-Systems (2)
Attn: Mark O'Neill
A. J. McDanal
P. O. Box 226118
Dallas, TX 75266

General Electric Co.
Attn: Ron Hodge
P. O. Box 527
King of Prussia, PA 19406

International Rectifier
Attn: Harold Weinstein
235 Kansas Street
El Segundo, CA 91214

Intersol Power Corp.
Attn: John Sanders
7400 W. Radcliff Avenue
Littleton, CO 80123

Jet Propulsion Lab (2)
Attn: K. Shimada
R. Ferber
4800 Oak Grove Drive
Pasadena, CA 91109

Martin Marietta (4)
Attn: S. Broadbent
M. Imamura
D. Hughes
J. Baumann
P.O. Box 179
Denver, CO 80201

Microwave Associates
Attn: Jonathon Chapple-Sokol
South Avenue MS-116
Burlington, MA 01803

3M
Attn: Sanford Cobb
Industrial Optics
235 2D15
3M Center
St. Paul, MN 55144

Motorola
Attn: Keith Kingston
GED
8201 E. McDowell
Scottsdale, AZ 85252

NASA, HQ
Attn: John Loria
Code RET-1
Washington, DC 20546

New Shelter Home Magazine
9317 Shoshone
Albuquerque, NM 87111

Oak Ridge National Lab
Attn: Steve Kaplan
P. O. Box X
Oak Ridge, TN 37830

Oklahoma University
571 South University Blvd.
Norman, OK

Photowatt (2)
Attn: William Taylor
Mike Keeling
2414 W. 14th Street
Tempe, AZ 85281

Power Hybrids
Attn: Jeff Meyer
1742 Crenshaw Blvd.
Torrance, CA 90501

PRC
Attn: E. Stirewalt
5201 Leesburg Pike
Suite 400
Falls Church, VA 22070

Purdue University (2)
Attn: Richard Schwartz
Mark Lundstrom
Electrical Engineering Dept.
West Lafayette, IN 47907

Ray Bahm & Associates
Attn: Ray Bahm
2513 Kimberly Court NW
Albuquerque, NM 87130

Research Triangle Institute
Attn: Mayrant Simons
Box 12194
Research Triangle Park, NC 27709

Rockwell International
Microelectronics Research &
Development Center
Attn: Stan Zehr
1049 Camino Dos Rios
Thousand Oaks, CA 91360

SERI (3)
Attn: Gene Blakeslee
Lee Cole
John Benner
1617 Cole Blvd.
Golden, CO 80401

SERI, Library (2)
1536 Cole Blvd., Bldg. #4
Golden, CO 80401

Southern Cal Edison
Attn: Spencer Carlisle
2244 Walnut Grove Ave.
Rosemead, CA 91770

Spectrolab
Attn: Brian Elm
12500 Gladstone Avenue
Sylmar, CA 91342

Star Light Energy
Attn: J. Furber
1717 18th Street NW
Washington, DC 20009

Strategies Unlimited
201 San Antonio Circle
Suite 205
Mountain View, CA 94040

Solar Works
Attn: Paul Wilkins
Route 2, Box 274
Santa Fe, NM 87501

Thermo Electron
Attn: Ron Scharlack
45 First Avenue
Waltham, MA 02154

UNM/NMERI
Attn: G. Leigh
Campus Box 25
Albuquerque, NM 87131

Varian & Associates (2)
Attn: Peter Borden
N. Kaminar
611 Hansen Way K-219
Palo Alto, CA 94303

Wright Patterson AFB
Attn: Jack Geis
AFWAL/POOC
Wright Patterson AFB, OH

Wyle Labs (2)
Attn: Dave Christenson
George Meares
7800 Governors Drive West
Huntsville, AL 35807

Alliance Tool Corp.
Attn: Helmut Walter
1300 Mt. Read Blvd.
Rochester, NY 14606

Spire (3)
Attn: S. Tobin
M. Nowlan
R. Little
Patriots Park
Bedford, MA 01730

2146 B. Hanson
2146 B. Nasby
2146 J. Rodriguez
2146 B. Rose
2146 H. Weaver
4700 E Beckner
4720 D. Schueler
4721 H. Gerwin
4721 W. Schimmel
4723 E. Burgess
4724 D. Arvizu
4724 L. Beavis
4724 E. Boes
4724 C. Chiang
4724 M. Edenburn
4724 D King
4724 A. Miash
4724 M. Rios
5133 R. Chaffin
5133 J. Wiczer
5811 R. Assink
8214 M. Pound
3141 L. Erickson (5)
3151 W. Garner (3)
3154-3 C. Dalin (25)
for DOE/TIC Unlimited
Distribution

☆U.S. GOVERNMENT PRINTING OFFICE: 1982-0-576-021/554